The varved sediments of Lake Żabińskie, Poland as a high-resolution archive of environmental change

Inauguraldissertation

der Philosophisch-naturwissenschaftlichen Fakultät
der Universität Bern

vorgelegt von

Paul David Zander

von South Lake Tahoe, Vereinigte Staaten von Amerika

Leiter der Arbeit:

Prof. Dr. Martin Grosjean

Universität Bern

Ko-Leiter der Arbeit:

Prof. Dr. Wojciech Tylmann

Universität Danzig

The varved sediments of Lake Żabińskie, Poland as a high-resolution archive of environmental change

Inauguraldissertation

der Philosophisch-naturwissenschaftlichen Fakultät
der Universität Bern

vorgelegt von

Paul David Zander

von South Lake Tahoe, Vereinigte Staaten von Amerika

Leiter der Arbeit:

Prof. Dr. Martin Grosjean

Universität Bern

Ko-Leiter der Arbeit:

Prof. Dr. Wojciech Tylmann

Universität Danzig

Von der Philosophisch-naturwissenschaftlichen Fakultät angenommen

Bern, 28.05.2021

Der Dekan:

Prof. Dr. Z. Balogh

Abstract

Human impacts to the global environment have accelerated in the past several decades resulting in global warming, pollution, modification of biogeochemical cycles and other major impacts to terrestrial and aquatic ecosystems. The diverse and growing field of paleoenvironmental reconstruction offers a long-term perspective of environmental change that is necessary to understand natural processes and what conditions were like prior to human impacts. Lake sediments are a particularly important archive of paleoenvironmental information because of their wide distribution on the continents, the potential for well-constrained chronologies, and the vast array of information that can be obtained from lake sediments. In this thesis, a 10,800-year record of environmental change is presented from Lake Żabińskie, Poland. This site is relatively unique because annual laminations (varves) are preserved over the majority of the past 10,800 years and a high sedimentation rate enables analyses at high temporal resolution. The site has been investigated extensively to understand modern processes as well as the past 2,000 years of the sedimentary record, but the full Holocene record had not been investigated until this thesis.

The first case study of the thesis (Chapter 3) investigates the application of cutting-edge techniques in radiocarbon measurements for dating lake sediments. Samples of plant macrofossils containing as little as 11 µg of carbon were measured for radiocarbon using a gas-source input to the mass spectrometer. Multiple samples were taken from the same stratigraphic levels in order to assess the accuracy and precision of these miniature radiocarbon samples. Additionally, the impact of miniature samples on age-depth models was assessed using simulations of different sampling scenarios. We found no evidence of age bias from miniature radiocarbon samples, and the precision of ages was not strongly affected by the technique used (gas-source or graphitized input). Simulated sampling scenarios indicate that increasing the number of ages can compensate for increased uncertainty produced by samples with small masses.

The second study (Chapter 4) focuses on reconstructing primary production and water column anoxia over the past 10,800 years. This was accomplished primarily by the use of ultra-high-resolution pigment measurements from hyperspectral imaging (HSI) core scanning, with complimentary evidence provided by elemental data from X-ray fluorescence scanning and pigment data from high-performance liquid chromatography. Reconstructions of primary productivity and anoxia were compared with local and regional climate and vegetation data to understand how these factors influenced conditions in the lake. The presence of bacteriopheopigments, a specific biomarker for water column anoxia, indicates that an extensive anoxic zone was present in the lake nearly continuously prior to approximately 2,800 cal yr BP. Several shifts in lake mixing regime occurred after that time and lead to variable water column oxygen concentrations. These shifts were linked to human modifications of forest cover, leading to the conclusion that forest cover was a primary control on lake mixing over the Holocene. Since the 17th century, intensive agricultural development and deforestation surrounding the lake caused major increases in erosional and nutrient inputs leading to major increases in primary production and biogeochemical cycling.

The third study (Chapter 5) investigates relationships between meteorological conditions and the structure and composition of varves over the period 1966-2019. This period was selected because a varve chronology could be established with no uncertainty over this interval. Ultra-high resolution spatially resolved biogeochemical data was obtained using micro X-ray fluorescence and hyperspectral imaging. Sub-varve scale patterns of geochemical data were used to classify varves into four varve types. The years associated with these varve types were shown to experience differing seasonal weather conditions, providing evidence that weather affects the composition of varves at sub-varve scale. Statistical analysis showed that total C and Ti could be used to reconstruct spring and summer temperature, and mass accumulation rate and Si could be used to reconstruct the frequency of windy days. This study shows the potential of bulk geochemical data from biochemical varves for paleoclimate reconstructions.

In the fourth study (Chapter 6), the relationship between spring temperatures sedimentary chloropigments was investigated, building upon previously published work that indicated chloropigments could be used as a proxy for spring temperature at Lake Żabińskie. Although a significant relationship between these two variables was found for the period 1779-2016 CE, there is no significant correlation over the period 1779-1906 CE. This result suggests that chloropigments are not a reliable temperature indicator at this site, and highlights the potential problems inherent to quantitative climate reconstructions based on the assumption that climate - proxy relationships remained stable through time.

Together, these studies demonstrate the variety of insights that can be gained from high quality lake sediments records. High-resolution scanning techniques, such as micro X-ray fluorescence (μXRF) and hyperspectral imaging (HSI), applied to varved sediments represent the cutting-edge of paleolimnological research in terms of measurement resolution. The feasibility of using hyperspectral imaging on resin-embedded sediment slabs was assessed; this would enable alignment of μXRF and HSI data with the greatest possible precision. However, for Lake Żabińskie sediments, resin-embedded sediments absorbed too much light, and it was not possible to apply HSI to resin-embedded slabs. Nonetheless, these high-resolution measurements enable investigation of sub-annual processes, and make it possible to detect rapid changes that cannot be observed with conventional proxy techniques. Additionally, the speed and low-cost of these non-destructive techniques make it possible to study long records in a relatively short amount of time. Therefore, these methods should be increasingly applied to cover sites across a wide variety of environments.

Table of Contents

List of Figures

List of Tables

List of Abbreviations

^{14}C	Radiocarbon
a.s.l.	Above sea level
AMS	Accelerator mass spectrometry
(CV-)RMSE	(Cross validated) Root Mean Square Error
(M)ANOVA	(Multivariate) analysis of variance
(µ)XRF	(micro) X-ray Fluorescence
BP	Before present (present = 1950 CE)
Bphe	Bacteriopheophytin
Cal BP	Calibrated years before present
CD/TC	Chlorophyll Derivatives/Total Carotenoids
CE (dates)	Common era
CE (statistic)	Coefficient of efficiency
CI	Confidence interval
CIT	Calibration-in-time
CNS	Carbon nitrogen sulfur
CONISS	Constrained Incremental Sums of Squares
CPI	Chlorophyll preservation index
d.s.	Dry sediments
DBD	Dry bulk density
DJF	December, January, February
GAM	Generalized additive model
HPLC	High-performance liquid chromatography
HSI	Hyperspectral imaging
JJA	June, July, August
ka	kiloannum
MAM	March, April, May
MAR	Mass accumulation rate
MICADAS	MIni CArbon DAting System

MMD	Mass movement deposit
MSWD	Mean square weighted deviation
PC(A)	Principal component (analysis)
PSB	Purple sulfur bacteria
PZ	Pigment zone
RABD	Relative absorption band depth
RDA	Redundancy analysis
RE	Reduction of error
RGB	Red green blue
SON	September, October, November
TC	Total carbon
TChl	Total chlorophyll
TIC	Total inorganic carbon
TN	Total nitrogen
TOC	Total organic carbon
TP	Tree pollen
UV-VIS	Ultra violet - visible (spectroscopy)
VT	Varve type

Preface

This thesis contains seven chapters. Chapter 1 introduces the thesis by summarizing the state of relevant research and includes the research questions tackled by this thesis. Chapter 2 includes a description of the Lake Żabińskie study site, previous research at the site, and summarizes the methods used in this thesis. Chapter 3 is a methodological study focused on the application of miniature radiocarbon samples for dating lake sediments. This chapter has been published in the journal *Geochronology* (Zander et al., 2020). Chapter 4 presents the full Holocene sedimentary sequence from Lake Żabińskie and focuses on past primary production and water-column mixing. This chapter has been published in *Science of the Total Environment* (Zander et al., 2021). Chapter 5 investigates relationships between seasonal meteorological conditions and varve composition over the period 1966-2019 CE. This chapter will be submitted to *Earth and Planetary Science Letters*. Chapter 6 explores the relationship between spring temperatures and sedimentary chloropigments to see if chloropigments in Lake Żabińskie sediments are suitable as a temperature proxy. This chapter has not been published. Chapter 7 summarizes the major findings of the thesis.

Chapter 1: Introduction

1.1 General motivation

Population growth and industrialization have led to intense impacts to the natural environment including global warming, pollution, loss of biodiversity, and various other impacts to ecosystems. Understanding how ecosystems function under both natural conditions and under the influence of human activities is critical for humans to continue to benefit from the services provided by ecosystems (Carpenter et al., 2009). Our understanding of the natural world and how we have impacted the environment is greatly enhanced by studying environmental conditions and processes in the past. This desire to understand the natural world by studying the past has led to the development of the interdisciplinary field of paleoenvironmental research. In this thesis, we focus on two important themes of paleoenvironmental research: understanding how lake trophic levels and anoxia varied in the past, and the use of lake sediments as indicators of past climatic change.

Increasing eutrophication of lakes and increasing persistence and extent of anoxia in lakes are recognized as global environmental problems (Jenny et al., 2016). Although the causes of these detrimental impacts to aquatic systems are known (primarily nutrient input from human activities), in many cases little is known about the natural conditions of lakes prior to human disturbance. Additionally, long-term records can increase our understanding of the processes that control aquatic productivity and anoxia, and inform management decisions to improve conditions in the future.

In the context of global warming, paleoclimate research has been essential to place the current warming in the context of natural variability, and to understand the mechanisms that have control climate change in the past (IPCC, 2013; Tierney et al., 2020). Still, there remain open questions about spatial variability of climate, and climate variability at interannual to multi-decadal scales. To answer these questions, a globally distributed network of high-resolution paleoclimate archives is required (PAGES2k Consortium, 2017; Kaufman et al., 2020). Lake sediments are an important component of this growing network. Therefore, it is important to understand how lake sediments record climate variations.

In this thesis, the sedimentary record of Lake Żabińskie is used to reconstruct changes in aquatic, terrestrial and atmospheric sectors of the environment. Additionally, interactions between each sector are investigated.

1.2 State of research

Sediments deposited in lakes are some of earth's most valuable archives of environmental change. This is because the properties and composition of lake sediments can reflect conditions in the lake, its catchment and the atmosphere (Smol et al., 2005). Lake sediments are uniquely valuable as geological archives because they are widely distributed on the continents and sedimentation is continuous, often with little variation in sedimentation rate. Therefore, lake sediments can be used to reconstruct multiple environmental parameters with relatively high chronological precision, especially in sediments with annual layers (varves). The array of environmental conditions and processes that can be reconstructed from lake

sediments is vast, including climate, vegetation, aquatic ecology, pollution, natural hazards and others (Figure 1.1). Paleoenvironmental research on lake sediments draws upon techniques from a wide variety of disciplines including biology, geology, chemistry, physics, environmental science, and many others. The following section summarizes current research relevant to the contents of this thesis.

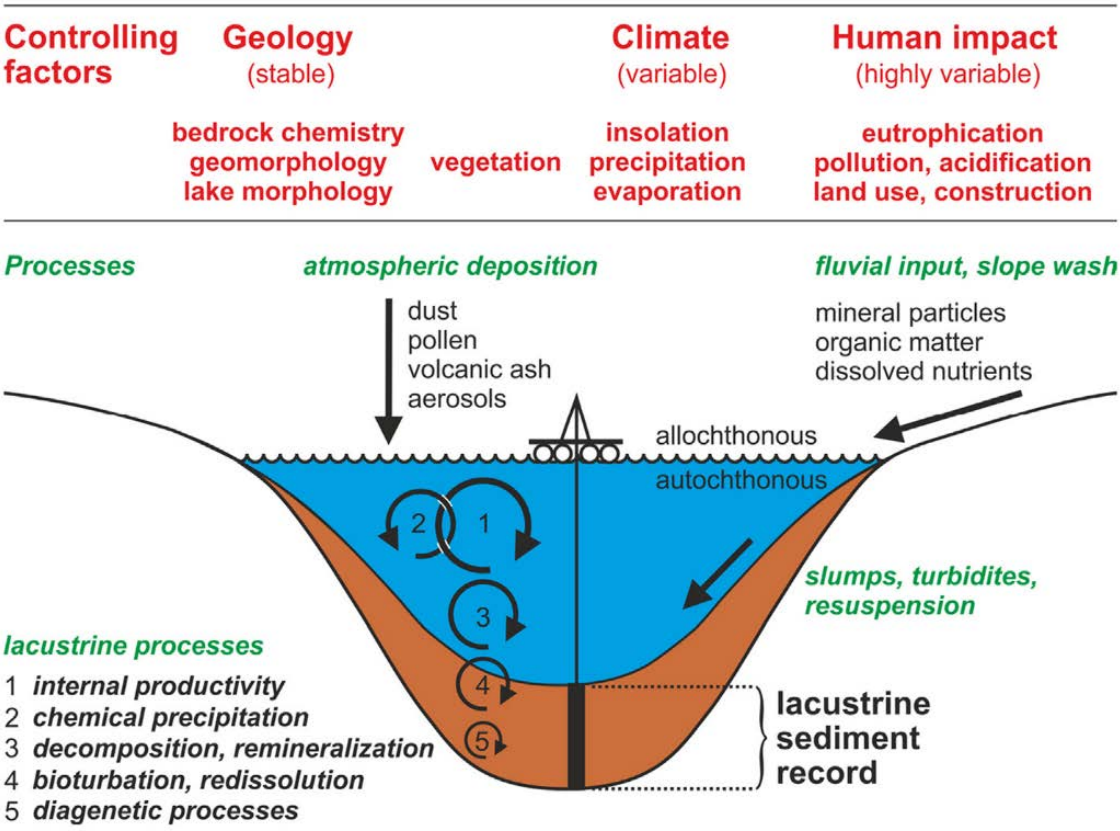

Figure 1.1: Summary of factors controlling lake sediment properties (figure from Zolitschka et al., 2015)

1.2.1 Dating lake sediments with radiocarbon and varve counting techniques

Chronological information about the depositional age of sediments is essential for comparing records from multiple sites and for constraining rates of change. Holocene lake sediment records are most often dated using radiocarbon (^{14}C) measurements. Radiocarbon ages are calculated based on the fraction of carbon in a sample that is ^{14}C and the known decay rate of this unstable isotope. Because the concentration of ^{14}C in the atmosphere has changed over time, radiocarbon ages must be calibrated to be placed on a calendar timescale (Reimer et al., 2013). Ideally, samples for radiocarbon measurements are obtained from terrestrial plant macrofossils to avoid radiocarbon reservoir effects (MacDonald et al., 1991). Technological improvements beginning with accelerator mass spectrometry (AMS; Linick et al., 1989) and continuing with innovations such as the gas-source input of the MIni CArbon DAting System have decreased the mass of sample material required for radiocarbon measurements (Ruff et al., 2007, 2010a). Smaller masses allow researchers to date sedimentary sections that have very low concentrations of suitable material for dating. Additionally, small sample masses allow researchers to investigate specific

organic fractions to understand their source and age, and to see which fractions are suitable for dating (Shah et al., 2008). Age-depth models are used to interpolate between dated levels by fitting a relationship between the depth of sediments and input ages. Bayesian age-depth models, such as Bacon (Blaauw and Christen, 2011) and the OxCal P-sequence (Bronk Ramsey, 2008, 2009), have become the standard approach for constructing sediment chronologies. These models use prior knowledge to constrain likely sedimentation rates and have been shown to provide appropriate estimates of age, sedimentation rate and age uncertainty in most cases (Blaauw et al., 2018). Evaluation of the true accuracy of radiocarbon-based age models requires independent age controls such as varve counts, tephra ages, or other methods.

Varve counting relies on an annual pattern in sedimentation creating seasonal layers that are recognizable. The utility of varves for chronologies and paleoclimatic reconstructions has been recognized for over 100 years (De Geer, 1908). Varve chronologies can offer significant advantages compared to radiocarbon chronologies because varve counts provide continuous age information (no interpolation required), there are no problems related to reservoir effects or reworking material, and varve counts can have very low uncertainties (typically errors are around 2%; Zolitschka et al., 2015). The uncertainty of varve chronologies depends on methodological choices used (automated counting versus manual; thin sections versus core images), but also the preservation quality of the annual layers. There is no consensus method for determining the uncertainty of a varve count. A common method is for multiple researchers to perform independent counts, with one count serving as the master count, and error calculated as the standard deviation of the multiple counts. Bonk et al. (2015b) proposed an alternative scheme that considers three independent counts as equally possible and assigns uncertainty asymmetrically based on the agreement or lack of agreement about individual varves. In some cases, varve counts are “floating”, meaning they are not tied to the present day, typically due to the presence of sedimentary section without preserved varves. In this case, the varve count must be tied to other age information, often radiocarbon ages (Hajdas et al., 1993). The OxCal V-sequence (Bronk Ramsey, 2008) provides a statistical routine to link radiocarbon ages and varve counts, taking into account uncertainty in both dating methods. By combining both types of age information, it is possible to achieve extremely precise chronologies. For instance, Rey et al. (2019) used this approach to date sediments from Moossee, Switzerland with mean 2σ error of ± 19 years over a 3000 year period.

1.2.2 Reconstruction of lake paleoproduction and anoxia

Due to growing concerns about eutrophication and increased extent and persistence of anoxic zones in lakes, there is a strong interest in using paleolimnological tools to reconstruct paleoproductivity and past periods of anoxia (Jenny et al., 2016; Dubois et al., 2018). Because monitoring data from lakes is often only decades long, long-term records from sediments are valued to understand ecological conditions over long time-scales (Mills et al., 2017). Paleo records improve our understanding of baseline ecological conditions prior to human disturbance (Bennion et al., 2011), natural variability, and how freshwater ecosystems respond to natural and human drivers of change.

Organic sedimentary proxies provide a variety of potential tools to reconstruct changes in trophic conditions. Measurements of bulk biogenic components such as organic carbon, nitrogen or biogenic silica can provide useful information about productivity and sources of organic matter (Meyers and Ishiwatari, 1993). Stable isotopes of carbon and nitrogen can provide information about the sources and recycling of these elements (Schelske and Hodell, 1995; Talbot, 2005). Even more detailed information about past environmental conditions can be obtained from microfossil assemblages, most commonly diatoms (Smol et al., 2005). Based on modern habitat preferences of these species, it is possible to reconstruct changes in nutrient levels, temperature, salinity, pH or other environmental parameters using transfer functions (Smol, 2010). Reconstruction of past redox conditions is also possible using chironomid assemblages (Clerk et al., 2000). Biomarkers are chemical compounds that can be linked to specific biotic sources (Bianchi and Canuel, 2011). A vast variety of biomarkers can be studied in the context of paleoproductivity or past anoxia (Castañeda and Schouten, 2011). For example, sterols were used to reconstruct diatom and dinoflagellate productivity in Lake Malawi (Castañeda et al., 2011). Pigments produced by photosynthetic organisms are a class of biomarkers that have proven particularly useful for reconstructing changes in algal community structure (Leavitt and Hodgson, 2002), trophic levels and nutrient concentrations (Guilizzoni et al., 2011a), and anoxia (Sinninghe Damsté and Schouten, 2006). Generally, the aforementioned methods require a great deal of time to perform the analyses, and destructive sampling (sometimes with relatively large sample volumes) is required. These two factors have limited the resolution of paleo records from such techniques, especially when applied to long timescales (1000s or 10,000s years).

Inorganic geochemical variables have also successfully been applied to reconstruct paleoproduction and redox changes in lakes. There are numerous methods to measure inorganic sediment components; however, X-ray fluorescence (XRF) core scanning has become particularly popular in paleolimnology because elemental abundances can be (rapidly) determined at sub-mm resolution (Croudace et al., 2019). Elements such as Br, Ca, or the Si/Ti ratio have been linked to paleoproductivity (Davies et al., 2015). Redox changes are frequently reconstructed using the Fe/Mn ratio (Naeher et al., 2013), but this ratio can be affected by other factors besides redox conditions (Makri et al., 2021b). Other elements such as Mo can also provide information about past redox conditions (Wirth et al., 2013).

Multi-proxy studies that base interpretations on multiple datasets are considered more reliable than those based on single proxies alone, and multi-proxy studies also provide more nuanced information about changes to aquatic ecosystems. Paleolimnological studies have demonstrated that it is possible to discern human impacts to aquatic ecosystems from natural variability (Mills et al., 2017; Dubois et al., 2018). These results have greatly improved our understanding of human impacts to aquatic ecosystems prior to lake monitoring, and have improved our understanding of the processes that control eutrophication or anoxia in lakes. Site-specific considerations often make it challenging to apply results from one lake to another, and this is one reason why paleolimnology will continue to be a valuable tool for environmental management.

1.2.3 Climate reconstruction using the calibration-in-time approach

Most quantitative paleoclimate reconstructions from lake sediments use either a calibration-in-time, or calibration-in-space approach. Whereas the calibration-in-space method uses modern-day climatic gradients over geographic distance to train reconstruction models (using transfer functions), the calibration-in-time (CIT) approach correlates proxy time series with historical instrumental climate time series. The calibration-in-space approach is generally not applicable to bulk sedimentary variables, because of differences in catchment properties (von Gunten et al., 2012). Therefore, in this thesis we focus on the CIT approach.

Methodological and site-specific considerations are highly important to achieve successful calibration-in-time paleoclimate reconstructions. Precise and accurate chronologies are required to enable comparisons between meteorological data and sedimentary data. Greater age uncertainty requires more smoothing of data prior to calibration, reducing the effective degrees of freedom. The CIT method relies on an assumption that the relationship between climate and proxy variables remained constant through time. However, this is not always the case (Blass et al., 2007), and instability of climate - proxy relationships should be expected in systems that have experienced significant anthropogenic disturbance. Long time series of meteorological data are beneficial to include greater environmental variability in the calibration period and to increase the degrees of freedom of the model. Long instrumental series also enable model validation using a split period approach (Cook et al., 1994). Autocorrelation of time series must be accounted for when testing the significance of correlations between climate variables and proxies. Bioturbation is an important factor to consider because this process smooths the signal of lacustrine proxies, leading to increased autocorrelation, and making it impossible to reconstruct high-frequency variability. Varved lake sediments are preferred for CIT studies because varved sediments can provide precise chronologies and their lack of bioturbation makes it possible to reconstruct climate parameters at annual resolution (Francus et al., 2002; Lapointe et al., 2020). High-resolution data (i.e. measurement intervals < 3 years) is generally required. Sites with higher sedimentation rates make it easier to make biogeochemical measurements at higher resolution. Non-destructive core-scanning techniques such as X-ray fluorescence spectroscopy and reflectance spectroscopy are ideal for CIT studies because measurements can be made at sub-mm scale (von Gunten et al., 2012); such high resolution is not possible with destructive sampling techniques (Croudace and Rothwell, 2015). Recently developed technologies continue to push the limits of analytical resolution, for instance: synchrotron radiation XRF (capable of 30 μm resolution; Alexandrin et al., 2018), XRF imaging (20 μm resolution; Shanahan et al., 2008), and hyperspectral imaging (30 μm resolution; Butz et al., 2015). As these techniques become more widely used, it will be possible to expand the geographic distribution of quantitative paleoclimate reconstructions from lake sediments.

CIT methods have been applied to a variety of proxy data, and across a variety of geographic regions from the tropics to the Arctic. In arctic or proglacial lakes with dominantly clastic sediments, varve thickness or other indicators of lithogenic flux have been used for quantitative reconstructions of winter

precipitation (Elbert et al., 2012), snowmelt (Francus et al., 2002), summer temperatures (Bird et al., 2009; Trachsel et al., 2010) and winter temperature (Amann et al., 2017). In more organic-rich sediments, sedimentary pigments have been used to reconstruct growing season temperatures (von Gunten et al., 2009; Amann et al., 2014), or layer thicknesses have been correlated with precipitation (Shanahan et al., 2009; Romero-Viana et al., 2011; Czymzik et al., 2016).

1.2.4 Hyperspectral imaging of lake sediments

Long, high-resolution, records of past lake productivity and anoxia are a desirable target of paleolimnological research, for reasons discussed in section 1.2.2. Conventional methods such as destructive chemical analyses or microfossil counts are not feasible for such high-resolution reconstructions. Hyperspectral imaging (HSI) has recently been applied to lake sediment cores, enabling rapid acquisition of biogeochemical data at sub-mm resolution (Butz et al., 2015). The HSI technique combines reflectance spectroscopy with imaging to produce an image in which each pixel contains a spectral profile of light reflectance. The spectral signature of the sediments can be used to obtain information about both inorganic and organic components (Butz et al., 2017). This method is well-suited for measurements of sedimentary pigments because of the unique spectral signatures of different pigment groups. For instance, chlorophyll-*a,* and it's derivatives, absorbs light around 660 nm. This absorbance can be quantified using a relative absorption band depth (RABD) index, and these RABD indices can be correlated with concentrations of pigments measured in sediments (Rein and Sirocko, 2002).

To date, two pigment groups have been measured using HSI: chloropigments (chlorophyll-*a* and -*b*, and their derivatives; maximum absorbance ~665 nm), and bacteriopheopigments-*a* and -*b* (derivatives of bacteriochlorophyll-*a* and -*b;* maximum absorbance ~845 nm). Chloropigments (TChl) are produced by phytoplankton, and therefore are indicative of aquatic primary production (Leavitt and Hodgson, 2002). Bacteriopheopigments-*a* and -*b* (Bphe) are produced by purple sulfur bacteria. These bacteria only live in strongly anoxic environments with high concentrations of sulfides, yet they are photosynthetic and also require light. Therefore, Bphe is a specific biomarker for anoxic conditions overlapping with the photic zone in aquatic environments (Sinninghe Damsté and Schouten, 2006). HSI-inferred pigment records have been used to reconstruct paleoproduction and anoxia over time periods ranging from decades to up to 20,000 years at sites from Switzerland (Schneider et al., 2018; Chiaia-Hernández et al., 2020; Makri et al., 2020; Tu et al., 2020), Poland (Sanchini et al., 2020a; Makri et al., 2021a; Zander et al., 2021) and Greece (Gassner et al., 2020). Holocene records of productivity and anoxia inferred from HSI have improved our understanding of human impacts to aquatic ecosystems by showing a close interplay between catchment land cover and aquatic productivity/anoxia in several small, deep, lakes.

1.3 Research gaps and questions

Previous research at Lake Żabińskie presented the sediment stratigraphy and paleoenvironmental reconstructions covering the past ~2000 years. Therefore, a central goal of this thesis is to establish a chronology and stratigraphy for the full sedimentary sequence recovered from Lake Żabińskie. High-

resolution (sub-decadal) long-term records of lake productivity and anoxia are incredibly rare. In this thesis, we use hyperspectral imaging and micro X-ray fluorescence techniques to reconstruct past productivity and anoxia at unprecedented resolution during the Holocene. Additionally, we explore how these high-resolution techniques can inform varve formation processes and linkages between climate and varve geochemistry. Research questions that guide Chapters 3-6 are presented below.

Chapter 3

In the context of radiocarbon-based chronologies for lake sediment records, it is well established that dating terrestrial plant macrofossils leads to more accurate results compared to bulk organic matter (MacDonald et al., 1991). Additionally, it is clear that increasing dating density (the number of dates per millennium) improves age-model reliability, accuracy and precision (Blaauw et al., 2018). Recently developed technologies, such as a gas-source input to an accelerator mass spectrometer, make it possible to obtain ^{14}C ages from incredibly small samples (as low as 10 µg C; Salazar et al., 2015; Gottschalk et al., 2018), with the disadvantage of increased analytical error. Smaller samples make it possible to obtain ages at greater density in organic-poor sediments, however it is not clear how to optimize age model performance with respect to sampling strategy (i.e. is it better to have few, large, samples to minimize the error of individual ages, or is it better to obtain more ages from smaller samples despite their greater error). Additionally, while it is known that terrestrial plant remains are preferred for dating, there is less known about age biases resulting from different types of plant macrofossils. To assess these research gaps, Chapter 3 aims to answer the following questions.

- **Q3.1:** How reliable and how precise are gas-source ^{14}C ages compared with conventional graphitized ages?
- **Q3.2:** What is the variability of ^{14}C ages obtained from a single stratigraphic level, and do certain types of plant macrofossils produce biased ages?
- **Q3.3:** How do analytical precision and dating density affect the accuracy and precision of age-depth models for lake sediments?

Chapter 4

Eutrophication and anoxia have increased in lakes across the globe (Jenny et al., 2016). However, there is little known about the variability of lake productivity and anoxia over timescales of thousands of years. Recent eutrophication is attributed to anthropogenic causes, mainly nutrient input, but much less is known about how lake ecosystems responded to climate and land cover change over the course of the Holocene. In Chapter 4, we use high-resolution HSI-inferred pigment data and µXRF scanning data from Lake Żabińskie sediments to answer the following questions:

- **Q4.1:** How have primary production and water column oxygen concentrations varied during the past 10,800 years?

- **Q4.2:** What role did natural and anthropogenic forces have in driving changes in primary production or lake mixing regime?

Chapter 5

Varved sediments have been used for paleoclimatic interpretation for over a century (De Geer, 1908), however paleoclimate interpretation of the properties of biogenic varves remains challenging due to the variety of possible mechanisms influencing of climate-sediment relationships. Demonstrations of climate-proxy relationships (focusing here on bulk sedimentary biogeochemical proxies, excluding microfossils or specific biomarkers) at annual resolution from biogenic varves are extremely rare. In theory, high-resolution scanning data of sub-varve structures could record meteorological conditions at event-to-seasonal temporal resolution. In Chapter 5, high-resolution μXRF and HSI data is compared with meteorological data over the period 1966-2019 to answer the following questions:

- **Q5.1:** Is the sequence of geochemical variables through a single varve influenced by seasonal meteorological conditions?
- **Q5.2:** Can varve composition be used to reconstruct seasonal meteorological conditions?

Chapter 6

Amann et al. (2014) demonstrated a significant correlation between spring temperatures and chloropigments (inferred from reflectance spectroscopy) in the sediments of Lake Żabińskie over the period 1907-2008 CE. This relationship suggested that chloropigments could be used to reconstruct spring temperatures over longer timescales. In Chapter 7, the relationship between chloropigments and spring temperature was explored using a longer instrumental temperature record from Warsaw, Poland to answer the following questions:

- **Q6.1**: Can HSI-inferred chloropigments improve upon the existing spring temperature - chloropigment calibration?
- **Q6.2:** Can the chloropigment - spring temperature calibration be extended over the period 1779-2016 CE?

1.4 References

Alexandrin, M.Y., Darin, A. V., Kalugin, I.A., Dolgova, E.A., Grachev, A.M., Solomina, O.N., 2018. Annual sedimentary record from lake donguz-orun (Central caucasus) constrained by high resolution SR-XRF analysis and its potential for climate reconstructions. Front. Earth Sci. 6. https://doi.org/10.3389/feart.2018.00158

Amann, B., Lamoureux, S.F., Boreux, M.P., 2017. Winter temperature conditions (1670-2010) reconstructed from varved sediments, western Canadian High Arctic. Quat. Sci. Rev. 172, 1-14. https://doi.org/10.1016/j.quascirev.2017.07.013

Amann, B., Lobsiger, S., Fischer, D., Tylmann, W., Bonk, A., Filipiak, J., Grosjean, M., 2014. Spring temperature variability and eutrophication history inferred from sedimentary pigments in the varved sediments of Lake Żabińskie, north-eastern Poland, AD 1907-2008. Glob. Planet. Change 123, 86-96. https://doi.org/10.1016/j.gloplacha.2014.10.008

Bennion, H., Battarbee, R.W., Sayer, C.D., Simpson, G.L., Davidson, T.A., 2011. Defining reference conditions and restoration targets for lake ecosystems using palaeolimnology: A synthesis. J. Paleolimnol. 45, 533-544. https://doi.org/10.1007/s10933-010-9419-3

Bianchi, T.S., Canuel, E.A., 2011. Chemical biomarkers in aquatic ecosystems. Princeton University Press.

Bird, B.W., Abbott, M.B., Finney, B.P., Kutchko, B., 2009. A 2000 year varve-based climate record from the central Brooks Range, Alaska. J. Paleolimnol. 41, 25-41. https://doi.org/10.1007/s10933-008-9262-y

Blaauw, M., Christen, J.A., 2011. Flexible paleoclimate age-depth models using an autoregressive gamma process. Bayesian Anal. 6, 457-474. https://doi.org/10.1214/11-BA618

Blaauw, M., Christen, J.A., Bennett, K.D., Reimer, P.J., 2018. Double the dates and go for Bayes — Impacts of model choice, dating density and quality on chronologies. Quat. Sci. Rev. 188, 58-66. https://doi.org/10.1016/j.quascirev.2018.03.032

Blass, A., Grosjean, M., Troxler, A., Sturm, M., 2007. How stable are twentieth-century calibration models? A high-resolution summer temperature reconstruction for the eastern Swiss Alps back to AD 1580 derived from proglacial varved sediments. The Holocene 17, 51-63. https://doi.org/10.1177/0959683607073278

Bonk, A., Tylmann, W., Goslar, T., Wacnik, A., Grosjean, M., 2015. Comparing varve counting and ^{14}C-Ams chronologies in the sediments of Lake Żabińskie, Northeastern Poland: Implications for accurate ^{14}C dating of lake sediments. Geochronometria 42, 157-171. https://doi.org/10.1515/geochr-2015-0019

Bronk Ramsey, C., 2009. Bayesian Analysis of Radiocarbon Dates. Radiocarbon 51, 337-360. https://doi.org/10.1017/s0033822200033865

Bronk Ramsey, C., 2008. Deposition models for chronological records. Quat. Sci. Rev. 27, 42-60. https://doi.org/10.1016/j.quascirev.2007.01.019

Butz, C., Grosjean, M., Fischer, D., Wunderle, S., Tylmann, W., Rein, B., 2015. Hyperspectral imaging spectroscopy: a promising method for the biogeochemical analysis of lake sediments. J. Appl. Remote Sens. 9, 096031. https://doi.org/10.1117/1.jrs.9.096031

Butz, C., Grosjean, M., Goslar, T., Tylmann, W., 2017. Hyperspectral imaging of sedimentary bacterial pigments: a 1700-year history of meromixis from varved Lake Jaczno, northeast Poland. J. Paleolimnol. 58, 57-72. https://doi.org/10.1007/s10933-017-9955-1

Carpenter, S.R., Mooney, H.A., Agard, J., et al., 2009. Science for managing ecosystem services: Beyond the Millennium Ecosystem Assessment. Proc. Natl. Acad. Sci. U. S. A. https://doi.org/10.1073/pnas.0808772106

Castañeda, I.S., Schouten, S., 2011. A review of molecular organic proxies for examining modern and ancient lacustrine environments. Quat. Sci. Rev. 30, 2851-2891. https://doi.org/10.1016/j.quascirev.2011.07.009

Castañeda, I.S., Werne, J.P., Johnson, T.C., Powers, L.A., 2011. Organic geochemical records from Lake Malawi (East Africa) of the last 700 years, part II: Biomarker evidence for recent changes in primary productivity. Palaeogeogr. Palaeoclimatol. Palaeoecol. 303, 140-154. https://doi.org/10.1016/j.palaeo.2010.01.006

Chiaia-Hernández, A.C., Zander, P.D., Schneider, T., Szidat, S., Lloren, R., Grosjean, M., 2020. High-Resolution Historical Record of Plant Protection Product Deposition Documented by Target and Nontarget Trend Analysis in a Swiss Lake under Anthropogenic Pressure. Environ. Sci. Technol. 54, 13090-13100. https://doi.org/10.1021/acs.est.0c04842

Clerk, S., Hall, R., Quinlan, R., Smol, J.P., 2000. Quantitative inferences of past hypolimnetic anoxia and nutrient levels from a Canadian Precambrian Shield lake. J. Paleolimnol. 23, 319-336. https://doi.org/10.1023/A:1008147127606

Cook, E.R., Briffa, K.R., Jones, P.D., 1994. Spatial regression methods in dendroclimatology: A review and comparison of two techniques. Int. J. Climatol. 14, 379-402. https://doi.org/10.1002/joc.3370140404

Croudace, I.W., Löwemark, L., Tjallingii, R., Zolitschka, B., 2019. Current perspectives on the capabilities of high resolution XRF core scanners. Quat. Int. 514, 5-15. https://doi.org/10.1016/j.quaint.2019.04.002

Croudace, I.W., Rothwell, R.G., 2015. Future Developments and Innovations in High-Resolution Core Scanning, in: Croudace, I.W., Rothwell, R.G. (Eds.), Micro-XRF Studies of Sediment Cores. Springer, Dordrecht, pp. 627-647. https://doi.org/10.1007/978-94-017-9849-5_27

Czymzik, M., Dreibrodt, S., Feeser, I., Adolphi, F., Brauer, A., 2016. Mid-Holocene humid periods reconstructed from calcite varves of the Lake Woserin sediment record (north-eastern Germany). The Holocene 26, 935-946. https://doi.org/10.1177/0959683615622549

Davies, S.J., Lamb, H.F., Roberts, S.J., 2015. Micro-XRF Core Scanning in Palaeolimnology: Recent Developments. https://doi.org/10.1007/978-94-017-9849-5_7

De Geer, G., 1908. On late quaternary time and climate. Geol. Föreningen i Stock. Förhandlingar 30, 459-464. https://doi.org/10.1080/11035890809445600

Dubois, N., Saulnier-Talbot, É., Mills, K., et al., 2018. First human impacts and responses of aquatic systems: A review of palaeolimnological records from around the world. Anthr. Rev. 5, 28-68. https://doi.org/10.1177/2053019617740365

Elbert, J., Grosjean, M., von Gunten, L., Urrutia, R., Fischer, D., Wartenburger, R., Ariztegui, D., Fujak, M., Hamann, Y., 2012. Quantitative high-resolution winter (JJA) precipitation reconstruction from varved sediments of Lago Plomo 47° S, Patagonian Andes, AD 1530-2002. Holocene 22, 465-474. https://doi.org/10.1177/0959683611425547

Francus, P., Bradley, R.S., Abbott, M.B., Patridge, W., Keimig, F., 2002. Paleoclimate studies of minerogenic sediments using annually resolved textural parameters. Geophys. Res. Lett. 29, 59-1-59-4. https://doi.org/10.1029/2002GL015082

Gassner, S., Gobet, E., Schwörer, C., et al., 2020. 20,000 years of interactions between climate, vegetation and land use in Northern Greece. Veg. Hist. Archaeobot. https://doi.org/10.1007/s00334-019-00734-5

Gottschalk, J., Szidat, S., Michel, E., Mazaud, A., Salazar, G., Battaglia, M., Lippold, J., Jaccard, S.L., 2018. Radiocarbon Measurements of Small-Size Foraminiferal Samples with the Mini Carbon Dating System (MICADAS) at the University of Bern: Implications for Paleoclimate Reconstructions. Radiocarbon 60, 469-491. https://doi.org/10.1017/RDC.2018.3

Guilizzoni, P., Marchetto, A., Lami, A., Gerli, S., Musazzi, S., 2011. Use of sedimentary pigments to infer past phosphorus concentration in lakes. J. Paleolimnol. 45, 433-445. https://doi.org/10.1007/s10933-010-9421-9

Hajdas, I., Ivy, S.D., Beer, J., Bonani, G., Imboden, D., Lotter, A.F., Sturm, M., Suter, M., 1993. AMS radiocarbon dating and varve chronology of Lake Soppensee: 6000 to 12000 ^{14}C years BP. Clim. Dyn. 9, 107-116. https://doi.org/10.1007/BF00209748

Jenny, J.P., Francus, P., Normandeau, A., Lapointe, F., Perga, M.E., Ojala, A., Schimmelmann, A., Zolitschka, B., 2016. Global spread of hypoxia in freshwater ecosystems during the last three centuries is caused by rising local human pressure. Glob. Chang. Biol. 22, 1481-1489. https://doi.org/10.1111/gcb.13193

Lapointe, F., Bradley, R.S., Francus, P., Balascio, N.L., Abbott, M.B., Stoner, J.S., St-Onge, G., de Coninck, A., Labarre, T., 2020. Annually resolved Atlantic sea surface temperature variability over the past 2,900 y. Proc. Natl. Acad. Sci. U. S. A. 117, 27171-27178. https://doi.org/10.1073/pnas.2014166117

Leavitt, P.R., Hodgson, D.A., 2002. Sedimentary Pigments, in: Tracking Environmental Change Using Lake Sediments. Springer, Dordrecht, pp. 295-325. https://doi.org/10.1007/0-306-47668-1_15

Linick, T.W., Damon, P.E., Donahue, D.J., Jull, A.J.T., 1989. Accelerator mass spectrometry: The new revolution in radiocarbon dating. Quat. Int. 1, 1-6. https://doi.org/10.1016/1040-6182(89)90004-9

MacDonald, G.M., Beukens, R.P., Kieser, W.E., 1991. Radiocarbon Dating of Limnic Sediments: A Comparative Analysis and Discussion. Ecology 72, 1150-1155. https://doi.org/10.2307/1940612

Makri, S., Rey, F., Gobet, E., Gilli, A., Tinner, W., Grosjean, M., 2020. Early human impact in a 15,000-year high-resolution hyperspectral imaging record of paleoproduction and anoxia from a varved lake in Switzerland. Quat. Sci. Rev. 239, 106335. https://doi.org/10.1016/j.quascirev.2020.106335

Makri, S., Lami, A., Tu, L., Tylmann, W., Vogel, H., Grosjean, M., 2021a. Holocene phototrophic community and anoxia dynamics in meromictic Lake Jaczno (NE Poland) using high-resolution hyperspectral imaging and HPLC data. Biogeosciences 18, 1839-1856. https://doi.org/10.5194/bg-18-1839-2021

Makri, S., Wienhues, G., Bigalke, M., Gilli, A., Rey, F., Tinner, W., Vogel, H., Grosjean, M., 2021b. Variations of sedimentary Fe and Mn fractions under changing lake mixing regimes, oxygenation and land surface processes during Late-glacial and Holocene times. Sci. Total Environ. 755, 143418. https://doi.org/10.1016/j.scitotenv.2020.143418

Meyers, P.A., Ishiwatari, R., 1993. Lacustrine organic geochemistry - an overview of indicators of organic matter sources and diagenesis in lake sediments. Org. Geochem. 20, 867-900. https://doi.org/10.1016/0146-6380(93)90100-P

Mills, K., Schillereff, D., Saulnier-Talbot, É., et al., 2017. Deciphering long-term records of natural variability and human impact as recorded in lake sediments: a palaeolimnological puzzle. Wiley Interdiscip. Rev. Water 4, e1195. https://doi.org/10.1002/wat2.1195

Naeher, S., Gilli, A., North, R.P., Hamann, Y., Schubert, C.J., 2013. Tracing bottom water oxygenation with sedimentary Mn/Fe ratios in Lake Zurich, Switzerland. Chem. Geol. 352, 125-133. https://doi.org/10.1016/j.chemgeo.2013.06.006

Reimer, P.J., Bard, E., Bayliss, A., et al., 2013. IntCal13 and Marine13 Radiocarbon Age Calibration Curves 0-50,000 Years cal BP. Radiocarbon 55, 1869-1887. https://doi.org/10.2458/azu_js_rc.55.16947

Rein, B., Sirocko, F., 2002. In-situ reflectance spectroscopy - Analysing techniques for high-resolution pigment logging in sediment cores. Int. J. Earth Sci. 91, 950-954. https://doi.org/10.1007/s00531-002-0264-0

Rey, F., Gobet, E., Szidat, S., Lotter, A.F., Gilli, A., Hafner, A., Tinner, W., 2019. Radiocarbon wiggle matching on laminated sediments delivers high-precision chronologies. Radiocarbon 61, 265-285. https://doi.org/10.1017/RDC.2018.47

Romero-Viana, L., Julià, R., Schimmel, M., Camacho, A., Vicente, E., Miracle, M.R., 2011. Reconstruction of annual winter rainfall since A.D.1579 in central-eastern Spain based on calcite laminated sediment from Lake La Cruz. Clim. Change 107, 343-361. https://doi.org/10.1007/s10584-010-9966-7

Ruff, M., Fahrni, S., Gäggeler, H.W., Hajdas, I., Suter, M., Synal, H.A., Szidat, S., Wacker, L., 2010. On-line radiocarbon measurements of small samples using elemental analyzer and MICADAS gas ion source. Radiocarbon 52, 1645-1656. https://doi.org/10.1017/S003382220005637X

Ruff, M., Wacker, L., Gäggeler, H.W., Suter, M., Synal, H.A., Szidat, S., 2007. A gas ion source for radiocarbon measurements at 200 kv. Radiocarbon 49, 307-314. https://doi.org/10.1017/S0033822200042235

Salazar, G., Zhang, Y.L., Agrios, K., Szidat, S., 2015. Development of a method for fast and automatic radiocarbon measurement of aerosol samples by online coupling of an elemental analyzer with a MICADAS AMS. Nucl. Instruments Methods Phys. Res. Sect. B Beam Interact. with Mater. Atoms 361, 163-167. https://doi.org/10.1016/j.nimb.2015.03.051

Sanchini, A., Szidat, S., Tylmann, W., Vogel, H., Wacnik, A., Grosjean, M., 2020. A Holocene high-resolution record of aquatic productivity, seasonal anoxia and meromixis from varved sediments of Lake Łazduny, North-Eastern Poland: insight from a novel multi-proxy approach. J. Quat. Sci. 35, 1070-1080. https://doi.org/10.1002/jqs.3242

Schelske, C.L., Hodell, D.A., 1995. Using carbon isotopes of bulk sedimentary organic matter to reconstruct the history of nutrient loading and eutrophication in Lake Erie. Limnol. Oceanogr. 40, 918-929. https://doi.org/10.4319/lo.1995.40.5.0918

Schneider, T., Rimer, D., Butz, C., Grosjean, M., 2018. A high-resolution pigment and productivity record from the varved Ponte Tresa basin (Lake Lugano, Switzerland) since 1919: insight from an approach that combines hyperspectral imaging and high-performance liquid chromatography. J. Paleolimnol. 60, 381-398. https://doi.org/10.1007/s10933-018-0028-x

Shah, S.R., Mollenhauer, G., Ohkouchi, N., Eglinton, T.I., Pearson, A., 2008. Origins of archaeal tetraether lipids in sediments: Insights from radiocarbon analysis. Geochim. Cosmochim. Acta 72, 4577-4594. https://doi.org/10.1016/j.gca.2008.06.021

Shanahan, T.M., Overpeck, J.T., Anchukaitis, K.J., Beck, J.W., Cole, J.E., Dettman, D.L., Peck, J.A., Scholz, C.A., King, J.W., 2009. Atlantic forcing of persistent drought in West Africa. Science (80-.). 324, 377-380. https://doi.org/10.1126/science.1166352

Shanahan, T.M., Overpeck, J.T., Hubeny, J.B., King, J., Hu, F.S., Hughen, K., Miller, G., Black, J., 2008. Scanning micro-X-ray fluorescence elemental mapping: A new tool for the study of laminated sediment records. Geochemistry, Geophys. Geosystems 9, n/a-n/a. https://doi.org/10.1029/2007GC001800

Sinninghe Damsté, J.S., Schouten, S., 2006. Biological markers for anoxia in the photic zone of the water column. Handb. Environ. Chem. Vol. 2 React. Process. 2 N, 127-163. https://doi.org/10.1007/698_2_005

Smol, J.P., 2010. The power of the past: Using sediments to track the effects of multiple stressors on lake ecosystems. Freshw. Biol. 55, 43-59. https://doi.org/10.1111/j.1365-2427.2009.02373.x

Smol, J.P., Birks, H.J.B., Last, W.M., 2005. Using Biology to Study Long-Term Environmental Change, in: Tracking Environmental Change Using Lake Sediments. pp. 1-3. https://doi.org/10.1007/0-306-47668-1_1

Talbot, M.R., 2005. Nitrogen Isotopes in Palaeolimnology, in: Tracking Environmental Change Using Lake Sediments. Kluwer Academic Publishers, pp. 401-439. https://doi.org/10.1007/0-306-47670-3_15

Trachsel, M., Grosjean, M., Schnyder, D., Kamenik, C., Rein, B., 2010. Scanning reflectance spectroscopy (380-730 nm): A novel method for quantitative high-resolution climate reconstructions from minerogenic lake sediments. J. Paleolimnol. 44, 979-994. https://doi.org/10.1007/s10933-010-9468-7

Tu, L., Zander, P., Szidat, S., Lloren, R., Grosjean, M., 2020. The influences of historic lake trophy and mixing regime changes on long-term phosphorus fractions retention in sediments of deep, eutrophic lakes: a case study from Lake Burgäschi, Switzerland. Biogeosciences 17, 2715-2729. https://doi.org/10.5194/bg-2019-389

von Gunten, L., Grosjean, M., Kamenik, C., Fujak, M., Urrutia, R., 2012. Calibrating biogeochemical and physical climate proxies from non-varved lake sediments with meteorological data: Methods and case studies. J. Paleolimnol. 47, 583-600. https://doi.org/10.1007/s10933-012-9582-9

von Gunten, L., Grosjean, M., Rein, B., Urrutia, R., Appleby, P., 2009. A quantitative high-resolution summer temperature reconstruction based on sedimentary pigments from Laguna Aculeo, central Chile, back to AD 850. The Holocene 19, 873-881. https://doi.org/10.1177/0959683609336573

Wirth, S.B., Gilli, A., Niemann, H., et al., 2013. Combining sedimentological, trace metal (Mn, Mo) and molecular evidence for reconstructing past water-column redox conditions: The example of meromictic Lake Cadagno (Swiss Alps). Geochim. Cosmochim. Acta 120, 220-238. https://doi.org/10.1016/j.gca.2013.06.017

Zander, P.D., Żarczyński, M., Vogel, H., Tylmann, W., Wacnik, A., Sanchini, A., Grosjean, M., 2021. A high-resolution record of Holocene primary productivity and water-column mixing from the varved

sediments of Lake Żabińskie, Poland. Sci. Total Environ. 755, 143713. https://doi.org/10.1016/j.scitotenv.2020.143713

Zolitschka, B., Francus, P., Ojala, A.E.K., Schimmelmann, A., 2015. Varves in lake sediments - a review. Quat. Sci. Rev. 117, 1-41. https://doi.org/10.1016/j.quascirev.2015.03.019

Chapter 2: Study site and methods

2.1 Lake Żabińskie

2.1.1 Site description

Lake Żabińskie (54.1318° N, 21.9836° E; Figure 2.) is located in the Masurian Lakeland of northeastern Poland. The catchment is 24.8 km^2 and includes two smaller lakes - Purwin and Łękuk. The geology and topography of the catchment is typical for the postglacial landscape of the Masurian Lakeland with gentle, undulating relief ranging from 110 to 230 m a.s.l. Surficial geology is dominated by deposits of glacial till, sandy moraines and fluvioglacial sands and gravels (Szumański, 2000). The study site was deglaciated following the Pomeranian Phase of the Vistulian glaciation, which was a regional readvance of the Scandinavian ice sheet ca. 17-16 ka BP (Marks et al., 2016). In current times, land cover in the catchment is a mixture of agricultural and woodland areas (primarily pine and oak-lime-hornbeam forests; Wacnik et al., 2016). The climate of the region is classified as humid continental warm summer (Dwb in the Köppen classification). The mean annual temperature during the period 1989-2019 (from the nearby Kętrzyn weather station; Polish Institute of Meteorology and Water Management - National Research Institute) was 8.1 °C, with pronounced seasonality (January: -2.1 °C; July: 18.4 °C). Annual precipitation averages 600 mm per year, with greater precipitation in summer than winter. The village of Żabinka (population, 100) is the largest settlement in the catchment and is located 0.5 km southeast of the lake. A recreational facility was established on the northern shore of the lake in the early 20th century.

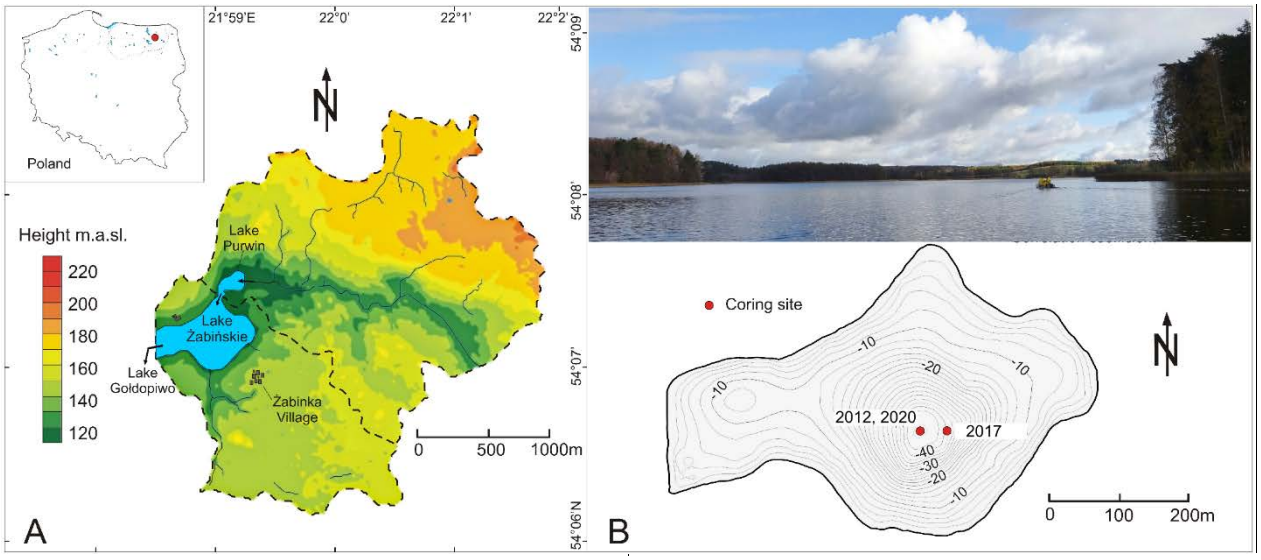

Figure 2.1: Study site map (modified from Amann et al., 2014). A) Topographic map of the Lake Żabińskie catchment with inset showing the location in Poland. B) Photograph of the study site (P. Zander) and bathymetric map (modified from Amann et al., 2014).

Lake Żabińskie is a kettle-hole lake and has typical morphometry of such lakes with high depth (maximum depth 44.4 m) relative to its surface area (41.6 ha), and a cone-shaped basin. There are three surface inflows to the lake and the outflow is a direct connection with the larger Lake Gołdopiwo. The lake is a eutrophic, hardwater lake with a variable mixing regime in which complete mixing occurs 0-2 times per

year (Bonk et al., 2015a). The high relative depth of the lake (6.1%) promotes thermal stratification, which leads to anoxic conditions in the water column throughout much of the year. Anoxia is also promoted by high primary production leading to high rates of oxygen consumption due to organic matter remineralization. Algal blooms during the spring and summer are associated with very low light penetration in the water column (Secchi depth ~ 1.2 m). Anoxic conditions have enabled preservation of biochemical varves in the sediments of Lake Żabińskie. Spring/summer layers are identified by their light color and abundant calcite and diatom remains, whereas fall/winter layers are darker in color and are composed of fine detrital material.

2.1.2 Limnological and paleoenvironmental research at Lake Żabińskie

The exceptional preservation of relatively thick varves at Lake Żabińskie has led to a great deal of research on both modern processes and paleoenvironmental reconstructions at Lake Żabińskie over the past decade. The exceptional quality of the sediments was recognized during a survey of lakes in Poland searching for varved sediments (Tylmann et al., 2013). Since 2011, limnological conditions and sediment traps have been monitored, providing high-quality information about modern processes at the site. As of this writing, at least 18 studies have been published in peer-reviewed journals that are focused primarily on Lake Żabińskie. These studies have focused on a variety of themes including modern processes (Bonk et al., 2015a; Ustrzycka et al., 2018), geochronology (Bonk et al., 2015b; Tylmann et al., 2016; Żarczyński et al., 2018; Zander et al., 2020), tephra (Kinder et al., 2020), climate reconstruction (Amann et al., 2014; Hernández-Almeida et al., 2014, 2015; Larocque-Tobler et al., 2015), and other paleoenvironmental reconstructions (Bonk et al., 2016; Wacnik et al., 2016; Hernández-Almeida et al., 2017; Witak et al., 2017; Żarczyński et al., 2019a, 2019b; Zander et al., 2021).

These studies resulted in several findings that are relevant to this thesis. Monitoring of limnological conditions and sedimentation using sediment traps established the annual pattern of sedimentation that forms varves in Lake Żabińskie (Bonk et al., 2015a). The robustness and precision of varve counting as a chronological tool was shown by comparisons with ^{210}Pb and ^{137}Cs profiles, tephra material from the Askja CE 1875 eruption (Tylmann et al., 2016), and radiocarbon ages over the past 2000 years (Bonk et al., 2015b; Żarczyński et al., 2018). Major changes in sediment properties during the period 1600-1720 CE record large increases in erosional input, algal production and lake mixing (Bonk et al., 2016; Hernández-Almeida et al., 2017). These changes were driven by the development of intensive agriculture and deforestation in the catchment (Wacnik et al., 2016). Further investigation using Fe/Mn ratios revealed changes to the lake mixing regime also during the first millennium CE due to weak anthropogenic modifications to forest cover surrounding the lake (Żarczyński et al., 2019b). A study of sedimentary pigments over the period 1907-2008 demonstrated changes in the algal community with increasing dominance of cyanobacteria in recent decades (Amann et al., 2014). This study also demonstrated the potential of chloropigments, inferred from reflectance spectroscopy core scanning, as a proxy for spring temperature. Additionally, climate reconstructions were developed using microfossil assemblages.

Chironomids were used to reconstruct summer temperature (Larocque-Tobler et al., 2015), and chrysophytes were used to reconstruct winter severity and wind velocities (Hernández-Almeida et al., 2014, 2015).

2.2 Methods

This section summarizes the key methodologies used in this thesis. More details about the methods can be found in the respective chapters (Chapters 3-6).

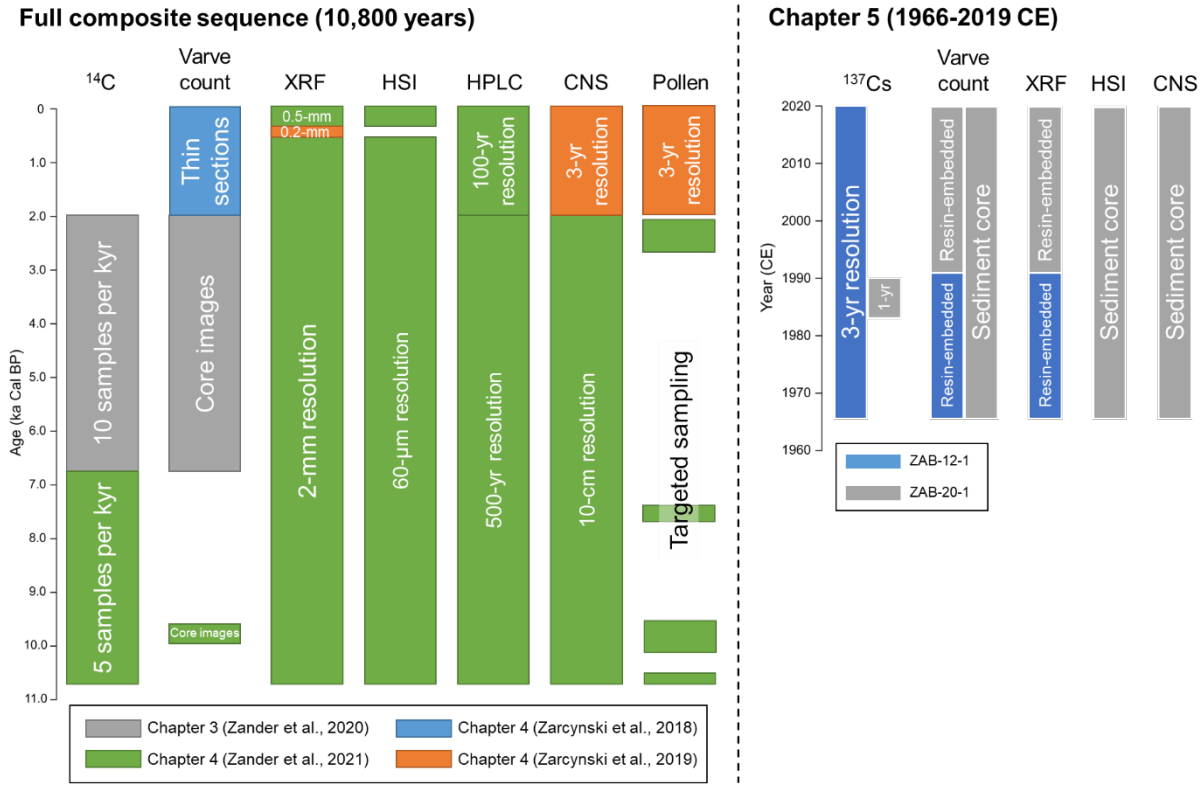

Figure 2.2: Schematic summary of datasets presented in this thesis. A) Full composite sequence covering 10,800 years. Different colored boxes indicate the chapters that discuss each dataset and the original publications. B) Datasets used in Chapter 5. Different colored boxes indicate the core each dataset was measured on.

2.2.1 Core retrieval and composite stratigraphy

Material for this thesis was retrieved during coring campaigns in 2012, 2017 and 2020. The full sediment sequence was recovered in 2012 using an UWITEC piston corer (90 mm diameter). Surface cores were extracted using UWITEC gravity corers (both 90 and 60 mm diameters) in 2017 and 2020. Cores were stored in dark at 4°C whenever possible. The 19.4-m-long composite sediment sequence was constructed by correlating distinct visual marker layers in overlapping core sections. Where possible, the same core sections that were used in Żarczyński et al. (2019b) were also used in this work, however in some cases core material was not available, and parallel cores were used. A 40-cm-long section of core (2.1-2.5 m composite depth) had no remaining material and could not be investigated in this thesis beyond previously

published data. A summary of cores and the composite stratigraphy is available in Table 2.1 and Fig. S4.1.

Table 2.1: Summary of sediment cores used in this thesis and their stratigraphic correlations

Core	Length (cm)	Section Top (cm)	Section Bottom (cm)	Composite Top (cm)	Composite Bottom (cm)	Notes
Full Composite Sequence (Chapters 3 and 4)						
ZAB 17-4	79.4	0.00	74.39	0.00	74.38	
ZAB 17-1-2	73.6	7.92	16.39	74.39	82.95	
ZAB 12-5-1-2	128.0	5.18	127.98	82.96	205.77	ca. 40 cm gap at bottom of this core (material was previously consumed)
ZAB 12-5-2-1	97.5	0.00	97.53	245.78	343.30	1.2 cm gap at bottom
ZAB 12-5-2-2	97.4	0.00	94.87	344.51	439.38	
ZAB 12-3-3-1	108.1	11.31	108.08	439.39	536.15	
ZAB 12-3-3-2	90.5	0.00	10.87	536.16	547.03	
ZAB 12-4-3-1	112.2	2.71	112.19	547.03	656.50	
ZAB 12-4-3-2	85.0	0.00	69.00	656.51	725.50	MMD, not used
ZAB 12-3-4-2	131.6	0.00	117.78	725.50	843.28	
ZAB 12-4-4-2	138.1	2.81	121.10	843.28	961.57	
ZAB 12-3-5-2	138.6	4.70	76.34	961.57	1033.21	
ZAB 12-4-5-1	140.3	26.99	124.69	1033.21	1130.91	
ZAB 12-5-6-1	115.7	9.60	115.68	1130.92	1236.99	
ZAB 12-5-6-2	80.7	0.00	72.46	1237.00	1309.45	
ZAB 12-4-6-2	125.6	9.11	99.12	1309.46	1399.46	
ZAB 12-3-7-1	116.0	58.31	109.28	1399.47	1450.43	
ZAB 12-4-7-1	139.0	13.30	126.00	1450.44	1563.13	
ZAB 12-3-8-1	124.4	10.29	117.59	1563.14	1670.43	
ZAB 12-4-8-1	74.8	22.58	74.80	1670.44	1722.65	
ZAB 12-4-8-2	122.8	0.00	104.33	1722.66	1826.98	
ZAB 12-3-9-2	123.7	10.01	123.72	1826.99	1940.69	
High-resolution sequence (Chapter 6)						
ZAB 12-1	200	10.17	28.88	15.80	34.51	Not used for HSI
ZAB 20-1	133.4	0.06	15.80	0.06	15.80	HSI data from this core

2.2.2 Chronological methods

The previously published varve count chronology for past 2000 years (Żarczyński et al., 2018) was used for the uppermost portion of the composite sequence. Where the original core material was not available, the varve count was transposed at easily identifiable marker layers and linearly interpolated between those marker layers. A mass movement deposit (labeled MMD-1) separates the sediments that had been investigated by Żarczyński et al. (2018) and those that had not been investigated prior to this thesis. To

date sediments below MMD-1, new varve counts and radiocarbon ages were used, and the methods for these techniques are presented below.

Varve counting

A section of well-preserved varves (7.3-13.1 m depth; 2.1-6.8 cal ka BP) was selected for varve counting to improve the precision of the chronology and as independent chronological information used to validate results obtained from miniature radiocarbon samples (Chapter 3). Varve counts were performed by three researchers using the software CooRecorder (Larsson, 2003) on core images obtained from a Specim PFD-CL-65-V10E hyperspectral linescan camera. Images were processed to RGB images using the method of Butz et al. (2015). The three independent varve counts were synthesized using the method of Żarczyński et al. (2018) whereby varves counted by only one researcher are not included in the master count, but are included as positive age uncertainty, and varves counted by two of three researchers are included in the master count and as negative age uncertainty. Varves counted by all three researchers do not contribute to the uncertainty. An additional varve count was made over the interval 17.0-16.4 m to constrain the chronology because two radiocarbon ages in this section gave conflicting ages. The varve count helped identify which age was more likely to be an outlier.

Radiocarbon

Samples were taken for radiocarbon dating from sediments older than 2000 years BP. Organic macrofossils were picked after wet sieving sediment slices (typically 1-cm-thick, maximum 2-cm-thick). Only material identified as terrestrial plant material was retained for analysis. Sample material was treated with an acid-base-acid (ABA) method to remove contamination. Radiocarbon measurements were done with the MIni CArbon DAting System (MICADAS) at the Laboratory for the Analysis of Radiocarbon, University of Bern. Samples smaller than 300 µg were input to the MICADAS gas ion source via combustion in an Elementar Vario EL Cube elemental analyzer (Salazar et al., 2015).

Age-depth modeling

An age-depth model for sediments below MMD-1 (sediments older than approximately 2000 cal BP) was developed using the software OxCal (Bronk Ramsey, 2008, 2009; Bronk Ramsey and Lee, 2013). Two different styles of age-depth models were integrated within OxCal. The P-sequence is a Bayesian depositional model that models sedimentation rates using Monte Carlo sampling to fit the input sequence of calibrated radiocarbon ages (calibration was done with IntCal13; Reimer et al., 2013). A parameter (k) controls the variability of sedimentation rates in the model. For the P-sequence models in this study, a uniformly distributed prior was used that allows k to vary between 0.01 and 100. The V-sequence was used for core sections with varve counts; this statistical routine uses the number of varves counted between dated levels (input as ‘gaps’, with uncertainty) to constrain the probability distribution of the calibrated radiocarbon ages. The composite model links two P-sequences (19.4-18.0 m, 16.4-13.1 m) and

two V-sequences (17.0-16.4 m, 7.3-13.1 m). Two MMDs were removed from the age model (18.0-17.0 m, 7.3-6.3 m).

2.2.3 Elemental analyses

X-ray fluorescence scanning

X-ray fluorescence (XRF) scanning was used to determine elemental abundances in the sediments. The majority of XRF data in this study was collected using an ITRAX core scanner (Cox Analytical Systems) at the University of Bern. The scanner was equipped with a Cr-tube, and the scanning parameters were exposure time 20 s, voltage 30 kV, current 50 mA. Two surface cores (ZAB-17-4 and ZAB-17-1) were scanned at the Swiss Federal Institute of Aquatic Science and Technology with an Avaatech XRF Core Scanner (Richter et al., 2006) equipped with a Rh-tube using voltage 10 kV, current 1.5 mA, and 15 s exposure time. Additional XRF data from an ITRAX core scanner at the University of Bremen with a Mo-tube (exposure time 10 s, voltage 30 kV, current 18 mA) was used to fill a gap where core material was not available (2.5-2.1 m composite depth). The scanning resolution was 2 mm for 19.4-2.5 m, 0.2 mm for 2.5-2.1 m, and 0.5 mm for 2.1-0 m. All XRF data were calculated as counts per second (cps) and then homogenized so that the standard deviation and mean for each element in overlapping core sections were equal. Key elements for analysis were selected based on data quality and interpretations of interest.

In addition to sediment core linescans, XRF data was acquired as elemental maps on resin-embedded sediment slabs using a Bruker M4 Tornado. The scanner was equipped with an Rh X-ray source and voltage and current were set to 50 kV and 300 µA, respectively. Counts were measured along the two-dimensional surface of the slabs with a measurement spot size of 20 µm and counting time of 20 ms/pixel. The measurement step (pixel size) was set to 60 µm. This approach has the advantage of high resolution and spatially resolved data. In addition, the resin-embedded blocks preserve fine structures in the laminated sediments that cannot be resolved as well on wet sediment core faces. These data were obtained from sediments representing the period 1960-2020 CE.

Destructive bulk element analysis

Previously published data on total inorganic carbon (TIC), total organic carbon (TOC), total nitrogen (TN), and total sulfur (TS) at 3-year resolution were used for the interval 6.1-0 m (Żarczyński et al., 2019b). For the interval 19.4-6.1 m these elements were measured at 10-cm resolution (1-cm-thick samples). A Vario El Cube elemental analyzer (Elementar) was used to measure TC, TN and TS. TIC was determined by (loss-on-ignition at 950 °C) - (loss-on-ignition at 550 °C) (Heiri et al., 2001). TOC was calculated by subtracting TIC from TC. Dry bulk density (DBD) was measured on the same samples used for CNS analyses by measuring the dry mass of one cm^3 of wet sediment. Mass accumulation rates (MAR) were calculated by multiplying dry bulk density and sedimentation rate (obtained from varve counts and OxCal age-depth model outputs).

2.2.4 Pigment analysis

Three distinct methods were used to measure sedimentary pigments, each with advantages and disadvantages.

Spectrophotometry

UV-VIS (ultraviolet-visible) spectrophotometry is a relatively simple method requiring little expertise and is capable of precise pigment concentration measurements; however, this method requires chemical extraction, limiting its utility for high-resolution measurements. Similar to HSI, it is a non-specific technique capable of determining concentrations of bulk pigment groups with similar absorption. In this thesis, spectrophotometry was used to calibrate HSI RABD indices to concentrations. Forty-one samples were taken from the core at a resolution of ~500 years for the period 10.8 to 2.0 ka cal BP and at ~100-year resolution for the most recent 2000 years. Pigments were extracted from freeze-dried sediments using 100% acetone using a modified version of the method of Amann et al. (2014). Concentrations of TChl and Bphe were measured using a Shimadzu UV-1800 spectrophotometer. The molar extinction coefficient for bacteriopheophytin-*a* from Fiedor et al. (2002) and the molar extinction coefficient for chlorophyll-*a* and chlorophyll derivatives-*a* from Jeffrey and Humphrey (1975) were used to calculate concentrations. These concentrations were used to calibrated RABD indices by applying a linear regression between concentrations (in µg/g dry sediments) and mean RABD index values from the sample area.

High-performance Liquid Chromatography

High-performance Liquid Chromatography (HPLC) is capable of quantitative concentration measurements of individual pigment compounds, providing much more detailed information than the spectroscopic techniques. However, this technique is labor-intensive and requires expert knowledge to operate the analytical equipment. The same pigment extracts that were used for spectrophotometer measurements were also used for HPLC measurements. We used an Agilent Infinity 1260 series HPLC equipped with a G7117C Diode-Array Detection detector and a G7121A fluorescence detector following the methods of Sanchini and Grosjean (2020). Pigment compounds were identified and quantified using reference standards (Table S4.1).

Hyperspectral Imaging

Hyperspectral imaging (HSI) produces data at exceptionally high temporal resolution and is acquired quickly (1-m-long core is scanned in 30 minutes). However, HSI-inferred pigment data is semi-quantitative and non-specific because it is based on absorption features that may be produced by multiple pigment compounds. Additionally, processing large volumes of data requires some expert knowledge. Hyperspectral core-scanning was done following the workflow outlined by Butz et al. (2015). A Specim PFD-65-V10E camera (Figure 2.) was used with exposure 90 ms, aperture f/1.9, field of view 78.7 mm, frame rate 10 Hz, and scanning speed 0.6 mm/s. Reflectance data were acquired across the visible and near-infrared spectrum from 400-1000 nm with a spectral resolution of 1.4 nm and a spatial resolution of

60 µm × 60 µm (pixel size). Data were processed using ENVI 5.1 and 5.4 (Exelisvis ENVI, Boulder, Colorado). Sedimentary pigment abundances were quantified using relative absorption band depth (RABD) indices. The index $RABD_{655\text{-}685max}$ measures total chloropigments (TChl; chlorophyll-*a* and -*b*, and their diagenetic products) and was calculated using the following formula (modified from Schneider et al., 2018):

$$RABD_{655-685max} = \left(\frac{X * R_{590} + Y * R_{730}}{X + Y}\right) / R_{655-685min}$$

Where R_λ is the reflectance at the wavelength (λ), $R_{655\text{-}685min}$ is the trough minimum (ie. lowest reflectance value measured between 655 and 685 nm), X is the number of spectral bands between R730 and the trough minimum, and Y is the number of spectral bands between the trough minimum and R590. $RABD_{845}$ measures bacteriopheophytin-*a* and -*b* (Bphe; derivatives of bacteriochlorophyll-*a* and -*b*) and was calculated using the following formula (Butz et al., 2015):

$$RABD_{845} = \left(\frac{34 * R_{790} + 34 * R_{900}}{68}\right) / R_{845}$$

RABD indices were calculated for every pixel creating maps of pigment abundances in the cores at a resolution of 60 µm. Depth profiles were calculated by averaging across a 2 mm wide subset; thus, each data point in the profile represents a 60 x 2000 µm area.

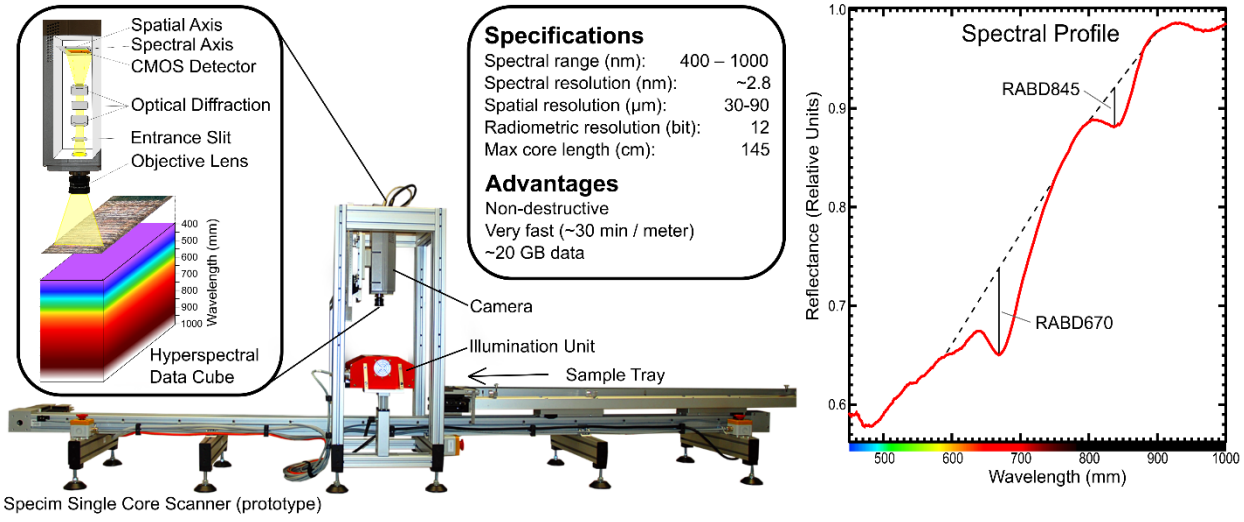

Figure 2.3: Specim Single Core Scanner and example of relative absorption band depth (RABD) index calculation. Figure modified from Butz et al. (2015).

Testing HSI on resin-embedded sediments

In order to utilize HSI data in conjunction with µXRF scanning data at the highest possible resolution, it would be optimal to obtain data from resin-embedded sediment slabs. Compared to fresh sediments, resin-embedded sediment slabs have the advantage of better preservation of fine sediment structures,

and the sediments are fixed in place unable to shift due to drying or smearing of the surface. This makes it possible to align scanning data from multiple instruments more precisely compared to fresh sediments.

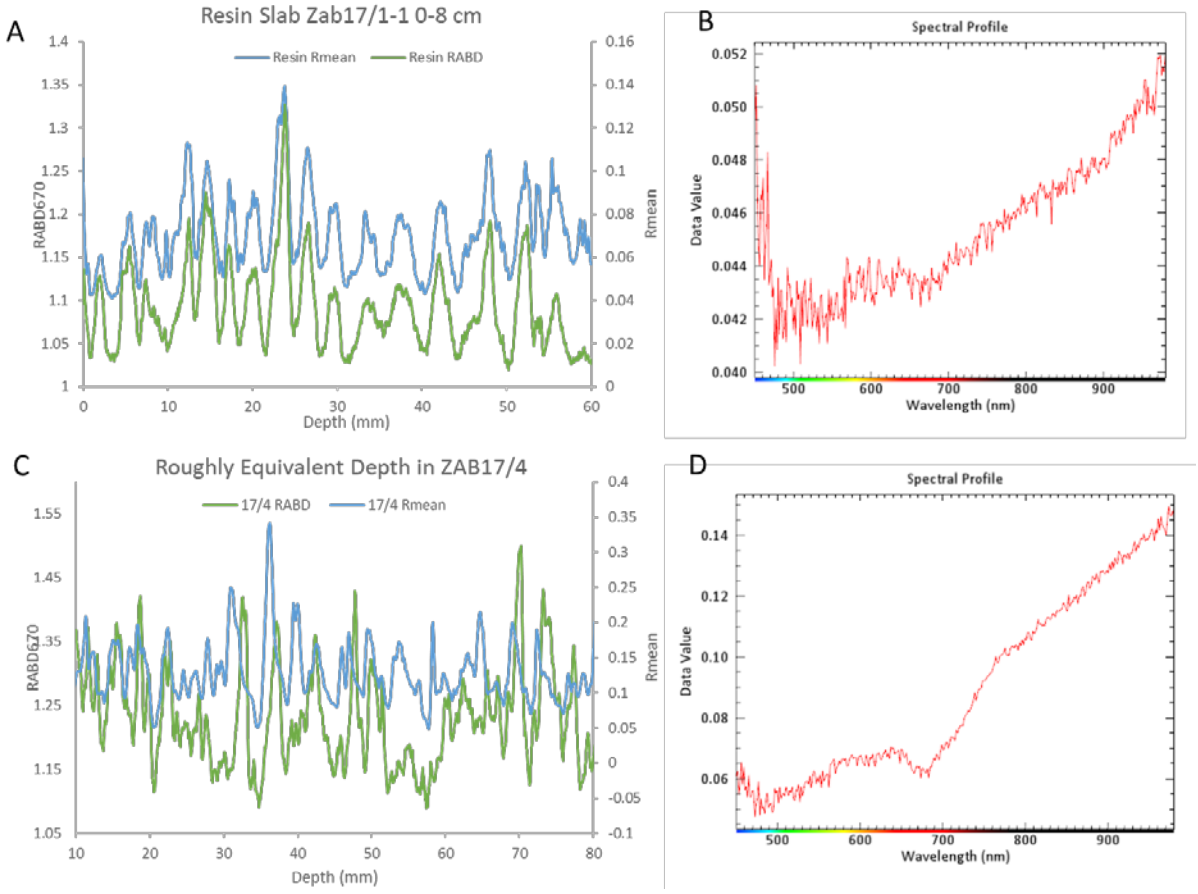

Figure 2.4: Comparison of HSI indices obtained from fresh sediment core and a resin-embedded sediment slab. A) Rmean and RABD670 from resin-embedded sediment slab showing that RABD values closely track Rmean values. B) Example spectral profile from dark lamination in resin slab with noisy spectral data due to low reflectance. C) Same as A, but for fresh sediments. Note that RABD peaks often occur below Rmean peaks. D) Same as B, but for dark lamination in fresh sediments. Absorbance near 670 nm from chloropigments is better detected due to higher reflectance.

Sediments were embedded in an epoxy resin chosen for its optical properties (EPOTEK301; 99% spectral transmission 382-980 nm) and then scanned with the hyperspectral camera to test if HSI was effective for resin-embedded sediments. Tests were also conducted on previously made slabs embedded in Araldite2020 epoxy resin. Very little light reflectance was measured from resin-embedded sediments, therefore an exposure of 140 ms and frame rate of 6 hz were applied. Despite these slower acquisition settings, average reflectance remained low, approximately 6% on average, whereas 10% or above is generally required to obtain good quality data with a high signal to noise ratio. The lack of reflectance affects the detection of chloropigments, as measured by an RABD index. Fig. 2.4 shows RABD670 and Rmean for a resin embedded slab and a roughly equivalent section of sediment in a fresh sediment core. In the resin embedded sediments, Rmean and RABD670 are synchronous, whereas in the fresh sediments, RABD670 tends to lead Rmean, with peaks in RABD670 typically occurring a few mm below

peaks in Rmean. The correlation between Rmean and RABD670 in the resin slab is 0.84, whereas in the fresh sediment core it is 0.26. This indicates that the brightness of the material is strongly affecting the detection of pigment absorption. When Rmean values are below about 6%, the absorption trough created by pigments becomes essentially indistinguishable from measurement noise in the spectral data, and therefore RABD values in these locations are very low. Based on this result, I deemed resin blocks unsuitable for HSI techniques, at least for Lake Żabińskie sediments.

2.2.5 Data analysis

Data analysis was performed in R (R Core Team, 2020). Full details of packages used are supplied in the respective chapters. For the full sediment sequence (Chapter 4), high-resolution scanning data was averaged to 1-cm resolution; this smooths the data, limiting the influence of outliers, and helps with small offsets that occurs when correlations XRF and HSI datasets. After log-transformation and normalization, this dataset was investigated and summarized using principle component analysis (PCA), stratigraphically constrained cluster analysis (CONISS) and kmeans cluster analysis. The HPLC pigment dataset was summarized with PCA and CONISS analyses. For the high-resolution study on the past 54 years (Chapter 5), varve types were classified based on a multivariate time-series dissimilarity score (psi, Benito and Birks, 2020). We tested the hypothesis that these varve types experienced different seasonal weather conditions by applying a MANOVA test to meteorological data organized by years associated to varve types. Generalized additive models were used to reconstruct climate variables (temperature and wind) from proxy data.

2.3 References

Amann, B., Lobsiger, S., Fischer, D., Tylmann, W., Bonk, A., Filipiak, J., Grosjean, M., 2014. Spring temperature variability and eutrophication history inferred from sedimentary pigments in the varved sediments of Lake Żabińskie, north-eastern Poland, AD 1907-2008. Glob. Planet. Change 123, 86-96. https://doi.org/10.1016/j.gloplacha.2014.10.008

Benito, B.M., Birks, H.J.B., 2020. distantia: an open-source toolset to quantify dissimilarity between multivariate ecological time-series. Ecography (Cop.). 43, 660-667. https://doi.org/10.1111/ecog.04895

Bonk, A., Kinder, M., Enters, D., Grosjean, M., Meyer-Jacob, C., Tylmann, W., 2016. Sedimentological and geochemical responses of Lake Żabińskie (north-eastern Poland) to erosion changes during the last millennium. J. Paleolimnol. 56, 239-252. https://doi.org/10.1007/s10933-016-9910-6

Bonk, A., Tylmann, W., Amann, B., Enters, D., Grosjean, M., 2015a. Modern limnology and varve-formation processes in lake Żabińskie, northeastern Poland: Comprehensive process studies as a key to understand the sediment record. J. Limnol. 74, 358-370. https://doi.org/10.4081/jlimnol.2014.1117

Bonk, A., Tylmann, W., Goslar, T., Wacnik, A., Grosjean, M., 2015b. Comparing varve counting and ^{14}C-Ams chronologies in the sediments of Lake Żabińskie, Northeastern Poland: Implications for accurate ^{14}C dating of lake sediments. Geochronometria 42, 157-171. https://doi.org/10.1515/geochr-2015-0019

Bronk Ramsey, C., 2009. Bayesian Analysis of Radiocarbon Dates. Radiocarbon 51, 337-360. https://doi.org/10.1017/s0033822200033865

Bronk Ramsey, C., 2008. Deposition models for chronological records. Quat. Sci. Rev. 27, 42-60. https://doi.org/10.1016/j.quascirev.2007.01.019

Bronk Ramsey, C., Lee, S., 2013. Recent and Planned Developments of the Program OxCal. Radiocarbon 55, 720-730. https://doi.org/10.1017/s0033822200057878

Butz, C., Grosjean, M., Fischer, D., Wunderle, S., Tylmann, W., Rein, B., 2015. Hyperspectral imaging spectroscopy: a promising method for the biogeochemical analysis of lake sediments. J. Appl. Remote Sens. 9, 096031. https://doi.org/10.1117/1.jrs.9.096031

Heiri, O., Lotter, A.F., Lemcke, G., 2001. Loss on ignition as a method for estimating organic and carbonate content in sediments: Reproducibility and comparability of results. J. Paleolimnol. https://doi.org/10.1023/A:1008119611481

Hernández-Almeida, I., Grosjean, M., Gómez-Navarro, J.J., et al., 2017. Resilience, rapid transitions and regime shifts: Fingerprinting the responses of Lake Żabińskie (NE Poland) to climate variability and human disturbance since AD 1000. Holocene 27, 258-270. https://doi.org/10.1177/0959683616658529

Hernández-Almeida, I., Grosjean, M., Przybylak, R., Tylmann, W., 2015. A chrysophyte-based quantitative reconstruction of winter severity from varved lake sediments in NE Poland during the past millennium and its relationship to natural climate variability. Quat. Sci. Rev. 122, 74-88. https://doi.org/10.1016/j.quascirev.2015.05.029

Hernández-Almeida, I., Grosjean, M., Tylmann, W., Bonk, A., 2014. Chrysophyte cyst-inferred variability of warm season lake water chemistry and climate in northern Poland: training set and downcore reconstruction. J. Paleolimnol. 53, 123-138. https://doi.org/10.1007/s10933-014-9812-4

Kinder, M., Wulf, S., Appelt, O., Hardiman, M., Żarczyński, M., Tylmann, W., 2020. Late-Holocene ultra-distal cryptotephra discoveries in varved sediments of Lake Żabińskie, NE Poland. J. Volcanol. Geotherm. Res. 402, 106988. https://doi.org/10.1016/j.jvolgeores.2020.106988

Larocque-Tobler, I., Filipiak, J., Tylmann, W., Bonk, A., Grosjean, M., 2015. Comparison between chironomid-inferred mean-August temperature from varved Lake Zabińskie (Poland) and instrumental data since 1896 AD. Quat. Sci. Rev. 111, 35-50. https://doi.org/10.1016/j.quascirev.2015.01.001

Larsson, L., 2003. COORECORDER v2. 3.13: Image Co-ordinate Recording Program.

Marks, L., Marks, L., Dzierżek, J., et al., 2016. Quaternary stratigraphy and palaeogeography of Poland. Acta Geol. Pol. 66, 403-427.

R Core Team, 2020. R: A Language and Environment for Statistical Computing.

Reimer, P.J., Bard, E., Bayliss, A., et al., 2013. IntCal13 and Marine13 Radiocarbon Age Calibration Curves 0-50,000 Years cal BP. Radiocarbon 55, 1869-1887. https://doi.org/10.2458/azu_js_rc.55.16947

Sanchini, A., Grosjean, M., 2020. Quantification of chlorophyll a, chlorophyll b and pheopigments a in lake sediments through deconvolution of bulk UV-VIS absorption spectra. J. Paleolimnol. 64, 243-256. https://doi.org/10.1007/s10933-020-00135-z

Schneider, T., Rimer, D., Butz, C., Grosjean, M., 2018. A high-resolution pigment and productivity record from the varved Ponte Tresa basin (Lake Lugano, Switzerland) since 1919: insight from an

approach that combines hyperspectral imaging and high-performance liquid chromatography. J. Paleolimnol. 60, 381-398. https://doi.org/10.1007/s10933-018-0028-x

Szumański, A., 2000. Objaśnienia do Szczegółowej Mapy Geologicznej Polski, Arkusz Giżycko, (Explanation to the Detailed Geological Map of Poland, Sheet Gizycko (104)). Warsaw, Poland.

Tylmann, W., Bonk, A., Goslar, T., Wulf, S., Grosjean, M., 2016. Calibrating 210 Pb dating results with varve chronology and independent chronostratigraphic markers: Problems and implications. Quat. Geochronol. 32, 1-10. https://doi.org/10.1016/j.quageo.2015.11.004

Tylmann, W., Zolitschka, B., Enters, D., Ohlendorf, C., 2013. Laminated lake sediments in northeast Poland: Distribution, preconditions for formation and potential for paleoenvironmental investigation. J. Paleolimnol. 50, 487-503. https://doi.org/10.1007/s10933-013-9741-7

Ustrzycka, A., Piotrowska, N., Bonk, A., Filipiak, J., Tylmann, W., 2018. Isotopic fingerprints of the Lake Żabińskie (NE Poland) hydrological system on contemporary carbonates precipitated in the lake. Isotopes Environ. Health Stud. 54, 225-243. https://doi.org/10.1080/10256016.2017.1349118

Wacnik, A., Tylmann, W., Bonk, A., Goslar, T., Enters, D., Meyer-Jacob, C., Grosjean, M., 2016. Determining the responses of vegetation to natural processes and human impacts in north-eastern Poland during the last millennium: combined pollen, geochemical and historical data. Veg. Hist. Archaeobot. 25, 479-498. https://doi.org/10.1007/s00334-016-0565-z

Witak, M., Hernández-Almeida, I., Grosjean, M., Tylmann, W., 2017. Diatom-based reconstruction of trophic status changes recorded in varved sediments of Lake Żabińskie (northeastern Poland), AD 1888-2010. Oceanol. Hydrobiol. Stud. 46, 1-17. https://doi.org/10.1515/ohs-2017-0001

Zander, P.D., Szidat, S., Kaufman, D.S., Żarczyński, M., Poraj-Górska, A.I., Boltshauser-Kaltenrieder, P., Grosjean, M., 2020. Miniature radiocarbon measurements (< 150 µg C) from sediments of Lake Żabińskie, Poland: effect of precision and dating density on age-depth models. Geochronology 2, 63-79. https://doi.org/10.5194/gchron-2-63-2020

Zander, P.D., Żarczyński, M., Vogel, H., Tylmann, W., Wacnik, A., Sanchini, A., Grosjean, M., 2021. A high-resolution record of Holocene primary productivity and water-column mixing from the varved sediments of Lake Żabińskie, Poland. Sci. Total Environ. 755, 143713. https://doi.org/10.1016/j.scitotenv.2020.143713

Żarczyński, M., Szmańda, J., Tylmann, W., 2019a. Grain-Size Distribution and Structural Characteristics of Varved Sediments from Lake Żabińskie (Northeastern Poland). Quaternary 2, 8. https://doi.org/10.3390/quat2010008

Żarczyński, M., Tylmann, W., Goslar, T., 2018. Multiple varve chronologies for the last 2000 years from the sediments of Lake Żabińskie (northeastern Poland) - Comparison of strategies for varve counting and uncertainty estimations. Quat. Geochronol. 47, 107-119. https://doi.org/10.1016/j.quageo.2018.06.001

Żarczyński, M., Wacnik, A., Tylmann, W., 2019b. Tracing lake mixing and oxygenation regime using the Fe/Mn ratio in varved sediments: 2000 year-long record of human-induced changes from Lake Żabińskie (NE Poland). Sci. Total Environ. 657, 585-596. https://doi.org/10.1016/j.scitotenv.2018.12.078

Chapter 3: Miniature radiocarbon measurements (< 150 µg C) from sediments of Lake Żabińskie, Poland: effect of precision and dating density on age-depth models

---

Declaration of contribution

The following study was published in *Geochronology* (Volume 2, 17 April 2020, p. 63-79). Paul Zander prepared samples, designed and performed the age modelling experiment, analyzed results, and prepared the manuscript with contributions from all authors. Martin Grosjean, Darrell Kaufmn, Sönke Szidat, and Paul Zander designed the strategy and goals of the study. Maurycy Żarczyński, Anna Poraj-Górska, and Paul Zander performed varve counting. Petra Boltshauser-Kaltenrieder identified and selected suitable macrofossils. Sönke Szidat oversaw ^{14}C analyses. Darrell Kaufman assisted with laboratory work. Core materials were supplied by Wojciech Tylmann. Edith Vogel and Gary Salazar assisted with ^{14}C sample measurements.

Miniature radiocarbon measurements (< 150 µg C) from sediments of Lake Żabińskie, Poland: effect of precision and dating density on age-depth models

Paul D. Zander[1], Sönke Szidat[2], Darrell S. Kaufman[3], Maurycy Żarczyński[4], Anna I. Poraj-Górska[4], Petra Boltshauser-Kaltenrieder[5], Martin Grosjean[1]

[1]Institute of Geography & Oeschger Centre for Climate Change Research, University of Bern, Bern, Switzerland

[2]Department of Chemistry and Biochemistry & Oeschger Centre for Climate Change Research, University of Bern, Bern, Switzerland

[3]School of Earth and Sustainability, Northern Arizona University, Flagstaff, USA

[4]Faculty of Oceanography and Geography, University of Gdańsk, Gdańsk, Poland

[5]Institute of Plant Sciences & Oeschger Centre for Climate Change Research, University of Bern, Bern, Switzerland

Correspondence to: Paul D. Zander (paul.zander@giub.unibe.ch)

Keywords: radiocarbon, MICADAS, lake sediments, OxCal, age-depth modeling

Abstract

The recent development of the MIni CArbon DAting System (MICADAS) allows researchers to obtain radiocarbon (^{14}C) ages from a variety of samples with miniature amounts of carbon (< 150 µg C) by using a gas ion source input that bypasses the graphitization step used for conventional ^{14}C dating with accelerator mass spectrometry (AMS). The ability to measure smaller samples, at reduced cost compared with graphitized samples, allows for greater dating density of sediments with low macrofossil concentrations. In this study, we use a section of varved sediments from Lake Żabińskie, NE Poland, as a case study to assess the usefulness of miniature samples from terrestrial plant macrofossils for dating lake sediments. Radiocarbon samples analyzed using gas-source techniques were measured from the same depths as larger graphitized samples to compare the reliability and precision of the two techniques directly. We find that the analytical precision of gas-source measurements decreases as sample mass decreases, but is comparable with graphitized samples of a similar size (approximately 150 µg C). For samples larger than 40 µg C and younger than 6000 yr BP, the uncalibrated 1σ age uncertainty is consistently less than 150 years (± 0.010 $F^{14}C$). The reliability of ^{14}C ages from both techniques is assessed via comparison with a best-age estimate for the sediment sequence, which is the result of an OxCal V-sequence that integrates varve counts with ^{14}C ages. No bias is evident in the ages produced by either gas-source input or graphitization. None of the ^{14}C ages in our dataset are clear outliers; the 95% confidence intervals of all 48 calibrated ^{14}C ages overlap with the median best-age estimate. The effects of sample mass (which defines the expected analytical age uncertainty) and dating density on age-depth models are evaluated via simulated sets of ^{14}C ages that are used as inputs for OxCal P-sequence age-depth models. Nine different sampling scenarios were simulated in which the mass of ^{14}C samples and the

number of samples were manipulated. The simulated age-depth models suggest that the lower analytical precision associated with miniature samples can be compensated for by increased dating density. The data presented in this paper can improve sampling strategies and can inform expectations of age uncertainty from miniature radiocarbon samples as well as age-depth model outcomes for lacustrine sediments.

3.1 Introduction

Radiocarbon (^{14}C) dating is the most widely used technique to date sedimentary sequences that are less than 50,000 years old. The robustness of age-depth models can be limited by the availability of suitable material for dating; this is particularly a problem for studies on sediments from alpine, polar, or arid regions where terrestrial biomass is scarce. Most accelerator mass spectrometry (AMS) labs recommend that samples contain 1 mg or more of carbon for reliable ^{14}C age estimations. It is well established that terrestrial plant macrofossils are the preferred material type for dating lake sediments because bulk sediments or aquatic macrofossils may have an aquatic source of carbon, which can bias ^{14}C ages (Groot et al., 2014; MacDonald et al., 1991; Tornqvist et al., 1992; Barnekow et al., 1998; Grimm et al., 2009). Furthermore, a high density of ^{14}C ages (i.e. one age per 500 years) is recommended to reduce the overall chronologic uncertainty of age-depth models (Blaauw et al., 2018). Researchers working on sediments with low abundances of terrestrial plant macrofossils face difficult choices about whether to date sub-optimal materials (e.g. bulk sediment or aquatic macrofossils), pool material from wide sample intervals, or rely on few ages for their chronologies. The problem of insufficient material can affect age estimates at all scales from an entire sedimentary sequence to a specific event layer which a researcher wishes to determine the age of as precisely as possible.

Recent advances have reduced the required sample mass for AMS ^{14}C analysis, opening new opportunities for researchers (Santos et al., 2007; Delqué-Količ et al., 2013; Shah Walter et al., 2015; Freeman et al., 2016). The recently developed MIni CArbon DAting System (MICADAS) has the capability to analyze samples with miniature masses via the input of samples in a gaseous form, thus omitting sample graphitization (Ruff et al., 2007, 2010a, 2010b; Synal et al., 2007; Szidat et al., 2014; Wacker et al., 2010a, 2010b, 2013). Samples containing as little as a few µg C can be dated using the gas-source input of the MICADAS. The analysis of such small samples provides several potential benefits for dating lake sediments: 1) the possibility to date sediments that were previously not dateable using ^{14}C due to insufficient material, 2) the ability to date sedimentary profiles with a greater sampling density and lower costs per sample, and 3) the ability to be more selective when selecting material to be analyzed for ^{14}C. The disadvantage of miniature samples is increased analytical uncertainty, which is a consequence of lower counts of carbon isotopes and the greater impact of contamination on the measurement results. The goal of this study is to assess the potential benefits and limits of applying miniature ^{14}C measurements to dating lake sediments. We aim to answer the following questions in this study: 1) How reliable and how precise are gas-source ^{14}C ages compared with graphitized ages? 2) What is the variability of ^{14}C ages

obtained from a single stratigraphic level? 3) How do analytical precision and dating density affect the accuracy and precision of age-depth models for lake sediments?

In this study, we use the sediments of Lake Żabińskie, Poland, as a case study to investigate the application of gas-source ^{14}C measurements to lake sediments. We focus on a continuously varved segment of the core, which spans from roughly 2.1 to 6.8 ka. We report the results of 48 radiocarbon measurements (17 using graphitization and 31 using the gas-source input) in order to compare the precision and reliability of gas-source ^{14}C ages with graphitized samples. The core was sampled such that up to five ages were obtained from 14 distinct stratigraphic depths. A floating varve chronology was integrated with the ^{14}C ages to produce a best-age estimate using the OxCal V-sequence routine (Bronk Ramsey, 2008). This best-age estimate is used as a benchmark for the ^{14}C results. The results of our ^{14}C measurements were used to constrain a statistical model designed to simulate sets of ^{14}C ages in order to test nine different hypothetical sampling scenarios in which we manipulate the number of ages and the mass of C per sample, which determines the analytical uncertainty of the simulated ages. By comparing the results of the simulated age-depth model outputs from these simulated ^{14}C ages with the best-age estimate from which the simulated ages were derived, we can improve our understanding of how the number of ages and their analytical precision influence the accuracy and precision of radiocarbon-based age-depth models.

3.2 Materials and methods

3.2.1 Core material and radiocarbon samples

Cores were obtained from Lake Żabińskie (coring site: 54.1318° N, 21.9836° E, 44 m water depth) in 2012 using an UWITEC piston corer (90 mm diameter). Lake Żabińskie is a small (41.6 ha), relatively deep (44.4 m) kettle-hole lake located at an altitude of 120 m a.s.l. The catchment is 24.8 km^2 and includes two other smaller lakes: Lake Purwin and Lake Łękuk. Average temperatures range from 17 °C in summer to -2 °C in winter. Annual precipitation is 610 mm, with the annual peak in summer (JJA). The geology of the catchment is primarily glacial till, sandy moraines and glacial fluvial sands and gravels (Szumański, 2000). Modern land cover in the catchment is a mixture of cultivated fields and primarily oak-lime-hornbeam and pine forests (Wacnik et al., 2016). The high relative depth (6.1%; calculated according to Wetzel et al., 1991) of Lake Żabińskie leads to strong seasonal stratification, bottom-water anoxia, and the preservation of varves in the sediments (Bonk et al., 2015a, 2015b; Tylmann et al., 2016; Żarczyński et al., 2018). Varve-based chronologies and ^{14}C measurements have been published for the most recent 2000 years of the Lake Żabińskie sedimentary sequence (Bonk et al., 2015b; Żarczyński et al., 2018). These studies show major changes to varve structure and a three-fold increase in sedimentation rates in response to increased cultivation and deforestation, beginning around 1610 CE. Prior to this time, land cover in the region was relatively stable, with forest/woodland cover dominating the landscape from the early Holocene until the 17th century CE (Wacnik, 2009a; Żarczyński et al., 2019b).

A composite sediment profile was constructed from overlapping, 2-m-long cores by correlating distinctive stratigraphic features. The composite sequence spans 19.4 m. Published downcore varve counts stop above a ~90-cm-thick slump/deformed unit. This slump event is dated to 1962-2071 cal yr BP (present = 1950 CE) based on an extension of the varve count published in Żarczyński et al., 2018. This study focuses on a section of core (7.3-13.1 m depth in our composite sequence) directly below this slump unit; this section was selected because it features continuous well-preserved varves throughout the section. Samples of 1- to 2-cm-thick slices of sediment were taken from the core (sample locations and core images are found in Supplementary File 1), then sieved with a 100 µm sieve. Macrofossil remains were identified and photographed (Supplementary File 2), and only identifiable terrestrial plant material was selected for ^{14}C measurements. Suitable macrofossils from a single stratigraphic level were divided into subsamples for analysis, with the goal of producing one graphitized ^{14}C age and 2-4 gas-source ages from each depth. When convenient, we grouped samples by the type of material (leaves, periderm, needles, seeds or woody scales), though 11 samples are a mixture of material types. In most cases, subsamples within a stratigraphic level are assumed to be independent, meaning they may have different true ages. However, there are some subsamples that were taken from single macrofossil fragments (six subsamples taken from two fragments sampled from two different depths), thus these samples have the same true age. It is also possible that subsamples from a single depth may be from the same original material without our knowledge (i.e. a macrofossil could break into several pieces while sieving, and these pieces could be analyzed as separate subsamples).

Sample material was treated with an acid-base-acid (ABA) method at 40°C, using 0.5 mol/L HCl, 0.1 mol/L NaOH and 0.5 mol/L HCl for 3 h, 2 h and 3 h, respectively. After drying at room temperature, samples were weighed, and those less than 300 µg were input to the gas ion source via combustion in an Elementar Vario EL Cube elemental analyzer (Salazar et al., 2015). Larger samples were graphitized following combustion using automated graphitization equipment (AGE) (Szidat et al., 2014). Radiocarbon data was processed using the software BATS (Wacker et al., 2010b). Additional corrections were applied to the data to account for cross contamination (carryover), and constant contamination (blanks) (Salazar et al., 2015; Gottschalk et al., 2018). The parameters for these corrections were calculated based on standard materials (the primary NIST standard oxalic acid II (SRM 4990C) and sodium acetate (Sigma-Aldrich, No. 71180) as ^{14}C-free material) run with the sample batches. We applied a constant contamination correction of 1.5 ± 0.2 µg C with 0.72 ± 0.11 $F^{14}C$ and a cross contamination correction of (1.2 ± 0.3 %) from the previously run sample. Measurement uncertainties were fully propagated for each correction. In total, 48 ages were obtained from 14 distinct stratigraphic levels (17 graphitized and 31 gas-source measurements).

3.2.2 Varve count

Varves in Lake Żabińskie are biogenic, with calcite-rich pale laminae deposited in spring and summer, and darker laminae containing organic detritus and fine clastic material deposited in winter (Żarczyński et al., 2018). We defined the boundary of each varve year by the onset of calcite precipitation (i.e., the upper boundary of dark laminae and lower boundary of light-colored laminae). Varves were counted using CooRecorder software (Larsson, 2003) on core images obtained from a Specim PFD-CL-65-V10E linescan camera (Butz et al., 2015). Three people performed independent varve counts, and these three counts were synthesized, and uncertainties calculated according to the methodology recommended by Żarczyński et al. (2018) yielding a master varve count with asymmetric uncertainties.

Because of the slump deposit above our section of interest, the varve chronology is 'floating' and must be constrained by the ^{14}C ages. Several different approaches were used to compare the varve count with the ^{14}C ages, all of which rely on some assumptions. One method is to tie the varve count to the radiocarbon based age at a chosen depth in the core. We tested this method using the median calibrated age of the uppermost dated level as the tie point. Such an approach assumes that the radiocarbon-based age at the tie point is correct. An additional drawback is that the choice of tie-point is arbitrary and can change the resulting varve count ages. Alternatively, we used least squares minimization to fit the varve count to all radiocarbon ages (Hajdas et al., 1995) by minimizing the offset between the varve count and the combined calibrated radiocarbon age at each dated level. However, we focus on a third, more sophisticated method, which is the OxCal 4.3 V-sequence (Bronk Ramsey, 2008, 2009; Bronk Ramsey and Lee, 2013). This technique integrates all available chronological information including varve counting and ^{14}C ages into a single model to determine a best-age estimate for the sequence (see sect. below for more details). The advantages of this approach are that all ages are considered equally likely to be correct (or incorrect), and the error estimate of the V-sequence is relatively consistent along the profile, whereas the error associated with the varve count is small at the top of the section, but increases downcore. Additionally, this technique allows for the possibility that the master varve count is incorrect (within the expected uncertainty of the count).

3.2.3 Age-depth modeling

Age-depth modeling was performed using OxCal 4.3 (Bronk Ramsey, 2008, 2009; Bronk Ramsey and Lee, 2013), which integrates the IntCal13 calibration curve (Reimer et al., 2013) for ^{14}C ages with statistical models that can be used to construct age-depth sequences. As an initial test to compare the reliability of gas-source ages and graphitized ages, and their effect on age-depth models, we produced three P-sequence models: one using all obtained ^{14}C ages, one using only graphitized ages, and one using only gas-source ages. For all OxCal models in this study, ages measured from the same depth were combined (using the function *R_combine*) into a single ^{14}C age with uncertainty before calibration and integration into the age-depth sequence. This choice was verified by the chi-squared statistic calculated by OxCal to test the agreement of ages sampled from a single depth. For every combination of ages except

one, we find that the chi-squared test is passed at 0.05 significance level. We justify the use of the combine function even for the grouping that failed to pass the chi-squared test (samples from 811 cm depth) because all ages in this group overlap, and there is no significant difference when models are run with the ages separated at this depth (less than 5 years difference for median age, and CI). The OxCal P-sequence uses a Bayesian approach in which sediment deposition is modelled as a Poisson (random) process. A parameter (k) determines the extent to which sedimentation rates are allowed to vary. For all P-sequence models in this study, we used a uniformly distributed prior for k such that $k_0 = 1$, and $\log_{10}(k/k_0) \sim U(-2, 2)$; this allows k to vary between 0.01 and 100. Sediment deposition sequences are constrained by likelihood functions produced by the calibration of radiocarbon ages. Thousands of iterations of sediment deposition sequences are produced using Markov Chain Monte Carlo (MCMC) sampling (Bronk Ramsey, 2008). These iterations can then be summarized into median age estimates, with confidence intervals.

The varve counts and all ^{14}C ages were incorporated into an OxCal V-sequence in an approach similar to that used by Rey et al. (2019). The V-sequence differs from the P-sequence in that it does not model sediment deposition. Instead, the V-sequence uses 'Gaps' (the amount of time between two points in a sequence) to constrain the uncertainty of radiocarbon ages. The Gap can be determined from independent chronological information such as varve counts or tree ring counts. We input the number of varves in 10 cm intervals to the V-sequence as an age 'Gap' with associated uncertainty. The OxCal V-sequence assumes normally distributed uncertainties for each gap, whereas our varve count method produces asymmetric uncertainty estimates. We used the mean of the positive and negative uncertainties as inputs to the V-sequence. However, OxCal sets the minimum uncertainty of each 'Gap' equal to 5 years, which in most cases is larger than the mean uncertainty in our varve count over a 10 cm interval. By including the varve counts as an additional constraint, the V-sequence produces a more precise age-depth relation than the P-sequence, which only considers the radiocarbon ages.

3.2.4 Age-depth model simulation

In order to test the effects of analytical uncertainty and dating density (number of ages per time interval) on age-depth models, we designed an experiment in which nine different sampling scenarios were simulated for the Lake Żabińskie sedimentary sequence to determine the expected precision and accuracy of resulting age-depth models. Three different sampling densities were simulated for the 5.8-m-long section: 5 ages, 10 ages, and 20 ages (equivalent to approximately 1, 2, and 4 ages per millennium, respectively). For each of these sampling densities three different sample-size scenarios were simulated: 35 µg C, 90 µg C, 500 µg C. These scenarios were designed to represent different sampling circumstances such as high or low abundances of suitable material for ^{14}C analysis, and different budgets for ^{14}C analysis. Radiocarbon ages were simulated using a technique similar to Trachsel and Telford (2017). In brief, we distributed the simulated samples evenly by depth across the 5.8-m-long section, and then used the median output of the OxCal V-sequence as the assumed true age for a given depth. This

calibrated assumed true age was back-converted to ^{14}C years using IntCal13 (Reimer et al., 2013). A random error term was added to the ^{14}C age to simulate the analytical uncertainty. The error term was drawn from a normal distribution with mean zero and standard deviation equivalent to the age uncertainty determined from the relationship between sample mass and age uncertainty found in the results of our ^{14}C measurements (Fig. 3.1A). The same expected analytical uncertainty was used for the age uncertainty for each simulated age. For a sample with 35 µg C, we expect a measurement uncertainty of ± 148 years (or ± 0.0114 $F^{14}C$), which is representative for the average age of all samples in this study (approximately 4000 ^{14}C yr BP). In reality, older samples would have greater age uncertainty, while younger samples would have less uncertainty. However, the effect of these differences on the performance of simulated age-depth models would be minimal as roughly half the ages would be more precise and half would be less precise. These simulated ^{14}C ages were input into an OxCal P-sequence using the same uniform distribution for the k-parameter as described in the previous section. This experiment was repeated 30 times for each scenario to assess the variability of possible age-model outcomes. We quantify the accuracy of the age-depth models as the deviation of the median modelled age from the best-age estimate at a given depth. We define precision as the width of the age-depth model confidence interval (CI).

3.3 Results

3.3.1 Radiocarbon measurements

In total, 48 radiocarbon measurements on terrestrial plant macrofossils were obtained from the section of interest yielding values from 0.475 - 0.777 $F^{14}C$ (2030 to 5990 ^{14}C yr BP; Table). Thirty-one ages were measured using the gas-source input; these samples contained between 11 and 168 µg C. Seventeen samples containing between 115 and 691 µg C were measured using graphitization. Analytical uncertainties for the ^{14}C measurements range from ± 0.0027 to ± 0.0306 $F^{14}C$ (± 41 to ± 328 years) with higher values associated with the smallest sample masses. The uncertainties for gas-source measurements and graphitized measurements are comparable for samples that contain a similar amount of carbon (Fig. 3.1). Samples containing less than 40 µg C (roughly equivalent to 80 µg of dry plant material) produce uncertainties greater than ± 150 years (1σ). We use a power-model fit with least-squares regression, to estimate the typical age uncertainty for a given sample mass ($r^2 = 0.90$, $p < 0.001$, Fig. 3.1). The resulting power model is nearly identical to what would be expected based on the assumed Poisson distribution of the counting statistics where the uncertainty follows the relationship $N^{-0.5}$ (N = the number of measured ^{14}C atoms).

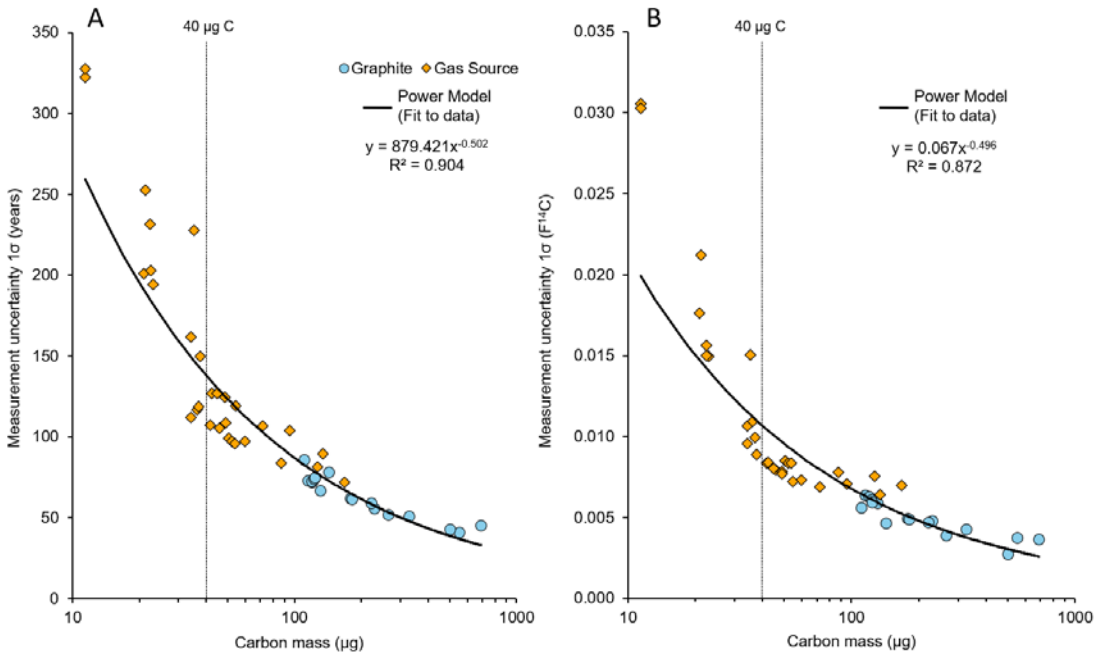

Figure 3.1: A) Age uncertainty of AMS radiocarbon ages (without calibration) versus the mass of carbon in the sample. Note that these samples date to approximately 2000-6000 BP; older ages will have greater age uncertainties. Note the logarithmic scale on the x-axis. The black line represents the best-fit power model for our dataset. B) Same as A, except uncertainties are plotted as measurement uncertainty in F14C units. This measure of uncertainty is not directly influenced by the age of the sample.

When comparing measurements taken from within a single sediment slice we find good agreement for all ^{14}C ages, regardless of whether the samples were analyzed with the gas-source input or via a graphitized target (Fig. 3.2), and no clear bias based on the type of macrofossil that was dated (Fig. 3.3). One method to test whether the scatter of ages is consistent with the expectations of the analytical uncertainty is a reduced chi-squared statistical test, also known as Mean Square Weighted Deviation (MSWD) in geochronological studies (Reiners et al., 2017). If the spread of ages is exactly what would be expected from the analytical uncertainty, the value of this statistic is 1. Lower values represent less scatter than expected, and larger values represent more scatter than expected. Of the 11 sampled depths with three or more ages, only one (811 cm, MSWD = 3.07) returned an MSWD that exceeds a 95% significance threshold for acceptable MSWD values that are consistent with the assumption that the age scatter is purely the result of analytical uncertainty.

Table 3.1: Results of the 48 ^{14}C analyses obtained for this study. Uncertainties of ^{14}C ages refer to 68% probabilities (1σ) whereas ranges of calibrated and modelled ages represent 95% probabilities.

Lab ID	Core ID	Top Core Depth (cm)	Bottom Core Depth (cm)	Centered Composite Depth (cm)	Carbon Mass (µg)	Gas/ Graphite	^{14}C age (BP)	Calibrated Age (Cal yr BP)[1]	Modelled Age from OxCal V-sequence (Cal yr BP)[2]	Material
BE-9791.1.1	ZAB-12-4-3-2	75	77	732.5	168	Gas	2028 ± 72	1823-2293	2106-2218	*Pinus sylvestris* seed fragments (seed wing, and fragments of seed)
BE-9793.1.1	ZAB-12-4-3-2	75	77	732.5	34	Gas	2149 ± 112	1867-2361	2106-2218	Terrestrial seed fragment
BE-9792.1.1	ZAB-12-4-3-2	75	77	732.5	11	Gas	2190 ± 322	1416-2968	2106-2218	Periderm (coniferous)
BE-9794.1.1	ZAB-12-4-3-2	75	77	732.5	11	Gas	2386 ± 328	1636-3325	2106-2218	Woody scale
BE-9503.1.1	ZAB-12-3-4-2	36	37	762	36	Gas	2273 ± 117	1998-2702	2297-2402	*Alnus* seed fragments
BE-9502.1.2	ZAB-12-3-4-2	85	86	811	87	Gas	2358 ± 84	2159-2715	2611-2703	Dicotyledonous leaf fragment[3]
BE-9502.1.1	ZAB-12-3-4-2	85	86	811	127	Gas	2379 ± 82	2183-2722	2611-2703	Dicotyledonous leaf fragment[3]
BE-9501.1.1	ZAB-12-3-4-2	85	86	811	21	Gas	2809 ± 201	2437-3447	2611-2703	Deciduous tree/shrub woody scales
BE-9500.1.1	ZAB-12-3-4-2	85	86	811	553	Graphite	2544 ± 41	2490-2754	2611-2703	Dicotyledonous leaf fragments, woody scales
BE-9497.1.1	ZAB-12-4-4-2	20	21	861	131	Graphite	2799 ± 67	2760-3076	2850-2929	*Pinus sylvestris* needle
BE-9498.1.1	ZAB-12-4-4-2	20	21	861	120	Graphite	2820 ± 72	2774-3143	2850-2929	Woody scale
BE-9496.1.1	ZAB-12-4-4-2	20	21	861	115	Graphite	2857 ± 73	2790-3174	2850-2929	*Pinus sylvestris* needle
BE-9499.1.1	ZAB-12-4-4-2	20	21	861	120	Graphite	2885 ± 72	2807-3229	2850-2929	Periderm (deciduous)
BE-9495.1.1	ZAB-12-4-4-2	61.5	62.5	902.5	21	Gas	3158 ± 252	2764-3984	3113-3187	Periderm, Dicotyledonous leaf fragments, woody scales
BE-9494.1.1	ZAB-12-4-4-2	61.5	62.5	902.5	54	Gas	2845 ± 96	2761-3215	3113-3187	Dicotyledonous leaf fragment
BE-9494.1.2	ZAB-12-4-4-2	61.5	62.5	902.5	50	Gas	2968 ± 99	2876-3374	3113-3187	Dicotyledonous leaf fragment
BE-9494.1.3	ZAB-12-4-4-2	61.5	62.5	902.5	52	Gas	2944 ± 97	2866-3358	3113-3187	Dicotyledonous leaf fragment
BE-9493.1.1	ZAB-12-4-4-2	61.5	62.5	902.5	230	Graphite	2980 ± 56	2979-3340	3113-3187	Dicotyledonous leaf fragments, periderm fragments

BE-9491.1.1	ZAB-12-4-4-2	100.5	101.5	941.5	37	Gas	3197 ± 119	3078-3700	3391-3462	Periderm
BE-9490.1.2	ZAB-12-4-4-2	100.5	101.5	941.5	123	Graphite	3296 ± 74	3375-3696	3391-3462	Dicotyledonous leaf fragments
BE-9490.1.1	ZAB-12-4-4-2	100.5	101.5	941.5	328	Graphite	3145 ± 51	3226-3466	3391-3462	Dicotyledonous leaf fragments
BE-9489.1.1	ZAB-12-3-5-2	44	45	1001.4	691	Graphite	3542 ± 45	3697-3965	3845-3915	Dicotyledonous leaf fragments
BE-9489.1.2	ZAB-12-3-5-2	44	45	1001.4	179	Graphite	3593 ± 62	3717-4084	3845-3915	Dicotyledonous leaf fragment[3]
BE-9489.1.4	ZAB-12-3-5-2	44	45	1001.4	222	Graphite	3603 ± 59	3724-4086	3845-3915	Dicotyledonous leaf fragment[3]
BE-9489.1.3	ZAB-12-3-5-2	44	45	1001.4	182	Graphite	3616 ± 62	3725-4141	3845-3915	Dicotyledonous leaf fragment[3]
BE-9489.1.5	ZAB-12-3-5-2	44	45	1001.4	124	Graphite	3631 ± 75	3721-4153	3845-3915	Dicotyledonous leaf fragment[3]
BE-9795.1.1	ZAB-12-4-5-1	24	26	1031.2	42	Gas	3724 ± 107	3829-4417	4084-4155	*Betula* seed fragments, terrestrial woody material, woody scale, periderm fragments
BE-9487.1.1	ZAB-12-4-5-1	25	26	1031.7	23	Gas	3856 ± 194	3731-4832	4084-4155	Leaf fragments
BE-9488.1.1	ZAB-12-4-5-1	25	26	1031.7	22	Gas	3856 ± 203	3725-4836	4084-4155	Wood fragment, Periderm fragments
BE-9485.1.1	ZAB-12-4-5-1	75	76	1081.7	60	Gas	4062 ± 97	4296-4837	4540-4616	Periderm, woody scales
BE-9486.1.1	ZAB-12-4-5-1	75	76	1081.7	46	Gas	4042 ± 105	4249-4832	4540-4616	*Betula alba* seed
BE-9484.1.1	ZAB-12-4-5-1	75	76	1081.7	266	Graphite	4065 ± 52	4421-4813	4540-4616	Periderm fragments
BE-9483.1.2	ZAB-12-4-5-1	118.5	119.5	1125.2	49	Gas	4387 ± 108	4655-5318	4960-5042	Periderm fragments
BE-9483.1.1	ZAB-12-4-5-1	118.5	119.5	1125.2	135	Gas	4475 ± 90	4860-5434	4960-5042	Periderm fragments
BE-9481.1.1	ZAB-12-5-6-1	54	55.5	1176.1	95	Gas	4850 ± 104	5321-5887	5500-5591	Woody seed fragments, leaf fragments, woody scales
BE-9482.1.1	ZAB-12-5-6-1	54	55.5	1176.1	22	Gas	5246 ± 232	5485-6536	5500-5591	Periderm fragments
BE-9480.1.1	ZAB-12-5-6-1	79	80	1200.8	35	Gas	5081 ± 228	5320-6315	5745-5832	Periderm fragments
BE-9479.1.1	ZAB-12-5-6-1	79	80	1200.8	42	Gas	5063 ± 127	5586-6178	5745-5832	Periderm, woody scale
BE-9478.1.1	ZAB-12-5-6-1	79	80	1200.8	111	Graphite	5197 ± 86	5745-6190	5745-5832	Periderm fragments and woody scales
BE-9476.1.1	ZAB-12-5-6-2	5	6	1242.5	49	Gas	5601 ± 125	6032-6718	6175-6267	Periderm and woody scale
BE-9475.1.1	ZAB-12-5-6-2	5	6	1242.5	72	Gas	5294 ± 107	5768-6300	6175-6267	Periderm
BE-9477.1.1	ZAB-12-5-6-2	5	6	1242.5	45	Gas	5410 ± 127	5920-6439	6175-6267	Periderm fragments

BE-9474.1.1	ZAB-12-5-6-2	5	6	1242.5	504	Graphite	5402 ± 43	6020-6294	6175-6267	*Pinus* periderm fragments
BE-9473.1.3	ZAB-12-5-6-2	45.5	46.5	1283	34	Gas	5988 ± 162	6479-7250	6531-6643	Dicotyledonous leaf fragments
BE-9473.1.2	ZAB-12-5-6-2	45.5	46.5	1283	55	Gas	5787 ± 119	6317-6880	6531-6643	Dicotyledonous leaf fragments
BE-9473.1.1	ZAB-12-5-6-2	45.5	46.5	1283	74	Gas	5868 ± 107	6415-6949	6531-6643	Dicotyledonous leaf fragments
BE-9473.1.4	ZAB-12-5-6-2	45.5	46.5	1283	38	Gas	5936 ± 150	6436-7165	6531-6643	Dicotyledonous leaf fragments
BE-9472.1.1	ZAB-12-5-6-2	45.5	46.5	1283	143	Graphite	5916 ± 78	6547-6946	6531-6643	Dicotyledonous leaf fragments, periderm fragment

[1] Ages calibrated using OxCal 4.3 with the IntCal13 calibration curve (Bronk Ramsey, 2009; Reimer et al., 2013). The range reported here represents the 95% confidence interval.

[2] Range represents 95% confidence interval.

[3] These samples were subsampled from a single fragment prior to analysis, thus samples within the same depth with this symbol have the same true age

3.3.2 Varve count and age-depth modeling

In total, 4644 (+155/- 176) varves were counted in the section of interest, with a mean varve thickness of 1.26 ± 0.58 mm (Fig. 3.4). Full varve count results are available at https://dx.doi.org/10.7892/boris.134606. Sedimentation rates averaged over 10 cm intervals range from 0.91 to 2.78 mm/year. All chronological data (^{14}C ages and varve counts) were integrated to generate a best-age estimate for the section of interest using an OxCal V-sequence (output of the Oxcal V-sequence is available at https://dx.doi.org/10.7892/boris.134606). This produced a well-constrained age-depth model with a 95% confidence interval (CI) width that ranges from 69 to 114 years (mean 86 years). OxCal uses an agreement index to assess how well the posterior distributions produced by the model (modelled ages at the depth of ^{14}C ages) agree with the prior distributions (calibrated ^{14}C ages). The overall agreement index for our OxCal V-sequence is 66.8%, which is greater than the acceptable index of 60%. Three of the fourteen dated levels in the V-sequence had agreement indices less than the acceptable value of 60% (A = 22.8, 48.5, 52.6% for sample depths = 1283.0, 1176.1, 732.5 cm, respectively), nonetheless we find the model fit acceptable as all 48 ^{14}C ages overlap with the median output of the V-sequence. We use the V-sequence as a best-age estimate for subsequent data comparisons and analyses. Alternative methods of linking the floating varve count with ^{14}C ages confirm that the ^{14}C ages are consistent with the varve count results. When the varve count is tied to the combined radiocarbon ages at the uppermost dated level (732.5 cm), we find that all other radiocarbon ages overlap with the varve count when considering the uncertainty of the varve count. If least squares minimization is used to minimize the offset between all radiocarbon ages and the varve count, we again find that all radiocarbon ages overlap with the master varve count (without considering varve count uncertainty). The result from the least squares minimization technique is highly similar to the OxCal V-sequence output.

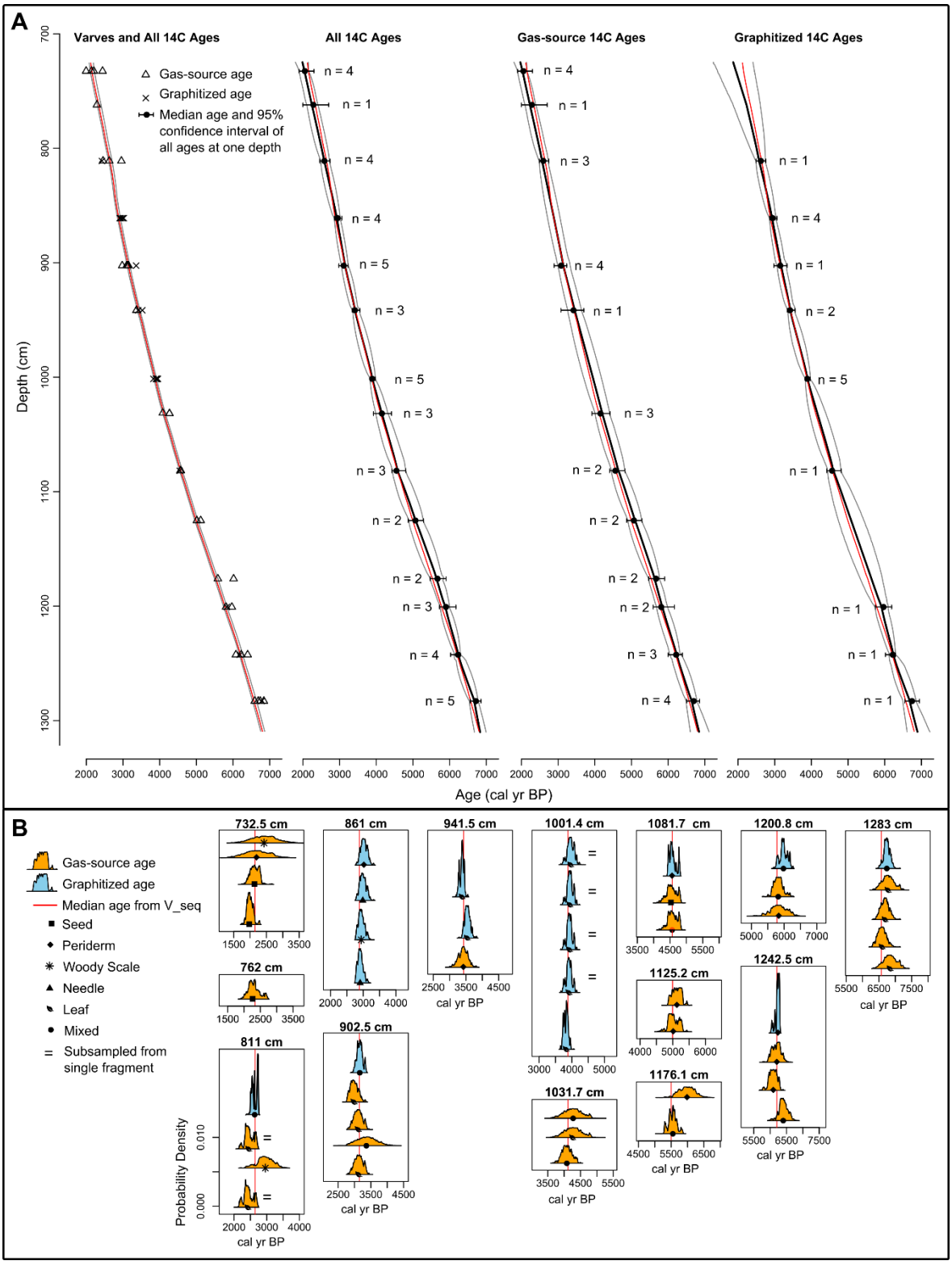

Figure 3.2: A) Comparison of age-depth model outputs from OxCal (Bronk Ramsey, 2008, 2009; Bronk Ramsey and Lee, 2013; Reimer et al., 2013). From left to right: OxCal V-sequence using all ^{14}C ages as well as varve counts as inputs; OxCal P-sequence using all ^{14}C ages as inputs; OxCal P-sequence using only gas-source ^{14}C ages; OxCal P-sequence using only graphitized ^{14}C ages. The median age of the V-sequence is considered the best-age estimate and is repeated in all four panels as a red line. Gray lines represent the upper and lower limits of the 95% confidence interval of each model. Black lines represent the median ages of the P-sequences. B) Radiocarbon calibrated age probability density functions for each measured age, grouped by composite depth. The best-age estimates from the OxCal V-sequence are plotted as red lines for comparison. The = symbol adjacent to some probability density functions indicates that these ages (within a single depth) came from the same specimen and have the same true age.

To test the reliability of gas-source ages versus graphitized ages we created three OxCal P-sequences using: 1) all ^{14}C ages, 2) only graphitized ages, and 3) only gas-source ages. The results of all three of these age-depth models agree well with the best-age estimate of the V-sequence, although with larger 95% CIs (Fig. 3.2). The agreement index was greater than the acceptable value of 60 for all three models overall, and for each dated depth within all three models. The P-sequence using all ^{14}C ages spans 4838 ± 235 years, which is slightly greater than, but overlapping with, the total number of varves counted (the V-sequence estimates 4681 ± 79 years in the section). There is no clear bias observed in the age-depth models produced using either the gas-source or graphitized samples. The P-sequence outputs clearly show that a very precise age can narrowly constrain the age-model uncertainty at the depth of that sample, however, if dating density is low, the uncertainty related to interpolation between ages becomes large. Despite the lower precision of the gas-source ages, the model based on only gas-source ages actually has a lower mean CI width than the model with graphitized ages (mean 95% CI width: 373 years for the gas-source model, 438 years for the graphitized model). However, a direct comparison between the gas-source-only and the graphitized-only age models is confounded by differences in the number and spacing of samples. Specifically, there are no graphitized ages between the top of the section (724 cm) and 811 cm, and between 1082 and 1200 cm, which results in wide CI in these sections. On the other hand, uncertainty is reduced compared to the gas-source model in the depths adjacent to the graphitized ages due to higher precision such that 40% of the section (in terms of depth) has lower age uncertainty in the graphitized model.

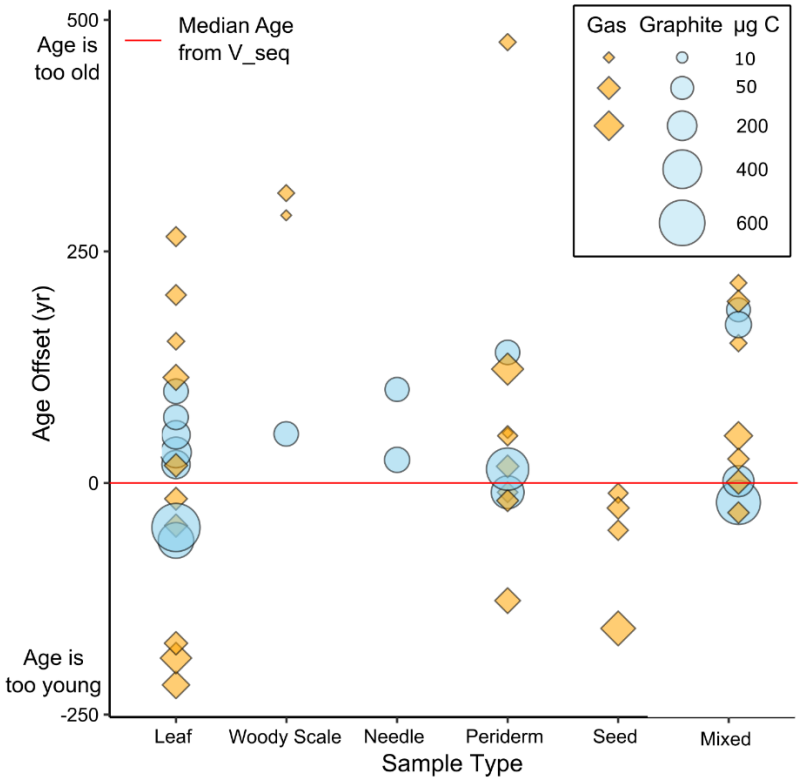

Figure 3.3: Offsets between median calibrated ^{14}C ages and the best age estimate from the OxCal V-sequence. Data are grouped by material type. Higher values indicate that the sample age is older than the best-age estimate.

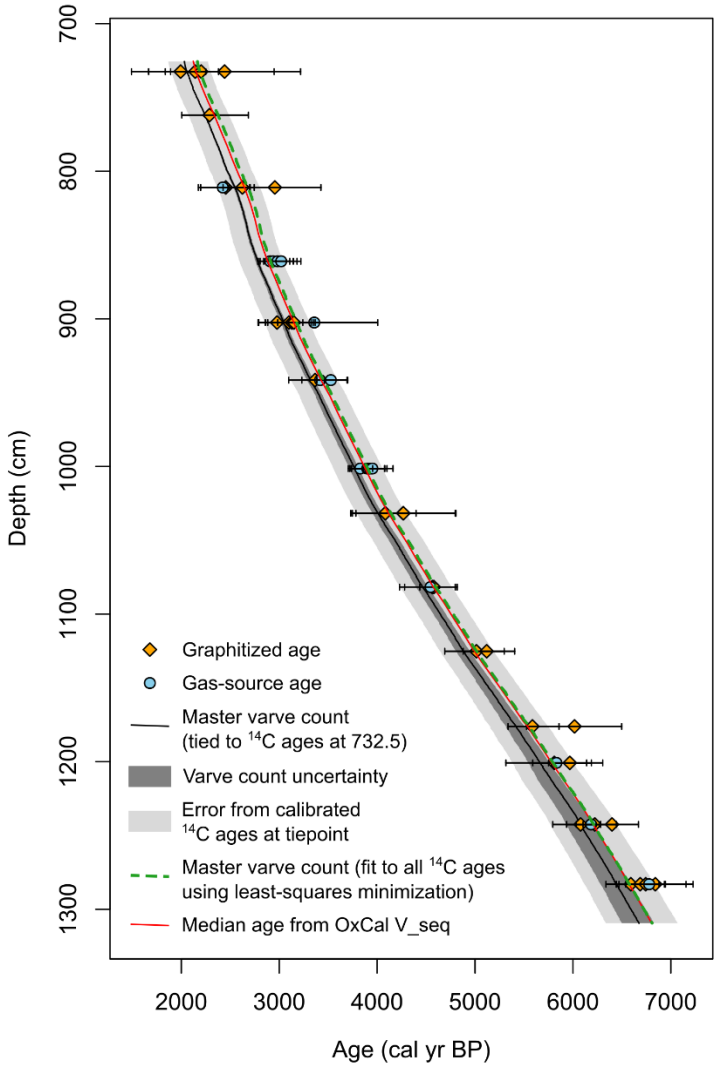

Figure 3.4: All radiocarbon ages and their 95% calibrated uncertainties plotted with the varve count results. The gray bands show the varve count tied to the combined calibrated age of the uppermost ^{14}C ages (at 732.5 cm) with dark grey representing the uncertainty calculated from the three replicated varve counts and light gray representing the uncertainty of the tie point. Dashed green is the varve count fit to the ^{14}C ages using least squares minimization of the offset between the varve age and the combined ^{14}C ages at each sampled depth.

3.3.3 Age-depth model simulations

Nine different sampling scenarios (described in Sect. 2.3) were simulated to test the effects of dating density and analytical precision on age-depth model confidence intervals. For each of the nine scenarios, sets of ^{14}C ages were simulated 30 times to create an ensemble of age-depth models for each scenario. One set of these simulated age-depth models is shown in Fig. 3.5, and an animation of the full set of simulated models is available online (Supplementary File 3). The age-depth models were evaluated for their precision (mean width of the 95% CI) and accuracy (the mean absolute deviation from the best-age estimate; summarized in Fig. 3.6 and Table 3.2). As expected, we find that increased dating density and increased sample masses improve both the accuracy and precision of the age-depth models. It is notable that increasing the number of ages can compensate for the greater uncertainty associated with smaller sample sizes. For instance, the mean CI of age-depth models based on ten, 90 µg C samples is narrower than age-depth models with five, 500 µg C samples (Table

3.2). However, the effect of analytical precision is greater on the mean absolute deviation from the best-age estimate. Increased dating density does tend to reduce the deviation from the best-age estimate (especially if the ages are imprecise), but the three scenarios that use 500 µg samples perform better than all other scenarios, in terms of deviation from the best-age estimate, regardless of the sampling density. Additionally, increased dating density does not improve the deviation from the best-age estimate for the 500 µg sample scenarios. This result may be due to the relatively constant sedimentation rates in our sedimentary sequence, which reduces errors caused by interpolation in scenarios with low dating density. Another prominent pattern in the simulations is the large spread of performance for models with relatively few and imprecise ages (Fig. 3.6). Increasing the number of samples and, especially, the mass of samples has a large impact on the agreement among the different iterations of each scenario.

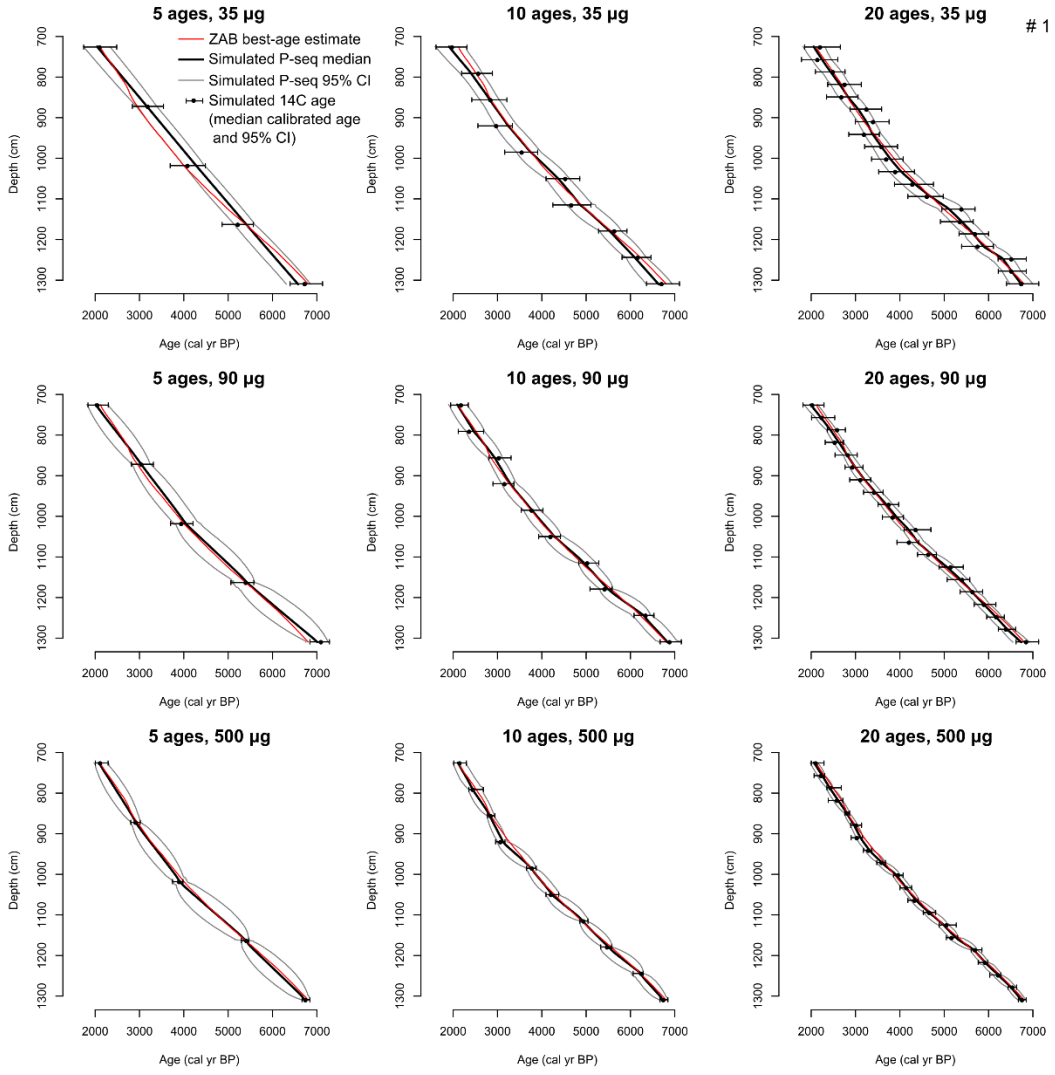

Figure 3.5: Results of age-model simulations to test the effects of sampling density and sample mass on age-model results. Each panel shows the output of an OxCal P-sequence using simulated ^{14}C ages as inputs compared with the best-age estimate from the V-sequence (shown in red). Simulated ^{14}C ages are based on the decalibrated best-age estimate of a given depth and the expected uncertainty associated with the mass C in the simulated ^{14}C age, which defines not only the age uncertainty, but also a random error term added to each simulated age. Plots show one ensemble member out of 30 simulations. An animation of all 30 simulations can be found in Supplementary File 3.3.

An additional measure of age-model quality is the Chron Score rating system (Sundqvist et al., 2014), which does not assess age-depth model fit, rather it assesses the quality of inputs used to generate an age-depth model. Thus the Chron Score provides an assessment of the 9 sampling scenarios that is independent of the choice of age-depth modelling software, or parameter selection during age-depth model construction. The Chron Score is calculated from three criteria used to assess the reliability of core chronologies: 1) delineation of downcore trend (D), 2) quality of dated materials (Q), and 3) precision of calibrated ages (P). These metrics are combined using a reproducible formula to provide a Chron Score (G) in which higher values represent more reliable chronologies:

$$G = -w_D D + w_Q Q + w_P P$$

We used the default weighting parameters (w_D, w_Q, and w_P = 0.001, 1 and 200) for each component of the Chron Score formula as described in Sundqvist et al. (2014). The quality (Q) parameter depends on two factors - the proportion of ages which are not rejected or reversed (i.e. an older age stratigraphically above a younger age), and a qualitative classification scheme for material types. We modified the threshold for determining if an age is considered a reversal such that if a ^{14}C age is older than a stratigraphically higher age by more than the age uncertainty (1σ), the age is considered to be stratigraphically reversed. This is different from the default setting, which is 100 years. For the material type classification (m), the simulated age models were assigned the value 4, which is the value assigned to chronologies based on terrestrial macrofossils. For more details on the Chron Score calculation see Sundqvist et al. (2014). The mean Chron Scores for the simulated age models (Table 3.2) show that doubling dating density substantially improves the Chron Score, but the effect is greater when moving from 5 to 10 ages than from 10 to 20 ages. The effect of increased precision on the Chron Score is also substantial; it is essentially defined by the Chron Score formula, in which precision is assessed as $P = s^{-1}$ where s is the mean 95% range of all calibrated ^{14}C ages. The effect of precision on the Chron Score is also determined by the weighting factors mentioned above.

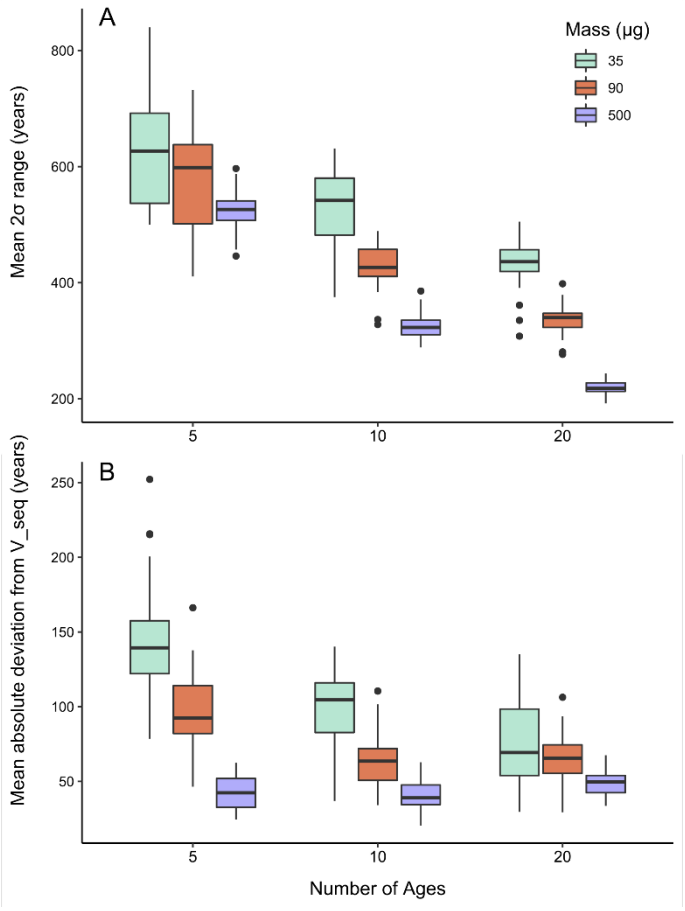

Figure 3.6: A) Boxplots showing the distribution of the mean 95% confidence interval widths produced by simulated age-depth models. Results are grouped by dating density along the x-axis, and by sample mass (smaller mass = greater uncertainty) using different colors. Each boxplot represents the distribution of results produced for 30 unique sets of simulated ^{14}C samples. Data points that are greater (less) than the 75th (25th) percentile plus (minus) 1.5 times the interquartile range are plotted as single points beyond the extent of the whiskers. B) Same as A, but showing the mean absolute deviation from the best-age estimate (median output of OxCal V-sequence).

3.4 Discussion

3.4.1 Radiocarbon measurements

The results of our ^{14}C measurements from repeated sampling of single stratigraphic levels provide useful information for other researchers working with miniature ^{14}C analyses, or any ^{14}C samples from lake sediments. We show that there is an exponential relationship between sample mass and the resulting analytical uncertainty (Fig. 3.1). We use the relationship shown in Fig. 3.1A to define the age uncertainty of our simulated ages, however it is important to note that this relationship is only valid for samples with a similar age to the samples in this study (approx. 2000-7000 cal yr BP). Older samples will yield greater age uncertainty for the same mass of C due to fewer ^{14}C isotopes (Gottschalk et al., 2018). The measurement uncertainty in F^{14}C units is not affected by age (Fig. 3.1B). The exact parameters of these relationships will also depend on laboratory conditions, however, the general shape of the relationship is valid. These data can inform researchers about the expected range of uncertainty for ^{14}C ages from samples of a given size. We find that samples larger than 40 µg C yield

ages that are precise enough to be useful for dating Holocene lake sediments in most applications, and even smaller samples can provide useful ages if no other material is available.

It is well documented that ^{14}C ages can be susceptible to sources of error that are not included within the analytical uncertainty of the measurements. Such errors can be due to lab contamination, sample material which is subject to reservoir effects (i.e. bulk sediments or aquatic organic matter; Groot et al., 2014; MacDonald et al., 1991; Tornqvist et al., 1992), or from depositional lags (terrestrial organic material which is older than the sediments surrounding it; Bonk et al., 2015; Howarth et al., 2013; Krawiec et al., 2013). Errors related to reservoir effects can be avoided by selecting only terrestrial plant material for dating (Oswald et al., 2005). Floating or shoreline vegetation should also be avoided as these plants may uptake CO_2 released by lake degassing (Hatté and Jull, 2015). Dating fragile material such as leaves (as opposed to wood) may reduce the chances of dating reworked material with a depositional lag, but generally this source of error is challenging to predict and depends on the characteristics of each lake's depositional system. To identify ages affected by depositional lags, it is necessary to compare with other age information. Consequently, the identification of outlying ages is facilitated by increased dating density.

In our dataset, multiple ^{14}C measurements were performed on material taken from a single layer, which enables outlier detection. We find that the scatter of ^{14}C ages obtained from the same depths is generally consistent with what would be expected based on the analytical uncertainties of the ages. There are no clear outliers in the data; every single ^{14}C age has a calibrated 95% CI that overlaps with the median of our best-age estimate OxCal V-sequence (and this result is confirmed by alternative methods of linking the varve count to ^{14}C ages). This agreement between the varve count and the ^{14}C ages is evidence that no age in this dataset is incongruent with the other available chronological information (other ^{14}C ages and varve counts). This notion is further demonstrated by the fact that 10 of 11 sampled levels from which we obtained three or more ages returned an MSWD within the 95% confidence threshold for testing age scatter (see Sect. 3.1; Reiners et al., 2017). This test is typically used for repeated measurements on the same sample material, however, in our study, many of the measurements from within a single sediment slice are from material that has different true ages. The MSWD test indicates that the variability in ages among samples from within a single sediment slice can reasonably be expected given the analytical uncertainty. However, in this study, no more than five samples were measured per depth, and thus the range of acceptable values for the MSWD is relatively wide due to the small number of degrees of freedom. Additionally, the analytical uncertainties are relatively large for the gas-source samples, allowing for wide scatter in the data without exceeding the MSWD critical value. Despite these caveats, the consistency between the variability among ages from one level and the analytical uncertainties allows us to make two important conclusions. 1) The analytical precision estimates are reasonable, even for miniature gas-source samples. 2) When material is carefully selected and taxonomically identified for dating, the sources of error that are not considered in the analytical uncertainty (e.g. contamination or depositional lags) are relatively minor in our case study. However, this second conclusion is highly dependent on the sediment transport and depositional processes, which are site specific. Depositional lags still likely have some impact on our chronology. Six ^{14}C ages from plant material collected from the Lake Żabińskie catchment in 2015

yielded a range of ages from 1978-2014 CE (Bonk et al., 2015) suggesting that the assumption that ^{14}C ages represent the age of the sediments surrounding macrofossils is often invalid. The scale of these age offsets is likely on the scale of a few decades for Lake Żabińskie sediments, which is inconsequential for many radiocarbon-based chronologies, but is the same order of magnitude as the uncertainty of our best-age estimate from the OxCal V-sequence, and should be considered when reporting or interpreting radiocarbon-based age determinations with very high precision.

The lack of outliers in our dataset is an apparent contrast with the findings of Bonk et al. (2015), who report that 17 of 32 radiocarbon samples taken from the uppermost 1000 years of the Lake Żabińskie core were outliers. The outlying ages were older than expected based on the varve chronology, and this offset was attributed to reworking of terrestrial plant material. The identification of outliers did not take into account uncertainties of the radiocarbon calibration curve and varve counts, which could explain some of the differences between the ^{14}C and the varve ages. Still, 8 of 32 ages reported by Bonk et al. (2015) have calibrated 2σ age ranges that do not overlap with varve count age (including the varve count uncertainty). The higher outlier frequency in the Bonk et al. (2015) data might be explained by their generally more precise ages and the fact that their varve count is truly independent from the ^{14}C ages.

Additionally, our dataset allows us to compare the results of ^{14}C ages obtained from different types of macrofossil materials, which we grouped into the following categories: leaves (including associated twigs), needles, seeds, periderm, woody scales, and samples containing mixed material types (Fig. 3.3). When comparing the calibrated median age of each sample to the median of our best-age estimate, we find that the difference between the age offsets of the different material types is not significant at the $\alpha = 0.05$ level (ANOVA, $F = 2.127$, $p = 0.08$). This is likely due to our selective screening of sample material, which only includes terrestrial plant material while avoiding aquatic insect remains or possible aquatic plant material, as well as the relatively small number of samples within each material type. There does appear to be a tendency for seeds to produce younger ages, and two of the three woody scale samples yielded ages that are approximately 300 years older than the best-age estimate. This could be due to the superior durability of woody materials compared with other macrofossil materials, which enables wood to be stored on the landscape prior to being deposited in the lake sediments. A larger number of samples would allow for more robust conclusions about the likelihood of certain material types to produce biased ages.

3.4.2 The OxCal V-sequence best-age estimate

In this study we have tested multiple approaches to assigning absolute ages from ^{14}C ages to a floating varve count (Fig. 3.4). Using a single tie-point relies on a potentially arbitrary selection of tie-point location and yields large uncertainty intervals when considering both the varve count uncertainty and the uncertainty of calibrated ages. Using least squares minimization of the offset between all radiocarbon ages and the varve count has the advantage of using all the ^{14}C ages rather than one tie-point, however this approach does not consider varve count uncertainties and does not directly yield an estimate of uncertainty derived from the radiocarbon age uncertainties. The OxCal V-sequence is unique in that all age information is integrated into a statistical framework including the probability

functions of ^{14}C ages and the uncertainty associated with the varve count as well. In contrast to the other two approaches, the V-sequence can change the total number of years in the sequence compared to the original varve count. However, the addition of 37 years in the V-sequence is well within the uncertainty of the varve count (+155/- 176). The V-sequence approach is expected to provide more precise and more reliable age estimates than either varve counting or radiocarbon-based age models alone. The resulting age-depth relation has a relatively narrow CI (mean 95% CI is 86 yr). Extremely precise age estimates were also produced using this method for Moossee, Switzerland by Rey et al. (2019). A combination of varve counts and ^{14}C ages from the Moossee sediments generated a V-sequence output with a mean 95% CI of 38 years. The higher precision in the Moossee study compared to our V-sequence output is primarily attributed to the higher dating density in Moosse with 27 radiocarbon ages over ~3000 years (3.9-7.1 ka) versus our study, which used 48 ages, but from only 14 unique depths, over ~4700 years. This comparison shows that repeated measurements from the same depth are less useful than analyses from additional depths. This approach to integrating varve counts and ^{14}C ages could potentially be improved by a better integration of varve count uncertainties into the OxCal program. Currently the uncertainties on age 'Gaps' in OxCal are assumed to be normally distributed and cannot be less than 5 years. Nevertheless, the result of the OxCal V-sequence is an age-depth model that is much more precise than those constructed only using ^{14}C ages and provides a useful reference to compare with the ^{14}C ages. It is important to note that the best-age estimate is not independent of the ^{14}C ages; it is directly informed by the ^{14}C ages.

3.4.3 Age-depth model simulations

The simulated age-depth modelling experiment allows us to assess the effects of dating density and sample mass (expected precision) on the outputs of age-depth models constructed for the section of interest in the Lake Żabińskie sediment core. Models based on relatively few, but very precise ages, are tightly constrained at the sample depths, but the CI widens further away from these depths (Fig. 3.5, Supplementary File 3). In contrast, models based on a greater sampling density produce confidence intervals with relatively constant width. If models are built using a high density of imprecise ages, the CI of the model output can actually be narrower than the CI of the individual ages. Bayesian age-depth models in particular can take advantage of the stratigraphic order of samples to constrain age-depth models to be more precise than the individual ages that make up the model (Blaauw et al., 2018), however this is only achievable when dating density is high enough. The results from this experiment suggest that, in the case of the Lake Żabińskie sequence, doubling the number of ages can approximately compensate for an increased analytical uncertainty of 50 years.

The choice of OxCal to produce age-depth models from these hypothetical sampling scenarios may have some influence on the results, however we expect that the key findings are replicable for any Bayesian age-depth model routine (i.e. Bacon or Bchron; Blaauw and Christen, 2011; Haslett and Parnell, 2008). To demonstrate this, we used Bacon (Blaauw and Christen, 2011, 2018) to generate age-depth models for one iteration of the simulated sampling scenarios, and compared the results to those generated by OxCal. We find that the Bacon-generated models are highly similar to the OxCal

models, and the patterns observed in terms of model precision and accuracy are reasonable similar to those obtained from Oxcal models. The Bacon results can be found in Supplementary File 4.

Table 3.2: Table summarizing the effect of dating density (number of ages) and analytical precision (sample mass) on the accuracy, precision and reliability of OxCal P-sequence models generated from simulated ^{14}C ages. Each of the nine scenarios was simulated 30 times; presented values are the mean of the 30-member ensemble. Precision is assessed by the mean width of the age-depth model 95% confidence interval. Accuracy is measured by the mean absolute deviation from the OxCal V-sequence best-age estimate, which is the reference from which ^{14}C ages were simulated. Chron Score is a metric designed to assessing the reliability of age-depth models where higher numbers represent greater reliability (Sundqvist et al., 2014).

			Number of ages in model		
Sample Mass (µg)	**Expected Uncertainty (yr)[1]**	**Expected Uncertainty ($F^{14}C$)**	**5 ages (1.07 per kyr)**	**10 ages (2.14 per kyr)**	**20 ages (4.27 per kyr)**
			Mean 95% CI width (yr)		
35	**± 148**	**± 0.011**	633	527	433
90	**± 92**	**± 0.007**	577	430	335
500	**± 39**	**± 0.003**	524	325	219
			Mean absolute deviation from OxCal V-sequence (yr)		
35	**± 148**	**± 0.011**	144	99	78
90	**± 92**	**± 0.007**	98	64	65
500	**± 39**	**± 0.003**	42	40	49
			Chron Score		
35	**± 148**	**± 0.011**	2.46	3.14	3.48
90	**± 92**	**± 0.007**	2.87	3.64	4.09
500	**± 39**	**± 0.003**	3.92	4.74	5.18

[1] Expected age uncertainty for an approximately 4000-year-old sample used to inform age-depth model simulations

The Chron Score results provide a succinct summary of the reliability of the chronologies produced in the different simulated sampling scenarios and is independent of model selection. The Chron Score becomes more sensitive to changes in precision as precision increases, so the difference in the Chron Scores between the 500 µg and 90 µg scenarios (1σ uncertainty of ± 39 and 92 years, respectively) is greater than the difference between the 90 µg and 35 µg scenarios (1σ uncertainty of ± 92 and 148 years, respectively). Increased dating density consistently improves the Chron Score results, with a stronger impact seen when shifting from 5 to 10 ages compared to shifting from 10 to 20 ages. The improvement of the Chron Score due to increased dating density is generally consistent for each of the different sample mass scenarios. This differs from the age-depth model statistics where increased dating density has a greater impact on precision in the larger sample mass scenarios (more precise ages). The opposite effect is seen in the mean absolute deviation results, where mean absolute deviation is reduced substantially as dating density increases for the smaller sample scenarios, and not at all for the 500 µg scenario. For all measures of chronologic performance, we find a greater improvement when increasing the number of ages from 5 to 10 ages compared to increasing from 10

to 20 ages, suggesting there are some diminishing returns from increased dating density. This result is in accordance with the results of Blaauw et al. (2018). While the Chron Score results are dependent on the parameters chosen for the calculation, they intuitively make sense. Because Chron Score results use only the simulated ^{14}C ages as input and are unaffected by the age modelling routine, the patterns exhibited in the scores may be more applicable to a variety of sedimentary records.

In real-world applications, there are additional advantages from increasing dating density. Many lacustrine sequences have greater variability in sedimentation rates than the sequence modelled here. More fluctuations in sedimentation rate require a greater number of ages to delineate the changes in sedimentation. Additionally, outlying ages and age scatter beyond analytical uncertainty are not considered in this modelling experiment. In most cases, detecting outlying ages becomes easier as dating density increases. Because this experiment is only applied to a single sedimentary sequence, the results may not be directly applicable for other sedimentary records with different depositional conditions. In the future, this type of age model simulation could be applied to a range of sedimentary sequences with a variety of depositional conditions.

3.4.4 Recommendations for radiocarbon sampling strategy

Radiocarbon sampling strategies will always be highly dependent on project-specific considerations such as how the chronology will affect the scientific goals of the project, budget and labor constraints, the nature of the sedimentary record in question, and the availability of suitable materials. A goal of this study is to provide data that can inform sampling strategies for building robust chronologies, particularly in cases where suitable material may be limited. Firstly, an iterative approach to ^{14}C measurements is preferred. An initial batch of measurements should target a low dating density of perhaps one date per 2000 years. Subsequent samples should aim to fill in gaps where age uncertainty remains highest (Blaauw et al., 2018), or where preliminary age-depth trends appear to be non-linear. In accordance with many previous studies (e.g. Howarth et al., 2013; Oswald et al., 2005), we advocate for careful selection of material identified as terrestrial in origin. If the mass of such material is limited, the MICADAS gas-source is useful for dating miniature samples, and we are convinced that miniature samples of terrestrial material are preferable to dating questionable material or bulk sediments. Samples as small as a few µg C can be measured using the MICADAS, though samples larger than 40 µg C are recommended for more precise results (mid to late Holocene samples containing 40 µg C are expected to have analytical uncertainty of ~138 years). Dating small amounts of material from single depths is also preferable to pooling material from depth segments that may represent long time intervals. A general rule of thumb is to avoid taking samples with depth intervals representing more time than the expected uncertainty of a ^{14}C age. To improve the accuracy of age-depth models, a higher priority should be placed on achieving sufficiently high dating density (ideally greater than one age per 500 years; Blaauw et al., 2018) using narrow sample-depth intervals. In most cases, this goal should be prioritized over the goal of gathering larger sample masses in order to reduce analytical uncertainties. The results of this study and others (e.g. Blaauw et al., 2018; Trachsel and Telford, 2017) clearly indicate that increased sampling density improves the accuracy, precision and reliability of age-depth models.

Multiple measurements from within a single stratigraphic depth, as we have done in this study, can be useful in sediments where age scatter (possibly from reworked material) is expected. In such cases, multiple measurements from a single depth could allow for identification of certain types of material that should be avoided. If age scatter is not expected, single measures of pooled macrofossils are more cost-effective than repeat measurements from a single depth.

Although increased dating density does incur greater cost, gas-source ages have lower costs compared to graphitized ages allowing for greater dating density at similar cost. Injecting CO_2 into the AMS rather than generating graphite and packing a target substantially reduces the effort to analyze a sample following pre-treatment, and additionally reduces some chance of contamination during graphitization. These advantages are partly offset by additional operator attention required during gas source measurements. How these differences translate to per-sample costs depends on the pricing structures implemented in each lab. Cost estimates from two MICADAS labs at the University of Bern and Northern Arizona University range between approximately 15 and 33% lower costs for gas-source measurements compared to graphitized samples. Use of smaller samples can also reduce the labor time required to isolate suitable material from the sediment, however handling and cleaning miniature samples can add additional challenges which increases labor time.

3.5 Conclusions

- AMS ^{14}C analysis of Holocene terrestrial plant macrofossils using the MICADAS gas-ion source produces unbiased ages with similar precision compared to graphitized samples that contain similar mass of carbon (approximately 120-160 µg C).
- The precision of a ^{14}C age can be approximately estimated based on the amount of carbon within a sample. Holocene samples containing greater than 40 µg C produce ^{14}C measurements with analytical uncertainty expected to be less than ± 0.01 $F^{14}C$ (150 years for samples than are approximately 4000 years old). Uncertainty increases exponentially as samples get smaller so 10 µg C samples are expected to have uncertainty of ± 0.021 $F^{14}C$ (277 years).
- The variability among ages obtained from 1- or 2-cm-thick samples in the Lake Żabińskie sediment core is compatible with the variability expected due to analytical uncertainty alone.
- We find no clear evidence in our dataset for age bias based on the type of macrofossil material dated, which we limited to terrestrial plant material.
- Judging from the output of age-depth models, the lower precision of miniature gas-source ages can be compensated for by increasing sampling density. Based on sets of simulated ^{14}C ages that mimic the ^{14}C ages of our study core, together with age-depth models generated using OxCal, doubling dating density roughly compensates for a decrease in analytical precision of 50 years.
- The effect of ^{14}C age precision is among several factors that influence chronological precision. The thickness of the depth interval used to obtain samples, the ability to select identifiable terrestrial materials or to analyze more than one type of material, the reliability of detecting age outliers, and the amount of variability in sedimentation rate all determine the accuracy and precision of an age-depth model, which are both improved by increasing the number of ages.

- This study can inform sampling strategies and provide expectations about radiocarbon-based age-depth model outcomes.

3.6 Acknowledgements

Core materials were supplied by Wojciech Tylmann, University of Gdańsk. Edith Vogel and Gary Salazar assisted with ^{14}C sample measurements. This project was funded by Swiss National Science Foundation grants 200021_172586 and IZSEZO-180887 and by the Polish National Science Centre grant 2014/13/B/ST10/01311.

Data availability

The key datasets associated with this manuscript (Varve count results and the best-age estimate OxCal V-sequence output) are available at the Bern Open Repository and Information System, https://dx.doi.org/10.7892/boris.134606

3.7 References

Blaauw, M., Christen, J.A., 2018. rbacon: Age-Depth Modelling using Bayesian Statistics. R package version 2.3.4. https://CRAN.R-project.org/package=rbacon 1-14.

Blaauw, M., Christen, J.A., 2011. Flexible paleoclimate age-depth models using an autoregressive gamma process. Bayesian Anal. 6, 457-474. https://doi.org/10.1214/11-BA618

Blaauw, M., Christen, J.A., Bennett, K.D., Reimer, P.J., 2018. Double the dates and go for Bayes — Impacts of model choice, dating density and quality on chronologies. Quat. Sci. Rev. 188, 58-66. https://doi.org/10.1016/j.quascirev.2018.03.032

Bonk, A., Tylmann, W., Amann, B., Enters, D., Grosjean, M., 2015a. Modern limnology and varve-formation processes in lake Żabińskie, northeastern Poland: Comprehensive process studies as a key to understand the sediment record. J. Limnol. 74, 358-370. https://doi.org/10.4081/jlimnol.2014.1117

Bonk, A., Tylmann, W., Goslar, T., Wacnik, A., Grosjean, M., 2015b. Comparing varve counting and ^{14}C-Ams chronologies in the sediments of Lake Żabińskie, Northeastern Poland: Implications for accurate ^{14}C dating of lake sediments. Geochronometria 42, 157-171. https://doi.org/10.1515/geochr-2015-0019

Bronk Ramsey, C., 2009. Bayesian Analysis of Radiocarbon Dates. Radiocarbon 51, 337-360. https://doi.org/10.1017/s0033822200033865

Bronk Ramsey, C., 2008. Deposition models for chronological records. Quat. Sci. Rev. 27, 42-60. https://doi.org/10.1016/j.quascirev.2007.01.019

Bronk Ramsey, C., Lee, S., 2013. Recent and Planned Developments of the Program OxCal. Radiocarbon 55, 720-730. https://doi.org/10.1017/s0033822200057878

Butz, C., Grosjean, M., Fischer, D., Wunderle, S., Tylmann, W., Rein, B., 2015. Hyperspectral imaging spectroscopy: a promising method for the biogeochemical analysis of lake sediments. J. Appl. Remote Sens. 9, 096031. https://doi.org/10.1117/1.jrs.9.096031

Delqué-Količ, E., Comby-Zerbino, C., Ferkane, S., et al., 2013. Preparing and measuring ultra-small radiocarbon samples with the ARTEMIS AMS facility in Saclay, France, in: Nuclear Instruments and Methods in Physics Research, Section B: Beam Interactions with Materials and Atoms. https://doi.org/10.1016/j.nimb.2012.08.048

Freeman, E., Skinner, L.C., Reimer, R., Scrivner, A., Fallon, S., 2016. Graphitization of small carbonate samples for paleoceanographic research at the godwin radiocarbon laboratory, University of Cambridge. Radiocarbon 58, 89-97. https://doi.org/10.1017/RDC.2015.8

Gottschalk, J., Szidat, S., Michel, E., Mazaud, A., Salazar, G., Battaglia, M., Lippold, J., Jaccard, S.L., 2018. Radiocarbon Measurements of Small-Size Foraminiferal Samples with the Mini Carbon Dating System (MICADAS) at the University of Bern: Implications for Paleoclimate Reconstructions. Radiocarbon 60, 469-491. https://doi.org/10.1017/RDC.2018.3

Groot, M.H.M., van der Plicht, J., Hooghiemstra, H., Lourens, L.J., Rowe, H.D., 2014. Age modelling for Pleistocene lake sediments: A comparison of methods from the Andean Fúquene Basin (Colombia) case study. Quat. Geochronol. 22, 144-154. https://doi.org/10.1016/j.quageo.2014.01.002

Hajdas, I., Bonani, G., Goslar, T., 1995. Radiocarbon dating the Holocene in the Gosciaz Lake floating varve chronology. Radiocarbon 37, 71-74. https://doi.org/10.1017/S0033822200014806

Haslett, J., Parnell, A., 2008. A simple monotone process with application to radiocarbon-dated depth chronologies. J. R. Stat. Soc. Ser. C Appl. Stat. 57, 399-418. https://doi.org/10.1111/j.1467-9876.2008.00623.x

Hatté, C., Jull, A.J.T., 2015. ^{14}C in Plant Macrofossils, in: Rink, J.W., Thompson, J.W. (Eds.), Encyclopedia of Scientific Dating Methods. Springer Science and Business Media, Dordrecht, pp. 1-79. https://doi.org/10.1007/978-94-007-6304-3

Howarth, J.D., Fitzsimons, S.J., Jacobsen, G.E., Vandergoes, M.J., Norris, R.J., 2013. Identifying a reliable target fraction for radiocarbon dating sedimentary records from lakes. Quat. Geochronol. https://doi.org/10.1016/j.quageo.2013.02.001

Krawiec, A.C.L., Kaufman, D.S., Vaillencourt, D.A., 2013. Age models and tephrostratigraphy from two lakes on Adak Island, Alaska. Quat. Geochronol. https://doi.org/10.1016/j.quageo.2013.07.002

Larsson, L., 2003. COORECORDER v2. 3.13: Image Co-ordinate Recording Program.

MacDonald, G.M., Beukens, R.P., Kieser, W.E., 1991. Radiocarbon Dating of Limnic Sediments: A Comparative Analysis and Discussion. Ecology 72, 1150-1155. https://doi.org/10.2307/1940612

Oswald, W.W., Anderson, P.M., Brown, T.A., Brubaker, L.B., Feng, S.H., Lozhkin, A. V., Tinner, W., Kaltenrieder, P., 2005. Effects of sample mass and macrofossil type on radiocarbon dating of

arctic and boreal lake sediments. Holocene 15, 758-767. https://doi.org/10.1191/0959683605hl849rr

Reimer, P.J., Bard, E., Bayliss, A., et al., 2013. IntCal13 and Marine13 Radiocarbon Age Calibration Curves 0-50,000 Years cal BP. Radiocarbon 55, 1869-1887. https://doi.org/10.2458/azu_js_rc.55.16947

Reiners, P.W., Carlson, R.W., Renne, P.R., Cooper, K.M., Granger, D.E., McLean, N.M., Schoene, B., 2017. Geochronology and thermochronology, Geochronology and Thermochronology. Wiley Blackwell. https://doi.org/10.1002/9781118455876

Rey, F., Gobet, E., Szidat, S., Lotter, A.F., Gilli, A., Hafner, A., Tinner, W., 2019. Radiocarbon wiggle matching on laminated sediments delivers high-precision chronologies. Radiocarbon 61, 265-285. https://doi.org/10.1017/RDC.2018.47

Ruff, M., Fahrni, S., Gäggeler, H.W., Hajdas, I., Suter, M., Synal, H.A., Szidat, S., Wacker, L., 2010a. On-line radiocarbon measurements of small samples using elemental analyzer and MICADAS gas ion source. Radiocarbon 52, 1645-1656. https://doi.org/10.1017/S003382220005637X

Ruff, M., Szidat, S., Gäggeler, H.W., Suter, M., Synal, H.A., Wacker, L., 2010b. Gaseous radiocarbon measurements of small samples. Nucl. Instruments Methods Phys. Res. Sect. B Beam Interact. with Mater. Atoms 268, 790-794. https://doi.org/10.1016/j.nimb.2009.10.032

Ruff, M., Wacker, L., Gäggeler, H.W., Suter, M., Synal, H.A., Szidat, S., 2007. A gas ion source for radiocarbon measurements at 200 kv. Radiocarbon 49, 307-314. https://doi.org/10.1017/S0033822200042235

Salazar, G., Zhang, Y.L., Agrios, K., Szidat, S., 2015. Development of a method for fast and automatic radiocarbon measurement of aerosol samples by online coupling of an elemental analyzer with a MICADAS AMS. Nucl. Instruments Methods Phys. Res. Sect. B Beam Interact. with Mater. Atoms 361, 163-167. https://doi.org/10.1016/j.nimb.2015.03.051

Santos, G.M., Southon, J.R., Griffin, S., Beaupre, S.R., Druffel, E.R.M., 2007. Ultra small-mass AMS ^{14}C sample preparation and analyses at KCCAMS/UCI Facility. Nucl. Instruments Methods Phys. Res. Sect. B Beam Interact. with Mater. Atoms. https://doi.org/10.1016/j.nimb.2007.01.172

Shah Walter, S.R., Gagnon, A.R., Roberts, M.L., McNichol, A.P., Gaylord, M.C.L., Klein, E., 2015. Ultra-Small Graphitization Reactors for Ultra-Microscale ^{14}C Analysis at the National Ocean Sciences Accelerator Mass Spectrometry (NOSAMS) Facility. Radiocarbon 57, 109-122. https://doi.org/10.2458/azu_rc.57.18118

Sundqvist, H.S., Kaufman, D.S., McKay, N.P., et al., 2014. Arctic Holocene proxy climate database - New approaches to assessing geochronological accuracy and encoding climate variables. Clim. Past 10, 1605-1631. https://doi.org/10.5194/cp-10-1605-2014

Synal, H.A., Stocker, M., Suter, M., 2007. MICADAS: A new compact radiocarbon AMS system. Nucl. Instruments Methods Phys. Res. Sect. B Beam Interact. with Mater. Atoms 259, 7-13. https://doi.org/10.1016/j.nimb.2007.01.138

Szidat, S., Salazar, G.A., Vogel, E., Battaglia, M., Wacker, L., Synal, H.-A., Türler, A., 2014. ^{14}C analysis and sample preparation at the new Bern Laboratory for the Analysis of Radiocarbon with AMS (LARA). Radiocarbon 56, 561-566. https://doi.org/10.2458/56.17457

Szumański, A., 2000. Objaśnienia do Szczegółowej Mapy Geologicznej Polski, Arkusz Giżycko, (Explanation to the Detailed Geological Map of Poland, Sheet Gizycko (104)). Warsaw, Poland.

Tornqvist, T.E., De Jong, A.F.M., Oosterbaan, W.A., Van Der Borg, K., 1992. Accurate dating of organic deposits by AMS ^{14}C measurement of macrofossils. Radiocarbon 34, 566-577. https://doi.org/10.1017/S0033822200063840

Trachsel, M., Telford, R.J., 2017. All age-depth models are wrong, but are getting better. Holocene 27, 860-869. https://doi.org/10.1177/0959683616675939

Tylmann, W., Bonk, A., Goslar, T., Wulf, S., Grosjean, M., 2016. Calibrating 210 Pb dating results with varve chronology and independent chronostratigraphic markers: Problems and implications. Quat. Geochronol. 32, 1-10. https://doi.org/10.1016/j.quageo.2015.11.004

Wacker, L., Bonani, G., Friedrich, M., et al., 2010a. MICADAS: Routine and high-precision radiocarbon dating. Radiocarbon 52, 252-262. https://doi.org/10.1017/S0033822200045288

Wacker, L., Christl, M., Synal, H.A., 2010b. Bats: A new tool for AMS data reduction. Nucl. Instruments Methods Phys. Res. Sect. B Beam Interact. with Mater. Atoms 268, 976-979. https://doi.org/10.1016/j.nimb.2009.10.078

Wacker, L., Fahrni, S.M., Hajdas, I., Molnar, M., Synal, H.A., Szidat, S., Zhang, Y.L., 2013. A versatile gas interface for routine radiocarbon analysis with a gas ion source, in: Nuclear Instruments and Methods in Physics Research, Section B: Beam Interactions with Materials and Atoms. https://doi.org/10.1016/j.nimb.2012.02.009

Wacnik, A., 2009. From foraging to farming in the Great Mazurian Lake District: Palynological studies on Lake Miłkowskie sediments, northeast Poland. Veg. Hist. Archaeobot. 18, 187-203. https://doi.org/10.1007/s00334-008-0196-0

Wacnik, A., Tylmann, W., Bonk, A., Goslar, T., Enters, D., Meyer-Jacob, C., Grosjean, M., 2016. Determining the responses of vegetation to natural processes and human impacts in north-eastern Poland during the last millennium: combined pollen, geochemical and historical data. Veg. Hist. Archaeobot. 25, 479-498. https://doi.org/10.1007/s00334-016-0565-z

Wetzel, R.G., Likens, G.E., Wetzel, R.G., Likens, G.E., 1991. Lake Basin Characteristics and Morphometry, in: Limnological Analyses. Springer New York, pp. 1-14. https://doi.org/10.1007/978-1-4757-4098-1_1

Żarczyński, M., Tylmann, W., Goslar, T., 2018. Multiple varve chronologies for the last 2000 years from the sediments of Lake Żabińskie (northeastern Poland) - Comparison of strategies for varve counting and uncertainty estimations. Quat. Geochronol. 47, 107-119. https://doi.org/10.1016/j.quageo.2018.06.001

Żarczyński, M., Wacnik, A., Tylmann, W., 2019. Tracing lake mixing and oxygenation regime using the Fe/Mn ratio in varved sediments: 2000 year-long record of human-induced changes from Lake Żabińskie (NE Poland). Sci. Total Environ. 657, 585-596. https://doi.org/10.1016/j.scitotenv.2018.12.078

3.8 Supplementary material

The following supplemental files are available online at https://doi.org/10.5194/gchron-2-63-2020-supplement:

Supplementary File S3.1: Core images and location of ^{14}C ages.

Supplementary File S3.2: Microscope images of macro- fossils used for ^{14}C dating.

Supplementary File S3.3: Animation of OxCal P-sequence age-depth models for all 30 iterations of simulated sampling scenarios (animated version of Fig. 3.4).

Supplementary File S3.4: Comparison of Bacon and OxCal simulated age-depth models.

Chapter 4: A high-resolution record of Holocene primary productivity and water-column mixing from the varved sediments of Lake Żabińskie, Poland

---

Declaration of contribution

The following study was published in *Science of the Total Environment* (Volume 755, 10 February 2021, 143713). Paul Zander and Martin Grosjean designed the study. Paul Zander did primary laboratory analyses and data analysis. Hendrik Vogel and Paul Zander did XRF scanning. Agnieszka Wacnik did pollen and charcoal analysis. Andrea Sanchini assisted with pigment analysis and interpretation. Wojciech Tylmann and Maurycy Żarczyński provided core material and data. Paul Zander wrote the manuscript with contributions from all authors. Sönke Szidat, Gary Salazar, Edith Vogel, Ron Lloren, Irene Brunner, Stamatina Makri, Linus Rösler, Petra Boltshauser-Kaltenrieder, and Daniela Fisher also contributed to analyses in this study.

A high-resolution record of Holocene primary productivity and water-column mixing from the varved sediments of Lake Żabińskie, Poland

Paul D. Zander[1*], Maurycy Żarczyński[2], Hendrik Vogel[3], Wojciech Tylmann[2], Agnieszka Wacnik[4], Andrea Sanchini[1], Martin Grosjean[1]

[1] Institute of Geography & Oeschger Centre for Climate Change Research, University of Bern, Bern, Switzerland

[2] Faculty of Oceanography and Geography, University of Gdańsk, Gdańsk, Poland

[3] Institute of Geological Sciences & Oeschger Centre for Climate Change Research, University of Bern, Bern, Switzerland

[4] W. Szafer Institute of Botany, Polish Academy of Sciences, Cracow, Poland

[*] Correspondence E-mail address: paul.zander@giub.unibe.ch

Keywords: Hyperspectral imaging, Pigments, Varves, Anoxia, Eutrophication, Holocene

Abstract

Eutrophication and anoxia are increasing in lakes worldwide. However, our understanding of variations of primary productivity and anoxia in lakes over thousands of years is limited. Long-term records are needed to understand the natural variability of lake ecosystems, and to improve our understanding of drivers of productivity and anoxia. In this study, we used the varved sediment record of Lake Żabińskie, Poland to answer the following research questions: 1) How have primary production and water column oxygen concentrations varied during the past 10,800 years?; 2) What role did natural and anthropogenic forces have in driving changes in primary production or lake mixing regime? Recently developed hyperspectral imaging (HSI) techniques were used to quantify sedimentary chloropigments-*a* and bacteriopheopigments-*a* (Bphe-*a*) at sub-annual resolution. These data, combined with elemental data from micro X-ray fluorescence (µ-XRF) and pigment assemblage data from high-performance liquid chromatography (HPLC) measurements, were used to reconstruct paleolimnological conditions. Bphe-*a* was used as an indicator of anoxia, and its presence suggests that an extensive anoxic zone was present nearly continously from 10.8 to 2.8 ka BP. Anoxic conditions, driven by thermal stratification, were promoted by closed forest cover during that time, which limited wind-driven mixing of the water column. After 2.8 ka BP, water column oxygenation occurred more frequently, particularly during periods of increased human agricultural activity and forest opening. Pronounced anoxia was again present continuously from ~610-1470 CE, concurrent with a period of reforestation. After ~1610 CE, deforestation caused increases in erosion rates, algal production, and water column oxygenation. Pigment assemblages indicate that the algal community during the past 150 years was different from any other time during the Holocene. This study demonstrates a clear link between lake biogeochemical processes and forest cover and shows the potential of HSI to produce extremely high-resolution records of past productivity and redox conditions from varved lake sediments.

Highlights

- Aquatic productivity and anoxia were inferred from a 10,800-year sediment core
- Sedimentary pigments were quantified using hyperspectral imaging (HSI)
- Anoxia was persistent during the Holocene prior to human-mediated deforestation
- HSI on varves enables sub-annual reconstruction of past productivity and anoxia

Graphical abstract

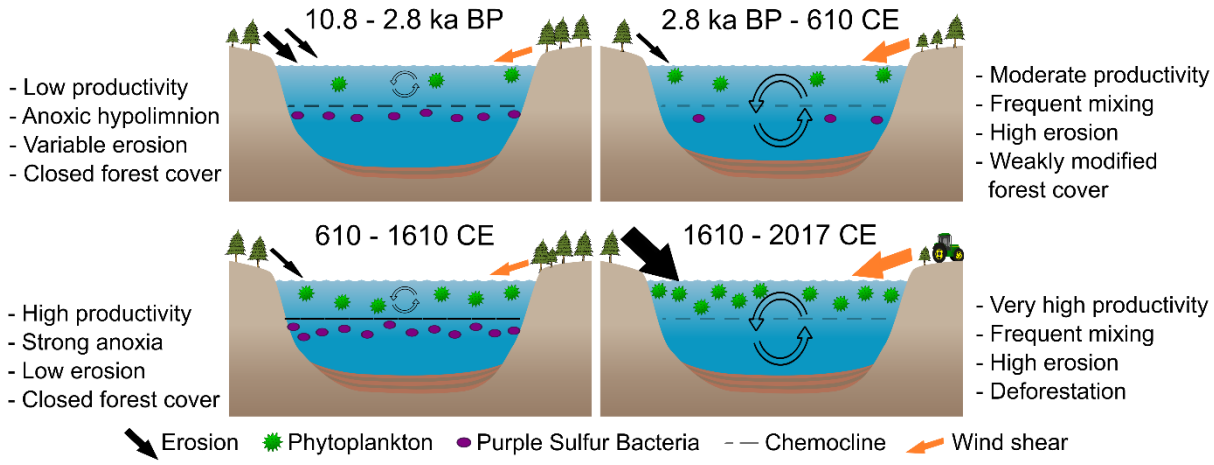

4.1 Introduction

Anthropogenic impacts to freshwater ecosystems have led to a global increase in eutrophication of lakes and increased occurrence and extent of anoxic or hypoxic zones (Carpenter, 2005; Friedrich et al., 2014; Jenny et al., 2016). These changes have primarily been attributed to higher nutrient loads and warmer summer temperatures that have, together, increased primary production in many lakes across a variety of ecosystems (Smith, 2003; Mills et al., 2017). Efforts to restore lake ecosystems have focused on nutrient reductions to slow eutrophication, however high primary production and hypoxia can persist for decades after management efforts are implemented (Jenny et al., 2016). Additionally, anthropogenic global warming is expected to increase anoxia in lakes because warmer temperatures enhance thermal stratification, which decreases oxygen transport to the hypolimnion, and warmer temperatures reduce oxygen solubility (Woolway and Merchant, 2019). To better understand the natural variability of lake ecosystems and the drivers controlling aquatic production and oxygenation, there is a need for long-term records of primary production and water column oxygen concentrations. Paleolimnological records can inform target conditions for restoration efforts and lake management (Bennion et al., 2011), and illuminate the sensitivity of lake ecosystems to forcing factors such as climate, land cover and land use, nutrient inputs and their combinations.

A variety of paleolimnological methods have been used to reconstruct past changes in lake trophic status and water column oxygen concentrations. Paleoproductivity has been reconstructed using changes in organic carbon (Meyers, 2006), C:N ratios, carbon and nitrogen stable isotopes (Schelske and Hodell, 1995; Talbot, 2005), assemblages of diatoms or other microfossils (Hall and Smol, 1999),

pigments (Leavitt and Hodgson, 2002), and other sediment variables. The majority of these methods require time-consuming laboratory analyses, which limits the resolution of paleoproductivity reconstructions over Holocene timescales. Past changes in oxygen concentration have been inferred from pigments and DNA associated with anoxygenic bacteria (Lotter, 2001; Sinninghe Damsté and Schouten, 2006; Wirth et al., 2013), and from microfossil assemblages (Clerk et al., 2000; Ursenbacher et al., 2020). Another approach is to use redox-sensitive elements such as Fe and Mn (Mackereth, 1966). This approach has become widely applied, in part because µ-XRF core scanners readily enable measurements of these elements at high resolution (Naeher et al., 2013; Wirth et al., 2013; Żarczyński et al., 2019). However, interpretation of these elements depends on site-specific characteristics and often requires complementary data from other sediment variables (Boyle, 2005; Davies et al., 2015). Due to these limitations, caveats should be considered when interpreting Fe and Mn as redox proxies (Naeher et al., 2013). The preservation of varves has also been used as an indicator of anoxic bottom-waters (Jenny et al., 2013; Zolitschka et al., 2015). Studies of sedimentary pigments have proven particularly useful for tracing changes in bacterial and algal communities, which can be used to reconstruct both productivity and oxygen concentrations. Conventional analyses of pigments are time-consuming and costly, leading to low-resolution reconstructions when applied to sediment records covering the Holocene or longer time-scales. Recently developed Hyperspectral Imaging (HSI) techniques enable rapid quantification of bulk pigment groups at sub-mm resolution (i.e. 60 x 60 µm pixel size) and these techniques have been used to investigate past lake productivity and oxygen concentrations at unprecedented temporal resolution (Butz et al., 2015, 2017; Schneider et al., 2018; Gassner et al., 2020; Makri et al., 2020; Tu et al., 2020).

Recent studies using HSI have demonstrated that land cover changes associated with Neolithic and Bronze Age agricultural development strongly influenced lake mixing regimes in small, relatively deep lakes (Gassner et al., 2020; Makri et al., 2020; Sanchini et al., 2020b). However, less is known about the evolution of productivity and lake mixing in settings with minimal human impact throughout the Holocene. To investigate this question, we selected Lake Żabińskie in the Masurian Lakeland of northern Poland, where forest cover was not strongly modified by humans until ~1610 CE (Wacnik et al., 2016). Żarczyński et al. (2019) reconstructed major variations in bottom water oxygen at Lake Żabińskie during the past 2000 years based on Fe/Mn ratios and related these inferred mixing regime changes to changes in surrounding forest cover. In this study, we aimed to answer the following research questions: 1) How have primary production and water column oxygen concentrations varied during the past 10,800 years?; 2) What role did natural and anthropogenic forces have in driving changes in primary production or lake mixing regime? We hypothesized that land cover was the primary control on lake mixing throughout the Holocene. To investigate these research questions, we measured pigments in a long sediment core using Hyperspectral Imaging (HSI) and high-performance liquid chromatography (HPLC) and combined these with geochemical data (µ-XRF and CNS analysis). The Lake Żabińskie sediment record covers the past 10,800 years and is annually laminated throughout most of its length, making it an excellent archive to apply ultra-high-resolution scanning techniques. Calibrated HSI-inferred chloropigment and bacteriopheopigment concentrations enabled us to reconstruct past primary production and oxygen concentrations at sub-annual resolution.

4.2 Study Site

Lake Żabińskie is a eutrophic hard-water lake located in the post-glacial landscape of the Masurian Lakeland in northeastern Poland (54.1318° N, 21.9836° E; Fig. 4.1). The lake is a kettle-hole with a small surface area (41.6 ha) relative to its maximum depth (44.4 m), and a catchment area of 24.8 km^2. The catchment geology is dominated by glacial till, sandy moraines and fluvioglacial sands and gravels (Szumański, 2000). Land cover in the catchment is a mixture of agrarian and woodland areas (primarily oak-lime-hornbeam and pine forests; Wacnik et al., 2016). The lake has three inflows, including one from smaller Lake Purwin, and the outflow is a direct connection to much larger Lake Gołdopiwo. The site has been extensively studied for several years, with a focus on modern limnological and sedimentological processes, as well as multi-proxy investigations of the most recent 2000 years of the sediment record. Limnological monitoring showed inter-annual differences in the lake mixing regime with complete mixing occurring 0-2 times per year (Bonk et al., 2015a). Ice-cover typically lasts 2-4 months. Thermal stratification leads to anoxic conditions in the hypolimnion each summer. In some years the hypolimnion remains anoxic throughout the year, whereas in other years, mixing in the spring or fall brings oxygen into the bottom waters (Bonk et al., 2015a). The strong thermal stratification is attributed to the high relative depth of the lake (6.1 %; Wetzel et al., 1991) and steep basin morphology. Investigations of the sediment record identified major anthropogenic impacts starting in the 17th century, which led to increased catchment erosion, shifts in the algal communities, and eutrophication (Bonk et al., 2016; Hernández-Almeida et al., 2017). Żarczyński et al. (2019) showed that changes in bottom water oxygenation (inferred from Fe/Mn ratios) were caused by changes to the density of forest cover surrounding the lake.

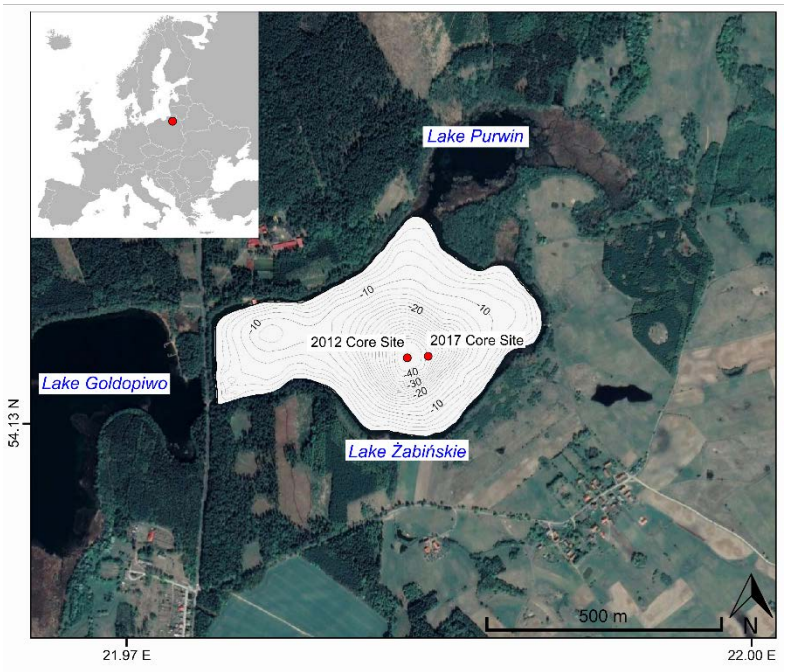

Figure 4.1: Study area and bathymetric map. Imagery from Google Earth (April 29, 2019). Additional maps of catchment geology, and land cover can be found in Bonk et al. (2015a) and Wacnik et al. (2016).

4.3 Methods

Sediment cores were retrieved in 2012 using an UWITEC piston corer (ø90 mm), and surface cores were retrieved in 2017 using an UWITEC gravity corer (ø60 mm). Overlapping sections were visually correlated using distinctive stratigraphic layers to form a composite sequence of 19.4 m (Fig. S4.1). All depths mentioned in this study are composite depths below lake floor.

4.3.1 Geochronological methods

The chronology presented here is a combination of previously published chronological data for the upper 13.1 m of the record and new chronological data for the section 19.4-13.1 m, which is published here for the first time (Fig. 4.2). The uppermost 6.3 m (corresponding to the last ~2000 years) was dated using varve counting as described in Żarczyński et al. (2018), and this chronology was transposed to our composite sequence. The reliability of the varve count was validated by radiocarbon ages (Bonk et al., 2015b; Żarczyński et al., 2018), ^{137}Cs chronostratigraphic markers, a ^{210}Pb profile, and identification of the 1875 CE Askja (Tylmann et al., 2016) and 860 CE White River Ash (Mount Churchill) tephras (Kinder et al., 2020). A mass movement deposit (MMD-2) from 7.3-6.3 m was removed from the chronology. The chronology from 13.1-7.3 m (~6.8-2.1 ka cal BP) was established by Zander et al. (2020), and is based on a V-sequence age model from the software OxCal (Bronk Ramsey, 2008, 2009; Bronk Ramsey and Lee, 2013), which combines age information from varve counts and radiocarbon ages.

The chronology for the remainder of the composite sequence is published here for the first time and is based primarily on radiocarbon ages. Eighteen samples of taxonomically identified terrestrial plant macrofossils were measured for ^{14}C by AMS analysis at the University of Bern (Table S4.3). Detailed information about the radiocarbon sample preparation can be found in Zander et al., 2020. We used the age-depth modeling software OxCal (Bronk Ramsey, 2008, 2009; Bronk Ramsey and Lee, 2013) to generate an age-depth relation that links two P-sequences (16.4-13.1 m, and 19.4-18.0 m) with a V-sequence (17.0-16.4 m). MMD-1 (18.0-17.0 m) was excluded from age-depth modeling. The P-sequence is a Bayesian age-depth modeling routine that calibrates radiocarbon ages using IntCal13 (Reimer et al., 2013) and models sedimentation rates to fit the ages. Details about the chronologic methods can be found in the supplementary material (S1.1).

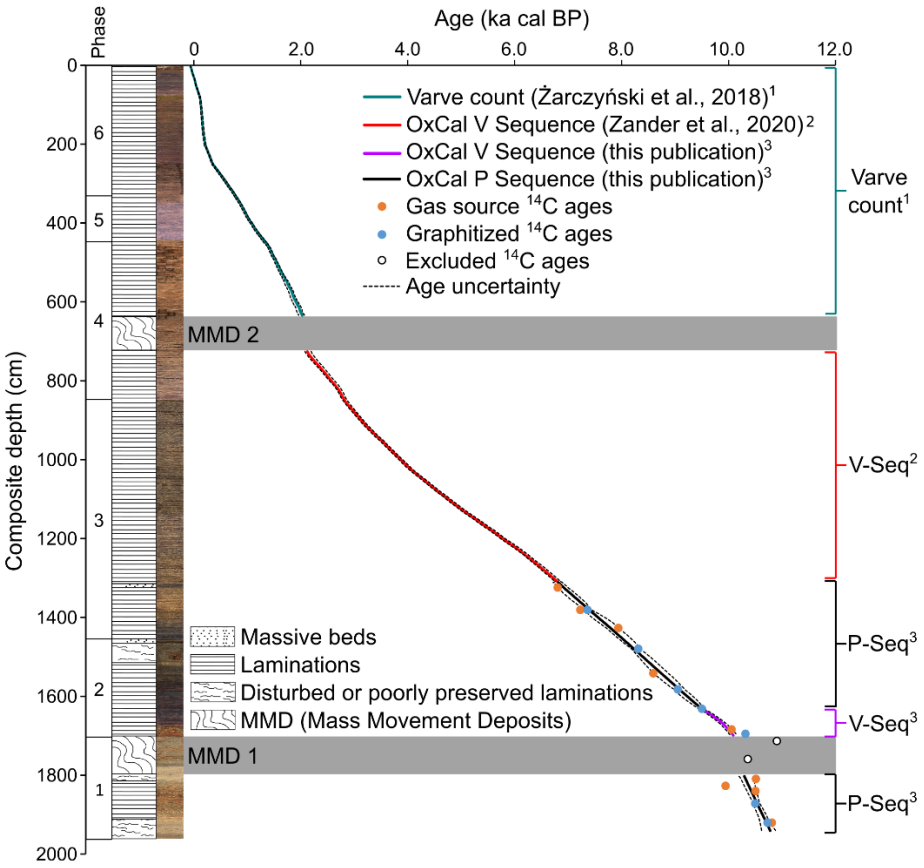

Figure 4.2: Age-depth relation and core stratigraphy. Only newly reported radiocarbon ages are shown. Gas source ages contain < 150 µg C, graphitized ages contain > 150 µg C. The varve count chronology of the past 2000 years is from Żarczyński et al. (2018) and the OxCal V-sequence spanning 2.1-6.8 ka from Zander et al. (2020). The age uncertainty (dashed lines) of the varve count section was determined by comparing the counts of 3 different researchers (Żarczyński et al., 2018). For the OxCal models, the uncertainty is the 2σ range of the model output.

4.3.2 Geochemical analyses

µ-XRF scanning on the 2017 sediment-water interface cores (83-0 cm in our composite profile) was performed at the Swiss Federal Institute of Aquatic Science and Technology with an Avaatech XRF Core Scanner (Richter et al., 2006) equipped with a Rh-tube. Lighter elements were measured using 10 kv, 1.5 mA, and 15 s exposure time. Heavier elements (Cu, Zr) were measured using 40 kv, 2.0 mA, and 40 s exposure time. The scanning resolution was 0.5 mm. For the interval 2.5-2.1 m we used previously published µ-XRF data (Bonk et al., 2016; Żarczyński et al., 2019b) to fill a gap where all core material had been sampled prior to scanning. These data were obtained using an ITRAX core scanner (Cox Analytical Systems) at the University of Bremen with a Mo-tube (exposure time 10 s, 30 kV, 18 mA), at a resolution of 0.2 mm. All other cores were scanned at the University of Bern using an ITRAX core scanner equipped with a Cr-tube (exposure time 20 s, 30 kV, 50 mA). The scanning resolution was 0.5 mm for 2.1-0.8 m and 2 mm resolution for 19.4 -2.5 m. All XRF data were calculated as counts per second (cps) and then homogenized such that the standard deviation and mean for each element in overlapping core sections were equal. We selected key XRF elements for analysis based on data quality and interpretations of interest. Interpretations followed those of Davies et al. (2015) for XRF on lake sediments and previous work from the study site (Żarczyński et al.,

2019b). We used K, Zr and Ti as proxies for lithogenic input from the catchment; Fe, Mn, S and P as indicators of changing redox conditions; Cu and P as indicators of aquatic production or organic matter content, Ca/Ti ratio for endogenic calcite precipitation, and Si/Ti ratio for biogenic silica (diatom and chrysophyte abundance).

Total inorganic carbon (TIC), total organic carbon (TOC), total nitrogen (TN), and total sulfur (TS) measurements for the interval 6.1-0 m were obtained at 3-year resolution, as reported in Żarczyński et al. (2019). For the interval 19.4-6.1 m these elements were measured at 10-cm resolution (1-cm-thick samples). TC, TN and TS were measured on these samples using a Vario El Cube elemental analyzer (Elementar). TIC was determined using loss-on-ignition at 950 °C (after samples were previously burned at 550 °C) (Heiri et al., 2001), and TOC was calculated by subtracting TIC from TC.

Dry bulk density (DBD) was measured on the same samples used for CNS analyses. Mass accumulation rates (MAR) were calculated by multiplying dry bulk density and sedimentation rate. Sedimentation rate was obtained from varve thickness over the section 13.1-0 m depth, and calculated from the OxCal age-depth model output for 19.4-13.1 m depth. To account for the variable measurement resolution of DBD, a LOESS regression was used to smooth the DBD data prior to the MAR calculation. Fluxes were calculated by multiplying concentrations by MAR (a 60-year running mean was first applied to MAR for the sections with varve counts).

4.3.3 Pigment analysis

Pigment extractions were performed on 41 lyophilized samples weighing 0.2 to 0.6 g using 100% acetone, using a modified version of the method described in Amann et al. (2014). Samples were taken at ~500-year resolution for the period 10.8 to 2.0 ka cal BP and at ~100-year resolution from 2.0 ka cal BP to present. Extracts were measured using a spectrophotometer (Shimadzu UV-1800) for bulk concentrations of TChl-*a* (Total Chloropigments-*a*, defined as chlorophyll-*a* and chlorophyll derivatives-*a*) and Bphe-*a* (Bacteriopheopigments-*a*). We used the molar extinction coefficient for Bacteriopheophytin-*a* from Fiedor et al. (2002), and the molar extinction coefficient for chlorophyll-*a* and chlorophyll derivatives-*a* from Jeffrey and Humphrey (1975). The same pigment extracts were also analyzed using HPLC (Agilent Infinity 1260 series equipped with a G7117C Diode-Array Detection detector and a G7121A fluorescence detector) for specific pigment measurements following the procedures of Sanchini and Grosjean (2020). Sixteen pigment compounds were identified by comparisons to reference standards (Table S4.1). Two samples taken from within single varves were not considered for the pigment stratigraphy because the pigments represent seasonal deposition. The remaining 39 samples represent 2.5-23 years (mean = 8.5) of sedimentation per sample. All HPLC pigment concentrations were normalized to nmol per g of organic matter.

Hyperspectral imaging (HSI) was done using a Specim PFD-CL-65-V10E linescan camera following the methods of Butz et al. (2015). Relative absorption band depth (RABD) indices were used to quantify absorption features associated with sedimentary pigments. Measurements were done at a resolution of 60 × 60 µm (pixel size). Details on the scanning methodology and index calculations can be found in the supplementary material. The $RABD_{655\text{-}685max}$ index represents TChl-*a* and is interpreted as representative of total algal abundance (Rein and Sirocko, 2002; Wolfe et al., 2006; Butz et al.,

2017; Schneider et al., 2018). The $RABD_{845}$ index represents Bphe-*a*, a specific biomarker for purple sulfur bacteria (PSB). PSB live at the chemocline of stratified water bodies and require both light and reduced sulfur to photosynthesize (Van Gemerden and Mas, 1995). Therefore, the presence of Bphe-*a* indicates that the oxic/anoxic boundary was within the photic zone of the lake (Sinninghe Damsté and Schouten, 2006). Both RABD index values were calibrated to concentrations (µg/g dry sediments) via linear regression between the spectrophotometer measurements and the average RABD index values of the sample locations.

Interpretations of pigment taxonomic affiliations follow those of Bianchi and Canuel (2011), Guilizzoni and Lami (2003), Leavitt and Hodgson (2002), and Swain (1985). The CD/TC (Chlorophyll Derivatives/Total Carotenoids) ratio is used as an indicator of lake trophic state and/or preservation conditions because cyanobacteria produce more carotenoids than chloropigments, and carotenoids are better preserved under anoxic conditions (Swain, 1985). The Chlorophyll Preservation Index (CPI; (chlorophyll-*a*/(pheopigments-*a* + chlorophyll-*a*)) is an indicator of pigment preservation/degradation (Buchaca and Catalan, 2008). The ratio DDX+DT/Chl-*a* (DDX = Diadinoxanthin; DT = Diatoxanthin) is used as an indicator of light penetration (Hager, 1980; Riegman and Kraay, 2001).

4.3.4 Pollen

A 2000-year record of pollen from Żarczyński et al. (2019) was supplemented here with pollen samples targeting specific sediment sections with oxic/anoxic transitions to investigate the relationship between vegetation changes and shifts in lake mixing regime. We sampled four periods: 10,700-10,500 cal BP, 10,100-9600 cal BP, 7,700-7,400 cal BP, and 2,700-2,100 cal BP with 2-cm-thick samples (each sample represents 7-20 years). The methods of sample preparation and pollen counting are the same as in Żarczyński et al. (2019).

4.3.5 Data analysis

Statistical analyses were conducted using R 3.6 (R Core Team, 2020). The packages ‘ggplot2’ (Wickham, 2016), ‘factoextra’ (Kassambara and Mundt, 2017), ‘rioja’ (Juggins, 2017), ‘corrplot’ (Wei and Simko, 2017) and ‘zoo’ (Zeileis and Grothendieck, 2005) were used for data analyses and visualization. Data from µ-XRF and HSI scanning and MARs were averaged to 1 cm resolution. Data from mass movement deposits or cracks were removed, and the data were log-transformed and scaled prior to statistical analyses. Principal component analysis (PCA) and an unconstrained cluster analysis were performed on this dataset to understand the relationships between different geochemical proxies and their variations over time. A broken-stick model was used to determine the number of significant principal components (Bennett, 1996). The cluster analysis was done using the kmeans method (1000 iterations). A stratigraphically constrained hierarchical cluster analysis (CONISS) was performed using ‘rioja’ (Juggins, 2017) for the HSI and µ-XRF dataset to identify geochemically similar stratigraphic units.

Statistical analysis of the HPLC pigment dataset was done separately. Pigment concentrations were square-root transformed and scaled prior to analysis. PCA and CONISS analyses were also applied to the HPLC pigment data to identify zones of similar pigment assemblages and to aid interpretation. A

broken-stick model was used to determine the number of zones in the pigment assemblage, as well as the number of significant principal components (Bennett, 1996).

4.4 Results and interpretation

4.4.1 Core lithology and geochemical results

The base of the 19.4-m-long sediment record was dated to 10,780 +102/-160 cal BP (Fig. 4.2). Details about chronological results are available in the supplementary material (S1.2). The sediments are generally composed of laminated (varved) carbonate- and organic-rich mud. Varves are preserved in approximately 16.2 m, representing ~93% of the record, excluding mass-movement deposits. Most varves consist of couplets of calcite-rich pale brown laminae (summer) and dark brown laminae composed of organic detritus and fine mineral matter (winter), though more complicated varve structures are also present. Żarczyński et al. (2018) presented detailed varve microfacies descriptions for the past 2000 years. Two mass movement deposits from 18.0-17.0 m and 7.3-6.3 m were identified by deformed laminae, massive beds, and fining-upwards sequences. We identified five lithotypes based on the results of the kmeans cluster analysis on HSI, XRF and MAR data (Fig. 4.3; Fig. 4.4). Example images of each lithotype and corresponding pigment maps from HSI are shown in Fig. 4.4.

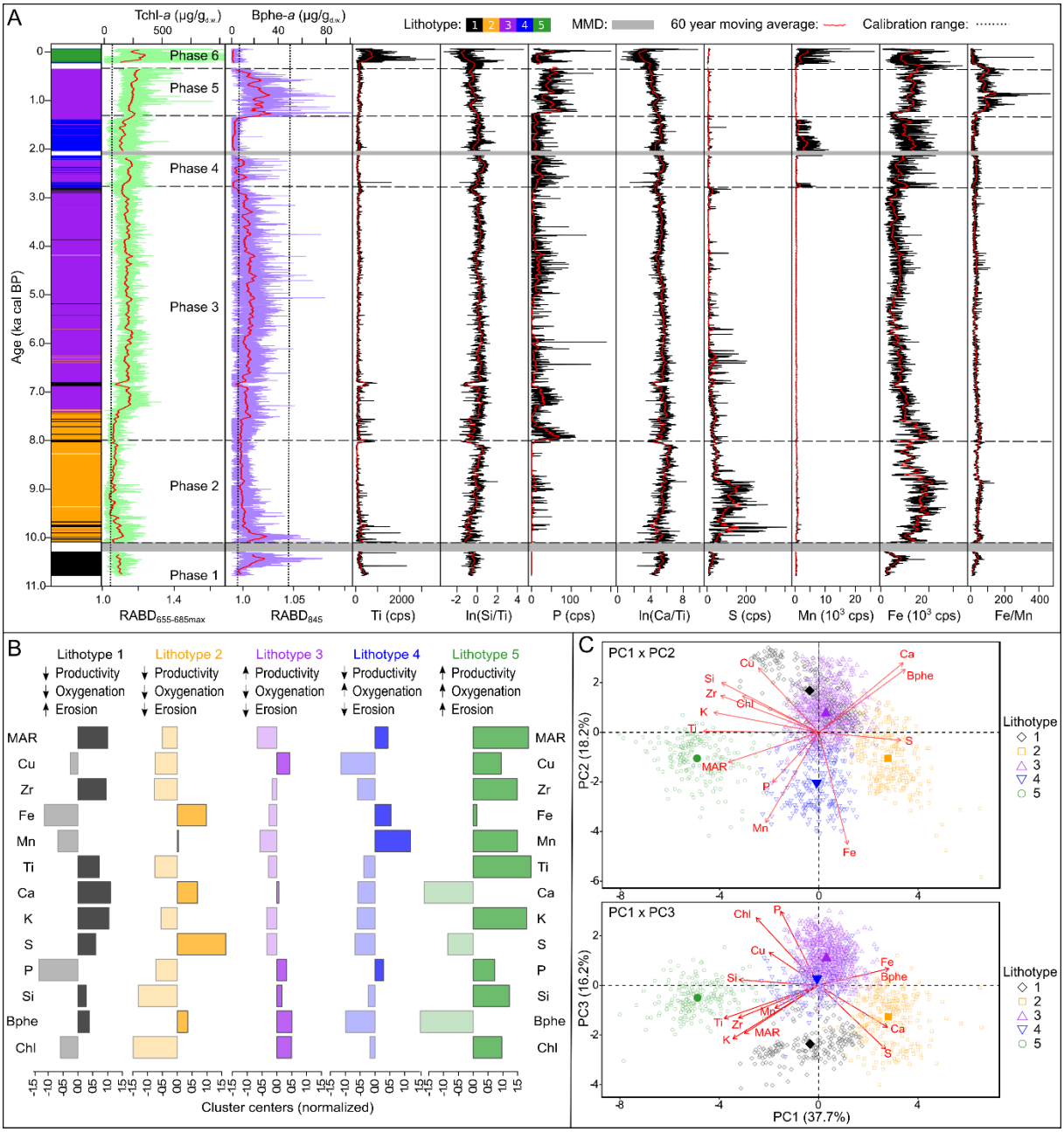

Figure 4.3: A) Selected geochemical variables plotted by age. Colored bar on left shows lithotypes identified by kmeans cluster analysis. B) Cluster centers of each lithotype (normalized mean values of each geochemical variable within each lithotype). C) Principal component biplots showing first three principal components with loadings of each variable depicted as red arrows. Data points are grouped by cluster/lithotype, which is indicated by different colors and symbols, with the larger filled-in symbols representing the cluster center.

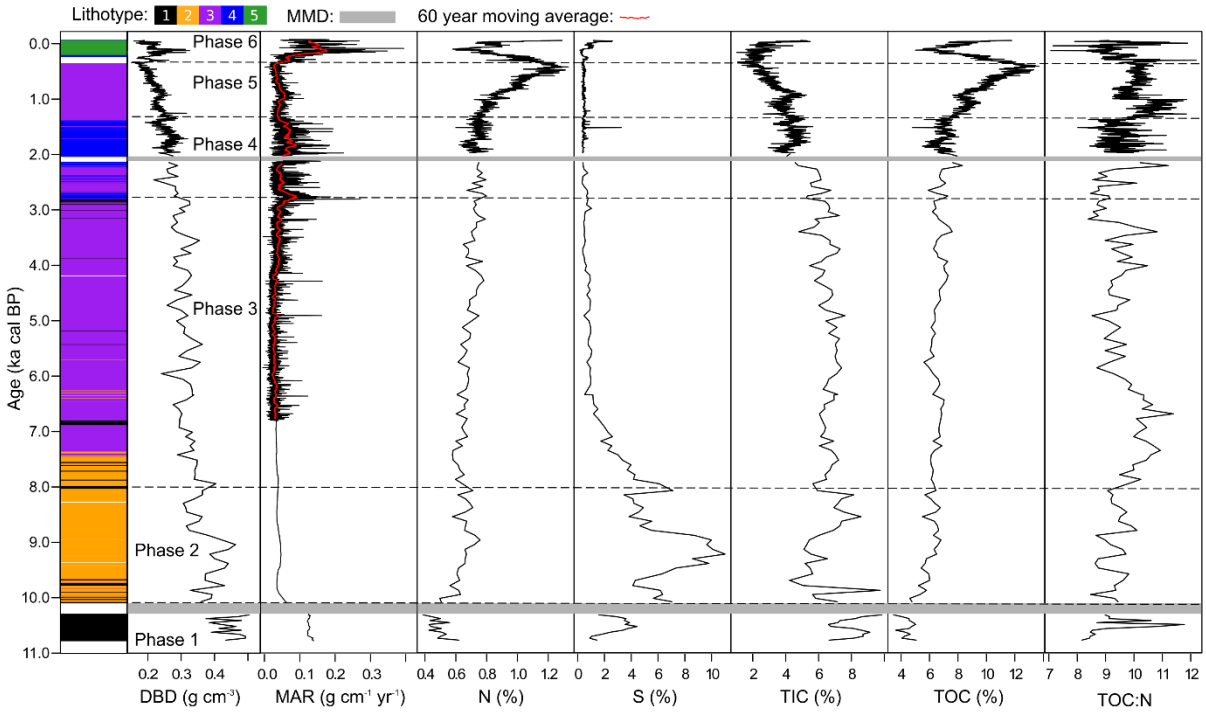

Figure 4.4: Dry Bulk Density (DBD), Mass accumulation rate (MAR), and C, N, S elemental data. Red line in MAR is 60-yr average.

Lithotype 1 (example image Fig. 4.5e) is defined by high MAR, Ca, and erosion indicators (Ti, K, Zr), whereas Fe, Mn, P and TChl-*a* are low. Sediments tend to be grayish in color, with relatively low TOC and high lithogenic content. Varve preservation ranges from good to absent; this lithotype represents more non-varved sediments than any other lithotype. Lithotype 1 primarily occurs from 10.8 to 10.3 ka cal BP, but is also identified occasionally throughout the record where more siliciclastic sediments occur. We interpret this lithotype as representative of periods with relatively high catchment erosion and low aquatic productivity. Bphe-*a* values vary across this lithotype, but are clearly high from 10.6 to 10.3 ka cal BP, indicating strongly anoxic conditions, and this interpretation is supported by the presence of varves and low Fe and Mn in this period.

Lithotype 2 (example image Fig. 4.5d) is characterized by very high values of Fe and S, and very low TChl-*a* and Si. Erosional indicators and MAR are relatively low, whereas Bphe-*a* and Ca are relatively high. Sediments of this type are very dark, with the lowest light reflectance of any lithotype (Fig. S4.2). Varves are usually present, though faint at times, and there are some sections with disturbed varves or massive beds. This lithotype occurs almost exclusively in the interval 10.1-7.4 ka cal BP. We interpret this lithotype as representative of periods with low catchment erosion and low aquatic productivity. The formation of iron sulfides suggests that the hypolimnion was anoxic (Boyle, 2005), and Bphe-*a* concentrations above the detection limit confirm this.

Lithotype 3 (example image Fig. 4.5c) is the most common lithotype, and has very well-preserved varves with little variation in varve structure or thickness. Concentrations of TChl-*a* and Bphe-*a* are relatively high, as are Cu and P counts, whereas MAR, erosional indicators and Mn are low. Lithotype 3 is the dominant sediment type from 7.4 to 2.8 ka cal BP and from ~610 to 1610 CE. This lithotype is

indicative of a strongly stratified water column and persistent hypolimnetic anoxia. Erosional input was relatively low, and aquatic production was relatively high.

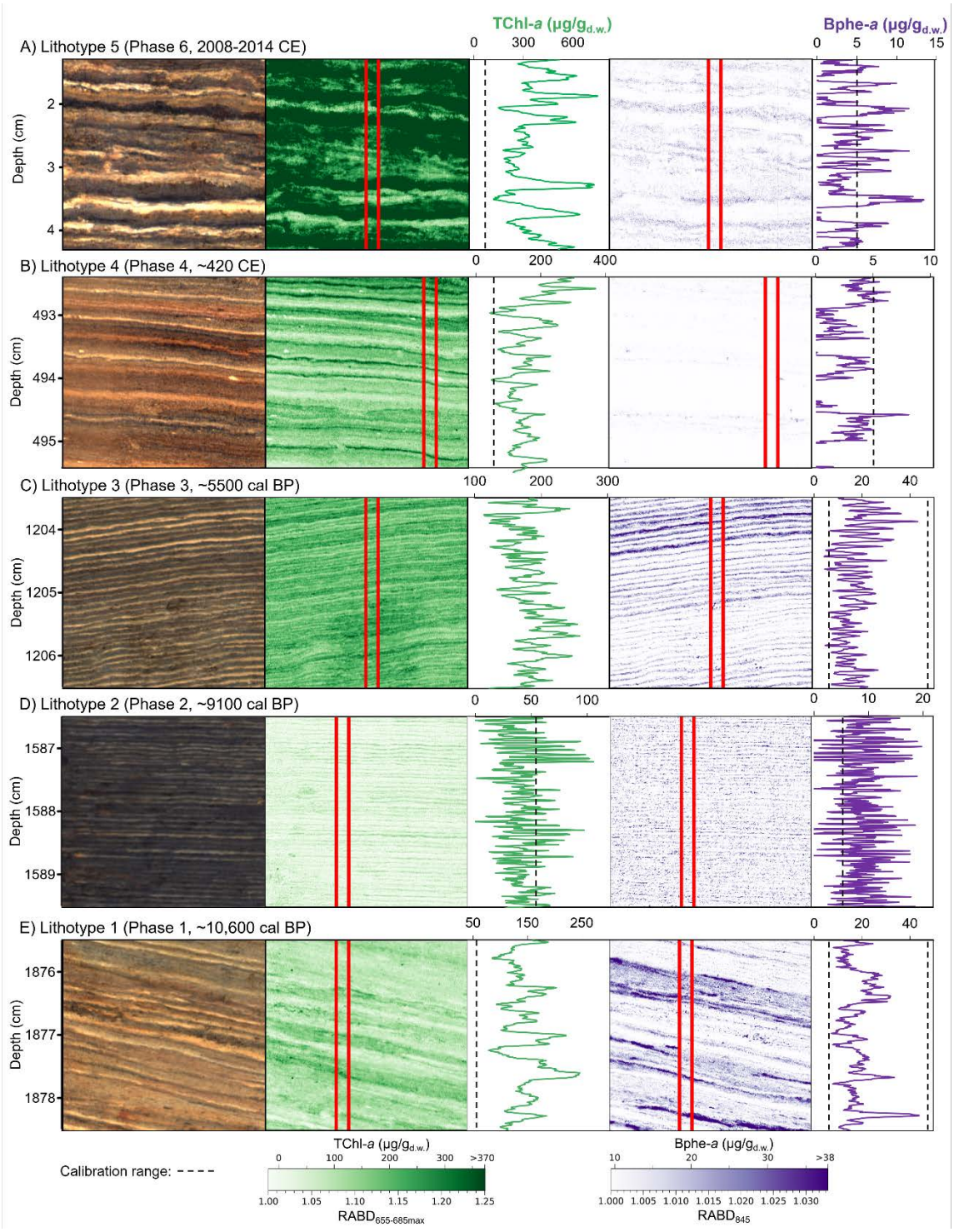

Figure 4.5: Close-ups of example sections for each lithotype to show varve structure and seasonal variations of pigments detected by Hyperspectral Imaging. Each image represents 3 cm of sediments (sediment depth of composite core). Note that the axis scales change for pigment plots. A) Lithotype 5: modern sediments with high productivity and traces of Bphe-*a*. B) Lithotype 4: Fe- and Mn-rich varves during a period of more intense mixing. C) Lithotype 3: strongly stratified conditions with anoxia during the mid-Holocene. D) Lithotype 2: Dark-colored varves rich in iron-sulfides with relatively low pigment concentrations. E) Lithoytpe 1: Varves with relatively high minerogenic content, yet also Bphe-*a* present, indicating anoxia during the early Holocene.

Lithotype 4 (example image Fig. 4.5b) is characterized by high counts of Fe and Mn, high MAR, and low Bphe-*a* and erosional indicators. Sediments of this type show a more variable varve structure with reddish laminae rich in Fe and Mn present in many years. This lithotype is present mainly from 2.8 to 1.3 ka cal BP. The high abundance of Mn implies that this lithotype represents periods when the lake mixed completely, and bottom waters were seasonally oxygenated.

Lithotype 5 (example image Fig. 4.5a) has a distinct geochemical signature with high or very high values of all considered elements except Ca and S. MAR is at maximum levels. TChl-*a* is highly variable, but reaches maximal concentrations in this lithotype, and fluxes of TChl-a are very high (Fig. S4.3). Bphe-*a* is very low in this lithotype. Varves are much thicker in this lithotype, with multiple calcite laminae visible in some years. This lithotype represents the most recent 300 years of sedimentation. This period is characterized by high erosional input from the catchment, high aquatic productivity, and complete seasonal mixing of the water column.

4.4.2 Pigment analysis

HSI pigment indices were calibrated and quantified using pigment concentrations measured by spectrophotometer. TChl-*a* was measured in 41 samples via spectrophotometer and these concentrations are significantly correlated with $RABD_{655\text{-}685max}$ ($r = 0.97$, $p<0.001$, RMSEP = 5.4%, Fig. S4.4). Bphe-*a* was detected in only 28 samples with the spectrophotometer, yet yields a significant correlation with $RABD_{845}$ ($r = 0.79$, $p<0.001$, RMSEP = 13.8%, Fig. S4.4). These correlations were confirmed by comparisons with HPLC data (Fig. S4.5). Bphe-*a* was measured in all samples by HPLC, and these measurements were used to estimate that the limit of detection for the $RABD_{845}$ index is ~0.992 (equivalent to approximately 5 $\mu g/g_{d.w.}$ Bphe-*a*).

The CONISS analysis on HPLC pigment data revealed four pigment zones (PZ; Fig. 4.6). The PCA analysis revealed two significant principal components (PCs). The first PC has positive loadings with all pigment compounds, and thus represents total pigment abundance, which is controlled by both lake productivity and pigment preservation. We interpret the second PC as indicative of community shifts between cyanobacteria (negative PC2 scores) and diatoms and chrysophytes (positive PC2 scores). This interpretation is based on negative PC2 loadings of canthaxanthin, echinenone, β,β-carotene, and {lutein + zeaxanthin} (these compounds were not separated chromatographically), and positive loadings of fucoxanthin, diatoxanthin, diadinoxanthin, and chlorophyll-*a.*

PZ-1 (Pigment Zone 1; 10.8-3.1 ka cal BP) represents the majority of the Holocene and is characterized by high concentrations of most pigments (high PC1 scores). A diverse and productive aquatic community is indicated by relatively high concentrations of β,β-carotene (total algal production), β,ε-carotene (cryptophytes and others), canthaxanthin (cyanobacteria), {lutein + zeaxanthin} (cyanobacteria/green algae), chlorophyll-*b* (green algae), and Bphe-*a* (PSB) (Leavitt and Hodgson, 2002; Bianchi and Canuel, 2011). Low PC2 scores and low CD/TC ratios (Swain, 1985) indicate cyanobacteria were relatively dominant in this zone.

PZ-2 (3.1-1.4 ka cal BP) is characterized by lower concentrations of most pigments. In particular, carotenoids such as {zeaxanthin + lutein} and echinenone reached their lowest values in this unit, and

Bphe-*a* concentrations were very low. Low CPI values (Buchaca and Catalan, 2008) and higher CD/TC ratios (Swain, 1985), indicate that poor preservation may play a role in lower pigment concentrations. PC2 scores are positive, suggesting a greater portion of the algal community was diatoms and/or chrysophytes, and cyanobacteria were less abundant.

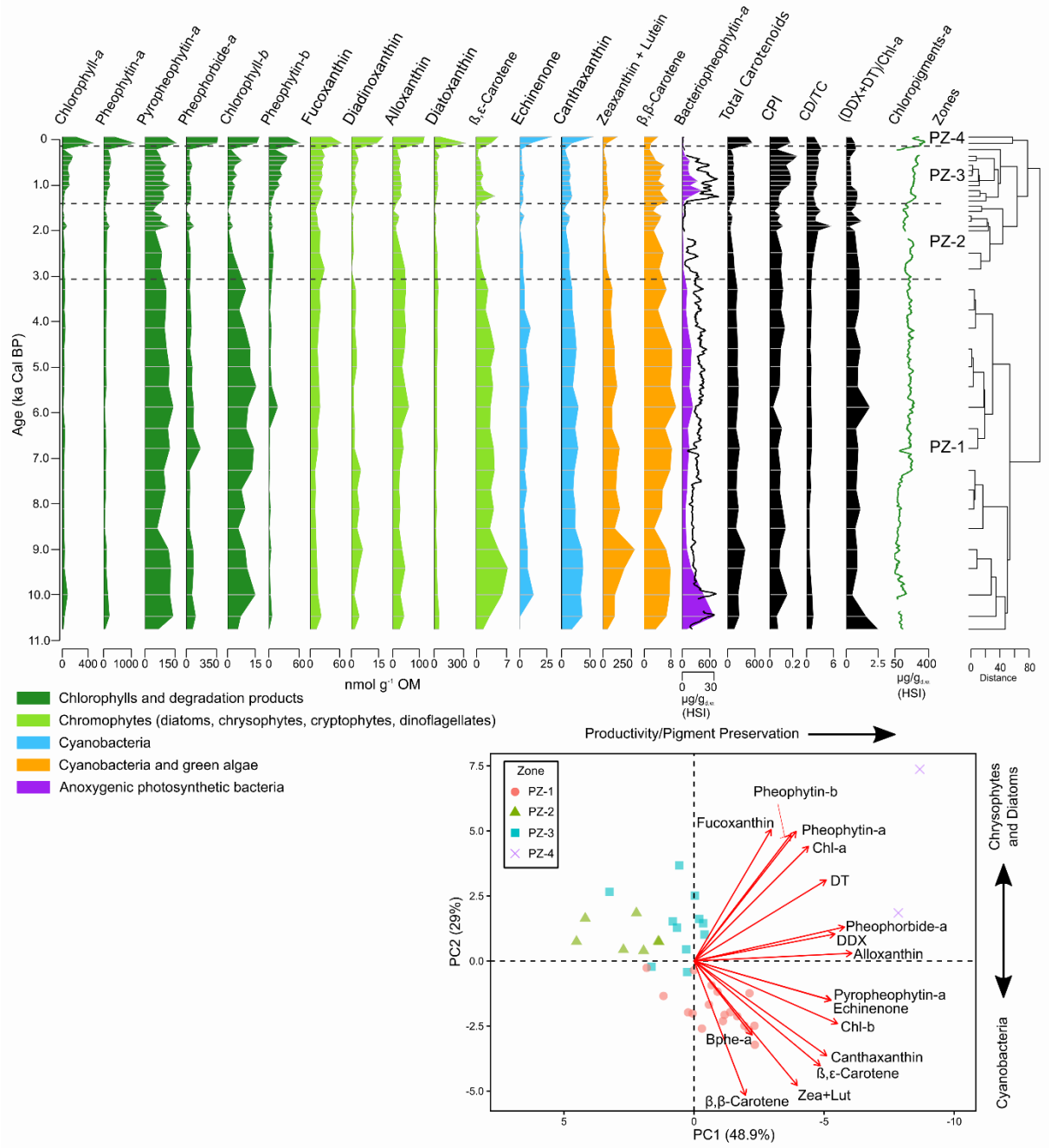

Figure 4.6: HPLC pigment stratigraphy. CPI = Chlorophyll Preservation Index, TC = Total Carotenoids, DC = Chlorophyll Derivatives, DDX = Diadinoxanthin, DT= Diatoxanthin. Zones defined by CONISS analysis.

PZ-3 (550-1800 CE) is characterized by an increase in pigment concentrations and abundant Bphe-*a*, suggesting anoxic conditions and increased pigment preservation. PC2 scores are high, indicating a similar algal assemblage to PZ-2 with diatoms and/or chrysophytes being relatively abundant, and cyanobacteria less abundant.

PZ-4 (1800 CE to present) contains the two most recent samples (dated ~1870 and 2009 CE), and has a unique pigment composition with a major increase in all pigment concentrations, except Bphe-*a*. Most pigments, particularly chloropigments, reached their highest values in the sample from 1870 CE. However, canthaxanthin, echinone, {zeaxanthin + lutein}, β,β-carotene, and β,ε-carotene all increased between 1870 and 2009, most likely indicating a shift toward cyanobacteria.

4.4.3 Paleolimnological reconstruction

We divided the record into six phases (1-6) based on lithology and the results of a CONISS analysis on the HSI and XRF datasets (summarized in Table S4.2). Here we discuss the limnological conditions during each of those periods.

Phase 1: 10.8-10.3 ka cal BP

The basal age of the core (10,780 +102/-160 cal BP) represents a minimum age of lake formation. Deglaciation of the area occurred following the Pomeranian phase stadial of Vistulian glaciation. Two cosmogenic ^{10}Be ages from erratic boulders north and south of Lake Żabińskie suggest that the area was deglaciated between 14.51 ± 1.0 ka cal BP and 12.9 ± 1.0 ka cal BP (Rinterknecht et al., 2005). These findings suggest lake formation likely occurred prior to our basal age of 10.8 ka cal BP.

Phase 1 sediments are predominantly lithotype 1, indicating high erosion rates and anoxic conditions. Bphe-*a* was detectable in the oldest sediments, suggesting a deep, seasonally stratified lake with hypolimnetic anoxia in summer. Erosion rates were high initially (indicated by high Ti and MAR), but declined substantially by ~10,620 cal BP. From ~10,620 to 10,300 cal BP laminations were preserved, and Bphe-*a* and Fe/Mn increased, suggesting that lake mixing weakened even further, leading to prolonged periods of anoxia. When accounting for the high mass accumulation rates at that time, Bphe-*a* flux reached the highest value of the entire record at ~10,420 cal BP (Fig. 4.7). TChl-*a* concentrations were relatively low, but fluxes were relatively high.

The algal community in this phase featured a high abundance of cyanobacteria, as indicated by relatively high concentrations of canthaxanthin, echinenone, and {zeaxanthin + lutein} (see PZ-1, above). Productive conditions and seasonal stratification were likely influenced by strong seasonality with warm summer temperatures (Tóth et al., 2015; Street-Perrott et al., 2018; Luoto et al., 2019) and high P input from weakly developed soils on glacial drift (Boyle et al., 2015). The abundance of cyanobacteria may be an indication of N-limiting conditions (Smith, 1983). High productivity and high (but decreasing) erosional input during the early Holocene were also found in several lakes in the Baltic region (Wacnik, 2009b; Lauterbach et al., 2011; Street-Perrott et al., 2018).

Phase 2: 10.1-8.0 ka cal BP

Phase 2 sediments are primarily lithotype 2, indicative of low erosional input and low productivity. Following the deposition of MMD-1 (mass movement deposit), anoxia quickly re-established, evidenced by good varve preservation and concentrations of Bphe-*a* above 10 $\mu g/g_{d.w.}$ within ~5 years after the mass movement event (Fig. S4.6). Lithogenic input was moderately high in the period following the event, but then decreased to very low values. Bphe-*a* concentrations peaked at ~9950

cal BP, and from ~10,060 cal BP until ~9,900 cal BP seasonal Bphe-*a* concentrations were below the detection limit in only six years. We interpret this period as a time of limited lake mixing, with most years not experiencing complete mixing.

From ~9,900 cal BP to ~8,800 cal BP, erosional input and concentrations of both TChl-*a* and Bphe-*a* decrease, while S and Fe counts are at their highest levels of the record. This suggests the presence of diagenetic iron sulfide formation, a clear indication that the sediments were anoxic and sulfidic during that time (Boyle, 2005). High sulfur concentrations were also found in Lake Łazduny (Sanchini et al., 2020) and Lake Suminko (Poland; Pedziszewska et al., 2015) during a similar time period, and in Lake Hańcza about 2000 years earlier (Lauterbach et al., 2011). The fact that high S deposition in the early Holocene is a common feature of these lakes suggests high S deposition may have been driven by sulfide oxidation in immature post-glacial soils. High availability of iron also enables sulfide formation (Boyle, 2005). Regional records report rising lake levels around 9,500 cal BP (Gałka et al., 2015; Pleskot et al., 2018), which could have caused the depth of the chemocline to increase, leading to lower PSB production (light limitation) despite strong stratification and anoxic bottom-waters.

From ~8,800 cal BP to ~8,050 cal BP Bphe-*a* and TChl-*a* concentrations are very low; yet Bphe-*a* was still detectable, suggesting that the hypolimnion remained anoxic, at least seasonally. Sediments are rich in fine organic detritus and endogenic calcite, with little lithogenic input (low Ti). Low Bphe-*a* in this section could be explained by low productivity overall, which would limit oxygen consumption, possibly shrinking the extent of the anoxic zone.

HPLC pigment measurements in phase 2 show little change from phase 1, and are still classified as PZ-1. The CD/TC ratio was at the lowest level of the record, which is often associated with eutrophic conditions (Swain, 1985; Guilizzoni and Lami, 2003). However, low concentrations of TChl-*a* suggest productivity was not particularly high during this phase. We interpret the low CD/TC ratio as an indication of relative dominance of cyanobacteria, driven by N-limiting conditions that may have occurred due to minimal nutrient recycling in the lake during to stratified conditions and a lack of N-fixing vegetation in the catchment, particularly prior to the establishment of *Alnu*s around 9.0 ka cal BP (Wacnik, 2009a)

Phase 3: 8.0-2.8 ka cal BP

This phase represents the majority of the record and is defined by moderately high TChl-*a* and Bphe-*a,* and very low Mn. This 6,200-year-long phase is characterized by anoxic and moderately productive conditions. The onset of the unit is defined by a drop in Fe and rise in P. Additionally, Ti counts increased at that time, associated with the deposition of several thin lithogenic beds from ~8,050 cal BP to ~6,800 cal BP. Regional records of paleohydrology show conflicting results about whether this period was relatively wet (Wacnik, 2009c; Dobrowolski et al., 2019) or dry (Gałka and Apolinarska, 2014; Gałka et al., 2015; Pleskot et al., 2018). Lower lake levels would have exposed easily eroded shoreline sediments, possibly explaining the higher Ti counts. Alternatively, wetter conditions and increased runoff could have increased catchment erosion.

At ~7,540 cal BP concentrations of Bphe-*a* and TChl-*a* increased. The geochemical data shift from lithotype 2 to lithotype 3, indicating more anoxic and productive conditions. From 7.5 ka cal BP until 2.8 ka cal BP proxies indicate remarkably stable conditions with low erosional input, moderately high primary production, and a strongly stratified water column. A brief period around ~6,840 cal BP is the only major deviation from these stable conditions, with a short-term increase in erosional input and a shift towards more oxic conditions. Lake mixing was generally weak from 7.5 to 2.8 ka cal BP, though brief seasonal mixing events likely did occur to limit PSB production. A close-up figure demonstrates that PSB production was highly seasonal during that time (Fig. 4.5a). Anoxic conditions were also found in Lake Łazduny (Sanchini et al., 2020) and Tiefersee (northern Germany) during the mid-Holocene (Dräger et al., 2017).

The pigment assemblage remains classified as PZ-1, characterized by abundant cyanobacteria-related pigments. Maximal concentrations of β,β-carotene during this phase indicate that total algal productivity was high (Bianchi and Canuel, 2011).

Phase 4: 2.8 ka cal BP - 610 CE

Phase 4 is characterized by the presence of lithotype 4, which is indicative of more frequent complete mixing of the lake. Prior to the deposition of MMD-2 at ~2030 cal BP, lithotype 4 was interbedded with lithotype 3 sediments, and after MMD-2, lithotype 4 became the dominant lithotype. Low Bphe-*a* and spikes in Mn indicate major mixing events that were unprecedented in the record prior to this phase, with enough oxygen in the bottom waters to preserve Mn-oxides (Wirth et al., 2013; Żarczyński et al., 2019b). Two periods of weakened mixing are indicated by peaks in Bphe-*a* from ~2,630 to ~2,520 cal BP and ~2,350 to ~2,200 cal BP.

HPLC measured pigments are classified as PZ-2, with generally lower concentrations, probably driven by reduced preservation associated with oxidation in the water column. This is reflected in relatively low CPI and CD/TC values (Swain, 1985; Buchaca and Catalan, 2008). Additionally, there is evidence (higher PC2 scores) of a shift from cyanobacteria to diatoms and/or chrysophytes.

Phase 5: 610-1610 CE

This phase is characterized by a return to lithotype 3 sediments and consistently high Bphe-*a* concentrations, indicating a strongly stratified water column and sustained anoxia overlapping with the photic zone. The transition to greater PSB production at ~610 CE occurred very rapidly. The seasonal maximum of Bphe-*a* increases from approximately 10 $\mu g/g_{d.w.}$ to a maximum of greater than 100 $\mu g/g_{d.w.}$ within 2 years (Fig. S4.7), suggesting a threshold effect occurred when anoxic and sulfidic conditions reached the photic zone of the lake. However, there are some indications that mixing was already weakening around ~550 CE, when Fe and Mn counts declined, and iron-rich reddish laminae became less frequent, suggesting that oxygenation of the bottom-waters was becoming less frequent. Bphe-*a* was also detected more frequently from ~530-610 CE compared to the previous four centuries. From ~610 to ~1470 CE, only 30 varves contained Bphe-*a* concentrations below the detection limit, suggesting that the lake was likely meromictic for the majority of this period. Interestingly, the Fe/Mn ratio (along with P counts) increased approximately 100 years after Bphe-*a*

increased, possibly because of delayed development of Fe and P saturation in the hypolimnion (Boehrer et al., 2017). Fe/Mn ratios stayed high throughout the remainder of the meromictic period. Ca/Ti ratios and % TIC declined throughout this phase, likely driven by depletion of Ca^{2+} ions in the epilimnion and/or dissolution of calcite in the cold, low-pH, hypolimnion (Wetzel, 2001; Hernández-Almeida et al., 2014). This dissolution would have strengthened the density gradient between hypolimnion and epilimnion and further limited water column mixing. This anoxic period is well-described by Żarczyński et al., (2019) and is associated with a period of reduced human activity and reforestation, as recorded by maximum tree pollen percentages (Fig. 4.8). The timing of this anoxic period is roughly similar to a period of anoxia in Tiefersee (Dräger et al., 2017), and maximum Bphe-*a* production in Lake Łazduny (Sanchini et al., 2020; Fig. 4.7).

After ~1470 CE, Bphe-*a* concentrations dropped below the detection limit with increasing frequency, indicating brief seasonal mixing events. From ~1560 to ~1610 CE, Bphe-*a* concentrations were consistently near or below the detection limit, and decreasing Fe/Mn ratios confirm greater oxygenation of the hypolimnion.

The pigment stratigraphy during this phase is classified as PZ-3 and shows improved preservation (higher CPI values) associated with more anoxic conditions. Assemblages remained similar to the previous phase with relatively high abundances of diatoms and chrysophytes.

Phase 6: 1610 to 2017 CE

The most recent sediments of Lake Żabińskie are mainly lithotype 5, characterized by very high MAR, high counts of erosion indicators Ti, K, Zr, and high TChl-*a* flux. These data, together, indicate major erosional input from the catchment and a shift towards more eutrophic conditions. These changes were associated with major deforestation and intensified agricultural land use surrounding the lake (Fig. 4.7; Wacnik et al., 2016, Żarczyński et al., 2019). Bphe-*a* concentrations were near or below the detection limit in this phase, and Mn counts reached high levels, indicating strengthened seasonal mixing and oxygenation of the hypolimnion.

Two pigment samples were measured in this zone, from ~1870 and 2009 CE, and these samples contain the highest concentrations of most pigments, showing a clear anthropogenic eutrophication effect as has been observed in numerous European lakes (Guilizzoni et al., 2002; Sanchini et al., 2020; Schneider et al., 2018b; Tõnno et al., 2019). Canthaxanthin, echinone, zeaxanthin, lutein, β,β-carotene, and β,ε-carotene were relatively low in the sample from ~1870 CE and increased greatly in the sample from 2009 CE, indicating a community shift towards cyanobacteria. This shift toward cyanobacteria dominance was found in a previous pigment study from Lake Żabińskie focused on the past century (Amann et al., 2014) and has been observed in lakes across the northern hemisphere (Taranu et al., 2015).

4.5 Discussion

4.5.1 Holocene aquatic productivity

Models of nutrient flux from catchment soils to lakes in postglacial landscapes suggest that P fluxes are greatest immediately after deglaciation, and decline exponentially over time (Boyle, 2007; Boyle et al., 2015). High TChl-*a* flux (Fig. S4.3) and high concentrations of carotenoids (Fig. 4.5) during phase 1 of the Lake Żabińskie record (10.8-10.3 ka cal BP) support this notion. However, TChl-*a* flux reached minimum values between 9.0 and 7.0 ka cal BP and then slowly increased to moderately high values from 3.0 ka cal BP to ~1600 CE. In contrast to the HSI-inferred TChl-*a* record, TC concentrations and CD/TC ratios, which have often been used as indicators of trophic levels (Swain, 1985; Guilizzoni and Lami, 2003; Guilizzoni et al., 2011b), suggest more eutrophic conditions prior to 3.3 ka cal BP, and less eutrophic conditions from 2.8 to 0.3 ka cal BP. These discrepancies may be explained by three possible factors: 1) sedimentary carotenoid concentrations are influenced by preservation conditions and anoxia in addition to trophic state (Swain, 1985; Leavitt and Hodgson, 2002); 2) TChl-*a* measurements from HSI may underestimate TChl-*a* concentrations in very dark sediments that occur from 9.9 to 7.5 ka cal BP; 3) nitrogen-limiting conditions may have promoted cyanobacteria dominance (Smith, 1983), particularly during the early Holocene, prior to the establishment of N-fixing plants, such as *Alnus* (established approximately 9.0 ka cal BP; Wacnik, 2009a).

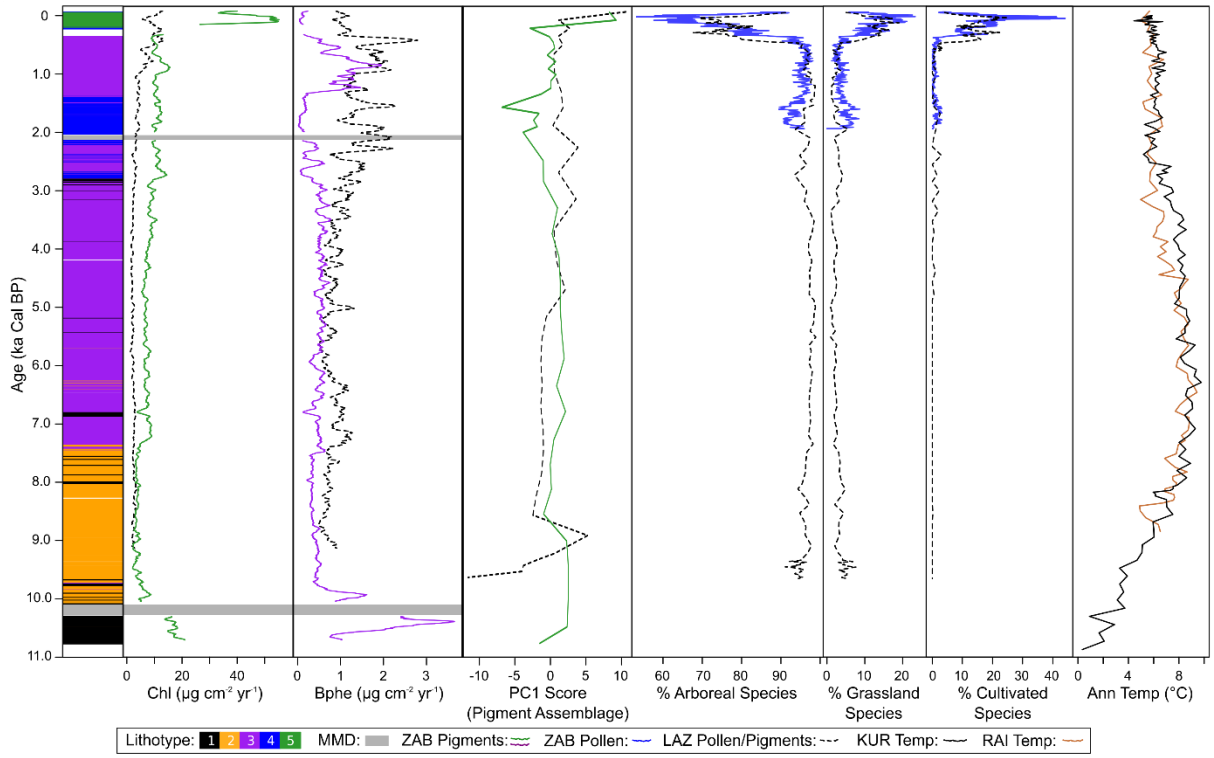

Figure 4.7: Comparison of Lake Żabińskie pigment data with regional data. LAZ = Lake Łazduny data plotted as dashed black lines (Sanchini et al., 2020). KUR = Lake Kurjanovas (Heikkilä and Seppä, 2010). RAI = Lake Raigastvere (Seppä and Poska, 2004). Pigment fluxes in the first two panels are shown as 60-year running means.

Several records in the region confirm an increasing trend in aquatic productivity during the Holocene, for instance, pigments from Lake Łazduny (30 km south of Lake Żabińskie, Sanchini et al., 2020; Fig.

4.7) and Lake Peipsi (Estonia, Tõnno et al., 2019), and biogenic silica data from Lake Suminko (northern Poland, Pedziszewska et al., 2015). Principal component analysis of pigment assemblages from Lake Łazduny revealed broadly similar Holocene trends in pigment assemblages as the Lake Żabińskie record (PC1 of each site is plotted in Fig. 4.7, see also Fig. S4.8), suggesting the patterns seen in Lake Żabińskie may be regionally representative for lakes with similar properties (i.e. small, relatively deep lakes). The trend towards higher productivity over the Holocene in several lakes suggests that ontogenetic processes led to natural eutrophication in these lakes (Fritz and Anderson, 2013). In contrast to the gradual ontogenetic increase in productivity, the effect of cultural eutrophication on Lake Żabińskie was sudden and severe. After ~1720 CE, TChl-*a* flux increased by 300% (Fig. 4.7), and the most recent two HPLC samples from ~1870 and 2009 CE show much higher pigment concentrations than all previous samples, with PC1 scores clearly outside the range of past natural variability. A similar result was obtained from Lake Łazduny pigment data (Fig. 4.7, Fig. S4.8).

4.5.2 Drivers of lake mixing regime

Lake stratification is influenced by a number of factors, such as exposure to wind, summer temperatures, aquatic production, and others (Boehrer and Schultze, 2008). Based on previous work using Fe/Mn ratios to trace oxygenation of Lake Żabińskie during the past 2000 years (Żarczyński et al., 2019b), we hypothesized that vegetative cover was the primary controlling factor of the mixing regime at Lake Żabińskie during the Holocene. Dense forest cover shelters the lake from wind, reducing vertical mixing of the water column. Fig. 4.7 compares the record of anoxia (as indicated by Bphe-*a* flux) in Lake Żabińskie with regional reconstructions of lake productivity, vegetation and temperature. Anoxic phases (high Bphe-*a*) occurred during the warm middle Holocene but also during cooler times in the early Holocene and during the past 2000 years. Anoxic phases tended to occur during times with higher algal production (indicated by TChl-*a* flux), but the relationship did not always hold, for instance during the period from ~1 to 600 CE. The more consistent driver of anoxia appears to be forest cover. Anoxic periods were associated with times of high tree pollen %, while periods with lower tree pollen were associated with greater oxygenation (low Bphe-*a*).

We investigated the relationship between lake stratification and forest cover more closely through selected case studies of periods when the mixing regime changed (Fig. 4.8, Fig. S4.9). The earliest phase of very high Bphe-*a* flux (~10,620-10,380 cal BP) occurred during a time when tree pollen (TP) represented more than 94% of pollen counts (Fig. S4.9). The pollen assemblage was dominated by *Pinus sylvestris* (up to 87%) and *Betula* (up to 22%), indicating that the lake was surrounded by pine dominated forests and pine-birch communities, probably with a greater share of birch on the lake shoreline. This forest, composed of tall trees species, would have shielded the small lake from wind, leading to meromixis.

Annual temperatures at that time were likely cooler than modern, but relatively warm in the summer; a pattern that is driven by the lingering Fennoscandian ice sheet (Stroeven et al., 2016) and high summer insolation (Laskar et al., 2004). Temperature reconstructions from pollen in the Baltic region (Sweden, Finland, Estonia, Latvia) suggest annual temperatures around 10.5 ka cal BP were 2-4 °C cooler than modern conditions, but similar to modern during summer months (Heikkilä and Seppä,

2010; Holmström et al., 2015). Chironomid-based summer temperature reconstructions from Żabieniec peat-bog in central Poland place summer temperatures close to modern values (Kotrys et al., 2019). Warm summers and cold winters create a favorable situation for meromictic conditions because there is less time during the year when the surface waters can be 4-5 °C, the temperature required for the lake to fully mix.

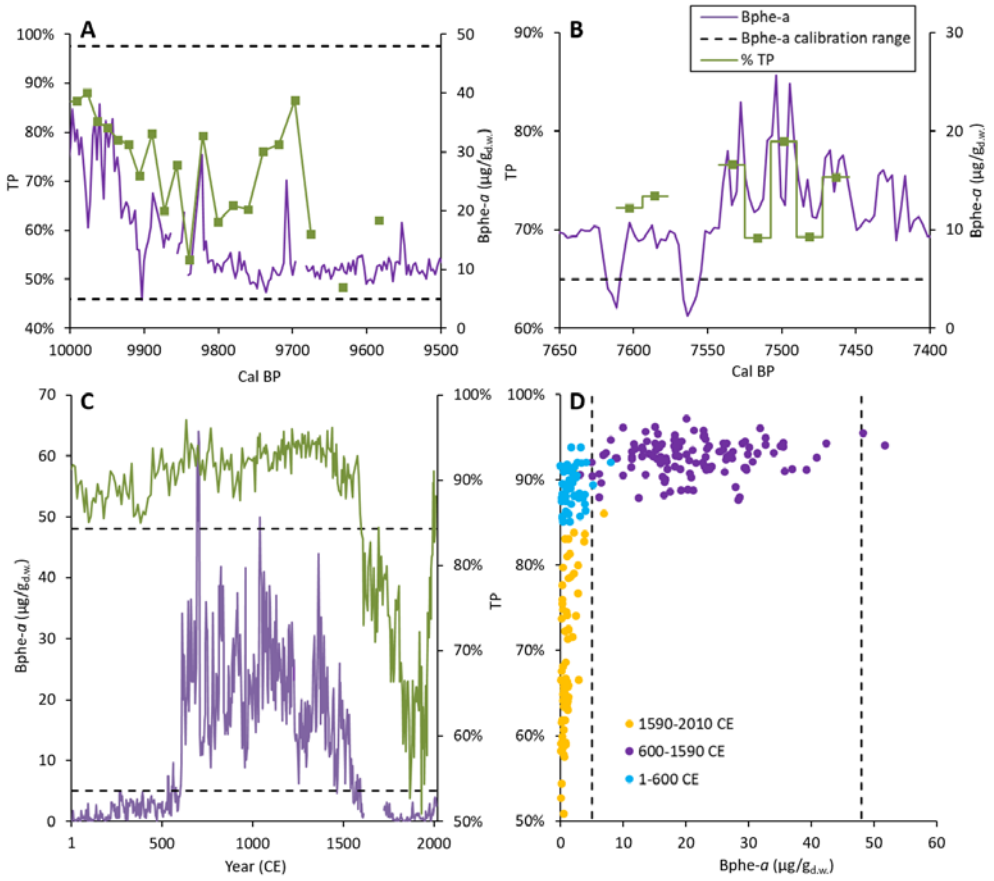

Figure 4.8: A) and B): Case study comparisons of % Tree Pollen (TP) and Bphe-*a*. Bphe-*a* data is 3-year aggregate averages. C) Comparison of % TP and Bphe-*a* during past 2000 years. Bphe-*a* data is 3-year aggregate averages. D) Cross plot of Bphe-*a* and % TP during the past 2000 years, demonstrating that more anoxic conditions occurred when TP% was greater than ~90%. Note that the axis scales change for each panel. Dashed black lines represent the calibration range of Bphe-*a.*

From ~10,000 to ~9,850 cal BP, Bphe-*a* concentrations declined substantially, and TP % decreased from 83% to 51% (Fig. 4.8a, Fig. S4.9). This regional shift in vegetation was driven mainly by *Corylus avellana* expansion and was accompanied by decreasing *Betula* and *Ulmus* after ~9,830 cal BP (Fig. S4.9). The formation of a scrub woodland dominated by hazel near the lake would have allowed more wind shear on the lake surface. Several brief peaks in Bphe-*a* between 9,900 and 9,700 cal BP are associated with short-term increases in TP (Fig. 4.8a), suggesting that lake mixing and plant cover were linked at decadal timescales. The long-term declining trend in Bphe-*a* continued until approximately 8.0 ka cal BP. This period of low Bphe-*a* corresponds with lower % arboreal pollen recorded in the Lake Łazduny sediment record from 8.9 to 7.8 ka cal BP (Fig. 4.7), providing further evidence that enhanced lake mixing, caused by increased wind shear, could have limited PSB production and that this was a regional phenomenon.

A shift toward strengthened stratification and more anoxic conditions occurred at ~7,540 cal BP. A slight shift toward more tree pollen also occurred at that time; however, inter-sample variability was high (Fig. 4.8b). Short-term increases in Bphe-*a* appear to track peaks in % TP between ~7,530 and ~7,460 cal BP, suggesting that the lake mixing regime was sensitive to decadal-scale variations in forest cover.

Proxy data indicate relatively little change in lake mixing regime from 7.5 to 2.8 ka cal BP. Stable, stratified, anoxic conditions promoted growth of PSB. Although the first cereal pollen are recorded in the region around 5,700 cal BP during the Neolithic period, forest cover was not significantly modified by humans at that time (Wacnik, 2009c). Pollen data from Lake Łazduny (Sanchini et al., 2020b) and Lake Miłkowskie (Wacnik, 2009b, 2009c) indicate generally stable and closed forest cover until the middle Bronze Age around 3.4-3.0 ka cal BP. After ~3.4 ka cal BP, agriculture became increasingly important for the economy of local human communities (Wacnik et al., 2012). Changes to forest cover at that time were local and impermanent. Nonetheless, declines in shares of arboreal taxa such as *Corylus*, *Tilia*, *Carpinus*, and *Picea* and increases of light-demanding *Betula* and herbaceous plants show that the forest cover was reduced via small clearings (Wacnik et al., 2012). These changes appear to have affected the mixing regime of Lake Żabińskie, as indicated by declining Bphe-*a* from ~2,960 to ~2,810 cal BP. Forest opening likely led to increased wind shear on the surface of the lake, leading to increased mixing. Pollen counts of cultivated species from Lake Żabińskie confirm human modification of forest cover near the lake by ~2,730 cal BP (Fig. S4.9; no samples were analyzed for pollen from 7.3 to 2.8 ka cal BP, so cultivation may have begun earlier).

A high-resolution pollen dataset for the past two millennia (Żarczyński et al., 2019b) enabled a close investigation of the link between lake mixing and forest cover (Fig. 4.8c, 4.8d). Between ~1 CE and ~540 CE, forest cover was relatively dense (average TP % = 89%). However, the presence of cultivated plants (Fig. 4.7) and charred microparticles provide clear evidence of human impacts to vegetation (Żarczyński et al., 2019b). Bphe-*a* was consistently near or below the detection limit during that time, indicating complete mixing of the lake. Between ~540 and ~610 CE, TP increased from 88% to 97%, and the percentage of cultivated plant pollen declined. Simultaneously, geochemical indicators suggest the lake was mixing less frequently (Fig. 4.8c). Meromictic conditions likely persisted from ~610 to ~1470 CE. During that time TP averaged 96%, and cultivated plant pollen averaged 0.2%. From ~1470 to ~1590 CE, TP declines slightly to 93% and cultivated plant pollen increases to 1.0%. These subtle changes led to a gradual decline in PSB production, with Bphe-*a* concentrations reaching the detection limit in several years, however PSB were clearly present until ~1560 CE, indicating stratified and anoxic conditions.

The percentage of TP decreased rapidly after ~1610 CE, reaching values as low as 53% by ~1870 CE. This strong deforestation of the lake catchment area caused major increases in erosion, and algal production, leading to a major increase in sedimentation rates. Low Fe/Mn ratios and Bphe-*a* concentrations below the detection limit during the past few centuries indicate that seasonal mixing was complete in most years.

In the decades following the Second World War, forests in the Masurian Lakeland have expanded (Wacnik et al., 2012), and this was true around Lake Żabińskie as well (Wacnik et al., 2016). Tree pollen averaged 86% from 1995 to 2010 CE, and a slight increase in Bphe-*a* is visible in the HSI data after ~2000 CE (Fig. 4.8c), but values are still near the detection limit. HPLC measurements also show a slight increase in Bphe-*a* in the most recent sample from 2009 CE compared to samples from ~1870 and ~1730 CE. This evidence, along with increased S concentrations, likely indicate a return to more stratified or anoxic conditions in the past few decades caused by recent afforestation. Limnologic conditions are, however, fundamentally different from conditions prior to human impacts (Hernández-Almeida et al., 2017) and may react to forcing differently. In particular, light penetration is restricted now because of higher epilimnetic productivity, and this may explain the low Bphe-*a* concentrations in the most recent sediments (Fig. 4.5a), despite stratified and anoxic conditions persisting throughout much of the year in modern limnological measurements (Bonk et al., 2015a). Evidence of light limitation for PSB is seen in the seasonal timing of Bphe-*a* in recent years (Bphe is low during spring/summer, and higher during fall/winter; Fig. 4.5a).

Comparisons of the Holocene Bphe-*a* record and vegetation reconstructions point to forest cover as the most important factor controlling stratification of Lake Żabińskie. Fig. 4.8d demonstrates the non-linear relationship between forest cover and Bphe-*a* production, whereby Bphe-*a* concentrations increase dramatically when TP is greater than ~90%. We summarize the occurrence of strongly stratified and anoxic conditions by observing the % of 3-year periods with average Bphe-*a* concentrations above the detection limit (5 $\mu g/g_{d.w.}$). Prior to 2.8 ka, when forests in the region experienced no, or weak, human impacts (Wacnik, 2009b; Karpińska-Kołaczek et al., 2014; Sanchini et al., 2020b), Bphe-*a* was present 97% of the time. From 2.8 ka cal BP to ~610 CE, when localized forest clearing for cultivation occurred (Wacnik, 2009b; Wacnik et al., 2012; Żarczyński et al., 2019), Bphe-*a* was present in only 23% of 3-year periods. During a period of reforestation from ~610 to ~1610 CE (Żarczyński et al., 2019), Bphe-*a* was present again 95% of the time. Since ~1720 CE, after extensive deforestation (Wacnik et al., 2016; Żarczyński et al., 2019b), there have been no 3-year periods with average Bphe-*a* concentrations above the detection limit. A relationship between forest cover and lake mixing has been observed in several small, deep lakes in Europe such as Tiefersee in northern Gemany (Dräger et al., 2017), Lake Łazduny in Poland (Sanchini et al., 2020), Soppensee (Lotter, 2001) and Moossee (Makri et al., 2020) in Switzerland, and Lake Zazari in Greece (Gassner et al., 2020). All of these lakes experienced stratified, anoxic conditions prior to large-scale forest clearing for agricultural expansion (Neolithic, Bronze Age or historic times).

Despite the clear importance of vegetation in controlling lake mixing, climate and lake productivity also likely influence the extent and persistence of anoxia. Low PSB production from 9.5 to 7.4 ka cal BP may have been influenced by low aquatic productivity overall. Additionally, summer temperatures may also be an important driver of lake stratification. In Lake Żabińskie, the prolonged period of high PSB production from 7.4 to 2.8 ka cal BP coincided with maximal Holocene temperatures (Fig. 4.7), and the shift towards more oxic conditions at 2.8 ka cal BP occurred during a grand solar minimum with relatively cool temperatures (Davis et al., 2003; Steinhilber et al., 2009). Additionally, oxic conditions during phase 4 (2.8 ka cal BP - 610 CE) and anoxic conditions during phase 5 (610-1610 CE)

coincided with relatively cool and warm periods, respectively (Luterbacher et al., 2016; Dobrowolski et al., 2019). However, highly resolved local temperature data are lacking prior to 1000 CE. During the last millennium, summer and winter temperature reconstructions from Lake Żabińskie based on chironomids and chrysophytes, respectively, show little relation to variations of Bphe-*a* (Hernández-Almeida et al., 2017). In all likelihood, prolonged stratification of Lake Żabińskie is only possible when minimum levels of summer warmth, primary production and forest density are exceeded.

4.5.3 Methodological advantages

The combination of high-resolution scanning techniques (µ-XRF and HSI) on varved sediments with specific HPLC pigment analysis enabled us to infer changes in past environmental conditions at unprecedented high temporal resolution and obtain detailed information about algal communities. HPLC measurements confirmed our interpretations and calibrations of the RABD indices to pigment concentrations (Fig. S4.6), which is critical for remotely sensed HSI data (Butz et al., 2015; Schneider et al., 2018). We also used HPLC measurements of Bphe-*a* to estimate the limit of detection of Bphe-*a* with the HSI method. This information is essential for interpretation of the HSI record of Bphe-*a*. HPLC techniques enabled us to measure specific pigment compounds that cannot be detected by HSI. By differentiating the chloropigments that make up the bulk absorption band $RABD_{655\text{-}685max}$, we gain insights about pigment preservation, light penetration, and organic matter cycling in the lake (e.g. CPI index, Buchaca and Catalan, 2008; Sanchini and Grosjean, 2020). Specific carotenoid pigments provide information about algal assemblages, making it possible to recognize the important role of cyanobacteria in lake productivity, whereas cyanobacteria are under-represented in the $RABD_{655\text{-}685max}$ index because of their lower chlorophyll production (Swain, 1985; Amann et al., 2014). Low (DDX+DT)/Chl-*a* ratios are indicative of reduced light penetration (Buchaca and Catalan, 2008; Hager, 1980; Riegman and Kraay, 2001). The fact that these ratios are low when Bphe-*a* is highest from ~610-1470 CE provides confirming evidence that PSB production was not driven by improved light penetration, but rather by more anoxic conditions.

Our HSI technique records seasonal-scale variations of Bphe-*a* and TChl-*a* deposition, enabling us to track changing aquatic conditions with unprecedented detail. For instance, we observed a 10-fold increase in seasonal Bphe-*a* concentration within 2 years at ~610 CE (Fig. S4.7). There is no visible change in lithology when the first blooms of PSB occur, so this observation is only made possible by the HSI technique. The HSI data also enabled investigation of the seasonal cycle of Bphe-*a* and TChl-*a* deposition. We find that seasonal maxima of Bphe-*a* typically occur simultaneously with maxima of TChl-*a* (Fig. 4.5c, d, e; Fig. S4.7). Both pigment groups usually peak immediately below (prior to) white calcite layers, indicating maximum PSB and phytoplankton production occurred in spring or early summer. However, during the most recent ~25 years, Bphe-*a* peaks were offset from TChl-*a* peaks and occur after calcite precipitation (Fig. 4.5a). This pattern is likely explained by reduced light availability caused by eutrophication in modern times. Suitable conditions for PSB now only occur during late summer when epilimnetic production is limited by low nutrient concentrations under strong lake stratification (Bonk et al., 2015a). An additional benefit of the HSI technique is that HSI

measurements of TChl-*a* appear to be less affected by preservation problems than HPLC measurements of specific pigments.

4.6 Conclusions and outlook

The use of hyperspectral imaging to quantify pigments in the varved sedimentary record of Lake Żabińskie enabled us to reconstruct changes in algal productivity and lake mixing at sub-annual resolution throughout the past 10,800 years. The combination of high-resolution, non-specific pigment measurements with low-resolution ,specific HPLC measurements strengthens our interpretation of the record. Bacteriopheopigments were used as an indicator of purple sulfur bacteria, which are indicative of anoxic conditions within the photic zone. We find that anoxia and a stratified water column persisted through the majority of the Holocene. Prior to 2.8 ka cal BP, Bphe-*a* concentrations were above the detection limit in ~97% of 3-year averages. After 2.8 ka cal BP the lake mixing regime alternated between periods of enhanced mixing and periods of strengthened stratification. Permanent anoxia and high PSB production persisted from ~610 to 1470 CE, concurrent with a reforestation period. During the past few centuries, forest clearing and increased agricultural land use have led to greater algal production, but also greater oxygenation of the water column. Through comparisons with other proxy data from our site and the region, we investigated how external drivers impact lake productivity and mixing regime. We found that the primary control on lake mixing is the density of forest cover surrounding the lake. However, temperature (mainly in summer) and lake productivity could also influence the extent and persistence of anoxia. We showed evidence of linkages between forest cover and lake mixing related to both anthropogenic (Bronze Age and later) and natural vegetation changes (Early and Middle Holocene). Changes to lake mixing occurred simultaneously with changes in forest cover.

This study shows the potential of HSI studies on sediment cores for inferring past environmental change at sub-annual resolution. Future studies can utilize this approach to investigate rates of change, regime shifts, and other questions that require datasets with very high resolution. We advocate for application of HSI pigment measurements in combination with HPLC techniques for long-term paleolimnological studies to understand short-term variability in limnological conditions and to gain a more complete understanding of changes in aquatic ecosystems and their catchments.

4.7 Acknowledgements

This project was funded by Swiss National Science Foundation grant 200021_172586, and Polish National Science Centre grant 2014/13/B/ST10/01311. The work of AW was additionally supported by the Statutory Research Tasks of the W. Szafer Institute of Botany (PAS). We thank Sönke Szidat, Gary Salazar, Edith Vogel, Ron Lloren, Irene Brunner, Stamatina Makri, Linus Rösler, Petra Boltshauser-Kaltenrieder, and Daniela Fisher for their contributions to this study.

Data Availability

Data produced for this project is publicly available at the Bern Open Repository and Information System (DOI: 10.7892/boris.147848).

4.8 References

Amann, B., Lobsiger, S., Fischer, D., Tylmann, W., Bonk, A., Filipiak, J., Grosjean, M., 2014. Spring temperature variability and eutrophication history inferred from sedimentary pigments in the varved sediments of Lake Żabińskie, north-eastern Poland, AD 1907-2008. Glob. Planet. Change 123, 86-96. https://doi.org/10.1016/j.gloplacha.2014.10.008

Bennett, K.D., 1996. Determination of the number of zones in a biostratigraphical sequence. New Phytol. 132, 155-170. https://doi.org/10.1111/j.1469-8137.1996.tb04521.x

Bennion, H., Battarbee, R.W., Sayer, C.D., Simpson, G.L., Davidson, T.A., 2011. Defining reference conditions and restoration targets for lake ecosystems using palaeolimnology: A synthesis. J. Paleolimnol. 45, 533-544. https://doi.org/10.1007/s10933-010-9419-3

Bianchi, T.S., Canuel, E.A., 2011. Chemical biomarkers in aquatic ecosystems. Princeton University Press.

Boehrer, B., Schultze, M., 2008. Stratification of lakes. Rev. Geophys. 46, 1-27. https://doi.org/10.1029/2006RG000210

Boehrer, B., von Rohden, C., Schultze, M., 2017. Physical Features of Meromictic Lakes: Stratification and Circulation, in: Gulati, R.D., Zadereev, E.S., Degermendzhi, A.G. (Eds.), Ecology of Meromictic Lakes. Springer International Publishing, pp. 15-34. https://doi.org/10.1007/978-3-319-49143-1_2

Bonk, A., Kinder, M., Enters, D., Grosjean, M., Meyer-Jacob, C., Tylmann, W., 2016. Sedimentological and geochemical responses of Lake Żabińskie (north-eastern Poland) to erosion changes during the last millennium. J. Paleolimnol. 56, 239-252. https://doi.org/10.1007/s10933-016-9910-6

Bonk, A., Tylmann, W., Amann, B., Enters, D., Grosjean, M., 2015a. Modern limnology and varve-formation processes in lake Żabińskie, northeastern Poland: Comprehensive process studies as a key to understand the sediment record. J. Limnol. 74, 358-370. https://doi.org/10.4081/jlimnol.2014.1117

Bonk, A., Tylmann, W., Goslar, T., Wacnik, A., Grosjean, M., 2015b. Comparing varve counting and ^{14}C-Ams chronologies in the sediments of Lake Żabińskie, Northeastern Poland: Implications for accurate ^{14}C dating of lake sediments. Geochronometria 42, 157-171. https://doi.org/10.1515/geochr-2015-0019

Boyle, J.F., 2007. Loss of apatite caused irreversible early-Holocene lake acidification. Holocene. https://doi.org/10.1177/0959683607077046

Boyle, J.F., 2005. Inorganic Geochemical Methods in Palaeolimnology, in: Tracking Environmental Change Using Lake Sediments. Kluwer Academic Publishers, pp. 83-141. https://doi.org/10.1007/0-306-47670-3_5

Boyle, J.F., Chiverrell, R.C., Davies, H., Alderson, D.M., 2015. An approach to modelling the impact of prehistoric farming on Holocene landscape phosphorus dynamics. Holocene. https://doi.org/10.1177/0959683614556381

Bronk Ramsey, C., 2009. Bayesian Analysis of Radiocarbon Dates. Radiocarbon 51, 337-360. https://doi.org/10.1017/s0033822200033865

Bronk Ramsey, C., 2008. Deposition models for chronological records. Quat. Sci. Rev. 27, 42-60. https://doi.org/10.1016/j.quascirev.2007.01.019

Bronk Ramsey, C., Lee, S., 2013. Recent and Planned Developments of the Program OxCal. Radiocarbon 55, 720-730. https://doi.org/10.1017/s0033822200057878

Buchaca, T., Catalan, J., 2008. On the contribution of phytoplankton and benthic biofilms to the sediment record of marker pigments in high mountain lakes. J. Paleolimnol. 40, 369-383. https://doi.org/10.1007/s10933-007-9167-1

Butz, C., Grosjean, M., Fischer, D., Wunderle, S., Tylmann, W., Rein, B., 2015. Hyperspectral imaging spectroscopy: a promising method for the biogeochemical analysis of lake sediments. J. Appl. Remote Sens. 9, 096031. https://doi.org/10.1117/1.jrs.9.096031

Butz, C., Grosjean, M., Goslar, T., Tylmann, W., 2017. Hyperspectral imaging of sedimentary bacterial pigments: a 1700-year history of meromixis from varved Lake Jaczno, northeast Poland. J. Paleolimnol. 58, 57-72. https://doi.org/10.1007/s10933-017-9955-1

Carpenter, S.R., 2005. Eutrophication of aquatic ecosystems: Bistability and soil phosphorus. Proc. Natl. Acad. Sci. U. S. A. 102, 10002-10005. https://doi.org/10.1073/pnas.0503959102

Clerk, S., Hall, R., Quinlan, R., Smol, J.P., 2000. Quantitative inferences of past hypolimnetic anoxia and nutrient levels from a Canadian Precambrian Shield lake. J. Paleolimnol. 23, 319-336. https://doi.org/10.1023/A:1008147127606

Davies, S.J., Lamb, H.F., Roberts, S.J., 2015. Micro-XRF Core Scanning in Palaeolimnology: Recent Developments. https://doi.org/10.1007/978-94-017-9849-5_7

Davis, B.A.S., Brewer, S., Stevenson, A.C., et al., 2003. The temperature of Europe during the Holocene reconstructed from pollen data. Quat. Sci. Rev. 22, 1701-1716. https://doi.org/10.1016/S0277-3791(03)00173-2

Dobrowolski, R., Mazurek, M., Osadowski, Z., Alexandrowicz, W.P., Pidek, I.A., Pazdur, A., Piotrowska, N., Drzymulska, D., Urban, D., 2019. Holocene environmental changes in northern Poland recorded in alkaline spring-fed fen deposits - A multi-proxy approach. Quat. Sci. Rev. 219, 236-262. https://doi.org/10.1016/j.quascirev.2019.05.027

Dräger, N., Theuerkauf, M., Szeroczyńska, K., Wulf, S., Tjallingii, R., Plessen, B., Kienel, U., Brauer, A., 2017. Varve microfacies and varve preservation record of climate change and human impact for the last 6000 years at Lake Tiefer See (NE Germany). Holocene 27, 450-464. https://doi.org/10.1177/0959683616660173

Fiedor, J., Fiedor, L., Kammhuber, N., Scherz, A., Scheer, H., 2002. Photodynamics of the Bacteriochlorophyll-Carotenoid System. 2. Influence of Central Metal, Solvent and β-Carotene on Photobleaching of Bacteriochlorophyll Derivatives. Photochem. Photobiol. 76, 145. https://doi.org/10.1562/0031-8655(2002)0760145POTBCS2.0.CO2

Friedrich, J., Janssen, F., Aleynik, D., et al., 2014. Investigating hypoxia in aquatic environments: Diverse approaches to addressing a complex phenomenon. Biogeosciences 11, 1215-1259. https://doi.org/10.5194/bg-11-1215-2014

Fritz, S.C., Anderson, N.J., 2013. The relative influences of climate and catchment processes on Holocene lake development in glaciated regions. J. Paleolimnol. 49, 349-362. https://doi.org/10.1007/s10933-013-9684-z

Gałka, M., Apolinarska, K., 2014. Climate change, vegetation development, and lake level fluctuations in Lake Purwin (NE Poland) during the last 8600 cal. BP based on a high-resolution plant macrofossil record and stable isotope data (δ13C and δ18O). Quat. Int. 328-329, 213-225. https://doi.org/10.1016/j.quaint.2013.12.030

Gałka, M., Tobolski, K., Bubak, I., 2015. Late Glacial and Early Holocene lake level fluctuations in NE Poland tracked by macro-fossil, pollen and diatom records. Quat. Int. 388, 23-38. https://doi.org/10.1016/j.quaint.2014.03.009

Gassner, S., Gobet, E., Schwörer, C., et al., 2020. 20,000 years of interactions between climate, vegetation and land use in Northern Greece. Veg. Hist. Archaeobot. https://doi.org/10.1007/s00334-019-00734-5

Guilizzoni, P., Lami, A., 2003. Paleolimnology: Use of Algal Pigments as Indicators, in: Encyclopedia of Environmental Microbiology. John Wiley & Sons, Inc. https://doi.org/10.1002/0471263397.env313

Guilizzoni, P., Lami, A., Marchetto, A., Jones, V., Manca, M., Bettinetti, R., 2002. Palaeoproductivity and environmental changes during the Holocene in central Italy as recorded in two crater lakes (Albano and Nemi). Quat. Int. 88, 57-68. https://doi.org/10.1016/S1040-6182(01)00073-8

Guilizzoni, P., Marchetto, A., Lami, A., Gerli, S., Musazzi, S., 2011. Use of sedimentary pigments to infer past phosphorus concentration in lakes. J. Paleolimnol. 45, 433-445. https://doi.org/10.1007/s10933-010-9421-9

Hall, R.I., Smol, John P., 1999. Diatoms as indicators of lake eutrophication, in: Stoermer, E.F., Smol, J.P. (Eds.), The Diatoms: Applications for the Environmental and Earth Sciences, Second Edition. Cambridge University Press, Cambridge, UK, pp. 128-168. https://doi.org/10.1017/CBO9780511763175.008

Heikkilä, M., Seppä, H., 2010. Holocene climate dynamics in Latvia, eastern Baltic region: A pollen-based summer temperature reconstruction and regional comparison. Boreas 39, 705-719. https://doi.org/10.1111/j.1502-3885.2010.00164.x

Heiri, O., Lotter, A.F., Lemcke, G., 2001. Loss on ignition as a method for estimating organic and carbonate content in sediments: Reproducibility and comparability of results. J. Paleolimnol. https://doi.org/10.1023/A:1008119611481

Hernández-Almeida, I., Grosjean, M., Gómez-Navarro, J.J., et al., 2017. Resilience, rapid transitions and regime shifts: Fingerprinting the responses of Lake Żabińskie (NE Poland) to climate variability and human disturbance since AD 1000. Holocene 27, 258-270. https://doi.org/10.1177/0959683616658529

Hernández-Almeida, I., Grosjean, M., Tylmann, W., Bonk, A., 2014. Chrysophyte cyst-inferred variability of warm season lake water chemistry and climate in northern Poland: training set and downcore reconstruction. J. Paleolimnol. 53, 123-138. https://doi.org/10.1007/s10933-014-9812-4

Holmström, L., Ilvonen, L., Seppä, H., Veski, S., 2015. A Bayesian spatiotemporal model for reconstructing climate from multiple pollen records. Ann. Appl. Stat. 9, 1194-1225. https://doi.org/10.1214/15-AOAS832

Jeffrey, S.W., Humphrey, G.F., 1975. New spectrophotometric equations for determining chlorophylls a, b, c1 and c2 in higher plants, algae and natural phytoplankton. Biochem. und Physiol. der Pflanz. https://doi.org/10.1016/s0015-3796(17)30778-3

Jenny, J.P., Arnaud, F., Dorioz, J.M., et al., 2013. A spatiotemporal investigation of varved sediments highlights the dynamics of hypolimnetic hypoxia in a large hard-water lake over the last 150 years. Limnol. Oceanogr. 58, 1395-1408. https://doi.org/10.4319/lo.2013.58.4.1395

Jenny, J.P., Francus, P., Normandeau, A., Lapointe, F., Perga, M.E., Ojala, A., Schimmelmann, A., Zolitschka, B., 2016. Global spread of hypoxia in freshwater ecosystems during the last three centuries is caused by rising local human pressure. Glob. Chang. Biol. 22, 1481-1489. https://doi.org/10.1111/gcb.13193

Juggins, S., 2017. rioja: Analysis of Quaternary Science Data, R package version (0.9-21).

Karpińska-Kołaczek, M., Kołaczek, P., Stachowicz-Rybka, R., 2014. Pathways of woodland succession under low human impact during the last 13,000 years in northeastern Poland. Quat. Int. 328-329, 196-212. https://doi.org/10.1016/j.quaint.2013.11.038

Kassambara, A., Mundt, F., 2017. factoextra: Extract and Visualize the Results of Multivariate Data Analyses. R package version 1.0.5.

Kinder, M., Wulf, S., Appelt, O., Hardiman, M., Żarczyński, M., Tylmann, W., 2020. Late-Holocene ultra-distal cryptotephra discoveries in varved sediments of Lake Żabińskie, NE Poland. J. Volcanol. Geotherm. Res. 402, 106988. https://doi.org/10.1016/j.jvolgeores.2020.106988

Kotrys, B., Płóciennik, M., Sydor, P., Brooks, S.J., 2019. Expanding the Swiss-Norwegian chironomid training set with Polish data. Boreas. https://doi.org/10.1111/bor.12406

Laskar, J., Robutel, P., Joutel, F., Gastineau, M., Correia, A.C.M., Levrard, B., 2004. A long-term numerical solution for the insolation quantities of the Earth. Astron. Astrophys. 428, 261-285. https://doi.org/10.1051/0004-6361:20041335

Lauterbach, S., Brauer, A., Andersen, N., et al., 2011. Multi-proxy evidence for early to mid-Holocene environmental and climatic changes in northeastern Poland. Boreas 40, 57-72. https://doi.org/10.1111/j.1502-3885.2010.00159.x

Leavitt, P.R., Hodgson, D.A., 2002. Sedimentary Pigments, in: Tracking Environmental Change Using Lake Sediments. Springer, Dordrecht, pp. 295-325. https://doi.org/10.1007/0-306-47668-1_15

Lotter, A.F., 2001. The palaeolimnology of Soppensee (Central Switzerland), as evidenced by diatom, pollen, and fossil-pigment analyses. J. Paleolimnol. 25, 65-79. https://doi.org/10.1023/A:1008140122230

Luoto, T.P., Kotrys, B., Płóciennik, M., 2019. East European chironomid-based calibration model for past summer temperature reconstructions. Clim. Res. 77, 63-76. https://doi.org/10.3354/cr01543

Luterbacher, J., Werner, J.P., Smerdon, J.E., et al., 2016. European summer temperatures since Roman times. Environ. Res. Lett. https://doi.org/10.1088/1748-9326/11/2/024001

Mackereth, F.J.H., 1966. Some chemical observations on post-glacial lake sediments. Philos. Trans. R. Soc. Lond. B. Biol. Sci. 250, 165-213. https://doi.org/10.1098/rstb.1966.0001

Makri, S., Rey, F., Gobet, E., Gilli, A., Tinner, W., Grosjean, M., 2020. Early human impact in a 15,000-year high-resolution hyperspectral imaging record of paleoproduction and anoxia from a varved lake in Switzerland. Quat. Sci. Rev. 239, 106335. https://doi.org/10.1016/j.quascirev.2020.106335

Meyers, P.A., 2006. An Overview of sediment organic matter records of human eutrophication in the Laurentian Great Lakes region, in: The Interactions Between Sediments and Water. Springer Netherlands, pp. 89-99. https://doi.org/10.1007/978-1-4020-5478-5_10

Mills, K., Schillereff, D., Saulnier-Talbot, É., et al., 2017. Deciphering long-term records of natural variability and human impact as recorded in lake sediments: a palaeolimnological puzzle. Wiley Interdiscip. Rev. Water 4, e1195. https://doi.org/10.1002/wat2.1195

Naeher, S., Gilli, A., North, R.P., Hamann, Y., Schubert, C.J., 2013. Tracing bottom water oxygenation with sedimentary Mn/Fe ratios in Lake Zurich, Switzerland. Chem. Geol. 352, 125-133. https://doi.org/10.1016/j.chemgeo.2013.06.006

Pedziszewska, A., Tylmann, W., Witak, M., Piotrowska, N., Maciejewska, E., Latałowa, M., 2015. Holocene environmental changes reflected by pollen, diatoms, and geochemistry of annually laminated sediments of Lake Suminko in the Kashubian Lake District (N Poland). Rev. Palaeobot. Palynol. 216, 55-75. https://doi.org/10.1016/j.revpalbo.2015.01.008

Pleskot, K., Tjallingii, R., Makohonienko, M., Nowaczyk, N., Szczuciński, W., 2018. Holocene paleohydrological reconstruction of Lake Strzeszyńskie (western Poland) and its implications for the central European climatic transition zone. J. Paleolimnol. 59, 443-459. https://doi.org/10.1007/s10933-017-9999-2

R Core Team, 2019. R: A Language and Environment for Statistical Computing. Vienna, Austria.

Rein, B., Sirocko, F., 2002. In-situ reflectance spectroscopy - Analysing techniques for high-resolution pigment logging in sediment cores. Int. J. Earth Sci. 91, 950-954. https://doi.org/10.1007/s00531-002-0264-0

Richter, T.O., Van Der Gaast, S., Koster, B., Vaars, A., Gieles, R., De Stigter, H.C., De Haas, H., Van Weering, T.C.E., 2006. The Avaatech XRF Core Scanner: Technical description and applications to NE Atlantic sediments. Geol. Soc. Spec. Publ. 267, 39-50. https://doi.org/10.1144/GSL.SP.2006.267.01.03

Rinterknecht, V.R., Marks, L., Piotrowski, J.A., Raisbeck, G.M., Yiou, F., Brook, E.J., Clark, P.U., 2005. Cosmogenic 10Be ages on the Pomeranian Moraine, Poland. Boreas 34, 186-191. https://doi.org/10.1111/j.1502-3885.2005.tb01014.x

Sanchini, A., Grosjean, M., 2020. Quantification of chlorophyll a, chlorophyll b and pheopigments a in lake sediments through deconvolution of bulk UV-VIS absorption spectra. J. Paleolimnol. 64, 243-256. https://doi.org/10.1007/s10933-020-00135-z

Sanchini, A., Szidat, S., Tylmann, W., Vogel, H., Wacnik, A., Grosjean, M., 2020. A Holocene high-resolution record of aquatic productivity, seasonal anoxia and meromixis from varved sediments of Lake Łazduny, North-Eastern Poland: insight from a novel multi-proxy approach. J. Quat. Sci. 35, 1070-1080. https://doi.org/10.1002/jqs.3242.

Schelske, C.L., Hodell, D.A., 1995. Using carbon isotopes of bulk sedimentary organic matter to reconstruct the history of nutrient loading and eutrophication in Lake Erie. Limnol. Oceanogr. 40, 918-929. https://doi.org/10.4319/lo.1995.40.5.0918

Schneider, T., Rimer, D., Butz, C., Grosjean, M., 2018. A high-resolution pigment and productivity record from the varved Ponte Tresa basin (Lake Lugano, Switzerland) since 1919: insight from an approach that combines hyperspectral imaging and high-performance liquid chromatography. J. Paleolimnol. 60, 381-398. https://doi.org/10.1007/s10933-018-0028-x

Seppä, H., Poska, A., 2004. Holocene annual mean temperature changes in Estonia and their relationship to solar insolation and atmospheric circulation patterns. Quat. Res. 61, 22-31. https://doi.org/10.1016/j.yqres.2003.08.005

Sinninghe Damsté, J.S., Schouten, S., 2006. Biological markers for anoxia in the photic zone of the water column. Handb. Environ. Chem. Vol. 2 React. Process. 2 N, 127-163. https://doi.org/10.1007/698_2_005

Smith, V.H., 2003. Eutrophication of freshwater and coastal marine ecosystems: A global problem. Environ. Sci. Pollut. Res. https://doi.org/10.1065/espr2002.12.142

Smith, V.H., 1983. Low nitrogen to phosphorus ratios favor dominance by blue-green algae in lake phytoplankton. Science (80-.). 221, 669-671. https://doi.org/10.1126/science.221.4611.669

Steinhilber, F., Beer, J., Fröhlich, C., 2009. Total solar irradiance during the Holocene. Geophys. Res. Lett. 36, 1-5. https://doi.org/10.1029/2009GL040142

Street-Perrott, F.A., Holmes, J.A., Robertson, I., Ficken, K.J., Koff, T., Loader, N.J., Marshall, J.D., Martma, T., 2018. The Holocene isotopic record of aquatic cellulose from Lake Äntu Sinijärv, Estonia: Influence of changing climate and organic-matter sources. Quat. Sci. Rev. 193, 68-83. https://doi.org/10.1016/j.quascirev.2018.05.010

Stroeven, A.P., Hättestrand, C., Kleman, J., et al., 2016. Deglaciation of Fennoscandia. Quat. Sci. Rev. https://doi.org/10.1016/j.quascirev.2015.09.016

Swain, E.B., 1985. Measurement and interpretation of sedimentary pigments. Freshw. Biol. 15, 53-75. https://doi.org/10.1111/j.1365-2427.1985.tb00696.x

Szumański, A., 2000. Objaśnienia do Szczegółowej Mapy Geologicznej Polski, Arkusz Giżycko, (Explanation to the Detailed Geological Map of Poland, Sheet Gizycko (104)). Warsaw, Poland.

Talbot, M.R., 2005. Nitrogen Isotopes in Palaeolimnology, in: Tracking Environmental Change Using Lake Sediments. Kluwer Academic Publishers, pp. 401-439. https://doi.org/10.1007/0-306-47670-3_15

Taranu, Z.E., Gregory-Eaves, I., Leavitt, P.R., et al., 2015. Acceleration of cyanobacterial dominance in north temperate-subarctic lakes during the Anthropocene. Ecol. Lett. 18, 375-384. https://doi.org/10.1111/ele.12420

Tõnno, I., Nauts, K., Belle, S., Nõmm, M., Freiberg, R., Kõiv, T., Alliksaar, T., 2019. Holocene shifts in the primary producer community of large, shallow European Lake Peipsi, inferred from sediment pigment analysis. J. Paleolimnol. 61, 403-417. https://doi.org/10.1007/s10933-019-00067-3

Tóth, M., Magyari, E.K., Buczkó, K., Braun, M., Panagiotopoulos, K., Heiri, O., 2015. Chironomid-inferred Holocene temperature changes in the South Carpathians (Romania). Holocene 25, 569-582. https://doi.org/10.1177/0959683614565953

Tu, L., Zander, P., Szidat, S., Lloren, R., Grosjean, M., 2020. The influences of historic lake trophy and mixing regime changes on long-term phosphorus fractions retention in sediments of deep, eutrophic lakes: a case study from Lake Burgäschi, Switzerland. Biogeosciences 17, 2715-2729. https://doi.org/10.5194/bg-2019-389

Tylmann, W., Bonk, A., Goslar, T., Wulf, S., Grosjean, M., 2016. Calibrating 210 Pb dating results with varve chronology and independent chronostratigraphic markers: Problems and implications. Quat. Geochronol. 32, 1-10. https://doi.org/10.1016/j.quageo.2015.11.004

Ursenbacher, S., Stötter, T., Heiri, O., 2020. Chitinous aquatic invertebrate assemblages in Quaternary lake sediments as indicators of past deepwater oxygen concentration. Quat. Sci. Rev. 231, 106203. https://doi.org/10.1016/j.quascirev.2020.106203

Van Gemerden, H., Mas, J., 1995. Ecology of phototrophic sulfur bacteria, in: Anoxygenic Photosynthetic Bacteria. Springer, Dordrecht, pp. 49-85. https://doi.org/10.1007/0-306-47954-0

Wacnik, A., 2009a. Vegetation development in the Lake Miłkowskie area, north-eastern Poland, from the Plenivistulian to the late Holocene. Acta Palaeobot. 49, 287-335.

Wacnik, A., 2009b. From foraging to farming in the Great Mazurian Lake District: Palynological studies on Lake Miłkowskie sediments, northeast Poland. Veg. Hist. Archaeobot. 18, 187-203. https://doi.org/10.1007/s00334-008-0196-0

Wacnik, A., Goslar, T., Czernik, J., 2012. Vegetation changes caused by agricultural societies in the Great Mazurian Lake District. Acta Palaeobot. 52, 59-104.

Wacnik, A., Tylmann, W., Bonk, A., Goslar, T., Enters, D., Meyer-Jacob, C., Grosjean, M., 2016. Determining the responses of vegetation to natural processes and human impacts in north-eastern Poland during the last millennium: combined pollen, geochemical and historical data. Veg. Hist. Archaeobot. 25, 479-498. https://doi.org/10.1007/s00334-016-0565-z

Wetzel, R.G., 2001. Limnology: Lake and River Ecosystems, third ed. Academic Press, San Diego, CA, USA. https://doi.org/10.1046/j.1529-8817.2001.37602.x

Wetzel, R.G., Likens, G.E., Wetzel, R.G., Likens, G.E., 1991. Lake Basin Characteristics and Morphometry, in: Limnological Analyses. Springer New York, pp. 1-14. https://doi.org/10.1007/978-1-4757-4098-1_1

Wickham, H., 2016. ggplot2: Elegant Graphics for Data Analysis.

Wirth, S.B., Gilli, A., Niemann, H., et al., 2013. Combining sedimentological, trace metal (Mn, Mo) and molecular evidence for reconstructing past water-column redox conditions: The example of meromictic Lake Cadagno (Swiss Alps). Geochim. Cosmochim. Acta 120, 220-238. https://doi.org/10.1016/j.gca.2013.06.017

Wolfe, A.P., Vinebrooke, R.D., Michelutti, N., Rivard, B., Das, B., 2006. Experimental calibration of lake-sediment spectral reflectance to chlorophyll a concentrations: Methodology and paleolimnological validation. J. Paleolimnol. https://doi.org/10.1007/s10933-006-0006-6

Woolway, R.I., Merchant, C.J., 2019. Worldwide alteration of lake mixing regimes in response to climate change. Nat. Geosci. 12, 271-276. https://doi.org/10.1038/s41561-019-0322-x

Zander, P.D., Szidat, S., Kaufman, D.S., Żarczyński, M., Poraj-Górska, A.I., Boltshauser-Kaltenrieder, P., Grosjean, M., 2020. Miniature radiocarbon measurements (< 150µgC) from sediments of Lake Żabińskie, Poland: effect of precision and dating density on age-depth models. Geochronology 2, 63-79. https://doi.org/10.5194/gchron-2-63-2020

Żarczyński, M., Tylmann, W., Goslar, T., 2018. Multiple varve chronologies for the last 2000 years from the sediments of Lake Żabińskie (northeastern Poland) - Comparison of strategies for varve counting and uncertainty estimations. Quat. Geochronol. 47, 107-119. https://doi.org/10.1016/j.quageo.2018.06.001

Żarczyński, M., Wacnik, A., Tylmann, W., 2019. Tracing lake mixing and oxygenation regime using the Fe/Mn ratio in varved sediments: 2000 year-long record of human-induced changes from Lake Żabińskie (NE Poland). Sci. Total Environ. 657, 585-596. https://doi.org/10.1016/j.scitotenv.2018.12.078

Zeileis, A., Grothendieck, G., 2005. Zoo: S3 infrastructure for regular and irregular time series. J. Stat. Softw. https://doi.org/10.18637/jss.v014.i06

Zolitschka, B., Francus, P., Ojala, A.E.K., Schimmelmann, A., 2015. Varves in lake sediments - a review. Quat. Sci. Rev. 117, 1-41. https://doi.org/10.1016/j.quascirev.2015.03.019

4.9 Supplementary material

4.9.1 Geochronological information

Geochronological methods

The chronology used in this study is a composite of previously published data, and newly generated age-depth models (Fig. S4.1 and S4.2). Żarczyński et al. (2018) presented a varve chronology for the past 2000 years, which represents the upper 6.3 m of the composite sequence. Of these 6.3 m, 1.4 m of our composite sequence uses the same core material as in Żarczyński et al., 2018. For the remaining core sections, varve counts were transposed to correlated sections using distinct stratigraphic markers, or in some sections, new varve counts were performed. We added an error term of ± 3 years to the original uncertainty in sections where varve counts were transposed to correlated core segments.

A MMD (mass movement deposit) from 7.3 to 6.3 m made it impossible to link varve counts below this depth to the varve chronology of the uppermost 6.3 m. Therefore, the chronology below this MMD is based on radiocarbon ages, which are further constrained by varve counts in some sections. The chronology from 13.1-7.3 m (~2100-6800 cal BP) was established by Zander et al., (2020) as part of a study assessing the use of miniature radiocarbon samples to date lake sediments. In that study, a floating varve chronology was combined with 48 ^{14}C ages using an Oxcal V-sequence age-depth modelling routine (Bronk Ramsey, 2009, 2008; Bronk Ramsey and Lee, 2013, Reimer et al., 2013). The V-sequence uses floating varve counts between dated levels, input as “Gaps”, to constrain the error range of calibrated ^{14}C ages. This method is described in more detail in Zander et al., 2020.

The chronology for 19.4-13.1 m is primarily based on radiocarbon ages and has not been published previously. Eighteen samples were measured for ^{14}C at the Laboratory for the Analysis of Radiocarbon with AMS at the University of Bern. Sample material was obtained from sieving 1-2-cm-thick slices of sediment, and terrestrial plant macrofossils were taxonomically identified and kept for measurement. Detailed information about the radiocarbon sample preparation can be found in Zander et al., 2020. MMD-1 (18.0-17.0 m depth) was removed from the chronology, and the two radiocarbon samples taken from this interval were excluded (Fig. S4.1). Above the MMD, two radiocarbon ages provided conflicting ages at 16.84 and 16.95 m; neither age could be dismissed as an outlier. To further constrain the age-depth relation in this section, we counted varves from 16.4 m to the top of the MMD

at 17.0 m. We used OxCal (Bronk Ramsey, 2009, 2008; Bronk Ramsey and Lee, 2013) to generate an age-depth relation which links two P-sequences (16.4-13.1 m, and 19.4-18.0 m) with a V-sequence from 17.0-16.4 m (the MMD from 18.0-17.0 m is excluded from age-depth modeling). The top of the lower P-sequence (18.0 m, bottom of MMD-1) is constrained to be equal in age or older than the bottom of the V-sequence (17.0 m, top of MMD-1), and the top of the V-sequence is defined to be equal to the bottom of the P-sequence which covers 16.4 to 13.1 m. The age at 13.1 m from Zander et al, 2020 was also input as the upper boundary of the upper-most P-sequence. The P-sequence is a Bayesian age-depth modeling routine that calibrates radiocarbon ages using IntCal13 (Reimer et al., 2013) and models the sedimentation rates which fit these ages. The parameter (k) determines the variability of sedimentation rates in the model. We used a uniformly distributed prior for k such that $k_0 = 1$, and $\log_{10}(k/k_0) \sim U(-2, 2)$; this allows k to vary between 0.01 and 100.

Geochronological Results

Based on the composite age-depth model, the basal age of the core is estimated to be 10,880-10,620 cal BP (Fig. 4.1, main text). This is well constrained by two ^{14}C ages at 19.21 m depth. One age (18.27 m, BE-9368.1.1) in phase 1 is an outlier that is clearly too young; the 95% confidence interval (CI) of the calibrated age does not overlap with the 95% CI of the age model. The other five ages in phase 1 fit the P-sequence age model well; the agreement index for all 5 ages is above 78% (above 60% is considered good model fit; Bronk Ramsey, 2008). Above MMD-1 a short floating varve count was done to constrain the radiocarbon ages in this section (16.99-16.42 m). We counted 604 ± 48 varves, which were input as 'Gaps' to an OxCal V-sequence along with two radiocarbon ages. The results of the integrated OxCal model indicate that MMD-1 was deposited 10,160-10,030 cal yr BP. The constraint of the varve count suggests that the ^{14}C age directly above the MMD (BE-9371.1.1, 16.95 m) is likely too old; the agreement index with the V-sequence model is only 12%. All other ages in the interval 17.0 to 13.1 m have agreement indices greater than 63%.

The P-sequence age model estimates relatively high sedimentation rates during phase 1 (approx. 2.9 mm/yr) but this result is consistent with varve thicknesses in this phase where varves are well preserved. The average varve thickness during the first decade after MMD-1 occurred was 2.0 mm. The sedimentation rate gradually decreased over the next 150 years, to around 1.2 mm/year. The sedimentation rate stayed consistently near this value from 9.9 ka cal BP until 2.8 ka cal BP, though sedimentation rates were determined by the P-sequence age model output rather than varve counts for the interval 9.6-6.8 ka cal BP. Based on varve counting, the sedimentation rate in phase 4 (2.8 ka cal BP to 610 CE) was approximately 2.6 mm/year and more variable than the previous 7,000 years. The sedimentation rate decreased slightly in phase 5 to 2.0 mm/year, and then rose dramatically in phase 6 to 5.9 mm/year, with some varves greater than 20 mm thick.

The uncertainties of age estimates along the sequence depend primarily on the methods used for each segment. Above MMD-2 varve counts were linked to the surface (2017 CE) resulting in uncertainty that increases downcore until MMD-2 at 2028 +43/-66 cal yr BP. Sections of the record that were modelled with OxCal P-sequences produced more uncertain age estimates, and the uncertainty in these segments is controlled mainly by the uncertainty of the calibrated ^{14}C ages. The P-

sequence from 16.4 to 13.1 m has an average uncertainty (2σ) of ± 108 years, and the maximum uncertainty for the record is ± 140 years at 15.4 m depth. The P-sequence for phase 1 has an average uncertainty of ± 93 years. The lack of a clear boundary with MMD-1 adds additional uncertainty to the age estimates in this phase that is not captured by the model. The OxCal V-sequence technique produces narrower age estimates because of the additional information provided by floating varve counts, which the model uses to constrain the calibrated radiocarbon age probability functions based on the number of years between radiocarbon samples. The OxCal V-sequence from 13.1 to 7.3 m has an average uncertainty of ± 43 years (Zander et al., 2020), and the V-sequence from 17.0 to 16.4 m has an average uncertainty of ± 60 years.

4.9.2 Hyperspectral imaging methods

Hyperspectral imaging (HSI) was done using a Specim PFD-CL-65-V10E linescan camera following the methods of Butz et al. (2015). Reflectance was measured from 400-1000 nm with a spectral resolution of 1.4 nm and a spatial resolution of 60 µm × 60 µm (pixel size). The scanning parameters were: exposure = 90 ms, aperture = f/1.9, field of view = 78.7 mm, frame rate = 10 Hz, and scanning speed = 0.6 mm/s. Hyperspectral data were processed using ENVI 5.4 (Exelisvis ENVI, Boulder, Colorado). Relative absorption band depth (RABD) indices were calculated to quantify the absorbance troughs caused by sedimentary chloropigments and bacteriopheophytins. The index $RABD_{655\text{-}685max}$ measures total chloropigments-*a* (TChl-*a*) and was calculated using the following formula (modified from Schneider et al., 2018):

$$RABD_{655-685max} = \left(\frac{X * R_{590} + Y * R_{730}}{X + Y}\right) / R_{655-685min}$$

Where R_λ is the reflectance at the wavelength (λ), R655-685min is the trough minimum (i.e. lowest reflectance value measured between 655 and 685 nm), X is the number of spectral bands between R730 and the trough minimum, and Y is the number of spectral bands between the trough minimum and R590. $RABD_{845}$ measures bacteriopheopigments-*a* using the following formula (Butz et al., 2015):

$$RABD_{845} = \left(\frac{34 * R_{790} + 34 * R_{900}}{68}\right) / R_{845}$$

These indices were calculated for every pixel, creating maps of pigment abundances at a resolution of 60 µm. Depth profiles were calculated by averaging across a 2-mm-wide subset; thus, each data point in the profile represents a 60 x 2000 µm area.

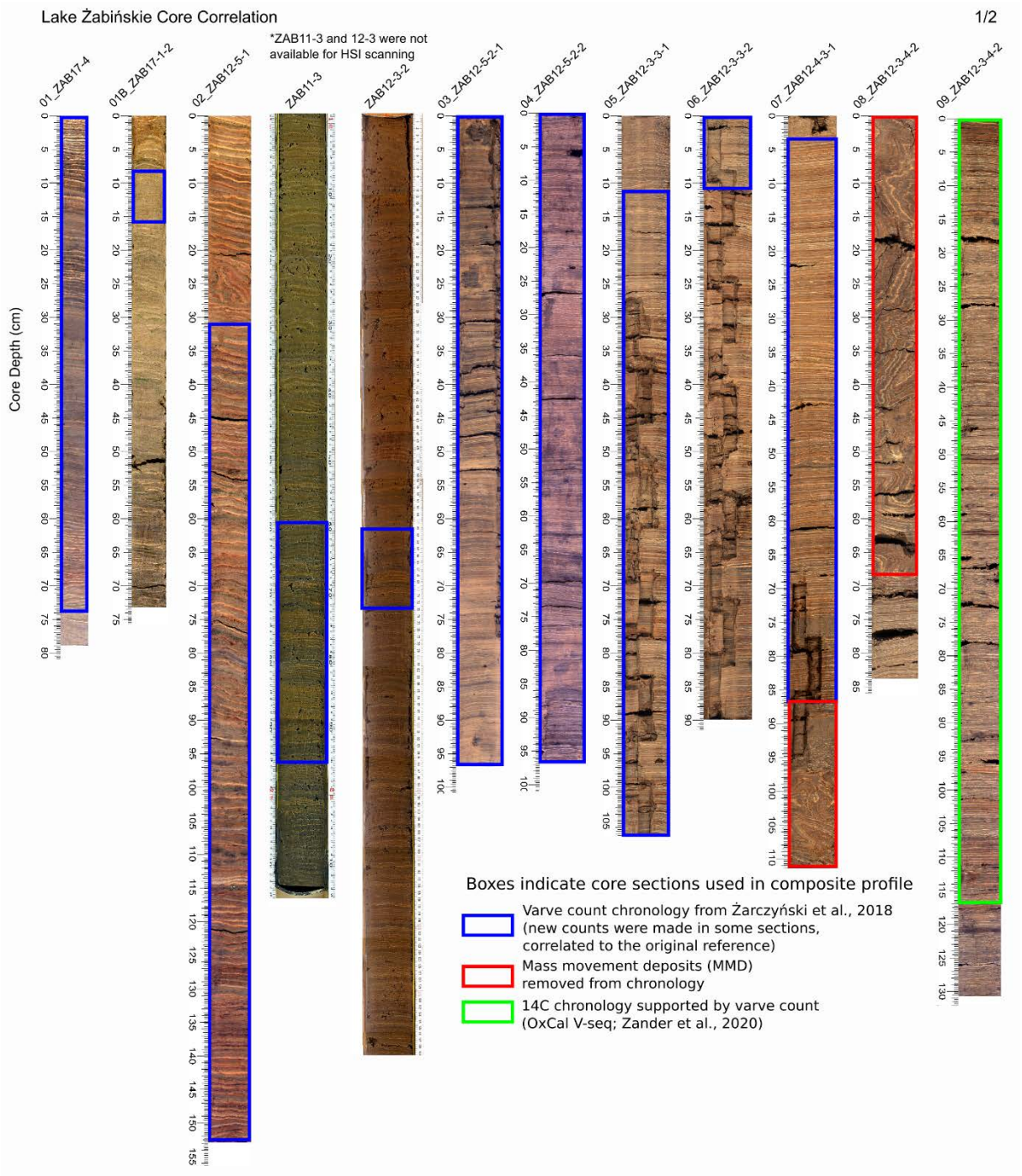

Figure S4.1: Core images showing core correlations used to build the composite profile. Colored boxes indicate the source of the chronology for that section.

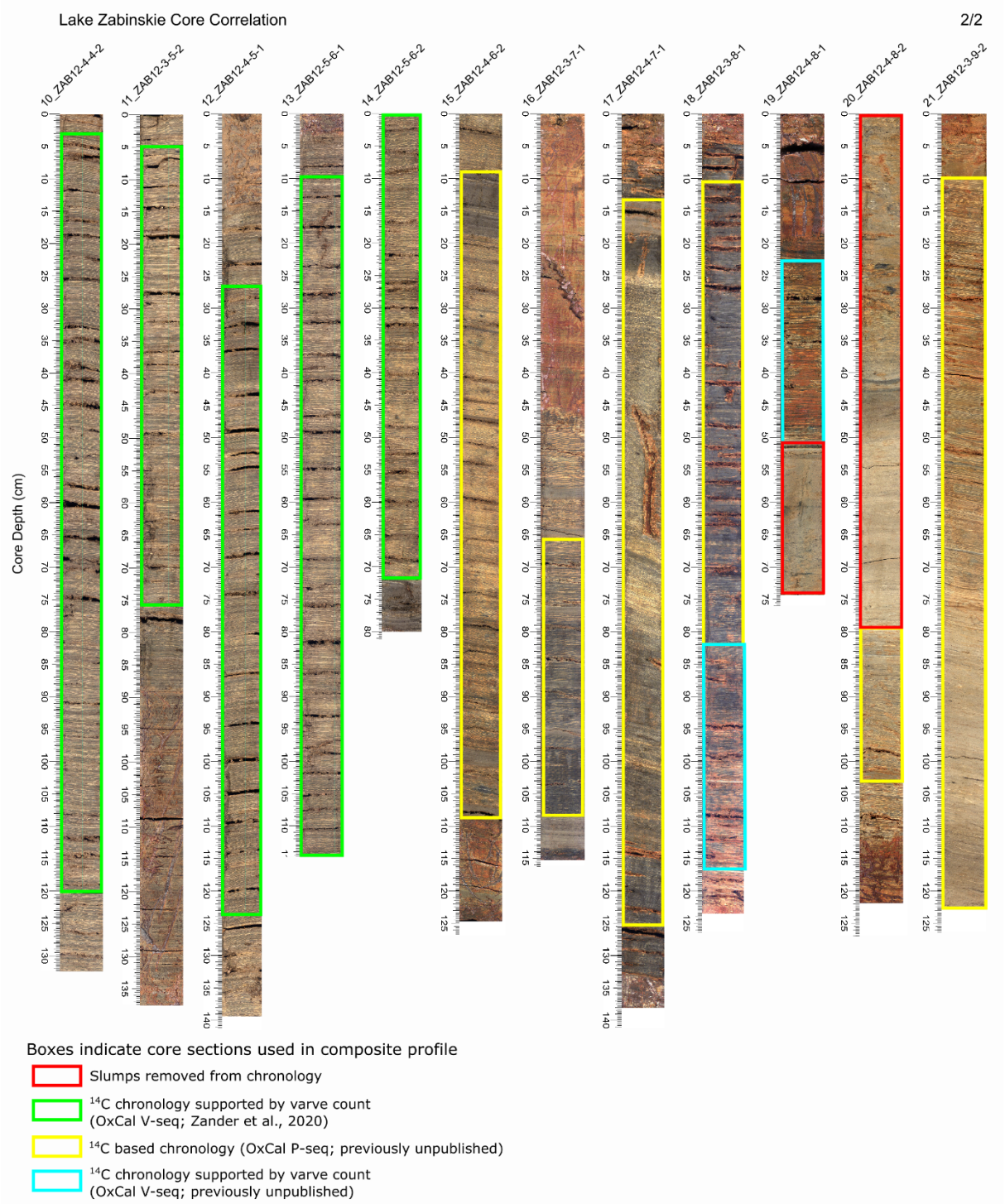

Figure S4.1 (continued): Core images showing core correlations used to build the composite profile. Colored boxes indicate the source of the chronology for that section.

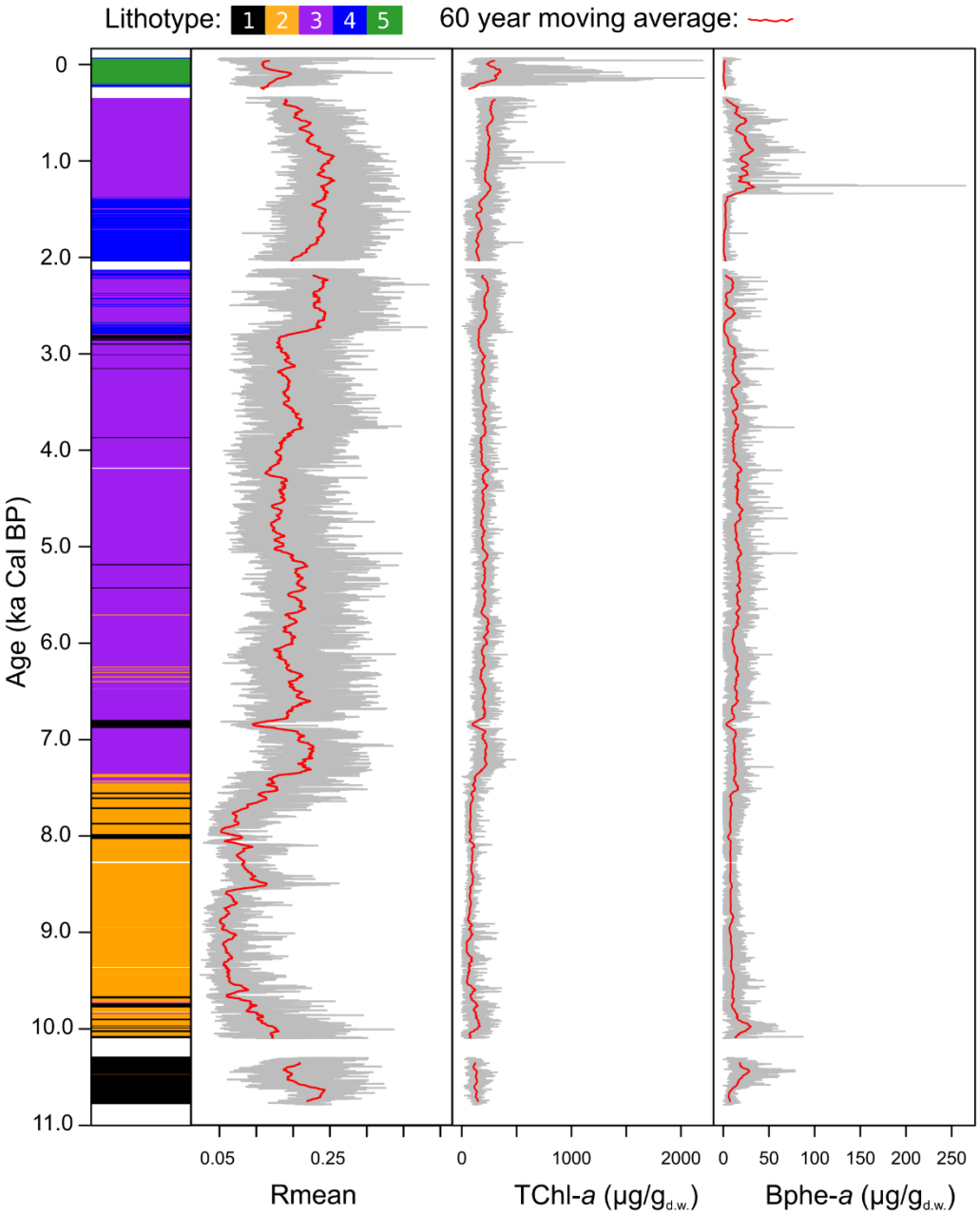

Figure S4.2: HSI indices comparing total reflectance (Rmean) and calibrated pigment concentrations.

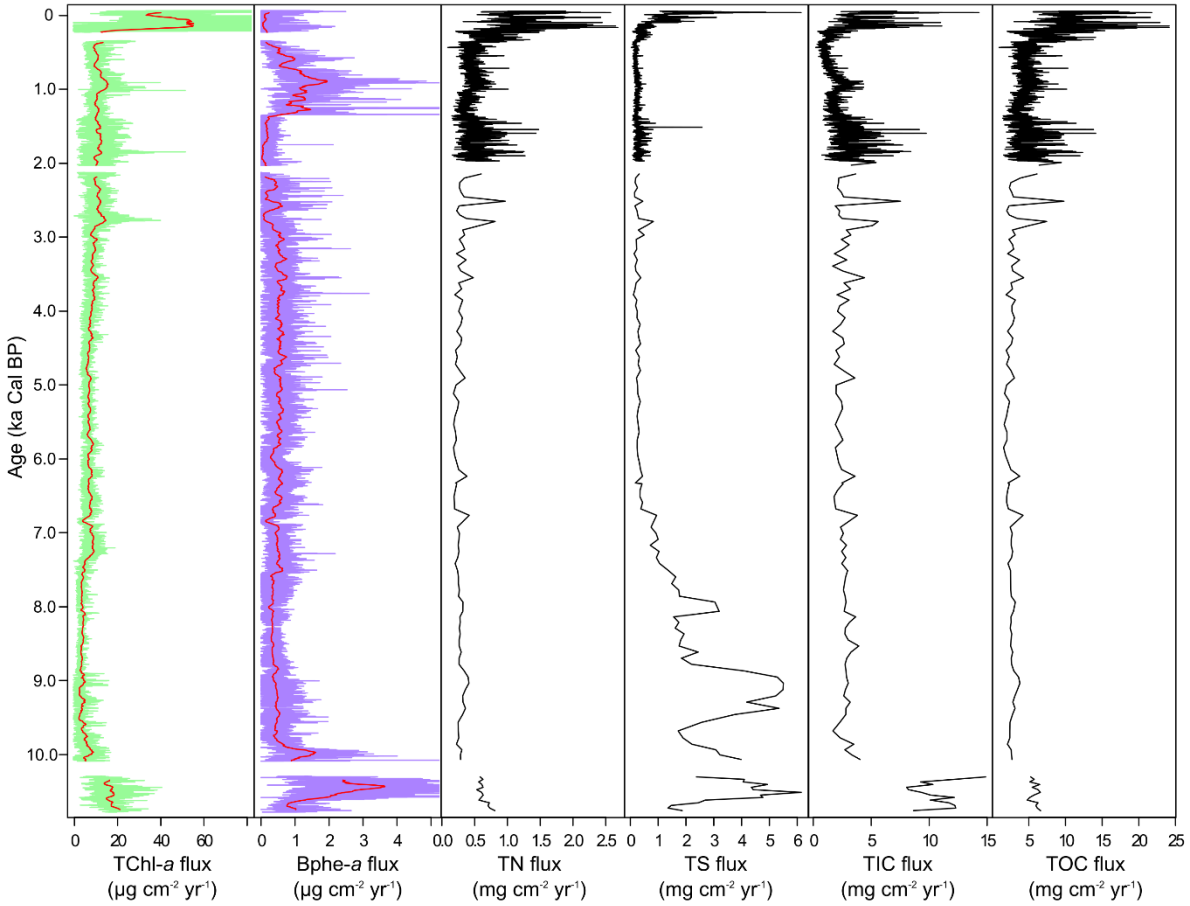

Figure S4.3: Fluxes of pigments (hyperspectral measurements), TN (Total Nitrogen), TS (Total Sulfur), TIC (Total Inorganic Carbon) and TOC (Total Organic Carbon).

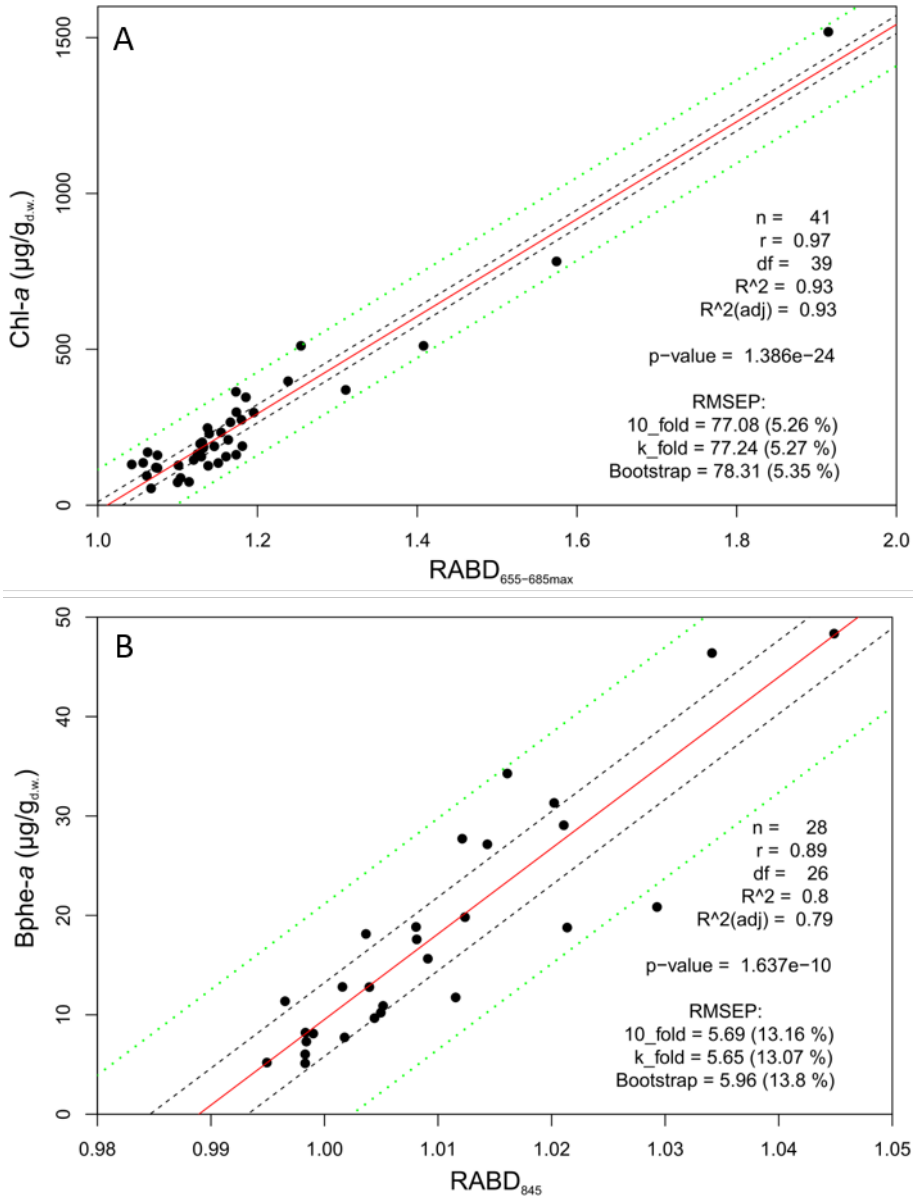

Figure S4.4: Linear correlation of RABD indices from HSI and bulk pigment concentrations determined by spectrophotometer measurements. A) $RABD_{655-685max}$ index and TChl-*a*. B) $RABD_{845}$ index and Bphe-*a*.

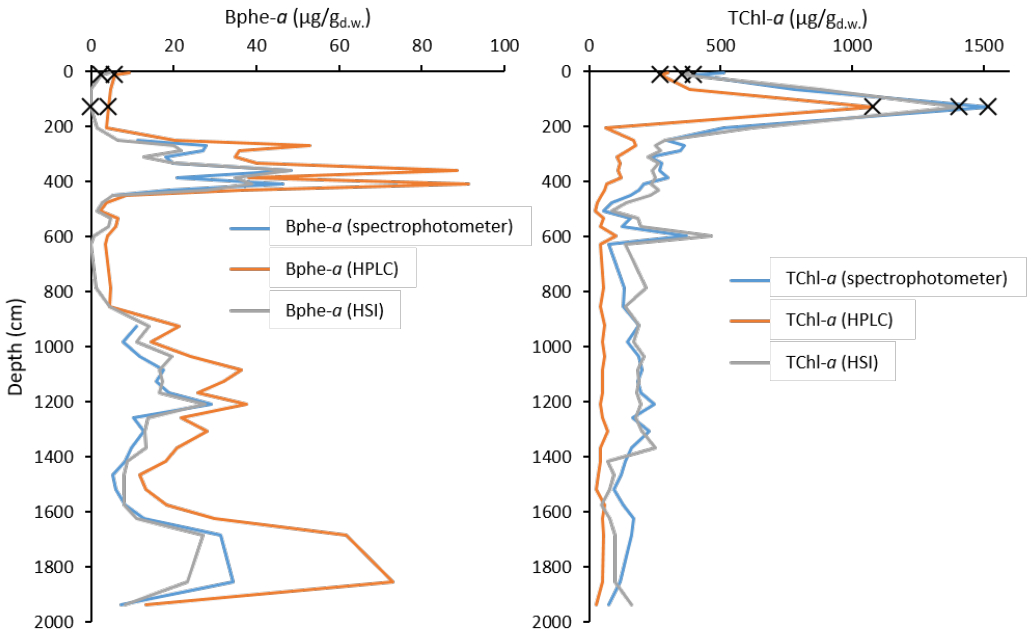

Figure S4.5: Comparison of pigment measurements made using spectrophotometer (blue), HPLC (orange) and HSI techniques (gray). Note that two samples (marked with black X's) included here are not included in the pigment stratigraphy of Fig. 4.6 because they represent seasonal pigment compositions.

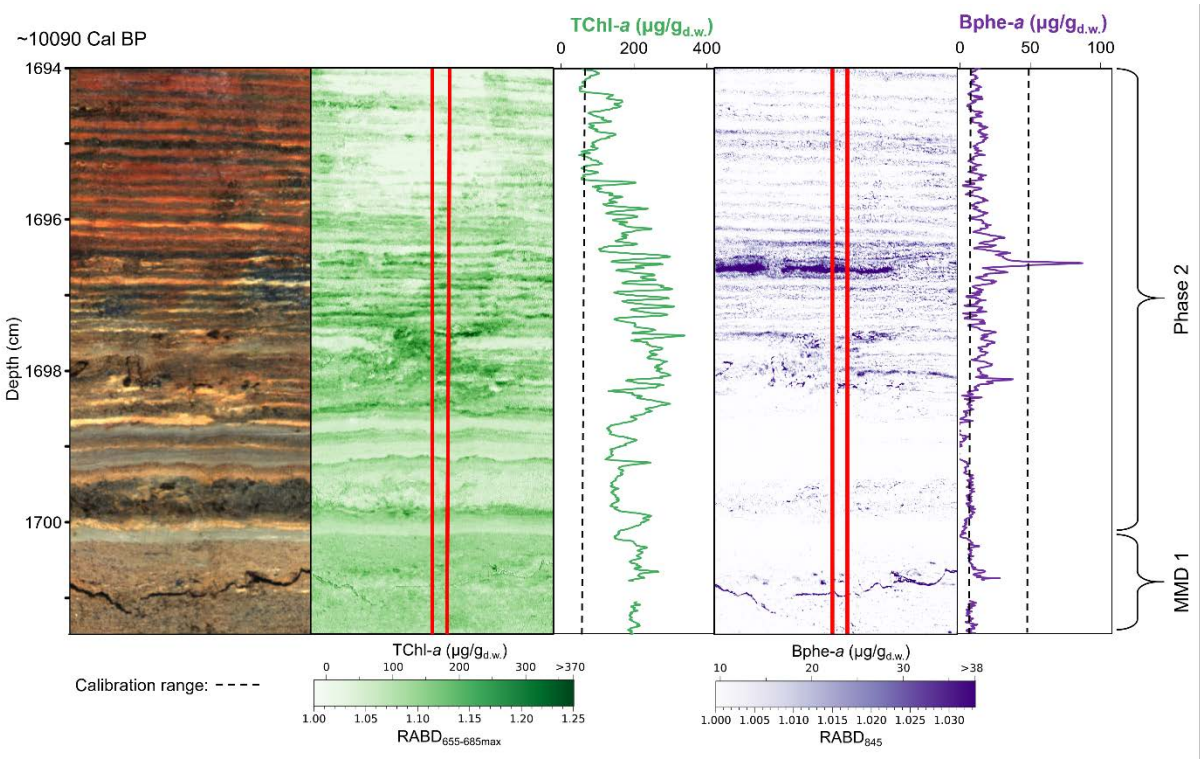

Figure S4.6: Onset of anoxic conditions following a mass movement event during the early Holocene. Bphe-*a* values above the detection limit (black dashed vertical line) at 1698 cm indicate the return of anoxic conditions in the lower photic zone (and growth of PSB) within less than 5 years after the mass movement event.

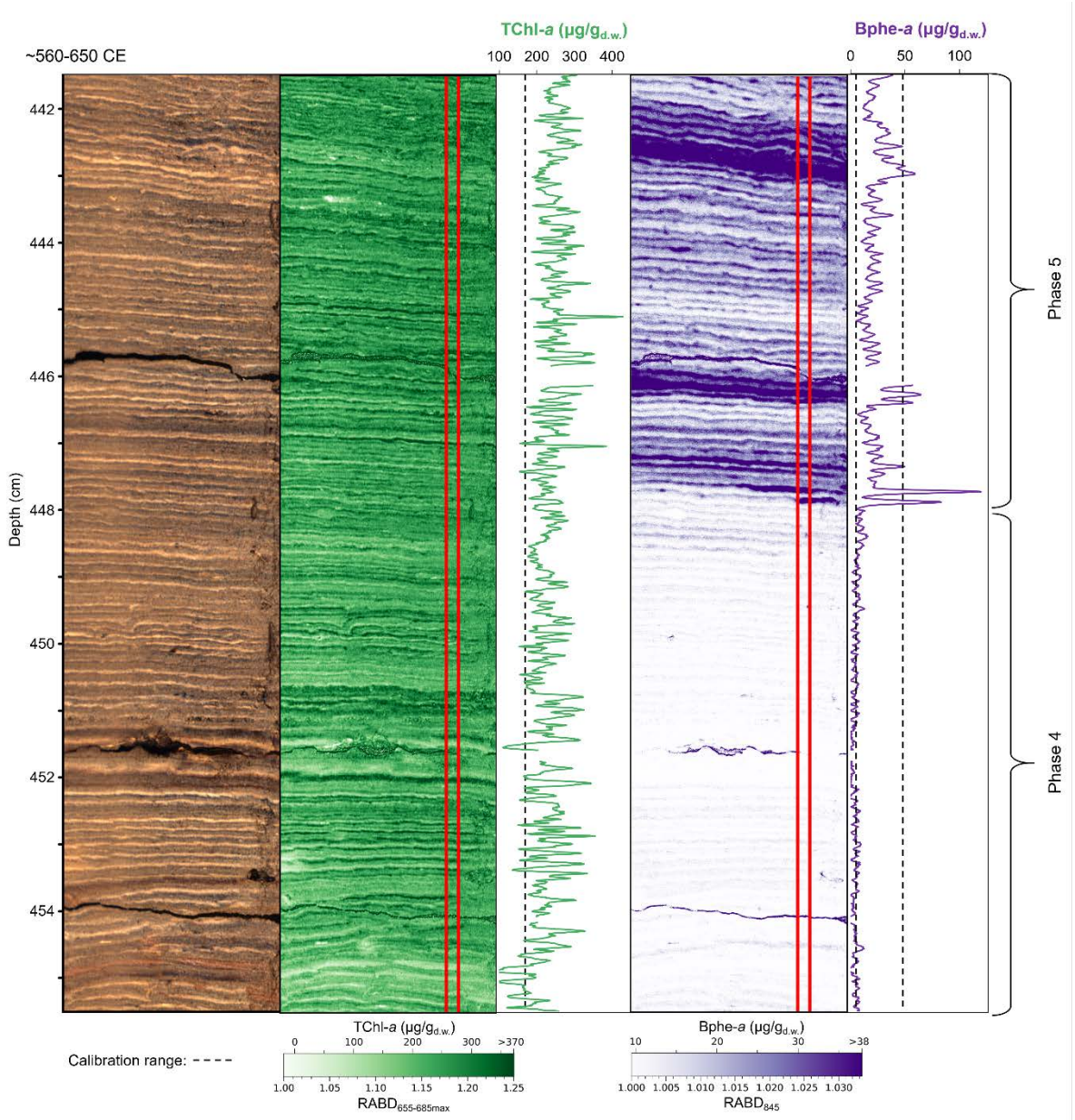

Figure S4.7: Close-up showing the rapid onset of PSB production (start of Phase 5) around 610 CE.

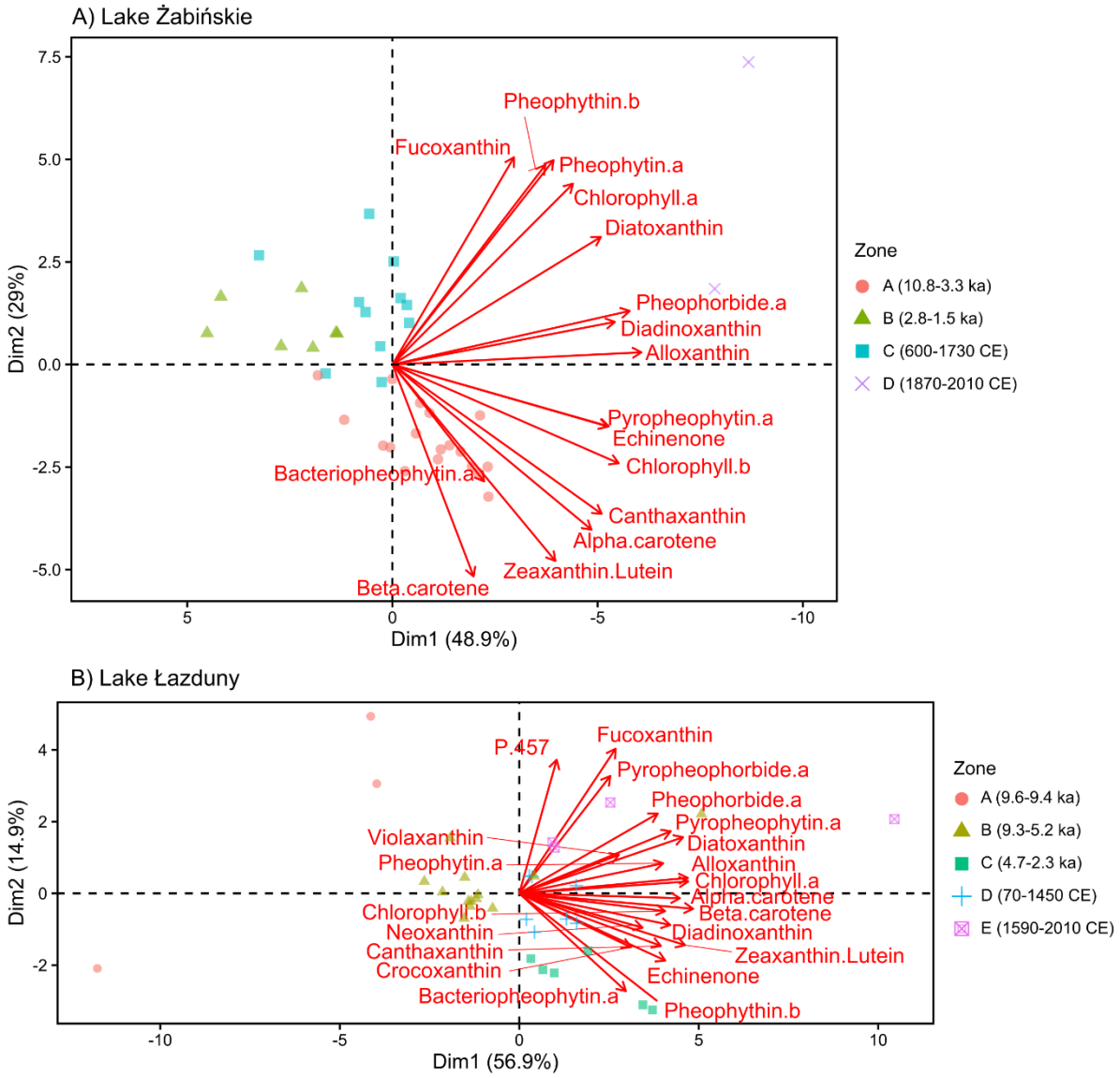

Figure S4.8: A) PCA and CONISS results for HPLC pigment data from Lake Żabińskie. B) PCA biplot from Lake Łazduny pigments (Sanchini et al, 2020).

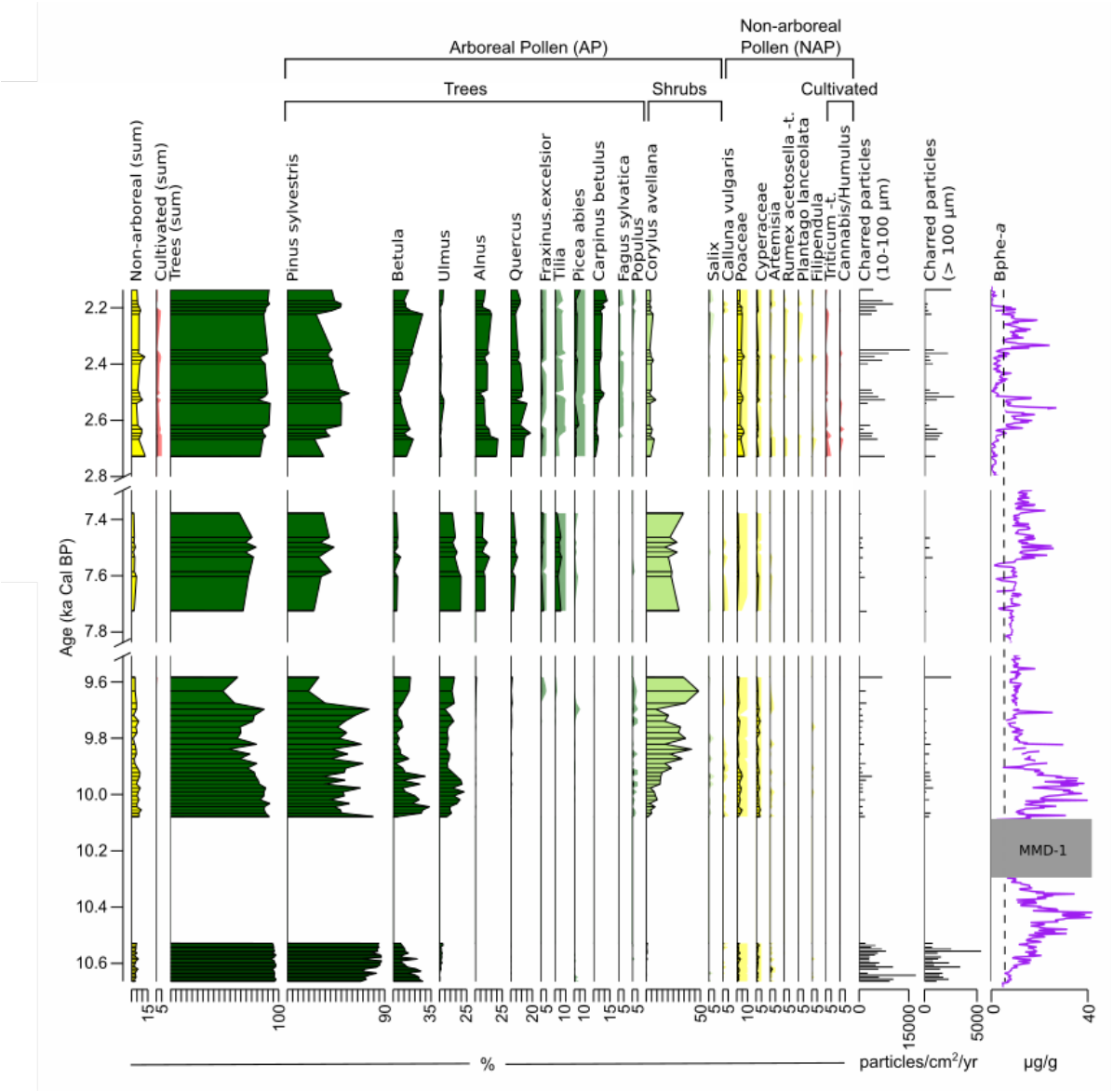

Figure S4.9: Summary of Lake Żabińskie pollen results of selected taxa from targeted sampling of periods with changes of lake mixing. Light shading represents 10x exaggeration of pollen percentages for taxa with less than 10% of counts. Bphe-*a* is plotted using 3-year averages for comparison. Vertical dashed line in Bphe-*a* plot represents the detection limit. Note breaks in the y-axis.

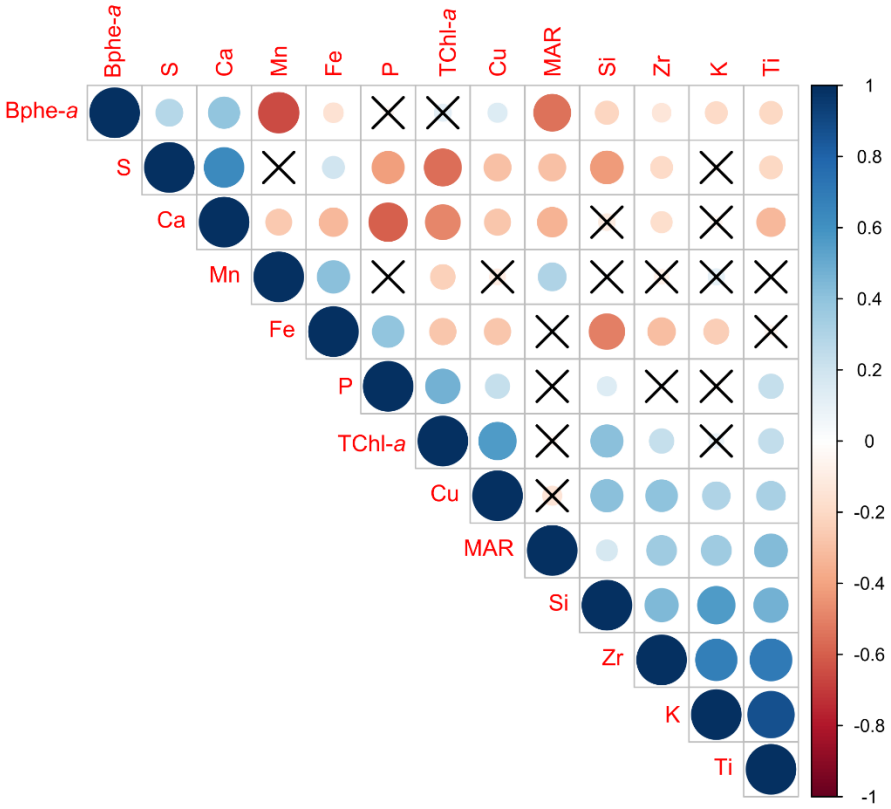

Figure S4.10: Correlation matrix of selected geochemical variables in which the size and color of the circles represent the Spearman's rank correlation coefficient. X symbols mark variable combinations where the correlation is not significant ($p > 0.05$). P-values were corrected for autocorrelation of the variables using the method of Bretherton et al. (1999). Data were averaged to 1 cm and log-transformed prior to the correlation analysis.

Table S4.1: List of reference standards used for pigment identification and calibration

Pigment	Company, Location	Standard Name	CAS	Purity	State
Fucoxanthin	Sigma-Aldrich, Buchs, Switzerland	FUCOXANTHIN analytical standard	3351-86-8	98.4% HPLC	powder
Pheophorbide-*a*	DHI, Copenhagen, Denmark	Pheophorbide a	15664-29-6	3.125 mg L-1,	liquid
Diadinoxanthin	DHI, Copenhagen, Denmark	Diadinoxanthin	18457-54-0	0.9600 mg L-1	liquid
Alloxanthin	DHI, Copenhagen, Denmark	Alloxanthin	2465-59-0	1.034 mg L-1	liquid
Diatoxanthin	Sigma-Aldrich, Buchs, Switzerland	DIATOXANTHIN analytical standard	31063-73-7	99.3% HPLC	powder
Zeoxanthin	Sigma-Aldrich, Buchs, Switzerland	ZEAXANTHIN analytical standard	144-68-3	99.2% HPLC	powder
Lutein	Sigma-Aldrich, Buchs, Switzerland	LUTEIN analytical standard	127-40-2	97.6% HPLC	powder
Canthaxanthin	Sigma-Aldrich, Buchs, Switzerland	CANTHAXANTHIN	514-78-3	96.8% HPLC	powder
Chlorophyll-*b*	Sigma-Aldrich, Buchs, Switzerland	CHLOROPHYLL B analytical standard	479-61-8	98.3% HPLC	powder
Pheophytin-*b*	*No standard available. Pheophytin-b was semi-quantified using calibration curve of Chlorophyll-b*				
Chlorophyll-*a*	Sigma-Aldrich, Buchs, Switzerland	CHLOROPHYLL A	479-61-8	99.5% HPLC	powder
Echinenone	Sigma-Aldrich, Buchs, Switzerland	ECHINENONE	432-68-8	98.5% HPLC	powder
Bacteriopheophytin-*a*	Sigma-Aldrich, Buchs, Switzerland	Bacteriochlorophyll from rhodopseudomonas sphaeroides	17499-98-8	~55%	powder
Pheophytin-*a*	DHI, Copenhagen, Denmark	Pheophytin *a*	603-17-8	3.356 mg L-1	liquid
β,β-carotene	Sigma-Aldrich, Buchs, Switzerland	β-Carotene	7235-40-7	93% UV	powder
β,ε-carotene	*No standard available. β,ε-carotene was semi-quantified using calibration curve of β,β-carotene*				
Pyropheophytin-*a*	Santa Cruz Biotechnology, Santa Cruz, USA	Pyropheophorbide a	24533-72-0	95% UV	powder

Table S4.2: Summary of lithological phases and their characteristics.

Phase	Depth (m)	Age	Brief Description	Lamination Thickness (mm)	TOC (%)	TIC (%)	TChl-*a* ($\mu g/g_{d.w.}$)	Bphe-*a* ($\mu g/g_{d.w.}$)
Phase 1	19.41-16.98	10.8-10.3 ka cal BP	Pale brown (10YR 6/3) carbonate mud with yellowish pale brown (10YR 8/4) laminations. Partially laminated.	1-5	4.4 +/- 0.5	8.0 +/- 1.0	127 +/- 23	14.7 +/- 8.2
MMD-1	18.02-16.98	10.1 ka cal BP	Indistinct contact with phase 1. Folded laminations, massive sediments, and coherent fragments of laminated sediments embedded within a matrix of massive sediments. Sharp contact with phase 2.					
Phase 2	16.98-14.51	10.1-8.0 ka cal BP	Very dark gray (7.5YR 3/1) carbonate mud with light grayish pale brown (10YR 7/2) laminations, and occasional massive beds. Lamination preservation is variable.	1.2 +/- 0.6	6.0 +/- 0.6	6.4 +/- 1.2	86 +/- 38	9.8 +/- 4.9
Phase 3	14.51-8.45	8.0-2.8 ka cal BP	Carbonate mud with well-preserved laminations and occasional massive beds. Laminations are dark grayish brown (2.5YR 4/2) and very pale brown (10 YR 8/4).	1.2 +/- 0.4	6.6 +/- 0.4	6.6 +/- 0.5	192 +/- 40	13.6 +/- 4.7
Phase 4	8.45-4.40	2.8-1.3 ka cal BP	Carbonate mud with well-preserved laminations. Simple dark grayish brown (10YR 4/2) and very pale brown (10 YR 8/4) laminations are interbedded with dark reddish-brown (5YR 3/4) Fe-rich laminations.	2.6 +/- 1.1	6.96 +/- 0.5	5.05 +/- 0.5	184 +/- 43	4.4 +/- 5.8
MMD-2	6.34-7.25	2.0 ka cal BP	MMD embedded within phase 4. Laminations are folded or vertical in the lower 80 cm, while the upper 11 cm is a graded bed					
Phase 5	4.40-2.50	610-1720 CE	Laminated carbonaceous silt with good preservation and consistent structure. Dark laminations are brown (7.5YR 4/3). Light laminations are very pale brown (10 YR 8/4).	2 .0 +/- 0.5	9.8 +/- 1.6	3.4 +/- 0.7	246 +/- 33	21.0 +/- 10.2
Phase 6	2.50-0	1720-2017 CE	Laminated carbonaceous silt with variable thickness and structure of laminations. Very pale brown Ca-rich (10 YR 8/4), dark reddish-brown (5YR 3/4) Fe-rich, and clastic-rich grayish brown (10YR 5/2) are present.	5.9 +/- 4.5	8.5 +/- 1.7	2.5 +/- 0.8	285 +/- 104	1.0 +/- 1.0

Table S4.3: Radiocarbon ages (only those not previously published are included here). Uncertainties of ^{14}C ages refer to 68% probabilities (1σ), whereas ranges of calibrated and modeled ages represent 95% probabilities. Calibration was done using OxCal 4.3 with the IntCal13 calibration curve (Bronk Ramsey, 2009; Reimer et al., 2013).

Lab ID	Core ID	Top Core Depth (cm)	Bottom Core Depth (cm)	Centered Composite Depth (cm)	Carbon mass (µg)	Gas/ Graphite	^{14}C age (BP)	Calibrated Age (Cal BP)	Modeled Age (Cal BP)	Material
BE-9796.1.1	ZAB-12-4-6-2	23.0	25.0	1324.4	68	Gas	5961 +/- 108	6534-7156	6816-6998	Dicotyledonous leaf fragments (stems), *betula* seed, woody scales
BE-9377.1.1	ZAB-12-4-6-2	80.0	81.0	1380.8	34	Gas	6332 +/- 166	6860-7566	7315-7436	*Betula alba* seed
BE-9376.1.1	ZAB-12-4-6-2	80.0	81.0	1380.8	432	Graphite	6450 +/- 50	7270-7435	7315-7436	Dicotyledonous leaf fragments
BE-10332.1.1	ZAB-12-3-7-1	85.0	87.0	1427.2	47	Gas	7117 +/- 105	7728-8167	7718-7954	Male anther, coniferous periderm
BE-9375.1.1	ZAB-12-4-7-1	42.0	43.0	1479.6	518	Graphite	7491 +/- 47	8198-8387	8185-8350	Coniferous periderm, woody scales, *Betula* seed fragments
BE-9374.1.1	ZAB-12-4-7-1	104.0	106.0	1542.1	132	Gas	7784 +/- 116	8391-8979	8590-8870	Periderm, woody scales, *Betula alba* seed fragments
BE-9373.1.1	ZAB-12-3-8-1	29.0	31.0	1582.8	185	Graphite	8110 +/- 76	8764-9291	8988-9187	*Pinus* periderm, woody scales
BE-9372.1.1	ZAB-12-3-8-1	78.0	80.0	1631.8	707	Graphite	8490 +/- 45	9445-9540	9442-9539	*Pinus* periderm, woody scales, *Betula alba* seed fragments
BE-10330.1.1	ZAB-12-4-8-1	35.0	37.0	1683.9	90	Gas	8965 +/- 88	9745-10257	9943-10065	*Betula alba* fruits, coniferous and deciduous periderm, deciduous bud scales
BE-9371.1.1	ZAB-12-4-8-1	47.0	48.0	1695.4	126	Graphite	9130 +/- 108	9936-10586	10012-10140	Woody scales, periderm

BE-9370.1.1	ZAB-12-4-8-1	65.0	66.0	1713.4	248	Graphite	9548 +/- 76	10660-11164	Not modeled[1]	Dicotyledonous leaf fragments, , decidous periderm, *Betula* seed fragments
BE-9369.1.1	ZAB-12-4-8-2	36.0	37.0	1759.2	219	Graphite	9187 +/- 76	10227-10555	Not modeled[1]	Periderm fragments, woody scales
BE-10329.1.1	ZAB-12-4-8-2	86.0	88.0	1809.7	103	Gas	9314 +/- 102	10238-10772	10234-10469	*Betula alba* fruit fragments, coniferous periderm, dicotyledonous leaf fragments
BE-9368.1.1	ZAB-12-4-8-2	104.0	105.0	1827.2	77	Gas	8875 +/- 138	9560-10235	10294-10500	*Betula alba* seeds, charcoal particles, woody scales
BE-10331.1.1	ZAB-12-3-9-2	23.0	24.0	1840.5	28	Gas	9279 +/- 194	9947-11168	10345-10525	*Betula alba* fruit fragments, coniferous periderm, coniferous woody scales
BE-9367.1.1	ZAB-12-3-9-2	54.0	56.0	1872.0	865	Graphite	9293 +/- 31	10306-10581	10450-10585	*Pinus* periderm, woody scales, *Betula alba* seed fragments
BE-9365.1.1	ZAB-12-3-9-2	103.0	104.0	1920.5	34	Gas	9503 +/- 248	10198-11605	10591-10781	*Pinus* periderm
BE-9366.1.1	ZAB-12-3-9-2	103.0	104.0	1920.5	990	Graphite	9488 +/- 31	10602-11066	10591-10781	Wood fragment

[1] These samples were taken from a MMD and were not included in the age model calculation

Chapter 5: Seasonal climate signals preserved in biochemical varves: insights from high-resolution sediment scanning techniques

Declaration of contribution

This manuscript will be submitted to *Earth and Planetary Science Letters.* Paul Zander, Martin Grosjean, Wojciech Tylmann and Maurycy Żarczyński designed the study. Paul Zander did hyperspectral scanning, numerical analysis and wrote the manuscript with contributions from all authors. Shauna-kay Rainford did the XRF scanning with assistance from Paul Zander. Maurycy Żarczyński and Joanna Piłczyńska performed analytical laboratory work.

Seasonal climate signals preserved in biochemical varves: insights from high-resolution sediment scanning techniques

Paul D. Zander[1*], Maurycy Żarczyński[2], Wojciech Tylmann[2], Shauna-kay Rainford[3], Martin Grosjean[1]

[1] Institute of Geography & Oeschger Centre for Climate Change Research, University of Bern, Bern, Switzerland

[2] Faculty of Oceanography and Geography, University of Gdańsk, Gdańsk Poland

[3] Institute of Plant Sciences & Oeschger Centre for Climate Change Research, University of Bern, Bern, Switzerland

[*] Correspondence E-mail address: paul.zander@giub.unibe.ch

Keywords: varves, XRF, hyperspectral imaging, lake sediments, climate change

Abstract

Varved lake sediments are exceptional archives of paleoclimatic information due to their precise chronological control and annual resolution. However, quantitative paleoclimate reconstructions based on the biogeochemical composition of biochemical varves are rare, due to the complexity of climate-proxy relationships and challenges associated with obtaining proxy data at annual resolution. In this study, novel high-resolution hyperspectral imaging and micro X-ray fluorescence imaging were used to obtain data on sedimentary pigments and elements in varved sediments of Lake Żabińskie, Poland over the period 1966–2019 CE at very high spatial (µm scale) and temporal (seasonal) resolution. The high resolution of the scanning data (60 µm), and excellent varve preservation (average thickness = 6.0 mm), enables detailed investigation of how changing climatic conditions influenced sediment composition and varve formation processes. Hierarchical clustering, based on the dissimilarity of within-varve geochemical time series, was used to classify four varve types. A multivariate analysis of variance shows that these varve types formed during significantly different seasonal meteorological conditions. Several significant correlations were found between varve geochemical data and spring/summer temperature and windiness. These correlations were used to inform variable selection for generalized additive models (GAMs) used to reconstruct seasonal climate conditions. Spring and summer (MAMJJA) temperature was reconstructed using Ti and total C (56.4% of deviance explained; cross validated root mean square error of prediction (CV-RMSE) = 0.7 °C, 14.7%). Windy days from March to December (mean daily wind speed > 7 m/s) were reconstructed using mass accumulation rate (MAR) and Si (49.6% of deviance explained, CV-RMSE = 18.4%). This study highlights the potential of high-resolution scanning techniques to improve our understanding of varve formation processes and thereby utilize the geochemical composition of biogenic varves for high-resolution paleoclimate reconstructions.

5.1 Introduction

Quantitative paleoclimatic reconstructions are essential for our understanding of how the climate system functions (IPCC, 2013). Spatially distributed, high-resolution paleoclimatic records are required to understand regional scale paleoclimate variability and to contextualize current climate change (Neukom et

al., 2019). Varved lake sediments have long been recognized as unique archives of climate (De Geer, 1908) because of the precise, annually-resolved, age control, and because of the wide variety of paleoenvironmental information preserved in varved sediments (Zolitschka et al., 2015). Numerous studies have identified close relationships between instrumental meteorological records and data obtained from varved sediments, in some cases at annual resolution, demonstrating the great potential of varves for high-resolution paleoclimatic reconstructions. The majority of these studies have related meteorological parameters with sedimentary variables in clastic varves that reflect transport of minerogenic material (e.g. Francus et al., 2002; Trachsel et al., 2010; Lapointe et al., 2020). Interpretation of climate signals recorded in the sedimentary properties of biochemical and biogenic varves has proven much more challenging than in clastic varves due to more complex and often non-linear interactions between climate forcing, ecological and hydrochemical response, endogenic organic matter and mineral formation, and sedimentation (Zolitschka et al., 2015). An extensive compilation of more than 1000 varve-related publications (http://www.pages.unibe.ch/science/end-aff/varves-wg/varve-related-publications, last updated 4 April 2019) includes only three studies (Tian et al., 2011; Swierczynski et al., 2012; Amann et al., 2014) that report significant correlation between meteorological data and bulk geochemical data from biogenic varves (excluding studies based on microfossils or layer thicknesses). More commonly, microfossil assemblages have been used to reconstruct climate variables from biogenic varves, however these techniques are generally challenging for sub-decadal scale analysis (Telford, 2019). Despite their widespread occurrence in temperate zones, biogenic and biochemical varves remain an under-utilized archive for high-resolution quantitative paleoclimate reconstructions.

During the past couple decades, high-resolution sediment scanning techniques, such as X-ray fluorescence (XRF) and reflectance spectroscopy have become increasingly popular for environmental reconstructions, including quantitative near-annually resolved climate reconstructions from varved (Trachsel et al., 2010; Amann et al., 2014; Lapointe et al., 2020) and non-varved lacustrine sediments (von Gunten et al., 2012). The speed and resolution of these non-destructive scanning measurements (often 0.2-2 mm resolution) is impossible to achieve with conventional biogeochemical methods that require destructive sampling of sediment cores. In this study, we use cutting-edge micro X-ray fluorescence (μXRF) imaging and hyperspectral imaging (HSI) methods that improve upon linescan techniques by producing two-dimensional images of geochemical data at 60 μm resolution. This improvement is critically important for sub-annual and annual resolution analyses because annual layers can be delineated more precisely and consistently using images of geochemical data. Additionally, 60 μm resolution yields an average of ~100 data points per varve at our site, enabling detailed investigation of sub-annual geochemical variability.

Here, these high-resolution imaging spectroscopy techniques were applied to sediments of Lake Żabińskie to gain insights into climate-proxy relationships in biochemical varves and to investigate how recent climatic variability is recorded varve composition. This site features varves with excellent preservation, high sedimentation rates (6 mm $year^{-1}$ during 1966-2019), and complex varve structures showing substantial year-to-year variations. Additionally, we focus on a 54-year period (1966-2019) in

which there is no uncertainty in the varve count chronology. These properties make the site ideal for studying the influence of weather on varve formation, structure and composition. This study aims to answer the following research questions: 1) how are seasonal weather conditions recorded in biochemical varves, and 2) how can varve composition be used to reconstruct seasonal meteorological conditions? Results show that at Lake Żabińskie, sub-annual geochemical patterns are influenced by seasonal meteorological conditions, and varve composition can be used to reconstruct spring/summer temperatures and windiness.

5.2 Materials and methods

5.2.1 Site description and core collection

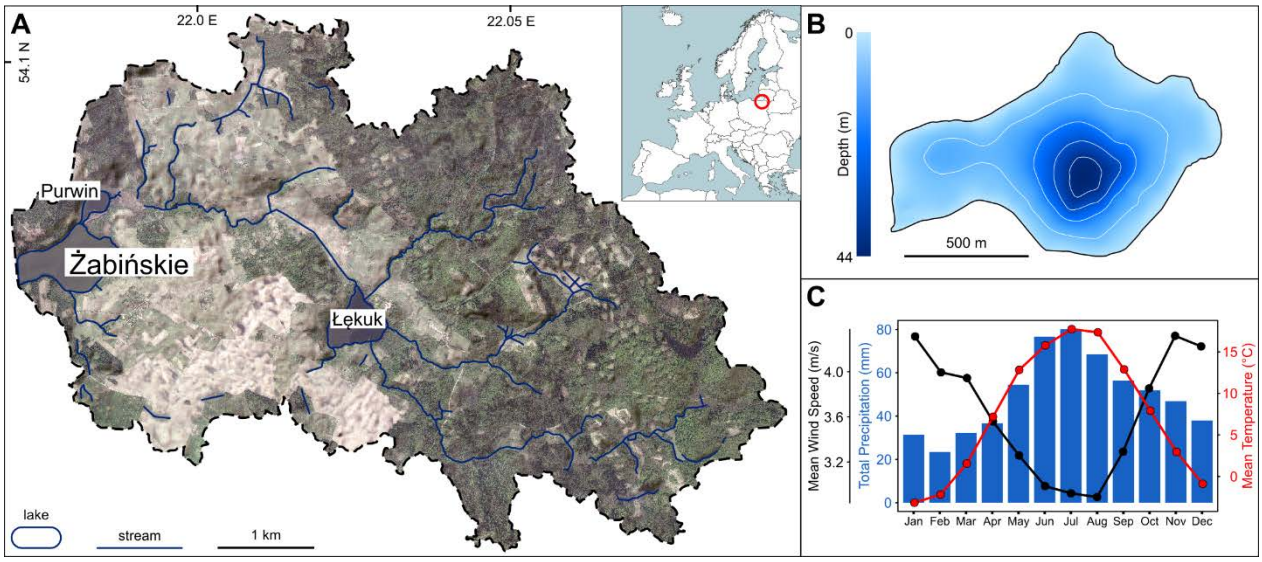

Figure 5.1: A) Orthophoto map of the Lake Żabińskie catchment. Dark green colors represent forests, lighter colors represent cultivated areas. B) Bathymetric map of Lake Żabińskie. C) Summary of monthly meteorological data over the period 1966-2019

Lake Żabińskie is a kettle-hole lake formed in the post-glacial landscape of the Masurian Lakeland in Poland (54.1318° N, 21.9836° E; Fig. 5.1). The basin is small (41.6 ha) and relatively deep (44.4 m), which promotes seasonal thermal stratification. Limnological data from 2011-2013 show that complete mixing of the water column occurs irregularly 0-2 times per year (Bonk et al., 2015). The catchment geology is mainly glacial till, sandy moraines and fluvioglacial sands and gravels. Anoxic and eutrophic conditions have led to good preservation of thick biochemical varves within the sediments. Previous investigations of the sedimentary record have documented changes to the lake mixing regime, trophy, and catchment erosion, with the most significant environmental changes occurring after major deforestation and the development of agriculture in the catchment during the 17th century (Bonk et al., 2016; Hernández-Almeida et al., 2017; Żarczyński et al., 2019; Zander et al., 2021).

Sediment cores used in this study were retrieved in 2012 (ZAB-12-1), and 2020 (ZAB-20-1) using an UWITEC gravity corer (ø90 mm). Resin-embedded sediment slabs and thin sections were produced following the method described in Żarczyński et al.(2018). Core correlation was done on a varve-by-varve basis using images of the cores, resin blocks, and thin sections.

5.2.2 Chronology

Varve counting was performed on scanned images of thin sections and these counts were transferred to core images and images of scanning measurement results. Identification of varve boundaries was facilitated by previous studies on varve microfacies in Lake Żabińskie (Żarczyński et al., 2018), as well as µXRF elemental measurements. The beginning of the varve year was defined as the onset of calcite precipitation as this point can be consistently identified for every year in both scanning data and thin sections. Multiple researchers confirmed the varve count for the period 1966-2019 with no uncertainty. The period 1966-1990 was counted on thin sections from ZAB-12-1, whereas for the period 1991-2019 thin sections from ZAB-20-1 were used. Varve thickness measurements were homogenized to account for differing sedimentation rates in the two cores by correcting the counting interval of each thin section to the actual depth covered by the same interval in the 2020 core. Dry bulk density was measured for each varve by sampling one cm^3 of wet sediment and measuring its weight after drying. Mass accumulation rates (MAR) were calculated by multiplying varve thickness and dry bulk density for each varve.

The varve count was validated using ^{137}Cs activity profiles to identify fallout from the 1986 Chernobyl incident, which could then be used as an independent time marker. ^{137}Cs activity was determined with gamma ray spectrometry (Tylmann et al., 2016). ZAB-12-1 was sampled for ^{137}Cs activity in 3-year intervals. Individual varves were sampled from ZAB-20-1 for the years 2017, 2011, 1989-1984 and 1966 to better resolve the 1986 Chernobyl peak and confirm baseline ^{137}Cs activities during years not affected by Chernobyl fallout.

5.2.3 Geochemical scanning measurements

µXRF measurements were conducted on resin-embedded sediment slabs extracted from the 2012 and 2020 cores using a Bruker M4 Tornado. The scanner was equipped with a Rh X-ray source with voltage and current set to 50 kv and 300 µA, respectively. Counts were measured along the two-dimensional surface of the slabs with a measurement spot size of 20 µm and counting time of 20 ms/pixel. The measurement step (pixel size) was set to 60 µm to achieve equivalent resolution to the hyperspectral images.

Hyperspectral imaging was performed on the fresh ZAB-20-1 core using a Specim PFD-CL-65-V10E linescan camera following methods described in Butz et al. (2015) and using the same scanning settings as in Zander et al. (2021). The scanning resolution (pixel size) was 60 µm. Relative absorption band depth (RABD) indices were used to quantify the abundance of bulk pigment groups in the sediments. $RABD_{655–685max}$ represents total chloropigments (TChl), and $RABD_{845}$ represents bacteriopheopigments-*a*. The RABD index values were calibrated to pigment concentrations ($µg/g_{d.s}$; d.s. = dry sediments) using the

calibration method described in Zander et al. (2021). TChl is used as a proxy for total algal productivity (Rein and Sirocko, 2002), whereas Bphe is produced by anoxygenic phototrophic sulfur bacteria and is a specific biomarker for anoxic conditions overlapping with the photic zone (Butz et al., 2015). An additional spectral index, Rmean (the average reflectance across the spectrum), was used as a proxy for calcite (Butz et al., 2017) to improve the alignment of HSI and μXRF data.

5.2.4 CNS Elemental Analysis

Total carbon (TC), total inorganic carbon (TIC), total nitrogen (TN), and total sulfur (TS) were quantified using a Vario El Cube elemental analyzer (Elementar) equipped with a SoliTIC module and thermal conductivity detector following methods described in Żarczyński et al. (2019). Samples were taken at annual resolution from ZAB-20-1 following varve boundaries. Total organic carbon (TOC) was calculated by subtracting TIC from TC. Individual varves were sampled and homogenized for these analyses. To account for loss due to decay of organic matter, TOC and TN values were corrected using the formulas developed by Gälman et al.(2008). The estimated TOC lost due to decay was added to TC values. All subsequent analyses were done with and without the correction; the results are robust and are weakly influenced by the correction.

5.2.5 Data Analysis

Downcore profiles of μXRF and HSI data were established by averaging rows of pixels across 2-mm-wide subsets of the rasterized geochemical data (thus each data point used for analysis represents a 60 x 2000 μm area). Data analysis was conducted in R 4.0.2 (R Core Team, 2020). The HSI pigment data (from the fresh ZAB-20-1 core) was aligned with the μXRF data (from resin-embedded slabs) using the location of varve boundaries manually identified on images of the core and resin-embedded slabs. This alignment was refined at the sub-varve scale using dynamic time warping ('dtw' package; Tormene et al., 2008) to maximize the correlation between Rmean (total reflectance; HSI) and Ca (μXRF) (Fig. S5.1). The largest allowed shift was less than the width of the thinnest varve, so data could not be shifted by more than one year (typically less).

To classify varve types, the package 'distantia' (Benito and Birks, 2020) was used to calculate the dissimilarity measure psi (ψ; Gordon and Birks, 1974), which measures the dissimilarity between pairs of multivariate time series. This ψ statistic was input as the distance matrix for the ward.d2 hierarchical clustering algorithm to identify groups of varves with a similar progression of geochemical data through the year. Data were detrended, log-transformed and scaled prior to classification. Four varve types (VTs) were identified based on the location of the elbow in a plot of ψ vs number of clusters. To determine if the years defined by VTs experienced differing seasonal meteorological conditions, a multivariate analysis of variance (MANOVA) test was performed using seasonal meteorological data from Kętrzyn, Poland, located 40 km west of the study site. Meteorological data were retrieved from the Polish Institute of Meteorology and Water Management – National Research Institute using open data API and climate 0.9.1 R package (Czernecki et al., 2020). We considered a 15-month period from March to May the following

year to account for the uncertainty of assigning the varve boundary to a fixed point in the year. We focus on mean daily temperature, the 90th percentile of daily precipitation, and the 90th percentile of daily mean wind speed based on the expectation that days with intense precipitation or wind would have a stronger effect on the sediments than mean seasonal values.

To further investigate relationships between seasonal meteorological conditions and varve composition, we performed a redundancy analysis (RDA) using the package 'vegan' (Oksanen et al., 2020) in which meteorological variables were used as explanatory variables, and annual mean geochemical data from varve layers were response variables. Additionally, a correlation analysis was performed between monthly meteorological variables and mean annual proxy data. The significance of linear correlations (Pearson's r) was assessed with p-values that were corrected for autocorrelation using the method of Bretherton et al (1999) and were corrected for multiple testing using the false discovery rate approach of Benjamini and Hochberg (1995).

Generalized additive models (GAMs) were used to reconstruct meteorological parameters from sedimentary variables. The target meteorological parameters for reconstruction were selected based on the results of the previous correlation analysis and analysis of variance, which identified temperatures in spring and summer, and windiness throughout multiple seasons as the most important variables driving variability in varve composition and structure. Predictor variables were selected based on the strength of their linear relations. Multiple combinations of possible predictor variables were evaluated and final models were selected based on their predictive power, but also mechanistic process understanding and plausibility. Models were fit with the R package mgcv using the restricted maximum likelihood (REML) smoothness selection (Wood, 2011). To assess the reconstruction skill of the GAM models, a split-period approach was used to calculate reduction of error (RE) and coefficient of efficiency (CE) (von Gunten et al., 2012).

5.3. Results and interpretation

5.3.1 Chronology

The varve count showed no uncertainty to the depth of the 1966 CE varve year, and correlation of varves between multiple cores from different coring years provided further confidence in the varve count. Average varve thickness in the period 1966-2019 was 6.0 mm. Fallout from the 1986 Chernobyl event, recorded in ^{137}Cs activities, peaks in the varves of 1985 and 1986 (Fig. 5.2). The ^{137}Cs activities in these two varves are indistinguishable within the measurement uncertainty (~8 Bq kg^{-1}). The similar activity values in these two varves is explained by the fact that the accident occurred in late April 1986 (roughly coincident with the varve boundary). Additionally, post-depositional diffusion of ^{137}Cs is expected (Klaminder et al., 2012). These results provide independent validation of the accuracy of the varve count.

5.3.2 Geochemical results

Varves in Lake Żabińskie are dominated by autochthonous organic material and calcite. Several long-term patterns (1966-2019) can be observed in the geochemical results (Fig. 5.2; Fig. 5.3). TOC, Ca and S show increasing trends toward the present while MAR, Fe, Si, and Mn decrease. The major increase in Ca is particularly notable, with much higher peaks after around 1992 indicating more calcite precipitation in the epilimnion. At the same time, Mn-rich layers become less frequent after 1992, most likely indicating less frequent seasonal mixing events. Mn layers are preserved during seasonal mixing of the water column that oxygenates the hypolimnion. Oxygenation of the bottom waters leads to precipitation of Mn that had previously been reductively dissolved in the normally anoxic hypolimnion (Schaller and Wehrli, 1996; Scholtysik et al., 2020). The trend toward less frequent mixing after 1992 is likely also responsible for increasing S towards the top of the core. TChl shows little long-term trend but significant year-to-year variability. Increasing TOC towards the present, stable TChl, and decreasing Si are interpreted as a result of a shift towards cyanobacteria and away from siliceous diatoms, as has previously been reported at Lake Żabińskie (Amann et al., 2014).

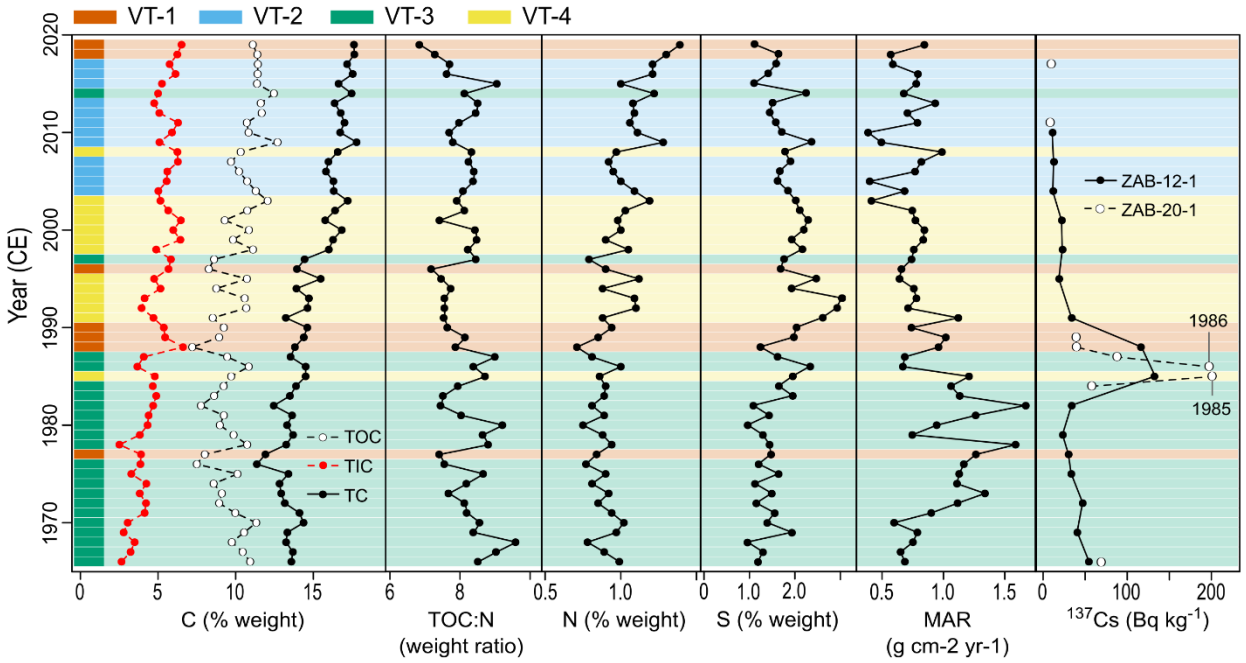

Figure 5.2: Results of CNS elemental analysis, mass accumulation rates, and ^{137}Cs activities displaying the 1986 peak from the Chernobyl accident.

Aligning and averaging all varve years to a fractional varve-year scale enables visualization and description of a 'canonical' varve year, which represents the typical sequence of geochemical variables through an annual cycle. (Fig. 5.4a). The typical varve year begins with the onset of calcite precipitation (as defined in our varve counting procedure), which occurs in the midst of peak primary production. Initial spring blooms of diatoms and other siliceous algae occur immediately after ice breakup, typically in March or April. Calcite precipitation follows after algal blooms uptake CO_2 and temperatures rise (Bonk et al.,

2015). Based on this information, the varve year represents an annual cycle beginning in late April or early May. Calcite precipitation continues throughout the summer with one to three distinct calcite laminae preserved. P typically tracks closely with Ca, suggesting co-precipitation of P with carbonates. TChl decline from relatively high values at the start of the varve year, and are low through late-summer and fall, before rising during winter deposition of fine organic detrital material and peaking during spring algal blooms marking the end of the varve year. Si counts follow a similar seasonal pattern as TChl, with major diatom blooms associated with the largest peaks in both Si and TChl. However, silicate minerals are also a major source of Si, and Si actually correlates better with K ($r = 0.36$, $p < 0.01$; Fig. S5.2) than TChl ($r = 0.24$, $p < 0.01$). Ti follows an opposite pattern compared to Ca with lowest values in the beginning of the varve year and maximal values near the end of the of varve year. High values of Ti are indicative of the period the lake is frozen and mainly fine lithogenic detrital material is deposited. Bphe concentrations are generally low, leading to more measurement noise than the other proxies. However, Bphe shows a clear pattern with highest values occurring in fall, when the anoxic boundary remains high, just before cooling temperatures in the epilimnion lead to mixing and lowering of the anoxic boundary. This terminal stratification period likely features greater light penetration compared to more productive times of spring and summer, ideal for growth of anoxygenic phototrophic bacteria that require light penetration at the chemocline (Sinninghe Damsté and Schouten, 2006). Fe and S show a less-pronounced seasonal pattern than other elements, but tend to reach highest values in late fall and winter. Fe often tracks Ti over the course of the year, indicating lithogenic detrital input is an important source of Fe. Mn has the most variable seasonal pattern with large peaks occurring at different points in the varve year; however, Mn peaks are generally absent in late summer/early fall, and some years show no Mn-rich layers (likely indicating a lack of deep mixing).

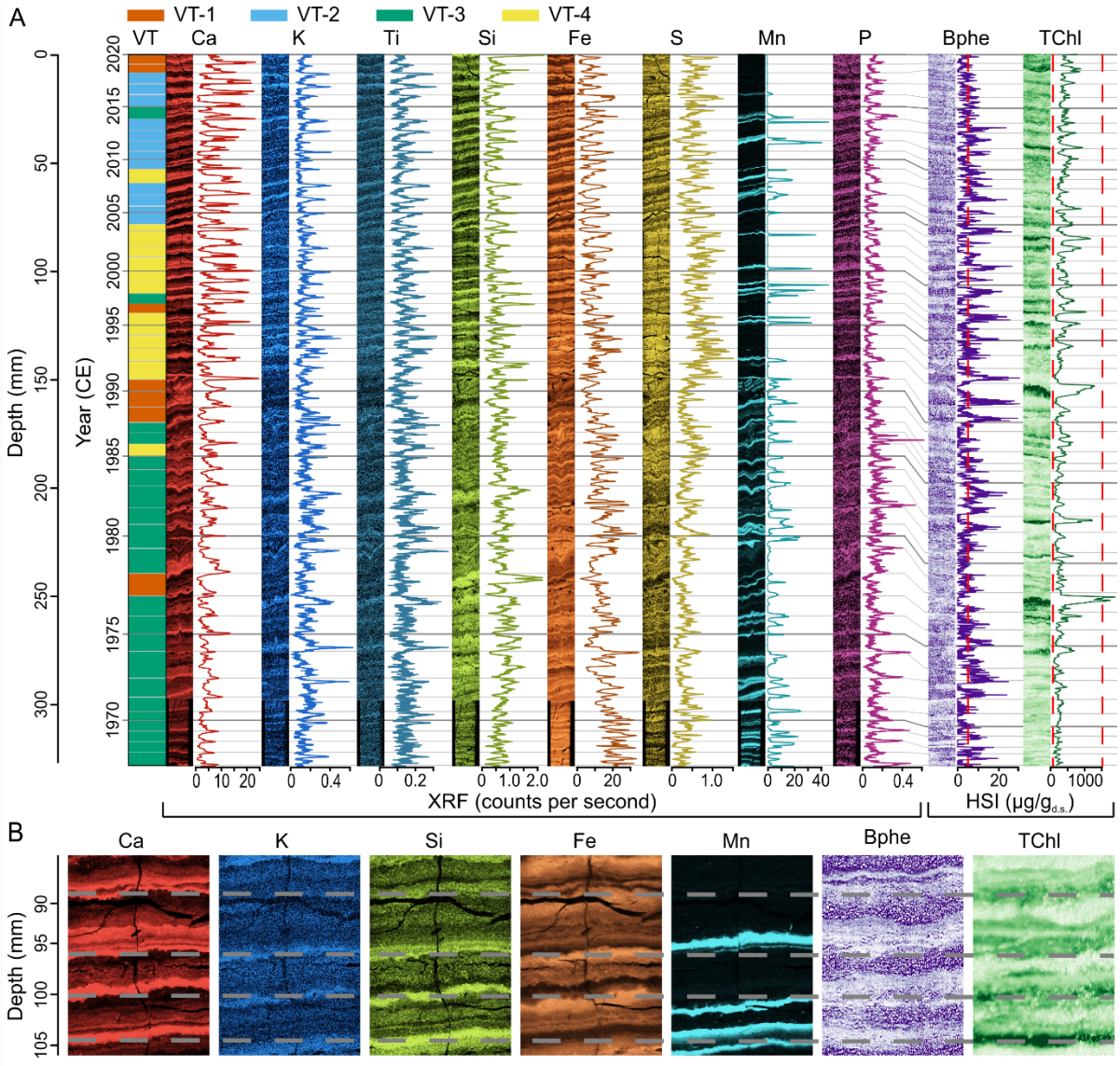

Figure 5.3: High-resolution geochemical data obtained from imaging spectroscopy (µXRF = micro X-Ray fluorescence, HSI = hyperspectral imaging). A) Composite sequence shown as both spatial maps and down-core profiles. Varve boundaries are shown as horizontal lines. Varve types (VTs) are plotted on the left side. µXRF data is from resin-embedded sediment slabs and the data from 1966-1990 is from the 2012 core, data from 1991-2019 is from the 2020 core. HSI data is from the wet 2020 core. Red dashed lines indicate the calibration range for pigment concentrations obtained using HSI. B) Close-ups of spatial distribution of elements and pigments in four varves.

5.3.3 Classification of varve type

The results of the hierarchical clustering algorithm based on the dissimilarity measure of multivariate time series (Fig. S5.3, S5.4) show distinct differences in the seasonal deposition of different elements and pigments (Fig. 5.4b), which correspond to different conditions in the lake and catchment.

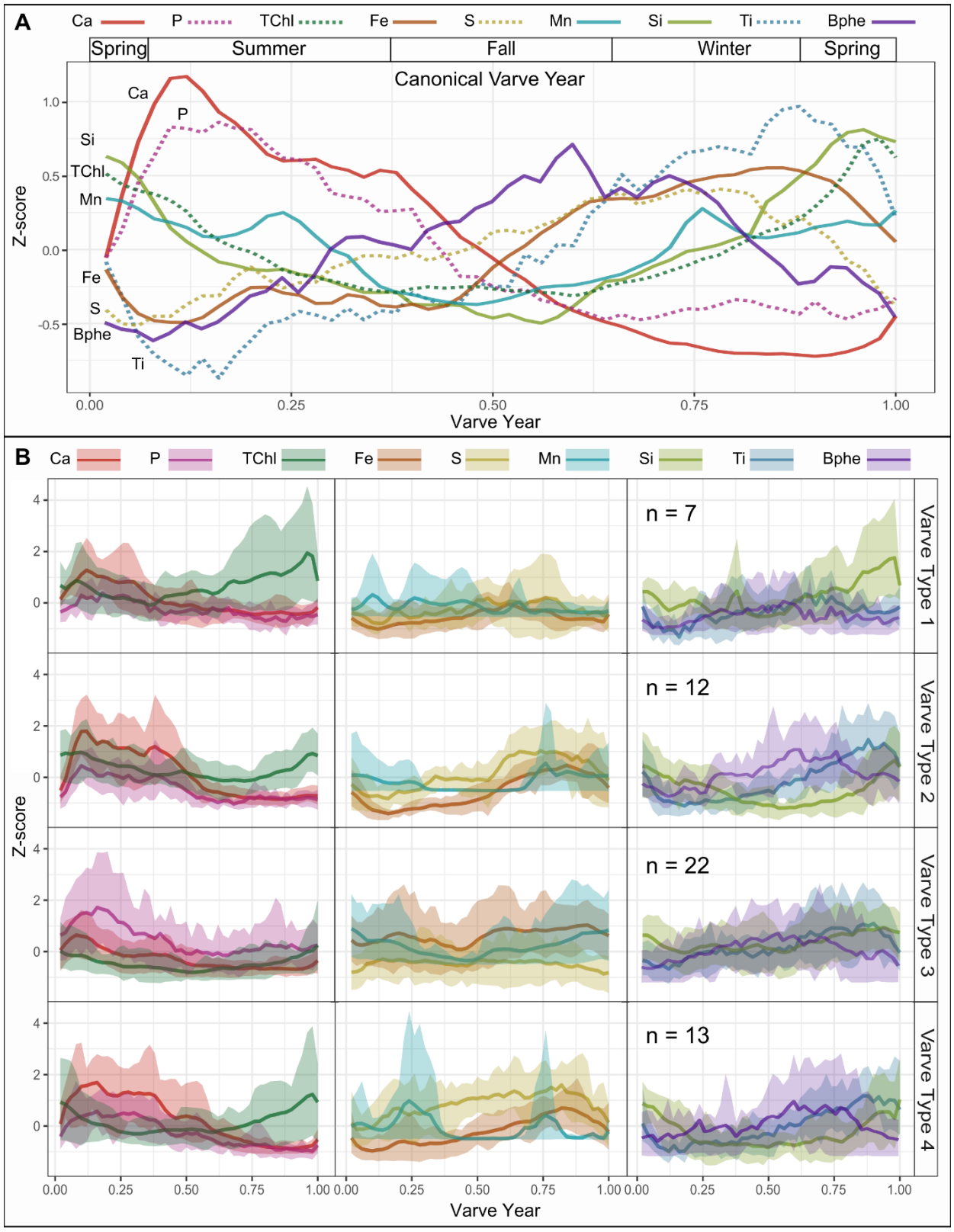

Figure 5.4: A) Average annual sequence of key geochemical variables across a varve year. Varve year begins in spring with calcite precipitation. B) Groups of annual time series determined from hierarchical clustering based on the dissimilarity measure ψ applied to the annual time series. Data plotted is means of varve types, with shaded regions representing 80% of the data for each group.

Varve type 1 (VT-1; n = 7, Fig. 5.4b) occurs occasionally throughout the record and is characterized by low lithogenic input (Ti), and generally lower counts of redox sensitive elements Fe, S, and Mn, though Mn peaks are occasionally present. This pattern indicates that, in the years with VT-1, the water column was strongly stratified and calm, with minimal erosional input or sediment focusing bringing detrital lithogenic material to the lake center. Additionally, elevated values of TChl and high Si near the end of the varve year indicate high productivity at the onset of the following spring prior to calcite deposition.

VT-2 (n = 12, Fig. 5.4b) occurs exclusively since 2004 and is the most common varve type in the past two decades. This type is defined by the highest Ca values in the first half of the varve year, a distinct rise in Bphe, Fe, S and Mn in the second half of the varve year, and relatively high Ti values in winter. This pattern indicates years with a warm and productive epilimnion in summer, leading to extensive anoxia in fall, promoting growth of anoxygenic phototrophic bacteria and formation of iron-sulfides. Mn peaks in some years indicate mixing in spring or late-fall.

VT-3 (n = 22, Fig. 5.4b) dominates during the period 1966-1987, and is identified in only two years after 1987. This type is defined by generally high values of Fe, Mn and P, and low values of Ca and TChl. The pattern of Fe is variable. High values of Mn and Fe throughout the varve year suggest that complete mixing of the water column occurred more often during these years. Detectable concentrations of Bphe in most years are evidence that strong thermal stratification and anoxic conditions still occurred in summer/early-fall. TChl is generally low, though there are some VT-2 years with large TChl peaks (algal blooms). Oxygenation of the water column may have limited TChl preservation (Leavitt and Hodgson, 2002).

VT-4 (n = 13, Fig. 5.4b) occurs primarily in the period 1991-2003 and is characterized by high Ca, TChl and S values. Mn is variable with very high peaks occurring in some years and no Mn in other years. Mn peaks tend to occur either in summer or late fall/early winter. Fe and Ti peak in winter. Bphe is again present mainly in fall. This varve type has higher S counts than the other types, likely indicating strongly reducing conditions in the hypolimnion and sediments (Håkanson and Jansson, 1983).

5.3.4 Relationships between varve composition and meteorological conditions

A MANOVA test was applied to test the hypothesis that the four different varve types (VTs) were formed in years with different typical seasonal meteorological conditions. The MANOVA test yields a significant result ($p = 0.001$), allowing us to reject the null hypothesis. Specifically, temperatures in spring (MAM), summer (JJA) and fall (SON) were significantly different ($p < 0.05$) in the years corresponding to the four varve types, and windiness in spring and fall also showed significant differences (Fig. 5.5). The differences in the meteorological data are consistent with the geochemical patterns defined by the VTs. VT-2 shows the greatest effect of weather conditions with consistently warmer temperatures and less wind in these years. The geochemical character of VT-2 indicates productive, well-stratified and anoxic conditions with intensive calcite precipitation (Fig. 5.4b). This suggests calcite precipitation in this lake is strongly influenced by epilimnetic temperatures, consistent with research in other lakes (e.g. Stabel, 1986). VT-3 is

associated with cooler temperatures and more wind (Fig. 5.5), which promoted more frequent lake mixing and lowered lake productivity, as evidenced by high Mn, P and Fe preservation and low TChl in these varves (Fig. 5.4b). Varve types 1 and 4 show more variability in the meteorological data (Fig. 5.5), with no clearly interpretable effect of weather on their formation.

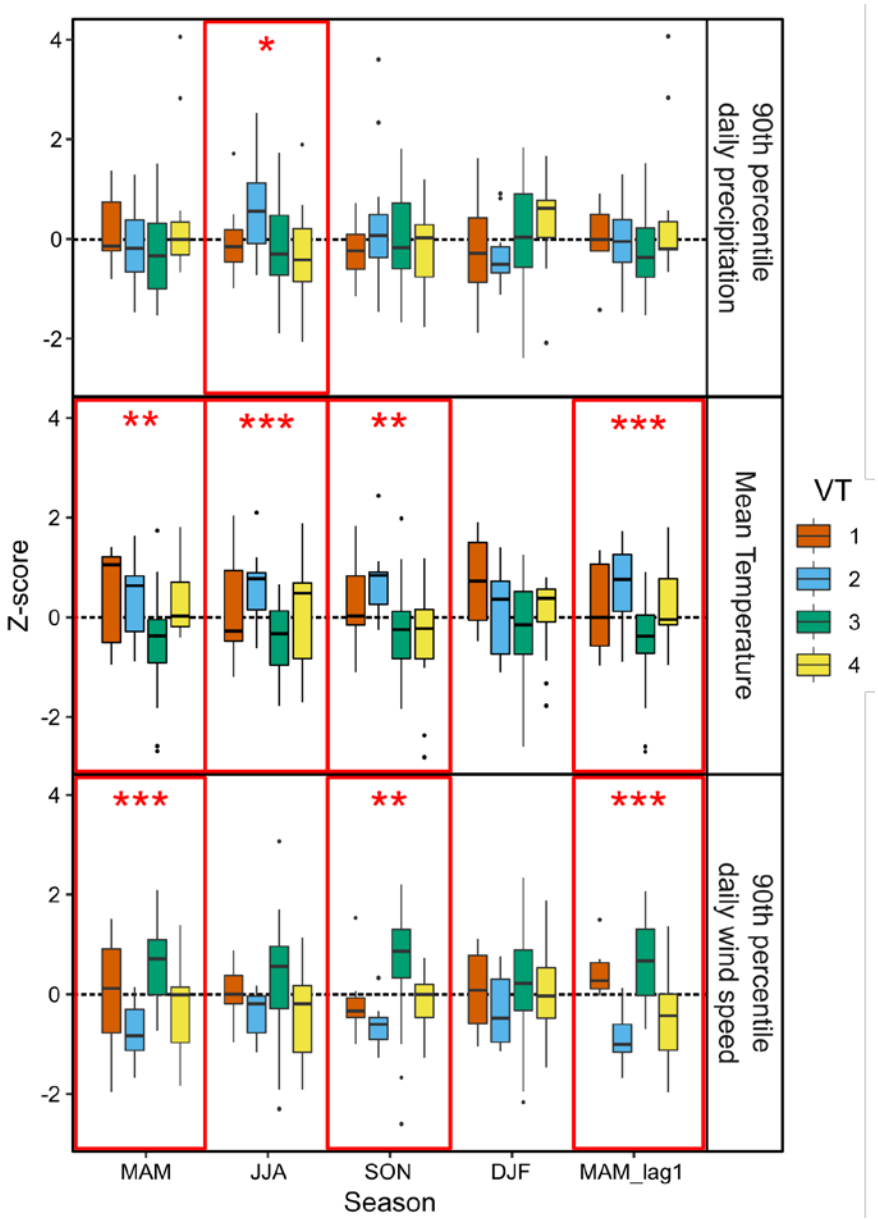

Figure 5.5: Boxplots of seasonal meteorological variables separate by varve types (VT). Red boxes and * symbols indicate meteorological variables with significantly ($p < 0.05$) different means for the four VTs, based on an analysis of variance test (* $p < 0.1$, ** $p < 0.05$, *** $p < 0.01$).

Relationships between meteorological conditions and varve composition were further explored by a redundancy analysis (RDA; Fig. S5.5) and correlation analysis between annual mean values of sedimentary variables and monthly/seasonal meteorological variables (Fig. 5.6;

Table 5.1). The results of the RDA indicate that 46.8% of the variance in the response variables (sedimentary variables) is shared with the explanatory variables (seasonal meteorology). The first RDA axis explains 28% of the variance and shows strong (opposing) effects of temperature and wind on several sedimentary variables, particularly MAR, Ca and TC. Precipitation shows very little similarity with the sedimentary data.

The monthly correlation analysis (Fig. 5.6) highlights how relationships between sedimentary variables and weather vary through the varve year. Temperatures are positively correlated to Ca, TC, TIC and TN, and negatively correlated with lithogenic elements (Ti, K). Spring and summer temperatures show the strongest relationship with the composition of varve layers; in particular TC is well correlated with MAMJJA temperatures ($r = 0.69$, $p_{adj} = 0.004$; Table 5.1). These correlations most probably reflect a combination of temperature-related mechanisms whereby warmer temperatures increase the duration of the growing season, increase algal growth rates (Butterwick et al., 2005), and lower the solubility of carbonates in the epilimnion (Plummer and Busenberg, 1982). Calcium carbonate solubility is controlled directly by water temperature and secondarily through CO_2 uptake from algal production (Stabel, 1986). Additionally, stronger thermal stratification and more extensive and persistent anoxia leads to increased carbon burial in sediments (Bartosiewicz et al., 2019). Negative correlations with Ti and K are likely driven by a dilution effect, whereby increased autochthonous carbonate and organic matter production decrease the concentration of lithogenic components of the mean composition of a varve. Warmer temperatures lengthen the growing season (and shorten ice cover), which increases the relative portion of autochthonous material and decreases the relative portion of lithogenic detritus. The geochemical patterns of VT-2 and -3 illustrate this mechanism. In VT-3, which formed during cooler years, high Ti values make up a greater portion of the varve year compared to VT-2 (warmer years). When calculated as mean values over the varve year, Ti is decreased in warmer years. Our results do not show a significant correlation between TChl and spring temperature, as was previously found by Amann et al. (2014) at Lake Żabińskie over the period 1907-2008 CE ($r = 0.36$, $p_{adj} < 0.05$ for annual resolution data). In our dataset the correlation is positive but not statistically significant ($r = 0.20$, $p_{adj} = 0.30$; Table 5.1), an example of how climate-proxy relationships are not always stable in time (Blass et al., 2007).

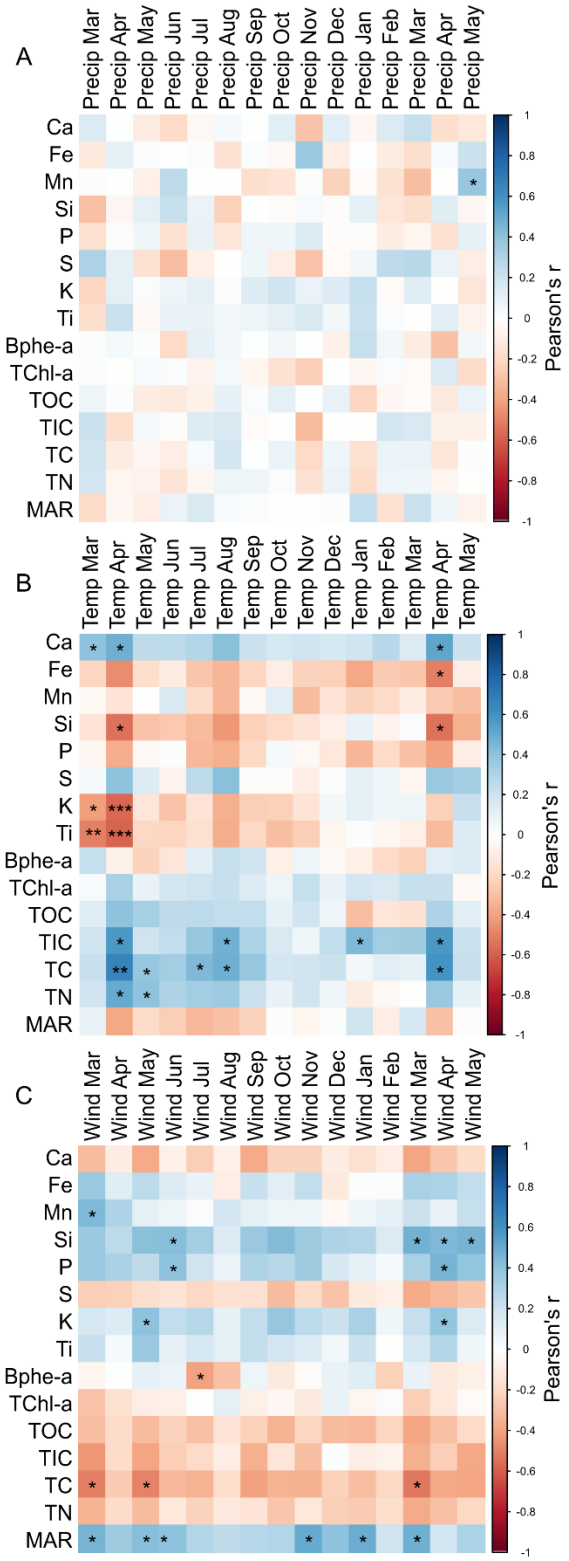

Figure 5.6: Correlation matrices of Pearson correlation coefficient (r) for sedimentary variables (annual mean values) and A) 90th percentile of daily precipitation for each month, B) mean monthly temperature, and C) 90th percentile of daily mean wind speeds for each month. Significance of correlations is identified by * symbols (* $p_{cor} < 0.1$, ** $p_{cor} < 0.05$, *** $p_{cor} < 0.01$).

Correlations between windiness and the data from varves show mostly an opposing pattern to temperature. The variable with the strongest relationship to windiness is MAR (mass accumulation rate). These positive correlations suggest a strong effect of sediment focusing due to wind driven turbulence in shallow parts of the lake, as has been observed in other lakes with varved sediments (e.g. Nuhfer et al., 1993; Roeser et al., 2021). The importance of sediment focusing at Lake Żabińskie was previously identified by higher than expected ^{210}Pb and ^{137}Cs inventories (Tylmann et al., 2016). Si also shows significant correlations with windiness. Resuspension of shallow sediments due to wind would likely transport siliciclastic and clay minerals, as well as benthic diatoms, into the depositional center of the lake. Additionally, wind driven mixing of the water column could help replenish the epilimnion with nutrients and dissolved Si, stimulating growth of siliceous algae (Conley et al., 1993). In addition to sediment focusing, wind strongly affects water column mixing and thereby, redox conditions within the lake. Positive correlations between wind and Mn, Fe and P can be attributed to deep mixing events driven by wind, particularly in spring (Naeher et al., 2013). Lowering of the anoxic boundary results in (re)precipitation of Mn and Fe (hydr)oxides and improves preservation of these elements in the sediments through 'geochemical focusing' (Schaller and Wehrli, 1996; Scholtysik et al., 2020). This geochemical focusing is also an important contribution to higher MARs during windier years (i.e VT-3; Fig. 5.4b, Fig. 5.5). The importance of wind shear on Lake Żabińskie biogeochemical cycling has previously been identified in the studies of the Holocene sedimentary record of Lake Żabińskie (Hernández-Almeida et al., 2014; Żarczyński et al., 2019; Zander et al., 2021). A significant negative correlation between bacteriopheophytin and July windiness could be explained by increased turbidity during windy summers (and limited light at the chemocline) and/or a lowering of the anoxic boundary below the photic zone; both effects would limit growth of anoxygenic phototrophic bacteria. As expected, February wind shows almost no correlation with any sedimentary variable; in February lake ice is consistently thick, shielding the lake from wind effects.

Table 5.1: Correlation matrix of Pearson correlation coefficients for selected meteorlogical variables and data from varves (annual mean values of geochemical data). Bold values indicate significant correlations ($p_{cor} < 0.05$). P-values were corrected for autocorrelation (Bretherton et al., 1999) and the false discovery rate (Benjamini and Hochberg, 1995).

	Temperature						**90th percentile Wind**				**Wind Days**
	MAM	**JJA**	**SON**	**DJF**	**Ann**	**MAMJJA**	**MAM**	**JJA**	**SON**	**DJF**	**Mar-Dec**
Ca	**0.58**	**0.45**	0.31	0.29	**0.58**	**0.61**	-0.32	-0.24	-0.36	-0.21	-0.50
Fe	-0.41	-0.33	-0.28	-0.39	**-0.55**	-0.44	0.31	0.12	0.30	0.02	0.41
Mn	-0.08	-0.17	-0.15	-0.26	-0.28	-0.14	**0.46**	0.09	0.00	-0.02	0.26
Si	**-0.44**	**-0.46**	-0.30	-0.01	-0.36	**-0.53**	**0.48**	**0.45**	0.49	0.40	**0.62**
P	-0.20	-0.31	-0.10	-0.30	-0.37	-0.29	**0.45**	0.25	0.38	0.14	0.41
S	0.26	0.29	-0.07	0.09	0.20	0.32	-0.31	-0.16	-0.14	-0.11	-0.33
K	**-0.57**	-0.35	-0.32	0.11	-0.30	**-0.55**	0.28	0.36	**0.50**	**0.41**	**0.45**
Ti	**-0.66**	-0.34	**-0.39**	-0.04	**-0.44**	**-0.60**	0.24	0.27	0.36	0.25	0.36
Bphe	0.03	0.12	0.13	-0.11	0.01	0.09	0.06	-0.30	-0.08	0.07	-0.05
TChl	0.20	0.28	0.25	0.20	0.34	0.28	-0.31	0.00	-0.22	-0.07	-0.24
TOC	**0.40**	0.35	0.29	-0.18	0.19	**0.44**	-0.41	-0.33	-0.36	**-0.44**	**-0.55**
TIC	**0.46**	**0.51**	0.27	**0.47**	**0.66**	**0.56**	-0.42	-0.29	-0.38	-0.14	**-0.44**
TN	**0.52**	**0.46**	0.27	-0.05	0.34	**0.58**	-0.40	-0.27	-0.27	-0.33	**-0.50**
TC	**0.59**	**0.59**	0.39	0.17	**0.57**	0.69	**-0.58**	-0.44	-0.51	-0.42	**-0.70**
MAR	-0.18	-0.40	-0.14	0.06	-0.17	-0.33	**0.51**	0.37	**0.52**	**0.56**	**0.63**

The correlation analysis (Fig. 5.6, Table 5.1) highlights proxies that are potentially suitable for paleoclimate reconstructions and for which seasons they are most sensitive. Warm season temperatures can be reconstructed using a combination of Ti and TC (or other carbonate/organic proxies), while wind can be reconstructed using MAR, Si, K or P though there is not a strong seasonal signal in the correlations. Bphe shows potential for reconstructing windsspecifically in summer, however the Bphe data is noisy due to concentrations near the detection limit, and summer wind speeds are relatively low, making this signal weak and less consistently reproducible compared to the other proxies (Fig. S5.6).

5.3.5 Temperature and wind reconstructions using generalized additive models

Based on the correlation analysis and investigation of relationships between varve types and meteorological variables, we selected spring and summer (MAMJJA) temperature and the number of windy days (mean daily wind speed > 7 m s^{-1}) from March to December as the most suitable targets for reconstruction. We chose the March to December timeframe for the wind reconstruction because this is the typical ice-free period, and therefore is expected to be most susceptible wind effects. The threshold for a wind day was selected based on the 95th percentile of daily wind speeds within a year to emphasize the importance of extreme wind events. We use the 95th percentile here rather than the 90th percentile used

for monthly and seasonal analysis because the time period is longer here, making the 95th percentile less susceptible to outliers.

Generalized additive models (GAM) were fit to predict meteorological conditions based on varve data at annual resolution. The GAMs method used here is analogous to multiple linear regression, but has the advantage of flexible predictor functions that can account for non-linear relationships between predictor and response variables. We found TC and Ti provided significant predictive power for MAMJJA temperature and a GAM fit to these variables explains 56.4% of the deviance in MAMJJA temperatures (Fig. 5.7). The 10-fold cross validated root mean square error (CV-RMSE) is 0.7 °C. Both predictor variables are significant ($p < 0.05$). Partial effect plots (Fig. S5.7) show the relationships between temperature and predictor variables are nearly linear. Residual analysis confirms the good fit of the model with no trends or significant autocorrelation apparent. The model captures the trends in temperature well, however it struggles to accurately predict temperatures in years with particularly warm or cold temperatures.

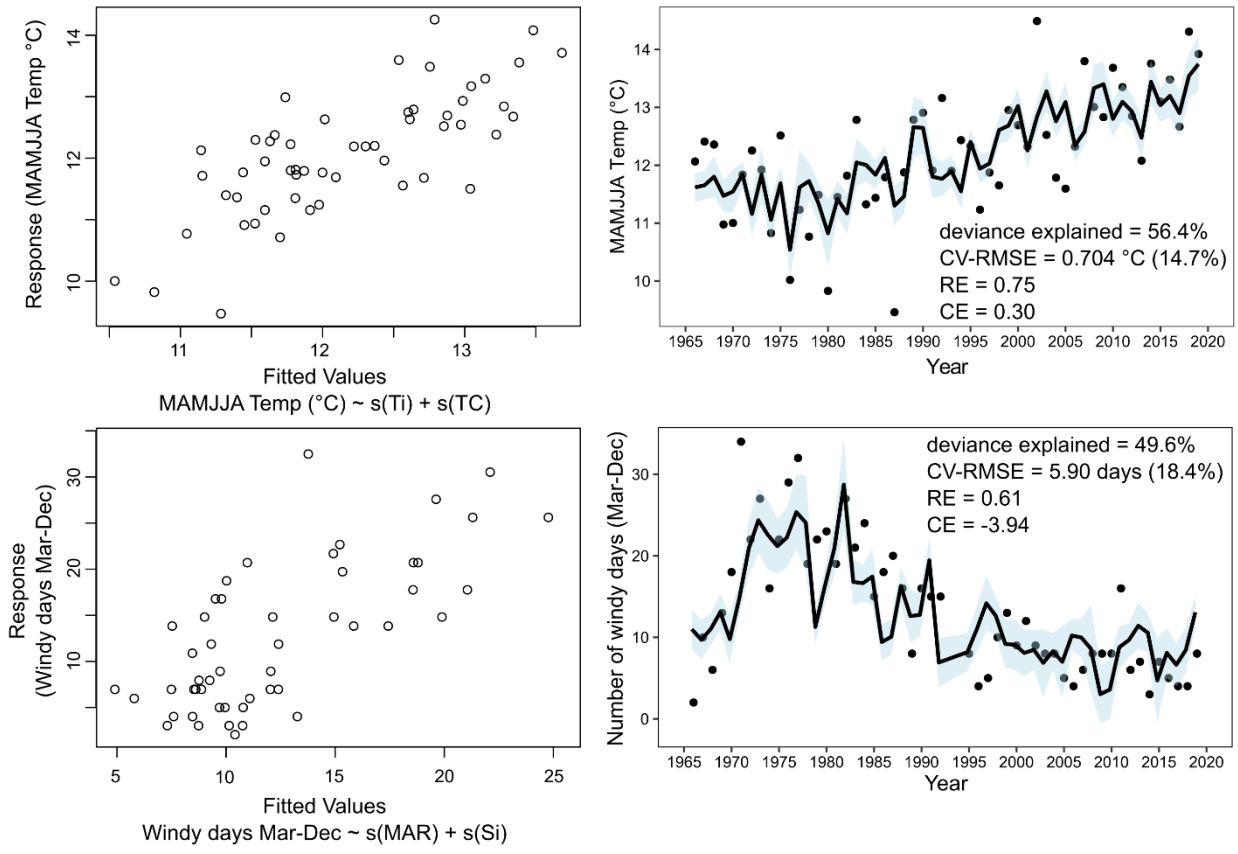

Figure 5.7: Results of generalized additive models used to predict spring and summer temperature and number of windy days from March to December (daily mean wind speeds > 7 m/s).

Wind days were successfully reconstructed using a model with predictors MAR and Si. The years 1993 and 1994 were removed prior to fitting the model because wind data were missing from these years. This model explains 49.6% of the deviance in wind days and has a 10-fold CV-RMSE of 5.9 days (18.4% of the

range) (Fig. 5.7). MAR and Si are significant predictors ($p < 0.05$). Partial effect plots show that the relationship between the predictor variables and wind days are approximately linear (Fig. S5.8). Wind speeds at Kętrzyn station show markedly higher values from 1970-1985, and the model is able to capture this trend well, however very low wind speeds in 1966 and 1968 are not well captured by the model.

The predictive skill of the models was assessed using the metrics reduction of error (RE) and coefficient of efficiency (CE) following von Gunten et al. (2012). These metrics are calculated using a split-period approach in which new GAMs were fit using the same variables and penalties but for a calibration period covering half the dataset: 1966-1992 for MAMJJA temperature and 1966-1991 for wind days (due to two years with missing data). This new model is then applied to the remaining observations (verification period). Positive RE values indicate that the calibration period model predicts observations over the verification period more accurately than using the mean of the calibration period as an unskilled prediction. Positive CE values indicate that the model outperforms the mean of the verification period for predictions over the verification period. The spring and summer temperature model shows predictive skill (RE = 0.75 and CE = 0.30), providing evidence that TC and Ti are potentially useful for temperature reconstructions from Lake Żabińskie, and possibly other sites with calcareous biochemical varves. The model for wind days outperforms the mean of the calibration period (RE = 0.61), but the CE is negative (-3.94) suggesting the model may lack predictive skill when applied beyond the calibration period. This negative CE value can be attributed to the large offset in the mean number of wind days for the calibration and verification periods; this highlights the challenges of reconstructing variables with significant decadal scale variability using such a short calibration period. Additionally, wind speeds are much more spatially variable than temperature, so it remains possible that local variations may lead to differences between wind speeds at Lake Żabińskie compared to the Kętrzyn station.

5.4 Discussion

Our results demonstrate that sub-annual and annual variations in geochemical composition can be related to meteorological conditions; however, there are several challenges in regards to high-resolution climate reconstructions that are worthy of discussion. Measurements of sedimentary variables include some degree of noise that generally becomes more significant as resolution is increased. Scanning data obtained from 2-mm-wide section of sediments are not likely fully representative of whole lake processes responding to meteorological conditions. Additionally, compositing data from different cores may introduce variability. However, repeated measurements on cores taken from different years strengthen our confidence in the reproducibility of our data (Fig. S5.6).

Furthermore, uncertainty is introduced when sampling annual layers for destructive analyses such as TC and DBD because it is easy to include some material from adjacent years. For this reason, high-resolution imaging spectroscopy techniques offer a major advantage because it is possible to consistently and precisely delineate varve boundaries on spatially resolved images of geochemical data. Annual resolution sampling is possible when varves are a few mm thick or more, such as in this study; however, this is not

possible in sediments with thinner varves. In such cases, non-destructive scanning data is essential for high-resolution analyses. Despite ideal material for this work with 6-mm-thick varves and no uncertainty in the varve count, uncertainty in assigning temporal values to data within a single varve remains a limitation of sub-annual analyses. This is because deposition rates are highly variable throughout the year. Determining the season of deposition of certain lamina may be possible (i.e. the first calcite lamina is deposited in April-June), but temporal uncertainty of a couple months or even more should be expected.

Moreover, time series of target meteorological variables for reconstruction are often correlated to one another, making it challenging to separate the influence of multiple potential controlling factors on proxy variables. For instance, the target climate variables used in this study for reconstructions (MAMJJA temperature and Mar-Dec wind days) are correlated ($r = -0.52$; Fig. S5.9), and both are significantly correlated (with opposing signs) with multiple sedimentary variables (Fig. 5.6, Table 5.1). This correlation confounds interpretation of the proxy data because changes in a single variable (for instance, TC) may be influenced by both temperature and wind variability. Furthermore, both proxy data from sediments and meteorological data autocorrelated. Although it is possible to account for this problem via the adjusted-n-technique (Bretherton et al., 1999) for correlations and by cross-validation of the calibration models, autocorrelation nevertheless weakens the strength of statistical inferences that can be made (Telford, 2019).

Non-climatic factors also influence the variability of varve structure and composition at a variety of timescales. The contribution of meteorological conditions to year-to-year variability of the within-varve geochemical time series was assessed by fitting a GAM with differences in seasonal meteorological values as predictor variables and the dissimilarity measure (ψ) as the response. This provides an answer to the question: do greater differences in meteorology between years correspond to greater differences in the within-varve time series? While most of the meteorological variables (9 out of 12) were significant predictors of dissimilarity, only 12.8% of the deviance in the dissimilarity values was explained by changes in meteorological conditions. The RDA investigates the relationship between weather conditions and mean annual sedimentary data, and presents a stronger link between weather and sediment properties with 46.8% of the variability in the sedimentary data redundant with variability in the seasonal meteorological data. Nonetheless, it is clear that other factors, such as human activity in the catchment, diagenetic effects, internal variability in biogeochemical cycling, or other possible factors, play an important role controlling the geochemical composition and structure of these varves. One such confounding variable is nutrient input to the lake. The proposed temperature reconstruction in this study assumes that algal production and calcite precipitation are driven to large extent by temperature variability. However, nutrient levels in the lake are likely also an important control on the carbon contents of the sediments (Fiskal et al., 2019). Diatom-based P reconstructions show an increasing trend over the period 1966-2010, similar to our temperature reconstruction (Witak et al., 2017). However, fertilizer use in the region is not well correlated with the diatom P reconstruction. It remains possible that the diatom signal is a response to meteorological changes rather than a separate external driver. One plausible feedback mechanism would be warmer

temperatures strengthen thermal stratification leading to more extensive anoxia and increased P release from sediments due to reductive dissolution of phosphates (Tu et al., 2020).

A further issue with the calibration-in-time approach used here is that the observational period is short and relationships between variables that are valid for this period may not apply to previous periods if reconstructions are applied further back in time (Blass et al., 2007). This is especially problematic for sites that have experienced major environmental changes (often human-induced) outside the calibration period, as is known for Lake Żabińskie (Hernández-Almeida et al., 2017). Nonetheless, positive CE and RE values for the spring and summer temperature model are a promising indicator that this reconstruction may be valid beyond the study period. Future work could investigate the climate-proxy relationships studied here over longer time-scales; however age uncertainty would require smoothing or aggregating data to lower temporal resolution.

Despite the aforementioned caveats, our results suggest that bulk geochemical variables, particularly from high-resolution scanning techniques, are a promising tool for high-resolution quantitative climate reconstructions from biochemical varves. Microfossil assemblages have generally been the method of choice for climate reconstructions from biogenic varves, however paleoecological transfer functions can also suffer from similar problems as those mentioned above, such as confounding variables, autocorrelation, and assumptions about the stability of climate proxy relationships through time. Additionally, the temporal resolution of such analyses is limited by the requirement for destructive sampling and time-consuming analyses. We find that the CV-RMSE for the spring and summer temperature reconstruction (0.7 °C) is comparable, or lower, than typical RMSE from climate transfer functions based on microfossil assemblages (Heiri et al., 2003). On the other hand, geochemical data are quickly measured at high-resolution using non-destructive scanning techniques such as XRF and reflectance spectroscopy; we propose that these data have untapped potential for quantitative climate reconstructions from biochemical varves.

5.5 Conclusions

The results of this study demonstrate the potential of high-resolution spectroscopy imaging techniques to enhance our understanding of sub-varve scale sedimentary processes. Relationships between meteorological conditions and varve composition and structure were explored through statistical techniques. The sequence of geochemical variables through the course of the varve year was shown to be influenced by changing seasonal meteorological conditions, though a large portion of variance in these within-varve time series remained unexplained by year-to-year meteorological variability. Correlation analysis identified spring and summer (MAMJJA) temperatures, and wind days during the ice-free season (Mar-Dec) as meteorological variables with the greatest potential for proxy-climate calibration from these sediments. GAMs were applied to reconstruct these two variables at annual resolution over the study period (1966-2019). Total C and Ti were used as predictors for MAMJJA temperature and yielded a reconstruction with good prediction performance (CV-RMSE = 0.7 °C, 14.7%). Mass accumulation rate

and Si were used to predict Mar-Dec wind days (CV-RMSE = 5.9 wind days, 18.4%). Split-period validation provides evidence that the temperature reconstruction model has predictive skill and may be applied outside the calibration period, whereas the wind reconstruction model warrants caution if applied beyond the calibration period. Our results provide a rare example of quantitative climate reconstruction based on bulk geochemical data from biochemical varves. The approach used in this study could be applied to other sites with varved sediments to generate paleoclimate reconstructions. Our results also provide evidence of the significant impact of recent climate change on lake biogeochemical cycling. Ultra-high-resolution spectroscopy imaging techniques, such as those applied in this study, show great potential for a variety of paleoenvironmental reconstructions from numerous archives beyond lake sediments such as speleothems, fossils, tree ring cores and many others.

5.6 Acknowledgements

This work was funded by Swiss National Science Foundation grant 200021_172586 and Polish National Science Centre project NCN 2015/18/E/ST10/00325. Joanna Piłczyńska assisted with lab analyses.

5.7 References

Amann, B., Lobsiger, S., Fischer, D., Tylmann, W., Bonk, A., Filipiak, J., Grosjean, M., 2014. Spring temperature variability and eutrophication history inferred from sedimentary pigments in the varved sediments of Lake Żabińskie, north-eastern Poland, AD 1907-2008. Glob. Planet. Change 123, 86-96. https://doi.org/10.1016/j.gloplacha.2014.10.008

Bartosiewicz, M., Przytulska, A., Lapierre, J., Laurion, I., Lehmann, M.F., Maranger, R., 2019. Hot tops, cold bottoms: Synergistic climate warming and shielding effects increase carbon burial in lakes. Limnol. Oceanogr. Lett. 4, 132-144. https://doi.org/10.1002/lol2.10117

Benito, B.M., Birks, H.J.B., 2020. distantia: an open-source toolset to quantify dissimilarity between multivariate ecological time-series. Ecography (Cop.). 43, 660-667. https://doi.org/10.1111/ecog.04895

Benjamini, Y., Hochberg, Y., 1995. Controlling the False Discovery Rate: A Practical and Powerful Approach to Multiple Testing. J. R. Stat. Soc. Ser. B 57, 289-300. https://doi.org/10.1111/j.2517-6161.1995.tb02031.x

Blass, A., Grosjean, M., Troxler, A., Sturm, M., 2007. How stable are twentieth-century calibration models? A high-resolution summer temperature reconstruction for the eastern Swiss Alps back to AD 1580 derived from proglacial varved sediments. The Holocene 17, 51-63. https://doi.org/10.1177/0959683607073278

Bonk, A., Kinder, M., Enters, D., Grosjean, M., Meyer-Jacob, C., Tylmann, W., 2016. Sedimentological and geochemical responses of Lake Żabińskie (north-eastern Poland) to erosion changes during the last millennium. J. Paleolimnol. 56, 239-252. https://doi.org/10.1007/s10933-016-9910-6

Bonk, A., Tylmann, W., Amann, B., Enters, D., Grosjean, M., 2015. Modern limnology and varve-formation processes in lake Żabińskie, northeastern Poland: Comprehensive process studies as a key to understand the sediment record. J. Limnol. 74, 358-370. https://doi.org/10.4081/jlimnol.2014.1117

Bretherton, C.S., Widmann, M., Dymnikov, V.P., Wallace, J.M., Bladé, I., 1999. The effective number of spatial degrees of freedom of a time-varying field. J. Clim. 12, 1990-2009. https://doi.org/10.1175/1520-0442(1999)012<1990:TENOSD>2.0.CO;2

Butterwick, C., Heaney, S.I., Talling, J.F., 2005. Diversity in the influence of temperature on the growth rates of freshwater algae, and its ecological relevance. Freshw. Biol. 50, 291-300. https://doi.org/10.1111/j.1365-2427.2004.01317.x

Butz, C., Grosjean, M., Fischer, D., Wunderle, S., Tylmann, W., Rein, B., 2015. Hyperspectral imaging spectroscopy: a promising method for the biogeochemical analysis of lake sediments. J. Appl. Remote Sens. 9, 096031. https://doi.org/10.1117/1.jrs.9.096031

Butz, C., Grosjean, M., Goslar, T., Tylmann, W., 2017. Hyperspectral imaging of sedimentary bacterial pigments: a 1700-year history of meromixis from varved Lake Jaczno, northeast Poland. J. Paleolimnol. 58, 57-72. https://doi.org/10.1007/s10933-017-9955-1

Conley, D.J., Schelske, C.L., Stoermer, E.F., 1993. Modification of the biogeochemical cycle of silica with eutrophication. Mar. Ecol. Prog. Ser. 101, 179-192. https://doi.org/10.3354/meps101179

Czernecki, B., Glogowski, A., Nowosad, J., 2020. Climate: An R Package to Access Free In-Situ Meteorological and Hydrological Datasets For Environmental Assessment. Sustainability. https://doi.org/10.3390/su12010394

De Geer, G., 1908. On late quaternary time and climate. Geol. Föreningen i Stock. Förhandlingar 30, 459-464. https://doi.org/10.1080/11035890809445600

Fiskal, A., Deng, L., Michel, A., et al., 2019. Effects of eutrophication on sedimentary organic carbon cycling in five temperate lakes. Biogeosciences 16, 3725-3746. https://doi.org/10.5194/bg-16-3725-2019

Francus, P., Bradley, R.S., Abbott, M.B., Patridge, W., Keimig, F., 2002. Paleoclimate studies of minerogenic sediments using annually resolved textural parameters. Geophys. Res. Lett. 29, 59-1-59-4. https://doi.org/10.1029/2002GL015082

Gälman, V., Rydberg, J., De-Luna, S.S., Bindler, R., Renberg, I., 2008. Carbon and nitrogen loss rates during aging of lake sediment: Changes over 27 years studied in varved lake sediment. Limnol. Oceanogr. 53, 1076-1082. https://doi.org/10.4319/lo.2008.53.3.1076

Gordon, A.D., Birks, H.J.B., 1974. Numerical methods in Quaternary palaeoecology: II. Comparison of pollen diagrams. New Phytol. 73, 221-249. https://doi.org/10.1111/j.1469-8137.1974.tb04621.x

Håkanson, L., Jansson, M., 1983. Principles of Lake Sedimentology, Principles of Lake Sedimentology. Blackburn Press. https://doi.org/10.1007/978-3-642-69274-1

Heiri, O., Birks, H.J.B., Brooks, S.J., Velle, G., Willassen, E., 2003. Effects of within-lake variability of fossil assemblages on quantitative chironomid-inferred temperature reconstruction. Palaeogeogr. Palaeoclimatol. Palaeoecol. 199, 95-106. https://doi.org/10.1016/S0031-0182(03)00498-X

Hernández-Almeida, I., Grosjean, M., Gómez-Navarro, J.J., et al., 2017. Resilience, rapid transitions and regime shifts: Fingerprinting the responses of Lake Żabińskie (NE Poland) to climate variability and human disturbance since AD 1000. Holocene 27, 258-270. https://doi.org/10.1177/0959683616658529

Hernández-Almeida, I., Grosjean, M., Tylmann, W., Bonk, A., 2014. Chrysophyte cyst-inferred variability of warm season lake water chemistry and climate in northern Poland: training set and downcore reconstruction. J. Paleolimnol. 53, 123-138. https://doi.org/10.1007/s10933-014-9812-4

IPCC, 2013. Climate Change 2013: The Physical Science Basis. Contribution of Working Group I to the Fifth Assessment Report of the Intergovernmental Panel on Climate Change. Cambridge University Press.

Klaminder, J., Appleby, P., Crook, P., Renberg, I., 2012. Post-deposition diffusion of ^{137}Cs in lake sediment: Implications for radiocaesium dating. Sedimentology 59, 2259-2267. https://doi.org/10.1111/j.1365-3091.2012.01343.x

Lapointe, F., Bradley, R.S., Francus, P., Balascio, N.L., Abbott, M.B., Stoner, J.S., St-Onge, G., de Coninck, A., Labarre, T., 2020. Annually resolved Atlantic sea surface temperature variability over the past 2,900 y. Proc. Natl. Acad. Sci. U. S. A. 117, 27171-27178. https://doi.org/10.1073/pnas.2014166117

Leavitt, P.R., Hodgson, D.A., 2002. Sedimentary Pigments, in: Tracking Environmental Change Using Lake Sediments. Springer, Dordrecht, pp. 295-325. https://doi.org/10.1007/0-306-47668-1_15

Naeher, S., Gilli, A., North, R.P., Hamann, Y., Schubert, C.J., 2013. Tracing bottom water oxygenation with sedimentary Mn/Fe ratios in Lake Zurich, Switzerland. Chem. Geol. 352, 125-133. https://doi.org/10.1016/j.chemgeo.2013.06.006

Neukom, R., Steiger, N., Gómez-Navarro, J.J., Wang, J., Werner, J.P., 2019. No evidence for globally coherent warm and cold periods over the preindustrial Common Era. Nature 571, 550-554. https://doi.org/10.1038/s41586-019-1401-2

Nuhfer, E.B.E., Anderson, R.Y.R., Bradbury, J.P., Dean, W.E., 1993. Modern sedimentation in Elk Lake, Clearwater County, Minnesota, in: Bradbury, J. P.Dean, W.E. (Ed.), Elk Lake, Minnesota: Evidence for Rapid Climate Change in the North-Central United States. Geological Society of America Special Paper 276, Boulder, CO, pp. 75-96. https://doi.org/10.1130/SPE276-p75

Oksanen, J., Blanchet, F.G., Friendly, M., et al., 2020. vegan: Community Ecology Package.

Plummer, L.N., Busenberg, E., 1982. The solubilities of calcite, aragonite and vaterite in CO2-H2O solutions between 0 and 90°C, and an evaluation of the aqueous model for the system CaCO3-CO2-H2O. Geochim. Cosmochim. Acta 46, 1011-1040. https://doi.org/10.1016/0016-7037(82)90056-4

R Core Team, 2020. R: A Language and Environment for Statistical Computing.

Rein, B., Sirocko, F., 2002. In-situ reflectance spectroscopy - Analysing techniques for high-resolution pigment logging in sediment cores. Int. J. Earth Sci. 91, 950-954. https://doi.org/10.1007/s00531-002-0264-0

Roeser, P., Dräger, N., Brykała, D., et al., 2021. Advances in understanding calcite varve formation: new insights from a dual lake monitoring approach in the southern Baltic lowlands. Boreas. https://doi.org/10.1111/BOR.12506

Schaller, T., Wehrli, B., 1996. Geochemical-focusing of manganese in lake sediments - An indicator of deep-water oxygen conditions. Aquat. Geochemistry 2, 359-378. https://doi.org/10.1007/bf00115977

Scholtysik, G., Dellwig, O., Roeser, P., Arz, H.W., Casper, P., Herzog, C., Goldhammer, T., Hupfer, M., 2020. Geochemical focusing and sequestration of manganese during eutrophication of Lake Stechlin (NE Germany). Biogeochemistry 151, 313-334. https://doi.org/10.1007/s10533-020-00729-9

Sinninghe Damsté, J.S., Schouten, S., 2006. Biological markers for anoxia in the photic zone of the water column. Handb. Environ. Chem. Vol. 2 React. Process. 2 N, 127-163. https://doi.org/10.1007/698_2_005

Stabel, H.-H., 1986. Calcite precipitation in Lake Constance: Chemical equilibrium, sedimentation, and nucleation by algae1. Limnol. Oceanogr. 31, 1081-1094. https://doi.org/10.4319/lo.1986.31.5.1081

Swierczynski, T., Brauer, A., Lauterbach, S., Martín-Puertas, C., Dulski, P., von Grafenstein, U., Rohr, C., 2012. A 1600 yr seasonally resolved record of decadal-scale flood variability from the Austrian Pre-Alps. Geology 40, 1047-1050. https://doi.org/10.1130/G33493.1

Telford, R.J., 2019. Review and test of reproducibility of subdecadal resolution palaeoenvironmental reconstructions from microfossil assemblages. Quat. Sci. Rev. 222, 105893. https://doi.org/10.1016/j.quascirev.2019.105893

Tian, J., Nelson, D.M., Hu, F.S., 2011. How well do sediment indicators record past climate? An evaluation using annually laminated sediments. J. Paleolimnol. 45, 73-84. https://doi.org/10.1007/s10933-010-9481-x

Tormene, P., Giorgino, T., Quaglini, S., Stefanelli, M., 2008. Matching Incomplete Time Series with Dynamic Time Warping: An Algorithm and an Application to Post-Stroke Rehabilitation. Artif. Intell. Med. 45, 11-34. https://doi.org/10.1016/j.artmed.2008.11.007

Trachsel, M., Grosjean, M., Schnyder, D., Kamenik, C., Rein, B., 2010. Scanning reflectance spectroscopy (380-730 nm): A novel method for quantitative high-resolution climate reconstructions from minerogenic lake sediments. J. Paleolimnol. 44, 979-994. https://doi.org/10.1007/s10933-010-9468-7

Tu, L., Zander, P., Szidat, S., Lloren, R., Grosjean, M., 2020. The influences of historic lake trophy and mixing regime changes on long-term phosphorus fractions retention in sediments of deep, eutrophic lakes: a case study from Lake Burgäschi, Switzerland. Biogeosciences 17, 2715-2729. https://doi.org/10.5194/bg-2019-389

Tylmann, W., Bonk, A., Goslar, T., Wulf, S., Grosjean, M., 2016. Calibrating 210 Pb dating results with varve chronology and independent chronostratigraphic markers: Problems and implications. Quat. Geochronol. 32, 1-10. https://doi.org/10.1016/j.quageo.2015.11.004

von Gunten, L., Grosjean, M., Kamenik, C., Fujak, M., Urrutia, R., 2012. Calibrating biogeochemical and physical climate proxies from non-varved lake sediments with meteorological data: Methods and case studies. J. Paleolimnol. 47, 583-600. https://doi.org/10.1007/s10933-012-9582-9

Witak, M., Hernández-Almeida, I., Grosjean, M., Tylmann, W., 2017. Diatom-based reconstruction of trophic status changes recorded in varved sediments of Lake Żabińskie (northeastern Poland), AD 1888-2010. Oceanol. Hydrobiol. Stud. 46, 1-17. https://doi.org/10.1515/ohs-2017-0001

Wood, S.N., 2011. Fast stable restricted maximum likelihood and marginal likelihood estimation of semiparametric generalized linear models. J. R. Stat. Soc. 73, 3-36.

Zander, P.D., Żarczyński, M., Vogel, H., Tylmann, W., Wacnik, A., Sanchini, A., Grosjean, M., 2021. A high-resolution record of Holocene primary productivity and water-column mixing from the varved sediments of Lake Żabińskie, Poland. Sci. Total Environ. 755, 143713. https://doi.org/10.1016/j.scitotenv.2020.143713

Żarczyński, M., Tylmann, W., Goslar, T., 2018. Multiple varve chronologies for the last 2000 years from the sediments of Lake Żabińskie (northeastern Poland) - Comparison of strategies for varve counting and uncertainty estimations. Quat. Geochronol. 47, 107-119. https://doi.org/10.1016/j.quageo.2018.06.001

Żarczyński, M., Wacnik, A., Tylmann, W., 2019. Tracing lake mixing and oxygenation regime using the Fe/Mn ratio in varved sediments: 2000 year-long record of human-induced changes from Lake Żabińskie (NE Poland). Sci. Total Environ. 657, 585-596. https://doi.org/10.1016/j.scitotenv.2018.12.078

Zolitschka, B., Francus, P., Ojala, A.E.K., Schimmelmann, A., 2015. Varves in lake sediments - a review. Quat. Sci. Rev. 117, 1-41. https://doi.org/10.1016/j.quascirev.2015.03.019

5.7 Supplementary material

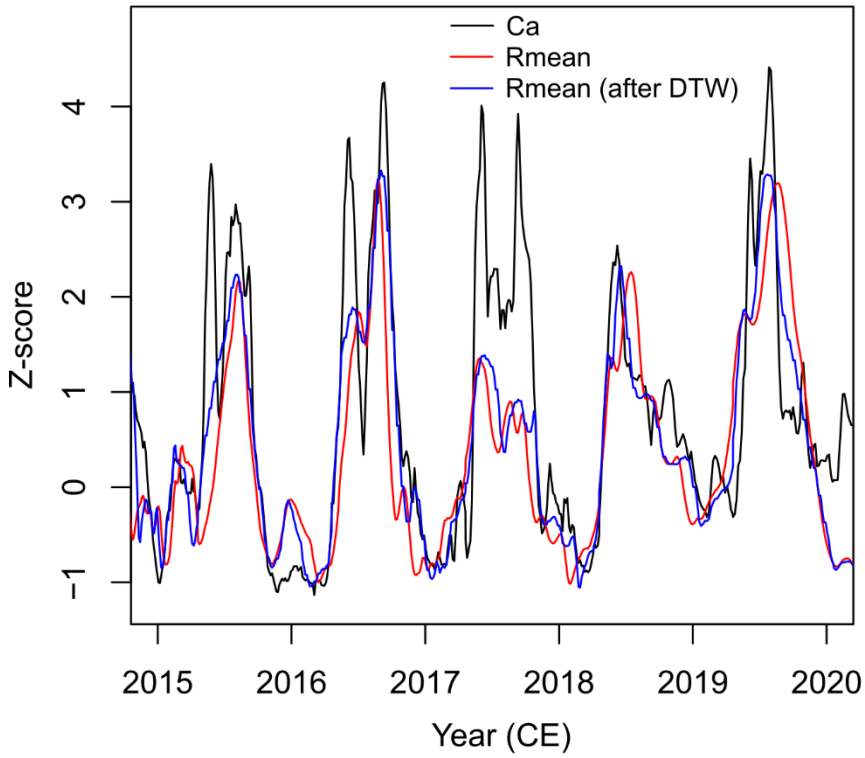

Figure S5.1: Example of the effect of dynamic time warping alignment used to align HSI and µXRF data at the sub-varve scale. Red line shows Rmean plotted on varve age scale from varve counting on HSI image. Blue line shows the same data after alignment to the Ca µXRF data. This new alignment was then applied to Bphe and TChl data from HSI before any other analyses.

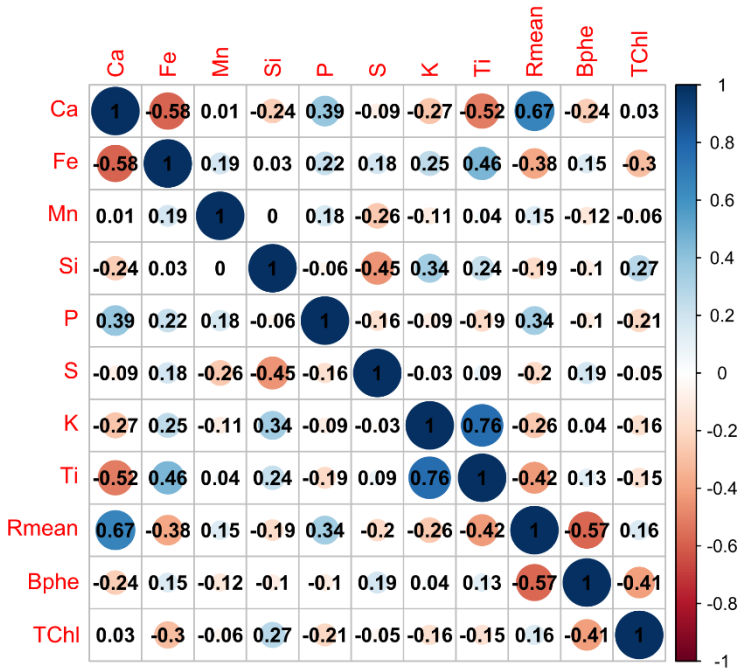

Figure S5.2: Correlation plot of high-resolution spectroscopy imaging data at original resolution (60 µm, n = 5631).

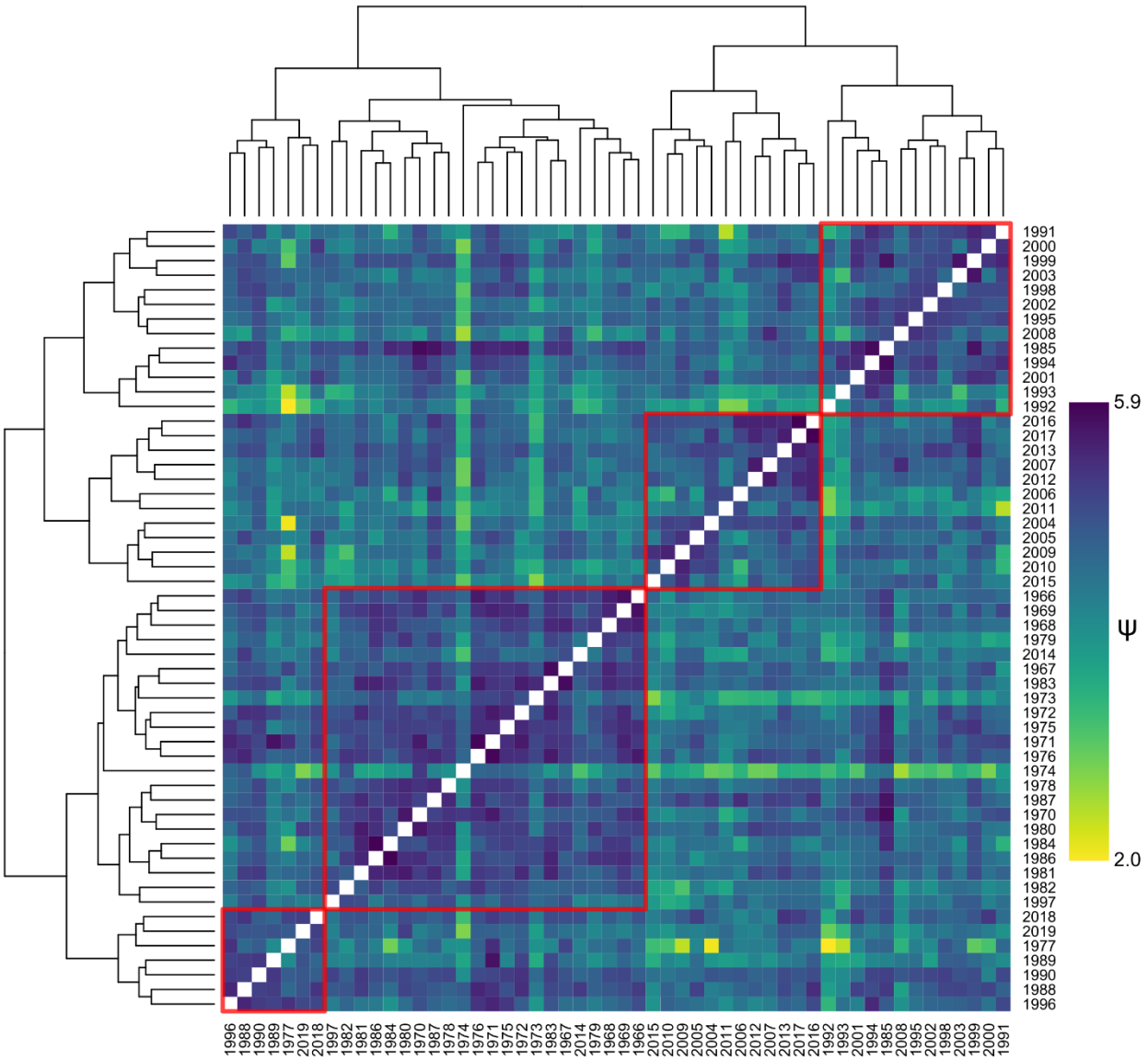

Figure S5.3: Matrix of dissimilarity values psi (ψ) and dendrogram resulting from hierarchical clustering. Red boxes identify varve type (VT) clusters.

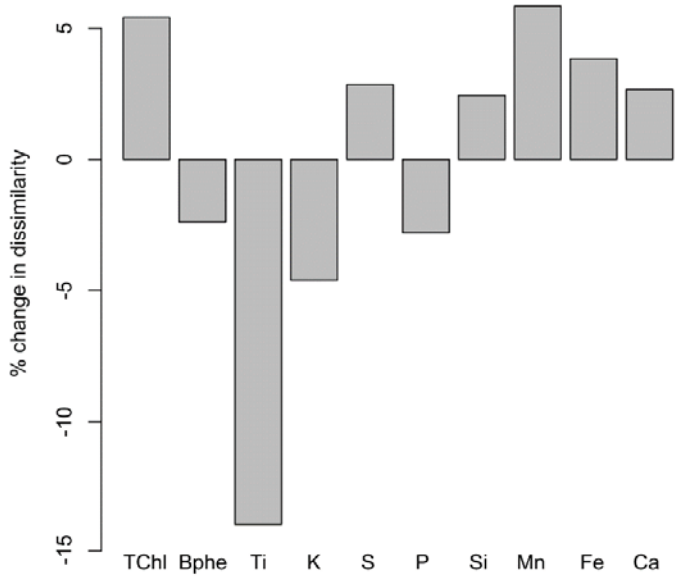

Figure S5.4: Percent change in dissimilarity (ψ) attributed to each variable. Positive values indicate the variable contributes to year-to-year dissimilarity in annual time series. Negative values indicate that the variable contributes to year-to-year similarity in annual time series.

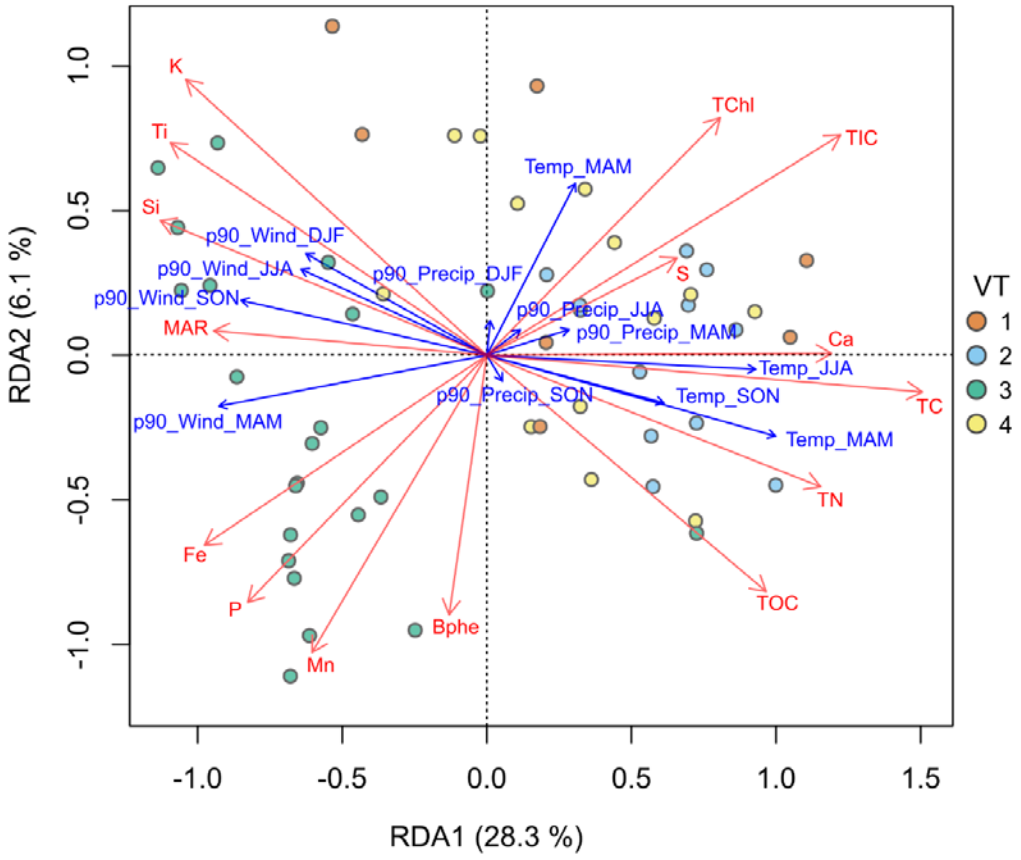

Figure S5.5: Results of a Redundancy Analysis (RDA) with mean annual proxy data as response variables and seasonal meteorological data as explanatory variables.

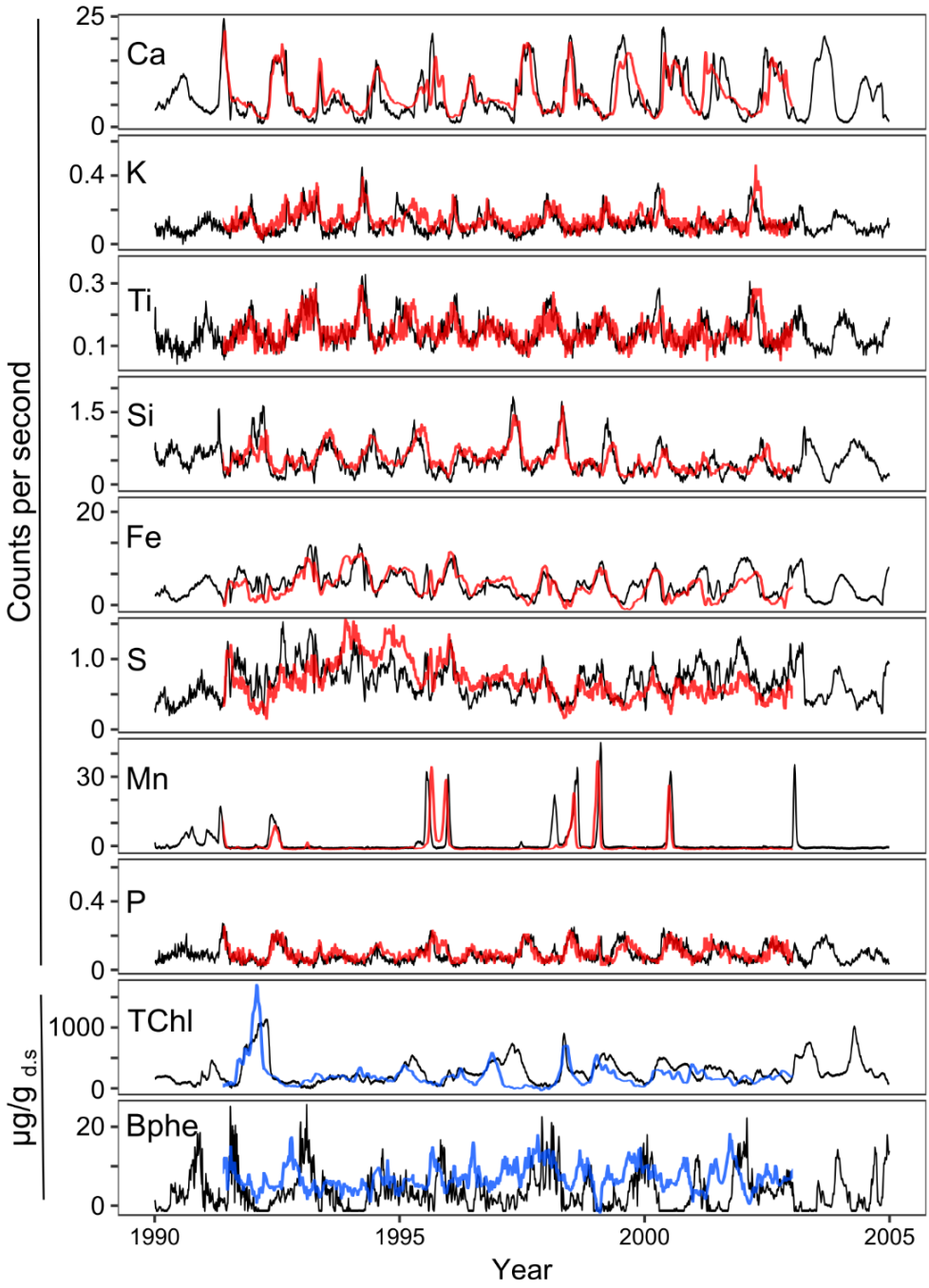

Figure S5.6: Plot demonstrating reproducibility of high-resolution scanning data by measurement of overlapping sections from different cores. Black lines represent data used in this study. Red lines represent an overlapping segment of the ZAB-12-1 core that was not used in the composite data for this study. Blue lines represent HSI data from an additional core (ZAB-19-1) not used for other analyses in this study.

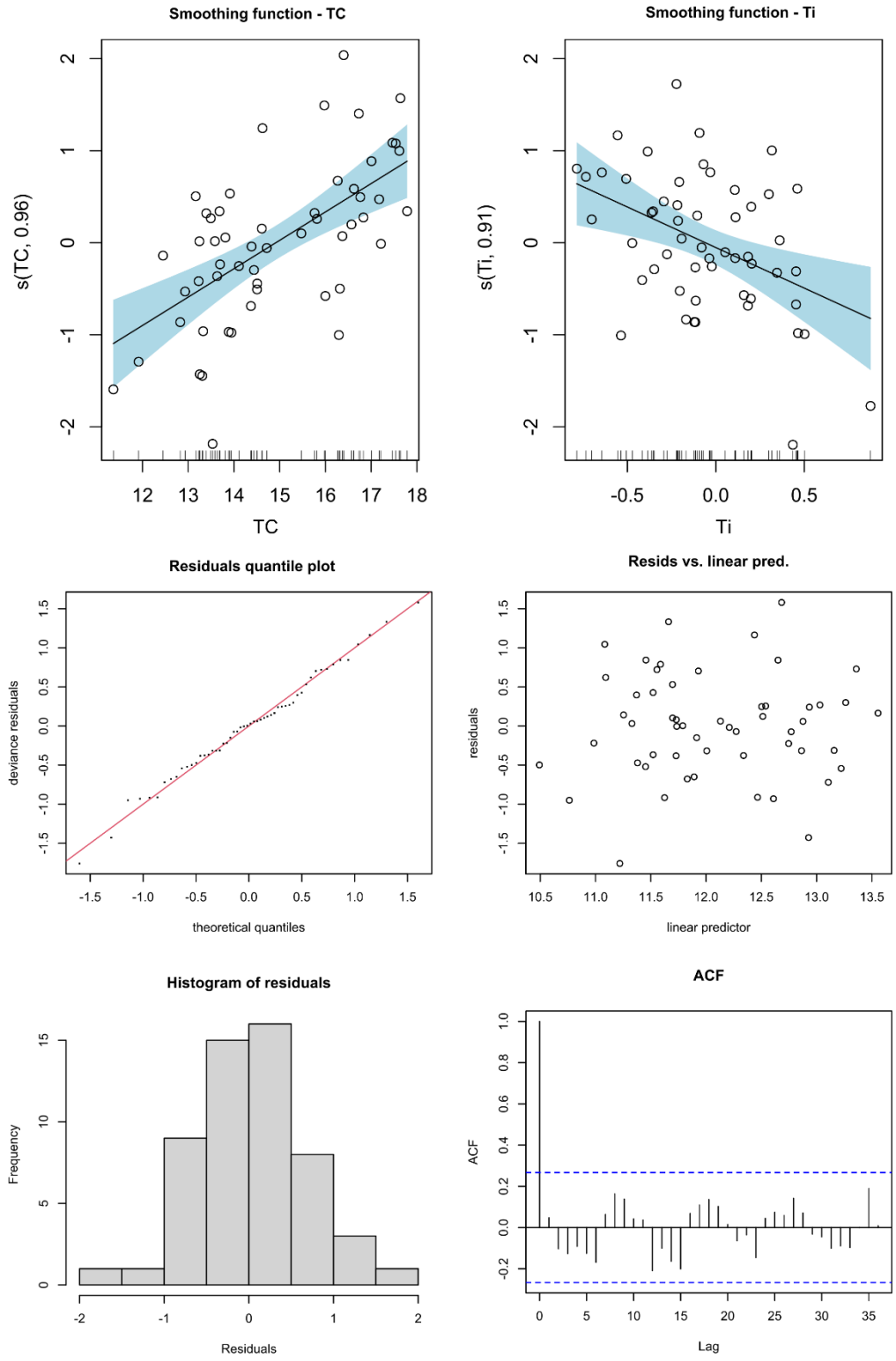

Figure S5.7: Partial effect plots and diagnostic plots for spring and summer temperature GAM reconstruction fit with TC and Ti.

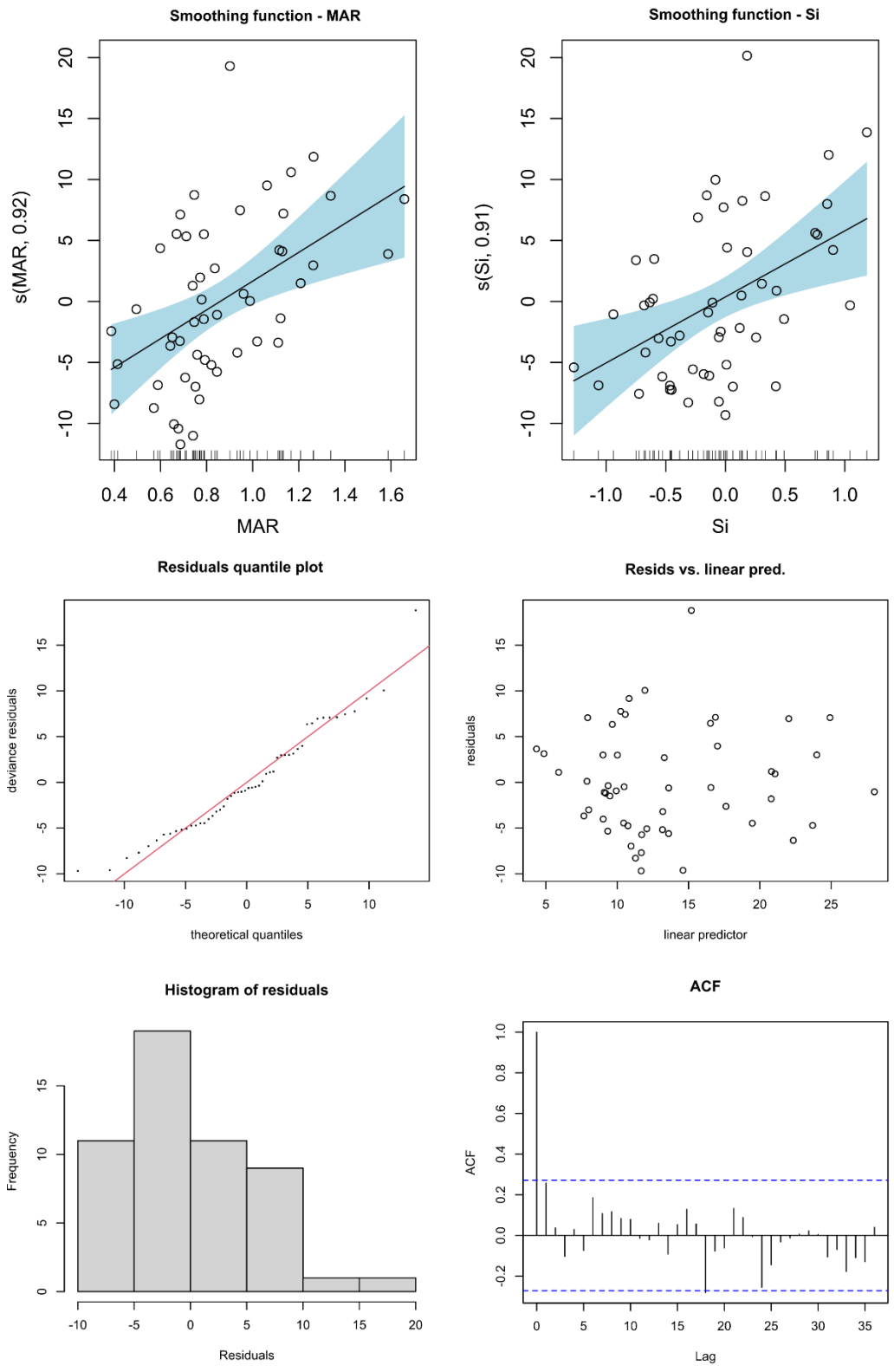

Figure S5.8: Partial effect plots and diagnostic plots of Mar-Dec wind days GAM reconstruction fit with MAR and Si.

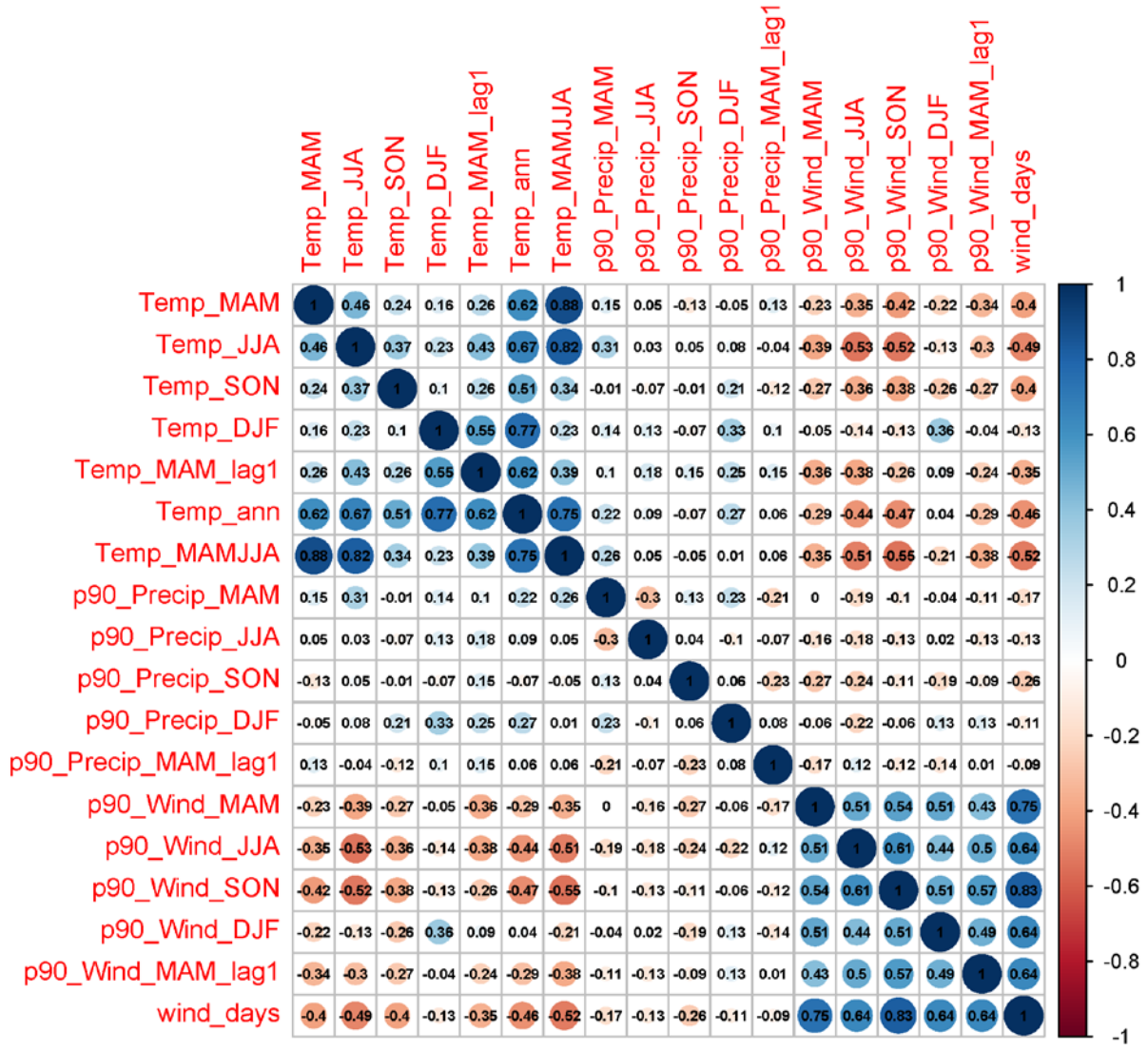

Figure S5.9: Correlation plot of selected meteorological variables.

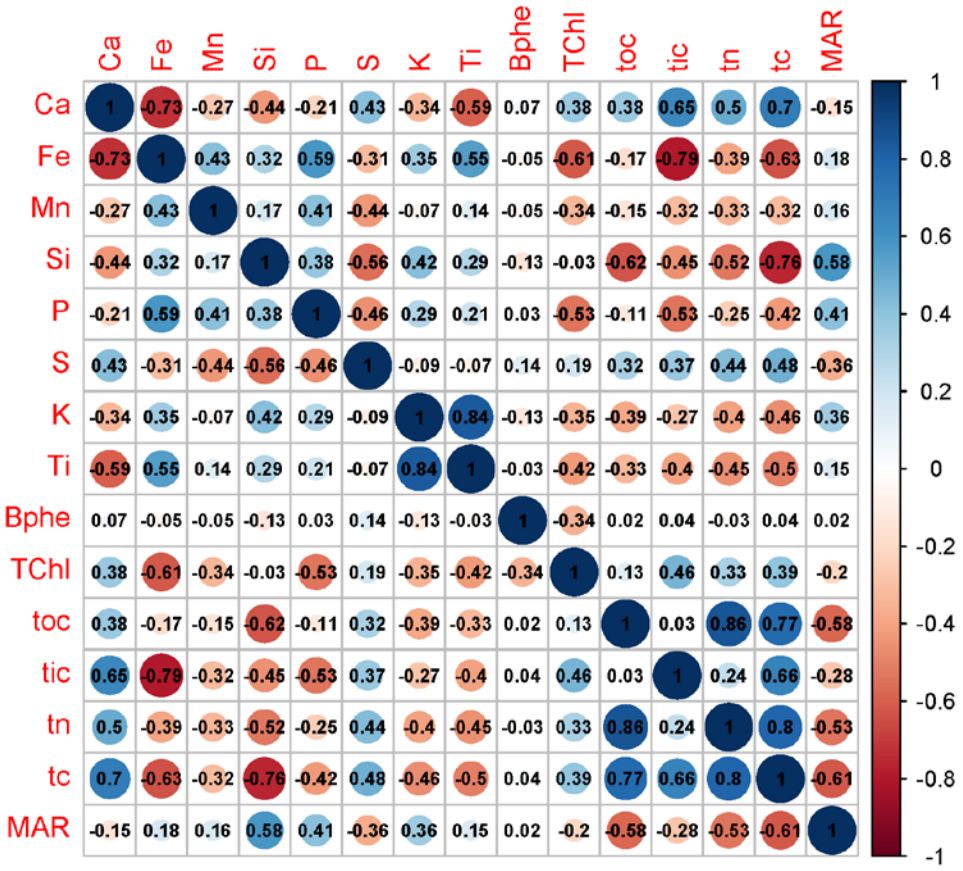

Figure S5.10: Correlation plot of proxy data at annual resolution (mean annual values, n = 54).

Chapter 6: Testing the suitability of sedimentary chloropigments as a proxy for spring temperature at Lake Żabińskie, Poland

Declaration of contribution

This study has not been published. Results were presented at the 14th International Paleolimnological Association Symposium, Stockholm, Sweden. Martin Grosjean and Paul Zander designed the study. Ronald Lloren, Irene Brunner and Henrik Vogel contributed to XRF scanning. Janusz Filipiak contributed meteorological data. Wojciech Tylmann and Maurycy Żarczyński contributed materials and data. Paul Zander did laboratory and numerical analysis, and wrote the text.

6.1 Introduction

Quantitative paleoclimate reconstructions are essential for understanding natural variability of the climate system as well as the forcing mechanisms that have controlled climate variability in the past (IPCC, 2013; Tierney et al., 2020). Varved lake sediments are highly valued as climate archives because of their precise chronologies, their ability to record information about multiple environmental variables, and the potential to obtain data at annual resolution (Brauer et al., 2009; Zolitschka et al., 2015).

In 2014, Amann et al. published a study of sedimentary pigments in Lake Żabińskie over the period 1907-2008 CE and found a statistically significant correlation between chloropigments and spring (MAM) temperature ($r = 0.36$, $p_{cor} < 0.05$ at annual resolution; $r = 0.63$, $p_{cor} < 0.05$ with a 5-year triangular filter). A calibration model was developed to reconstruct spring temperature variability, and the authors proposed that this proxy-climate calibration could be applied to longer time periods. Pigment data was obtained via reflectance spectroscopy at 2 mm resolution using a Gretag-Spectrolino (GretagMcBeth, Switzerland). The spectrally inferred pigment data was calibrated to measurements of chlorins (pheophytin-*a* and pyropheophytin-*a*) made using high-performance liquid chromatography. Recently, hyperspectral imaging (HSI) has been applied to sediment cores as a new technique to infer pigment abundances (Butz et al., 2015). Compared to the technology used by Amann et al. (2014), HSI offers several advantages. Most important is the measurement resolution, which is typically ~60 µm. Additionally, pigment abundances may be resolved spatially across the surface of the core. These two factors enable more precise delineation of annual layers, improving the accuracy and precision of annual time series. Another improvement is the greater spectral resolution of the reflectance data (2.8 nm for HSI compared to 10 nm for the Gretag-Spectrolino). This should improve the accuracy of pigment measurements by better resolving absorption features caused by pigments.

Exceptionally long instrumental temperature records are available from Warsaw extending back to 1779 CE at monthly resolution. This dataset provides an opportunity to test the calibration model over a much longer period than is typical for calibration-in-time studies (von Gunten et al., 2012). In this study, we aim to answer the following research questions: 1) Can HSI-inferred chloropigments improve upon the existing spring temperature and chloropigment calibration?; 2) Can the chloropigment - spring temperature calibration be extended over the period 1779-2016 CE?

6.2 Material and methods

6.2.1 Chronology

The data in this study was obtained on three sediment cores: ZAB-17-4, ZAB-17-1 (both retrieved in 2017), and ZAB-12-5-1 (retrieved in 2012). Cores were stratigraphically correlated using visual marker layers and X-ray fluorescence (XRF) data. Varve counting was done on core images obtained using a Specim PFD-CL-65-V10E hyperspectral linescan camera, with image processing done according to Butz et al. (2015). Two sections in the 2017 cores featured poor varve preservation, and linear interpolation

was used to determine ages in these segments (Figure 6.1). Stratigraphic tie points were established with the previously published varve chronology from (Żarczyński et al., 2018) based on peaks in K counts from XRF data. These tie points were used to assign ages at three locations so that ages could be assigned below the interpolated sections with poor preservation. The resulting chronology shows good agreement with the original varve count based on four other tie points that were not used to assign ages, but rather as a check of consistency between the chronologies. Each tie point is offset by no more than 2 years, which is within the range of counting uncertainty estimated by (Żarczyński et al., 2018).

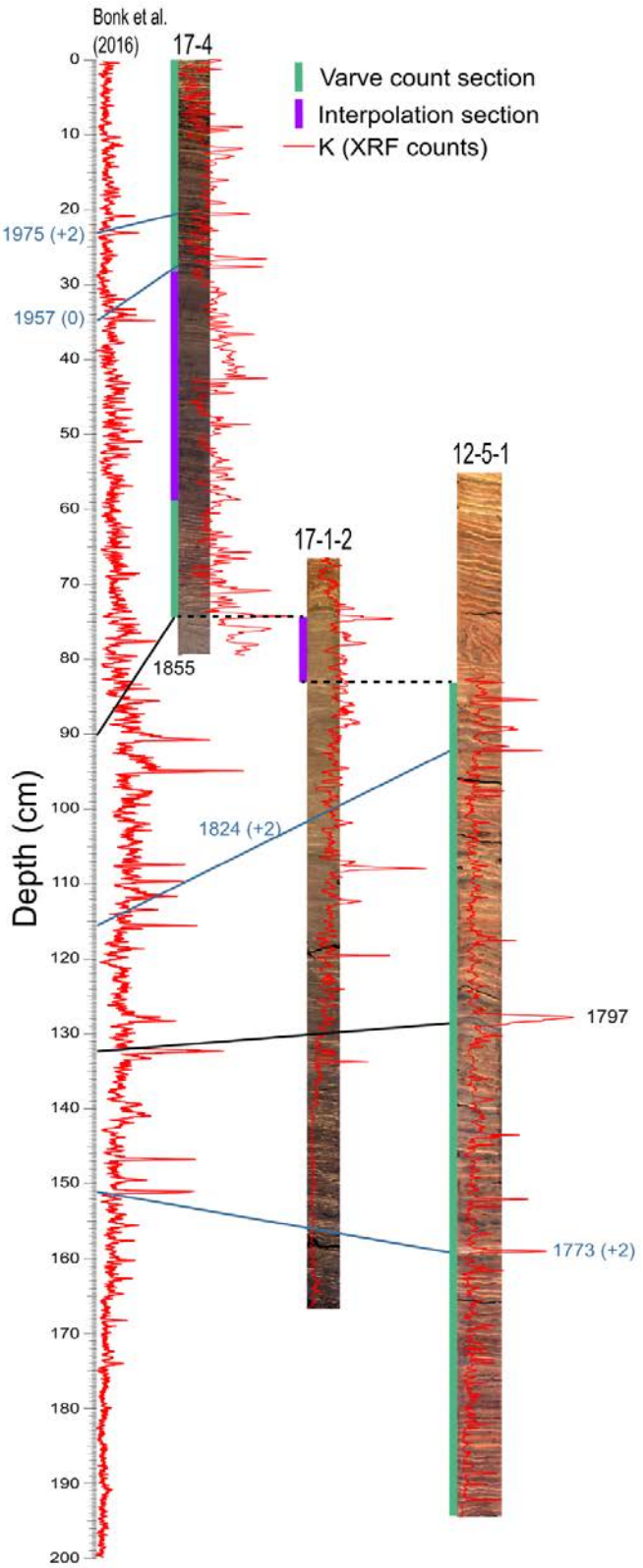

Figure 6.1: Stratigraphic correlations based on K XRF data (Bonk et al., 2016) used to align 2017 surface cores (ZAB-17-4 and ZAB-17-1) to the previously published chronology of Żarczyński et al. (2018). Tie points in black were used to assign ages to the new chronology. Tie points in blue were used as an uncertainty test, where the offset between the chronology established here and the original chronology is noted in parentheses.

6.2.2 Hyperspectral Imaging

Hyperspectral Imaging was performed using a Specim PFD-CL-65-V10E camera, following the workflow described by Butz et al. (2015). A relative absorption band depth (RABD) index was used to quantify absorption due to chloropigments according to the following formula (modified from Schneider et al., 2018):

$$\mathrm{RABD}_{655-685max} = \left(\frac{\mathrm{X} * \mathrm{R}_{590} + \mathrm{Y} * \mathrm{R}_{730}}{\mathrm{X} + \mathrm{Y}}\right) / R_{655-685min}$$

R_λ is the reflectance at the wavelength (λ), $R_{655\text{-}685min}$ is the trough minimum (ie. lowest reflectance value measured between 655 and 685 nm), X is the number of spectral bands between R730 and the trough minimum, and Y is the number of spectral bands between the trough minimum and R590. This $RABD_{655\text{-}685max}$ index represents total chloropigments, and can be considered a proxy for total algal productivity. This index is calculated slightly differently than the RABD index used by Amann et al. (2014), however, the two indices are directly comparable. Data from different cores was homogenized such that the standard deviation and mean in overlapping core sections were equal.

6.2.3 X-ray fluorescence scanning

Micro X-ray fluoresce (μXRF) scanning on the ZAB-17-4 and ZAB-17-1 was performed at the Swiss Federal Institute of Aquatic Science and Technology with an Avaatech XRF Core Scanner (Richter et al., 2006) equipped with a Rh-tube. Scanning parameters were 10 kV voltage, 1.5mA current, and 15 s exposure time. ZAB-12-5-1 was scanned at the University of Bern using an ITRAX core scanner equipped with a Cr-tube (exposure time 20 s, voltage 30 kV, current 50 mA). The scanning resolution was 0.5 mm for all three cores. All XRF data were calculated as counts per second (cps) and then homogenized as described for the HSI index above.

6.2.4 Meteorological data

Two metrological datasets were used in this study: 1) homogenized time series of monthly temperature data from Warsaw covering the period 1779-1999 CE (Lorenc, 2000); 2) temperature data for Lake Żabińskie (1885-2016 CE), calculated by spatial averaging and downscaling from nearby weather stations (Larocque-Tobler et al., 2015; J. Filipiak, personal communication). Here, we focus on spring (March, April, May) temperatures. Strong correlation between temperatures in Warsaw and Lake Żabińskie during the overlapping period ($r = 0.96$, $p_{cor} < 0.001$) indicate that Warsaw temperature variability is representative for the study site. A composite temperature record was created using Warsaw temperatures before 1885 CE and the Lake Żabińskie temperature data after 1885. Warsaw temperatures were scaled to match Lake Żabińskie temperatures using linear regression based on the overlapping period.

6.2.5 Data analysis

Data analysis was conducted in R (R Core Team, 2020). Annual values of $RABD_{655\text{-}685max}$ were calculated by averaging the index values over the depths assigned to a given year, based on the chronology. Correlations between $RABD_{655\text{-}685max}$ and spring temperatures (MAM) were calculated for data at yearly resolution, and after 3- and 5-year triangular filters were applied to both datasets. We tested if the correlations found by Amann et al. (2014) could be replicated or improved upon by first considering the same period used in the 2014 study (1907-2008 CE). We then calculated correlations over the full study period, and the period prior to 1907. The significance of correlations was assessed with p-values that were corrected for autocorrelation using the degrees of freedom adjustment of Bretherton et al. (1999). Additionally, correlations were calculated as a 31-year running mean (using 3-year triangular filtered data) over the full period to test the stability of the relationship over time.

6.3 Results

6.3.1 Geochemical results and interpretation

The chloropigment index $RABD_{655\text{-}685max}$ tracks algal productivity on a sub-annual scale, with peak values occurring immediately before or during the onset of calcite deposition (Figure 6.2). This observation confirms that sedimentary chloropigments are produced mainly in spring, as expected based on limnological monitoring (Bonk et al., 2015a).

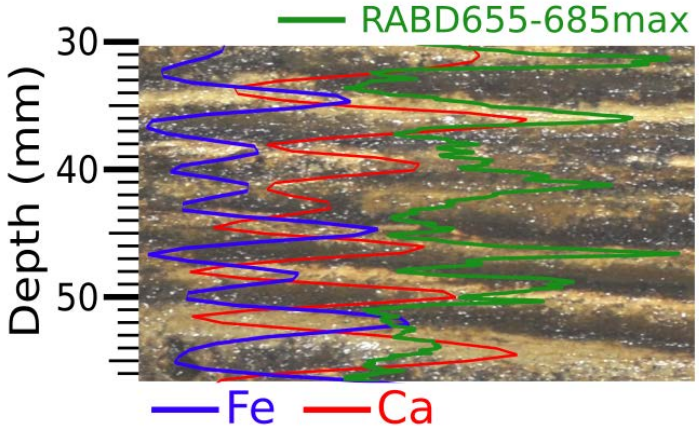

Figure 6.2: Close-up image showing varves. Light layers represent calcite deposition in spring/summer. Dark layers represent organic and lithogenic detrital material.

$RABD_{655\text{-}586max}$ shows little long-term trend (Figure 6.3). Somewhat lower values are found prior to 1850. Highest values are found between ~1860-1900. Lower values occur again from 1940-1970 before increasing towards the present. Ca also shows little long-term trend, though higher values are found in the most recent decades, as well as increased interannual variability. Ca in these sediments is mainly autochthonous calcite. Precipitation of calcite is driven by warm temperatures in the epilimnion in summer and uptake of CO_2 during algal blooms. K is representative of lithogenic input. Highest values occur prior to ~1845, and lowest values occur in the most recent few decades. Si reflects deposition of siliceous

algae, as well as silicate minerals, and therefore contains a mixed signal of productivity and lithogenic input. There is not a strong relationship between Si and RABD655-586max. Lower values of Si near the top of the core could reflect a shift in the algal community toward less siliceous algae and more cyanobacteria (Amann et al., 2014). Fe is influenced by lithogenic input, but also redox conditions (Naeher et al., 2013; Żarczyński et al., 2019b). Particularly high Fe values occur from ~1950-1970, which may have been a period of increased lake mixing, which would bring more oxygen into the bottom waters and improve preservation conditions for redox sensitive Fe compounds. Poor varve preservation in this section of core provides supporting evidence that this period featured more oxygenation of the hypolimnion. P tracks closely with Fe, suggesting either that P preservation is dependent on Fe concentrations in the sediments, or P preservation is also strongly influenced by changing redox conditions (Tu et al., 2020). Mn is also sensitive to redox conditions, with oxygenation events leading to preservation of Mn (Wirth et al., 2013). Mn also shows high values around 1950-1970, however in contrast to Fe and P, Mn values remain high in the uppermost portion of the core. S shows low values until 1860 and then increases to maximal values around 2000. S is better preserved in anoxic conditions.

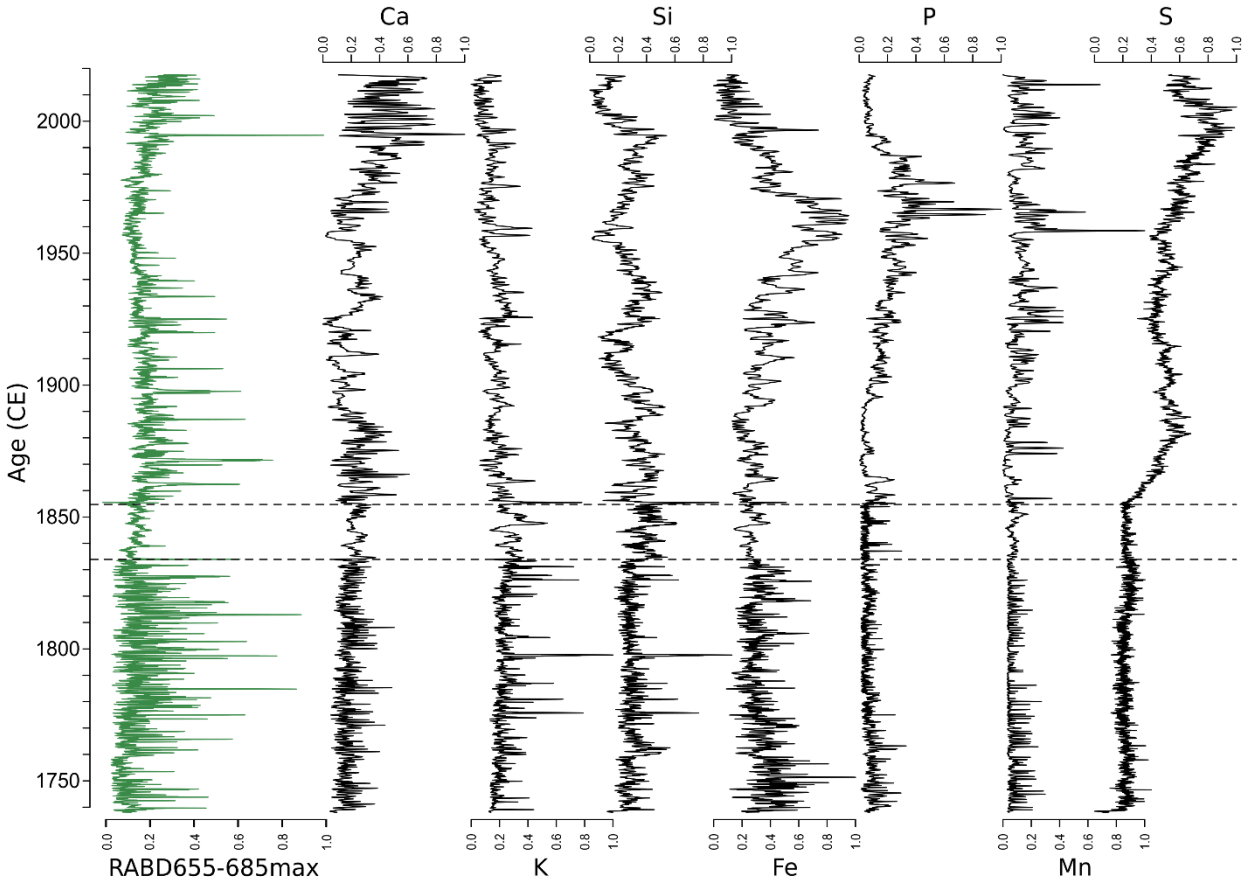

Figure 6.3: Key geochemical proxies from HSI and µXRF scanning. Dashed horizontal lines indicate tie points between different cores. All data are plotted on a standardized scale.

6.3.2 Correlations between spring temperature and chloropigments

The correlations between the chloropigment index and spring temperature found in Amann et al., 2014 are replicated with very similar values over the same period in our dataset (Table 6.1). The relationship between $RABD_{655\text{-}685max}$ and spring temperature is weaker over the full study period (1779-2016), though the correlations remain statistically significant ($p_{cor} < 0.05$ for 3-year filtered data). Correlation coefficients become larger as wider filters are applied. However, this smoothing increases autocorrelation, which decreases the corrected p-values. Generally, the 3-year filtered data seem to provide the best balance between optimizing for correlation strength and statistical significance. Correlations had not previously been investigated during the period 1779-1906, and we find no statistically significant relationship between chloropigments and spring temperature over this period. Figure 6.4 shows the 3-year filtered chloropigment and temperature data. At times, the sub-decadal variability in both datasets appears aligned, however the multi-decadal trends are often in disagreement. For instance, from 1870-1940 chloropigments decline while temperatures increase. The running correlation plot (Figure 6.5) shows that correlations were mostly positive from 1850-2016, however strong negative correlations are found during the first half of the 19th century.

Table 6.1: Correlation coefficients (Pearson's r) for RABD chloropigment index and spring (MAM temperature) for this study and Amann et al., 2014. Significance of correlations is indicated by * symbols (* $p_{cor} < 0.1$, ** $p_{cor} < 0.05$, *** $p_{cor} < 0.01$). P-values were corrected for autocorrelations using the method of Bretherton et al. (1999).

	MAM Temp (1907-2008)			MAM Temp (1779-2016)			MAM Temp (1779-1906)		
	yearly	3-yr	5-yr	yearly	3-yr	5-yr	yearly	3-yr	5-yr
$RABD_{655\text{-}685max}$ (this study)	0.31***	0.51***	0.64**	0.21***	0.37**	0.42*	0.06	0.19	0.25
$RABD_{660;670}$ (Amann et al., 2014)	0.35***	0.49**	0.58**	-	-	-	-	-	-

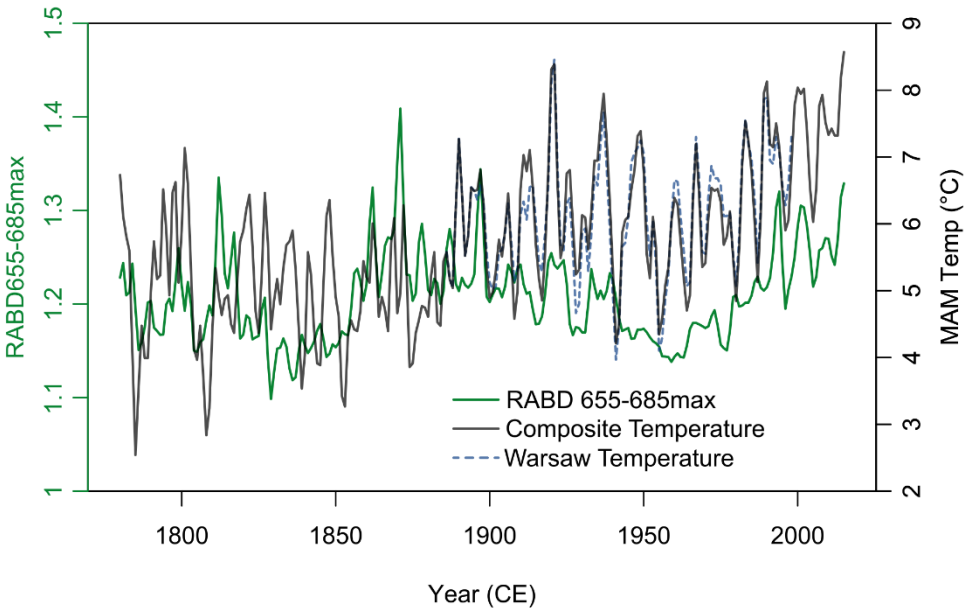

Figure 6.4: Plot showing $RABD_{655\text{-}685max}$ compared with instrumental spring (MAM) temperature data. All data shown are 3-year triangular filtered. Black line shows composite temperature record that combines the temperature data for Lake Żabińskie (1885-2016) with temperature data from Warsaw prior to 1885. Warsaw temperatures were scaled to match Lake Żabińskie values using linear regression. Blue dashed line shows scaled Warsaw temperatures over the period 1886-1999 to show the close similarity with Lake Żabińskie temperatures.

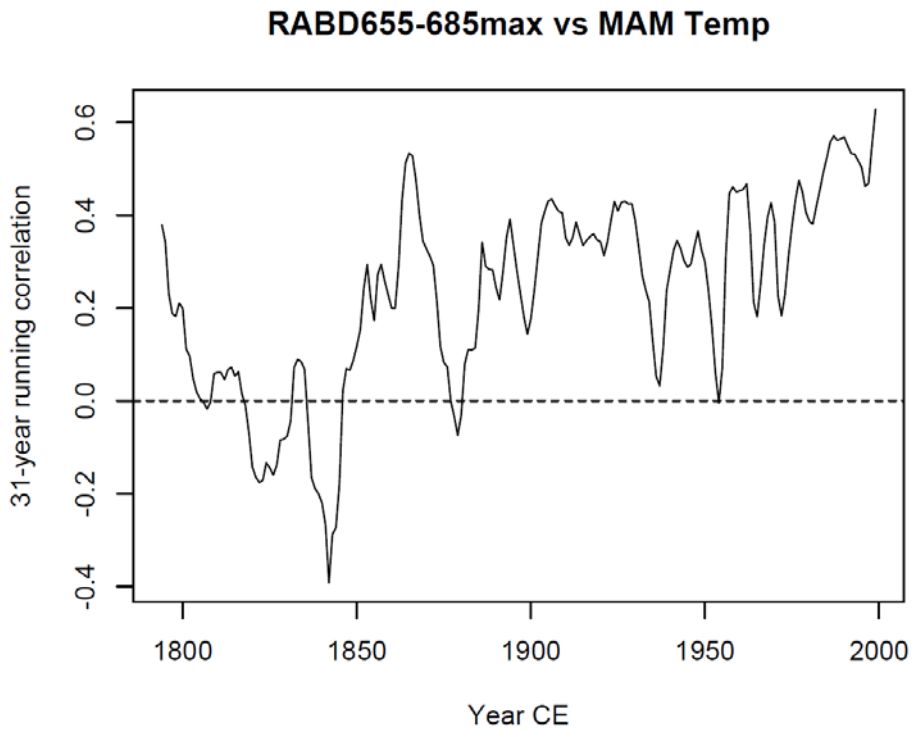

Figure 6.5: Plot of 31-year running correlations between $RABD_{655\text{-}685max}$ and spring temperature. Data were 3-year filtered prior to calculating the running correlation.

6.4 Discussion

Climate reconstructions based on the calibration-in-time approach rely on an assumption that the relationship between climate and proxy variables found in the calibration period remains stable outside that calibration period. Our results indicate that this is likely not the case for the relationship between spring temperature and chloropigments in Lake Żabińskie, casting doubt on the viability of chloropigments as a temperature proxy at this site. Instability of climate-proxy relationships is not uncommon (Wilson and Elling, 2004; Blass et al., 2007), and perhaps should be expected at sites such as Lake Żabińskie where major anthropogenic impacts have modified ecosystem function over the past few centuries (Bonk et al., 2016; Hernández-Almeida et al., 2017). Intensive agricultural development and deforestation after ~1590 CE lead to a major increase in catchment erosion and nutrient input to the lake, leading to approximately a four-fold increase in mass accumulation rates (Bonk et al., 2016). These impacts, as well as fertilizer use in the catchment and development of recreation facilities near the lake, certainly had a major effect on chloropigment concentrations in the sediments. Although the correlation between the two variables is statistically significant over the full study period ($r = 0.37$, $p < 0.05$, 3-yr triangular filtered data), the lack of statistically significant correlation over the period investigated here for the first time (1779-1906) is a strong indication that chloropigments are not a consistently good recorder of temperature variations at this time.

Another important consideration when interpreting the chloropigment record is consistency between cores. The data presented here is a composite of 2017 surface cores (ZAB-17-4, ZAB-17-1) and ZAB-12-5-1. ZAB-12-5-1 was taken closer to the deepest point of the lake; it features much better varve preservation, and higher sedimentation rates compared to the 2017 cores. These differences may also be related to the coring technique. ZAB-12-5-1 was collected with a piston corer and is 9 cm in diameter. These techniques cause less compaction than the gravity corer and 6 cm diameter used for ZAB-17 cores. Data from different cores were homogenized to account for these effects (raw data yielded poorer correlations with MAM temperatures), but this technique is imperfect. Additionally, varve preservation is poor in some sections of the 2017 cores, reducing the accuracy of calculated yearly values of the chloropigment index. $RABD_{655\text{-}685max}$ index values also tend to be lower when varve preservation is poor, possibly evidence that changes to lake mixing regime also affect chloropigment preservation (in both the water column and in sediments). Furthermore, it remains possible that there is a small error in the core correlation, which would impact the accuracy of the chronology. This may be an explanation for the poor correlations prior to 1850 CE (Figure 6.5).

6.5 Conclusion and outlook

In this study, we investigated correlations between sedimentary chloropigments and spring temperatures over the period 1779-2016 to assess the suitability of HSI-inferred chloropigments as a spring temperature proxy. We find that the results of Amann et al., 2014 are replicable using HSI to infer chloropigment abundances over the same study period (1907-2008). Over this period, the two chloropigment records are

strongly correlated ($r = 0.76$, $p < 0.01$, 3-yr triangular filtered data), and similar correlations are found with spring temperature. There is no clear improvement from the HSI technique in terms of relating chloropigments to temperature; however poorer varve preservation in the sediment cores used in this study may have limited or disguised any possible benefits achieved by the greater resolution of the HSI technique. When the calibration period was extended to 1779, the relationship between chloropigments and spring temperature breaks down. There is no significant correlation between the two variables in the 128 years from 1779-1907. Most likely, chloropigment abundance was strongly influenced by non-climatic factors such as soil erosion and/or fertilizer use.

A more consistent chloropigment record with improved chronological precision might be obtained from cores retrieved from the deepest point of the lake, where there is better varve preservation. However, given the major anthropogenic impacts to the lake ecosystem documented at Lake Żabińskie, it is not expected that climate was a dominant control on algal production (and thereby sedimentary chloropigment production) over the past several hundred years. This study highlights the potential danger of assuming that climate-proxy relationships are stable over time. Long calibration periods like used in this study can help identify this problem.

6.6 References

Amann, B., Lobsiger, S., Fischer, D., Tylmann, W., Bonk, A., Filipiak, J., Grosjean, M., 2014. Spring temperature variability and eutrophication history inferred from sedimentary pigments in the varved sediments of Lake Żabińskie, north-eastern Poland, AD 1907-2008. Glob. Planet. Change 123, 86-96. https://doi.org/10.1016/j.gloplacha.2014.10.008

Blass, A., Grosjean, M., Troxler, A., Sturm, M., 2007. How stable are twentieth-century calibration models? A high-resolution summer temperature reconstruction for the eastern Swiss Alps back to AD 1580 derived from proglacial varved sediments. The Holocene 17, 51-63. https://doi.org/10.1177/0959683607073278

Bonk, A., Kinder, M., Enters, D., Grosjean, M., Meyer-Jacob, C., Tylmann, W., 2016. Sedimentological and geochemical responses of Lake Żabińskie (north-eastern Poland) to erosion changes during the last millennium. J. Paleolimnol. 56, 239-252. https://doi.org/10.1007/s10933-016-9910-6

Bonk, A., Tylmann, W., Amann, B., Enters, D., Grosjean, M., 2015. Modern limnology and varve-formation processes in lake Żabińskie, northeastern Poland: Comprehensive process studies as a key to understand the sediment record. J. Limnol. 74, 358-370. https://doi.org/10.4081/jlimnol.2014.1117

Brauer, A., Dulski, P., Mangili, C., Mingram, J., Liu, J., 2009. The potential of varves in high-resolution paleolimnological studies. PAGES news 17, 96-98. https://doi.org/10.22498/pages.17.3.96

Bretherton, C.S., Widmann, M., Dymnikov, V.P., Wallace, J.M., Bladé, I., 1999. The effective number of spatial degrees of freedom of a time-varying field. J. Clim. 12, 1990-2009. https://doi.org/10.1175/1520-0442(1999)012<1990:TENOSD>2.0.CO;2

Butz, C., Grosjean, M., Fischer, D., Wunderle, S., Tylmann, W., Rein, B., 2015. Hyperspectral imaging spectroscopy: a promising method for the biogeochemical analysis of lake sediments. J. Appl. Remote Sens. 9, 096031. https://doi.org/10.1117/1.jrs.9.096031

Hernández-Almeida, I., Grosjean, M., Gómez-Navarro, J.J., et al., 2017. Resilience, rapid transitions and regime shifts: Fingerprinting the responses of Lake Żabińskie (NE Poland) to climate variability and human disturbance since AD 1000. Holocene 27, 258-270. https://doi.org/10.1177/0959683616658529

IPCC, 2013. Climate Change 2013: The Physical Science Basis. Contribution of Working Group I to the Fifth Assessment Report of the Intergovernmental Panel on Climate Change. Cambridge University Press.

Larocque-Tobler, I., Filipiak, J., Tylmann, W., Bonk, A., Grosjean, M., 2015. Comparison between chironomid-inferred mean-August temperature from varved Lake Zabińskie (Poland) and instrumental data since 1896 AD. Quat. Sci. Rev. 111, 35-50. https://doi.org/10.1016/j.quascirev.2015.01.001

Lorenc, H., 2000. serią temperatury powietrza w Warszawie oraz ocena jej wiekowych tendencji. Materiały Badawcze IMGW.

Naeher, S., Gilli, A., North, R.P., Hamann, Y., Schubert, C.J., 2013. Tracing bottom water oxygenation with sedimentary Mn/Fe ratios in Lake Zurich, Switzerland. Chem. Geol. 352, 125-133. https://doi.org/10.1016/j.chemgeo.2013.06.006

R Core Team, 2020. R: A Language and Environment for Statistical Computing.

Schneider, T., Rimer, D., Butz, C., Grosjean, M., 2018. A high-resolution pigment and productivity record from the varved Ponte Tresa basin (Lake Lugano, Switzerland) since 1919: insight from an approach that combines hyperspectral imaging and high-performance liquid chromatography. J. Paleolimnol. 60, 381-398. https://doi.org/10.1007/s10933-018-0028-x

Tierney, J.E., Poulsen, C.J., Montañez, I.P., et al., 2020. Past climates inform our future. Science (80-.). https://doi.org/10.1126/science.aay3701

Tu, L., Zander, P., Szidat, S., Lloren, R., Grosjean, M., 2020. The influences of historic lake trophy and mixing regime changes on long-term phosphorus fractions retention in sediments of deep, eutrophic lakes: a case study from Lake Burgäschi, Switzerland. Biogeosciences 17, 2715-2729. https://doi.org/10.5194/bg-2019-389

von Gunten, L., Grosjean, M., Kamenik, C., Fujak, M., Urrutia, R., 2012. Calibrating biogeochemical and physical climate proxies from non-varved lake sediments with meteorological data: Methods and case studies. J. Paleolimnol. 47, 583-600. https://doi.org/10.1007/s10933-012-9582-9

Wilson, R., Elling, W., 2004. Temporal instability in tree-growth/climate response in the Lower Bavarian Forest region: Implications for dendroclimatic reconstruction. Trees - Struct. Funct. 18, 19-28. https://doi.org/10.1007/s00468-003-0273-z

Wirth, S.B., Gilli, A., Niemann, H., et al., 2013. Combining sedimentological, trace metal (Mn, Mo) and molecular evidence for reconstructing past water-column redox conditions: The example of meromictic Lake Cadagno (Swiss Alps). Geochim. Cosmochim. Acta 120, 220-238. https://doi.org/10.1016/j.gca.2013.06.017

Żarczyński, M., Tylmann, W., Goslar, T., 2018. Multiple varve chronologies for the last 2000 years from the sediments of Lake Żabińskie (northeastern Poland) - Comparison of strategies for varve counting and uncertainty estimations. Quat. Geochronol. 47, 107-119. https://doi.org/10.1016/j.quageo.2018.06.001

Żarczyński, M., Wacnik, A., Tylmann, W., 2019. Tracing lake mixing and oxygenation regime using the Fe/Mn ratio in varved sediments: 2000 year-long record of human-induced changes from Lake Żabińskie (NE Poland). Sci. Total Environ. 657, 585-596. https://doi.org/10.1016/j.scitotenv.2018.12.078

Zolitschka, B., Francus, P., Ojala, A.E.K., Schimmelmann, A., 2015. Varves in lake sediments - a review. Quat. Sci. Rev. 117, 1-41. https://doi.org/10.1016/j.quascirev.2015.03.019

Chapter 7: Conclusion

7.1 Introduction

Lake Żabińskie offers a unique archive of paleoenvironmental change in northeastern Poland during the past 10,800 years. The well-preserved varves enabled relatively precise age control and, in conjunction with high-resolution scanning techniques, allow for analysis at annual and sub-annual resolution. This thesis builds upon previous research at Lake Żabińskie by investigating the full sedimentary sequence (previously only the past 2,000 years had been investigated). A central focus of the thesis was high-resolution non-destructive core-scanning techniques (micro X-ray fluorescence and hyperspectral imaging). The results of the thesis contribute knowledge to several important areas of paleoenvironmental research including strategies for dating lake sediments, how natural and anthropogenic factors influenced paleoproductivity and lake mixing over the Holocene, and quantitative reconstruction of climate variables from the biogeochemical composition of biogenic varves.

7.2 Conclusions of individual studies

In this section, I summarize the findings of the individual studies in the context of the research questions posed in Chapter 1.

7.2.1 Chapter 3: Miniature radiocarbon measurements (< 150 µg C) from sediments of Lake Żabińskie, Poland: effect of precision and dating density on age-depth models

The aim of this chapter was to assess the suitability and potential of miniature radiocarbon samples, measured using the recently developed gas-source input of the MICADAS, for dating lake sediments. This was assessed by measuring radiocarbon in multiple samples of various masses from the same core depths. Varve counts were used as additional chronological data to help assess bias of radiocarbon results. Additionally, simulations of sampling scenarios were performed to understand how choices about the number of samples taken, and the precision of resulting ages affect resulting age-depth models. The findings of this study are relevant to researchers designing sampling strategies for radiocarbon dating of sediment sequences, particularly sediments with limited suitable organic material for dating.

Q3.1: How reliable and how precise are gas-source ^{14}C ages compared with conventional graphitized ages?

Gas-source ages were found to be as reliable and precise as would be expected from graphitized ages of a similar mass. A comparison of gas-source ages and graphitized ages showed no bias in the ages obtained using the gas-source technique. The analytical precision of radiocarbon ages depends on the age of the sample and the mass of the sample. Gas-source ages are generally obtained on smaller samples, and therefore produce less precise ages. However, for samples with similar mass (samples containing 120-160 µg C were measured with both techniques), the analytical uncertainty is similar for both graphitized and gas-source ages. We found that over our study period (2.1-6.8 ka cal BP) the age

precision could be estimated reasonably well based on the mass of the sample, and the same relationship could be applied to ages obtained using both techniques.

Q3.2: What is the variability of ^{14}C ages obtained from a single stratigraphic level, and do certain types of plant macrofossils produce biased ages?

In our set of ages obtained from confirmed terrestrial plant macrofossils, the variability of ^{14}C ages was no greater than would be expected from analytical uncertainty alone. There was no clear evidence of bias based on the type of macrofossil material used for dating. Wood samples tended to yield older ages than other types of material, but this result was not statistically significant due to the small number of samples (3 samples of purely woody material were analyzed).

Q3.3: How do analytical precision and dating density affect the accuracy and precision of age-depth models for lake sediments?

Our simulated age-depth model experiment showed, unsurprisingly, that the accuracy and precision of age-depth models are both improved by increased dating density and increased analytical precision. Specifically, we investigated the trade-offs between few samples with greater mass, and therefore lower uncertainty, and more samples with low mass and greater uncertainty. We find that increased dating density can compensate for the greater uncertainty of miniature radiocarbon samples. Doubling the dating density decreased the age-model uncertainty range by approximately the same amount as would be expected by reducing analytical uncertainty by 50 years. In other words, an age-depth model based on 10 samples containing 500 µg C (expected uncertainty ± 39 years) has similar precision as a model based on 20 samples containing 90 µg C (expected uncertainty ± 92 years). Increased dating density had a greater effect on age-model precision for samples with larger masses, whereas age-model accuracy was only improved by increased dating density for samples with small masses. We note that dating density would more strongly affect age-model accuracy in sediment records with more variable sedimentation rates.

7.2.2 Chapter 4: A high-resolution record of Holocene primary productivity and water-column mixing from the varved sediments of Lake Żabińskie, Poland

This chapter presents the full 10,800 sedimentary record from Lake Żabińskie. The focus of the study was to reconstruct primary production and water column mixing regimes. Hyperspectral measurements of chloropigments and bacteriopheopigments at sub-mm resolution were the primary datasets used, with additional interpretations from XRF elemental data and pigment assemblages determined from HPLC. The findings of the paper elucidate how primary production and anoxia evolved over the Holocene and what were the most important drivers of changing limnological conditions. This study is relevant for researchers interested in understanding how natural and anthropogenic drivers influence trophic levels and lake mixing regimes over short and long timescales.

Q4.1: How have primary production and water column oxygen concentrations varied during the past 10,800 years?

Primary production was reconstructed at sub-annual resolution over the past 10,800 years using HSI-inferred chloropigments and anoxic conditions were recorded by HSI-inferred bacteriopheopigments. Fluxes of chloropigments were relatively high in the early part of the record (10.8 - 10.3 ka cal BP), then relatively low from 9.5 to 7.4 ka cal BP. Primary production increased gradually from 7.4 ka cal BP to ~1600 CE. Fluxes of chloropigments increased by over 300% after 1720 CE, with highest fluxes occurring during the 19th century. The presence of bacteriopheopigments (Bphe) indicates extensive anoxia and persistent lake stratification. Bphe was present nearly continuously prior to 2.8 ka cal BP, indicating persistent anoxic conditions. From 2.8 ka cal BP to ~610 CE, Bphe is present only occasionally, indicating more intensive lake mixing and higher oxygen concentrations. From ~610-1470 CE anoxia was again persistent. From 1470 CE to present, Bphe is very low. However, this may be due limited light penetration due to greater algal production, particularly after ~1800 CE. A slight increase in Bphe in the past few decades could be an indication that lake mixing is weakening and oxygenation of the hypolimnion is becoming less frequent.

Q4.2 What role did natural and anthropogenic forces have in driving changes in primary production or lake mixing regime?

Primary production appears to be strongly influenced by nutrient inputs, often linked to soil erosion. High values occurred in the early Holocene when P input from relatively immature soils was likely somewhat high. Natural eutrophication progressed slowly over thousands of years due to gradual build-up of nutrient pools within the lake and catchment soils. Intensive agricultural development and deforestation after 1620 CE caused major increases in aquatic production due to nutrient input from soil erosion, fertilizer use and other anthropogenic sources. Based on our results, the most important factor influencing lake mixing is forest cover surrounding the lake. Dense forests shield the lake from wind, thereby limiting wind-driven mixing. Even small reductions in forest cover, as recorded by pollen counts, led to increased mixing and oxygenation of the water column, evidenced by decreased Bphe and Fe/Mn ratios. Climate likely had some influence on lake mixing, with warmer conditions increasing thermal stratification; however, we observe little change in indicators of anoxia from 10.8 to 2.8 ka despite variable climate conditions, suggesting that climate did not exert a strong influence on lake mixing over the Holocene.

7.2.3 Chapter 5: Seasonal climate signals preserved in biochemical varves: insights from high-resolution sediment scanning techniques

The aim of this study was to investigate relationships between meteorological conditions and varve composition and structure to determine the potential of high-resolution sediment scanning techniques for reconstructing past climate or weather at Lake Żabińskie. We focused on the period 1966-2019 CE because varve counting results showed no uncertainty over this period, which was crucial to investigate these relationships at the highest possible resolution (sub-annual). The results of this study show the

potential of μXRF and HSI scanning for paleoclimate reconstructions, and are a rare demonstration of how climate influences the composition of biochemical varves.

Q5.1: Is the sequence of geochemical variables through a single varve influenced by seasonal meteorological conditions?

Yes. We classified varves into 4 varve types based on the similarity of the annual geochemical timeseries within each varve. A multivariate analysis of variance test showed that these groups of years experienced different seasonal meteorological conditions. In particular, temperatures in spring summer and fall, and windiness in spring and fall were shown to be related to the varve types.

Q5.2: Can varve composition be used to reconstruct seasonal meteorological conditions?

Yes. Statistically significant correlations between sedimentary geochemical variables and seasonal meteorological data show that varve composition has a strong potential for reconstructing past meteorological conditions. Specifically, spring and summer temperatures could be predicted by yearly means of total C and Ti within varves. The frequency of windy days could be predicted by mass accumulation rate and Si.

7.2.4 Chapter 6: Testing the suitability of sedimentary chloropigments as a proxy for spring temperature at Lake Żabińskie, Poland

This chapter aims to extend the previously published spring temperature calibration based on chloropigments from Lake Żabińskie (Amann et al., 2014) to cover a longer time period (1779-2016). Long time series of monthly temperature data from Warsaw make this long calibration period possible. The results of this study demonstrate the potential hazard of assuming climate - proxy relationships are stable through time.

Q6.1: Can HSI-inferred chloropigments improve upon the existing spring temperature - chloropigment calibration?

The HSI-inferred chloropigment record yields very similar results compared with the previously published chloropigment record for Lake Żabińskie that was obtained using a Spectrolino camera (Amann et al., 2014). Correlation coefficients between spring temperature and chloropigments are nearly identical over the same period.

Q6.2: Can the chloropigment - spring temperature calibration be extended over the period 1779-2016 CE?

Although there is a statistically significant correlation between spring temperature and chloropigments over the extended period (1779-2016 CE), the relationship between spring temperature and chloropigments is not stable over this period. In fact, there is no significant correlation found over the period that had not previously been investigated (1779-1906 CE). This finding casts doubt on the suitability of chloropigments as a proxy for spring temperature at Lake Żabińskie.

7.3 Final remarks

This thesis has demonstrated the value of Lake Żabińskie as an archive of environmental change. Changing conditions in aquatic, terrestrial and atmospheric sectors were reconstructed. The 10,800 year-long stratigraphy and chronology established in this work provide a foundation that future work at the site can build upon. Important insights were gained about the interplay between land cover change, aquatic ecological conditions and biogeochemical cycling. Because Lake Żabińskie has experienced significant anthropogenic impacts during the past few centuries, there are substantial challenges regarding the use of sedimentary properties from this site as climate indicators. Nonetheless, the results of this thesis give some indications about which sedimentary variables are most useful for climate reconstructions, while also being aware of the pitfalls associated with quantitative paleoclimate reconstructions.

The combination of methods used in this thesis provided unique and complementary data that were essential to a more complete understanding of processes investigated. Scanning data from XRF and hyperspectral imaging are powerful tools because of the high-resolution and rapid acquisition of these datasets. High-performance liquid chromatography provided complementary data that offered more detailed insights in the photosynthetic communities in the lake. We advocate for further use of these methods to understand long-term ecological dynamics at various lakes. The high-resolution sediment scanning techniques used in this thesis remain relatively young in their development and application in earth sciences. In this thesis, we have shown than hyperspectral imaging of varved sediments can provide insights into seasonal scale sedimentation and environmental conditions, however there remains much potential to explore these datasets for environmental reconstruction. The large volumes of data generated by this technique make it suitable for advanced computing and machine learning approaches. It is expected that these techniques will continue to expand the utility of hyperspectral imaging for paleoenvironmental research.

Acknowledgments

This thesis would not be possible without many people who have inspired, taught, and supported me along this path.

Most importantly, thank you to Prof. Dr. Martin Grosjean for his guidance, support and constructive feedback. I will always be thankful for the opportunity I was given to come to Bern and work on this project, and I appreciate the degree to which Martin allowed me to work independently to achieve my goals.

Thank you to Prof. Dr. Wojciech Tylmann for being my co-supervisor, providing many resources necessary for this work, and for being a great host during my visits to Gdańsk and the Masurian Lakeland. Many thanks to Prof. Dr. Willy Tinner for agreeing to be the Chair of my PhD defense and for letting me play with the fancy XRF at the Institute of Plant Sciences. Thanks as well to Prof. Dr. Bernd Zolitschka for reviewing this thesis.

A large share of credit for this work should go to Dr. Maurycy Żarczyński, the world's foremost expert on Lake Żabińskie. Thank you for kindly sharing data, many useful and entertaining discussions (not only about work), and graciously hosting me in Gdańsk.

Thank you to my co-authors whose important contributions made these studies possible: Prof. Dr. Darrell Kaufman (special thanks to Darrell for starting me down the path of lake sediments starting in 2010), Prof. Dr. Sönke Szidat, Dr. Maurycy Żarczyński, Anna Poraj-Górska, Dr. Petra Boltshauser-Kaltenrieder, Dr. Hendrik Vogel, Dr. Agnieszka Wacnik, Dr. Andrea Sanchini, and Dr. Shauna-kay Rainford. It was a pleasure working with all of you.

Dr. Daniela Fischer, Edith Vogel, Dr. Gary Salazar, Ron Lloren, Irene Brunner, Dr. Stamatina Makri, Linus Rösler, Joanna Piłczyńska, Dr. Alicja Bonk, Dr. Christoph Butz, Dr. Benjamin Amann, Dr. Marina Morlock, Dr. Janusz Filipiak, Dr. André Lotter, and Willy Tanner also contributed to this work.

Special thanks to the past and present members of the Paleolimnology Group: Dr. Tobias Schneider, Dr. Christoph Butz, Dr. Benjamin Amann, Dr. Stamatina Makri, Dr. Andrea Sanchini, Dr. Christoph Dätwyler, Dr. Luyao Tu, Giulia Wienhues, Dr. Raphael Neukom, Michael Faden, Dr. Aurea C. Chiaia-Hernández, Yunuén Temoltzin-Loranca, Linus Rösler, Nicole Fahrni, Carlo Egger and Luc Hächler. Thank you for the help, lunch break conversations, and social activities over the past few years.

Thank you to my family and friends for love and support over the years. None of this would be possible without the love, support and courage of my wife Hilary Woodhams. She encouraged me to look for PhD positions in Switzerland in the first place!

This work was funded by Swiss National Science Foundation grant 200021_172586, and Polish National Science Centre grants NCN 2014/13/B/ ST10/01311 and NCN 2015/18/E/ST10/00325.

Declaration of consent

on the basis of Article 18 of the PromR Phil.-nat. 19

Name/First Name: Zander, Paul

Registration Number: 17-108-960

Study program: Climate Sciences

Bachelor ☐ Master ☐ Dissertation ☑

Title of the thesis: The varved sediments of Lake abi skie, Poland as a high-resolution archive of environmental change

Supervisor: Prof. Dr. Martin Grosjean

I declare herewith that this thesis is my own work and that I have not used any sources other than those stated. I have indicated the adoption of quotations as well as thoughts taken from other authors as such in the thesis. I am aware that the Senate pursuant to Article 36 paragraph 1 litera r of the University Act of September 5th, 1996 and Article 69 of the University Statute of June 7th, 2011 is authorized to revoke the doctoral degree awarded on the basis of this thesis.
For the purposes of evaluation and verification of compliance with the declaration of originality and the regulations governing plagiarism, I hereby grant the University of Bern the right to process my personal data and to perform the acts of use this requires, in particular, to reproduce the written thesis and to store it permanently in a database, and to use said database, or to make said database available, to enable comparison with theses submitted by others.

Bern, 09.04.21

Place/Date

Paul Zander Digitally signed by Paul Zander Date: 2021.04.09 17:16:19 +02'00'

Signature